

Discrimination of fabric mechanical properties and buckling deformations in a novel fabric handle evaluation system

Yiyi Wang

Submitted in accordance with the requirements for the degree of
Doctor of philosophy

The University of Leeds
School of Design

September, 2016

The candidate confirms that the work submitted is her own, except where work which has formed part of jointly-authored publications has been included. The contribution of the candidate and the other authors to this work has been explicitly indicated below. The candidate confirms that appropriate credit has been given within the thesis where reference has been made to the work of others.

Wang, Y. and Mao, N. 2015. The influences of pre-tensions on the deformations of woven fabric shells during cyclic axial compression buckling processes. In: the 9th Textile Bioengineering and Informatics Symposium, Zadar, Croatia.

Mao, N., Wang, Y. and Qu, J. 2016. Smoothness and roughness: characteristics of fabrics-to-fabric self-friction properties. In: *The 90th textile institute world conference, Poznan, Poland*.

This copy has been supplied on the understanding that it is copyright material and that no quotation from the thesis may be published without proper acknowledgement.

Acknowledgements

I would like to give special thanks to my supervisor, Dr. Ningtao Mao for his valuable advice, guidance, constructive criticism, patience, and support during this work.

I would like to thank Dr. Jianguo Qu for his help with the software and the support in the laboratory work.

I also thank the staff in fashion design department for providing the test fabrics.

I also thank my family, my friends and colleagues for their support, encouragement during this work.

Abstract

This research is to study the characteristics of fabric properties measured in an innovative fabric test system, Leeds University Fabric Handle Evaluation System (LUFHES); it is designed for objectively evaluating fabric handle in a simpler, relatively low cost and automatic method. The quantification of fabric handle in the LUFHES is based on the energy consumption of fabric shells during their cyclic shear twisting and cyclic axial compression buckling deformations, as well as the fabric surface properties evaluated from fabric-fabric self-friction process.

In this study, low stress fabric mechanical properties measured in the cyclic axial compression buckling, shear twisting and fabric-fabric friction of fabric shells in LUFHES were analysed to establish the new technological approach in relation to fabric handle analysis. In addition, the fabric properties measured in the LUFHES were compared with the fabric properties measured in fabric unidirectional deformation processes such as the Kawabata Evaluation System for Fabric (KES-F) and the Fabric Assurance by Simple Testing (FAST) to disclose the differences of these three fabric measurement systems.

Properties of 29 fabrics including 12 woven fabrics, 7 knitted fabrics and 10 nonwoven fabrics were studied in this project in order to understand the mechanical properties of fabrics which are made from different fibres, having different fabric structures, fabric weight and thickness measured by using the LUFHES system.

The suitable pre-tension for the LUFHES tests was determined by analysing the effect of pre-tensions on the energy consumption of various fabric deformations in cyclic fabric shell compression buckling-recovery processes, and suitable pre-tension force for fabric measurements in the LUFHES was identified in the range of 1.2N/m and 2N/m.

Fabric shear and buckling properties measured in the LUFHES were compared with shear and bending properties obtained in both the KES-F and FAST systems to investigate the differences between these three systems in discriminating fabrics. It was found that fabric shear properties obtained in the FAST were different from those obtained in the LUFHES shear tests for woven fabrics due to insufficient shear deformations in woven fabrics in FAST test. It was also found that shear properties obtained in the KES-F shear tests were not in agreement with those obtained in the LUFHES tests due to greater extension forces applied on fabrics leading to greater fabric elongation before its shear test in the KES-F system for some fabrics such as knitted and nonwoven fabrics. Thus, fabric

discriminations in terms of fabric shear properties obtained in these three testing systems will be different.

The correlation between critical buckling force and bending properties was found to depend on the fabric types and measurement methods. Critical buckling forces of woven and nonwoven fabrics obtained in the LUFHES were found to correlate well with bending rigidity obtained in the KES-F system, while critical buckling forces of knitted fabrics correlated well with the bending rigidity obtained in the FAST system.

It was found that there are several unique advantages using the fabric-fabric self-friction method in objective measurement of fabric handle over other methods such as fabric-metal and fabric-artificial finger frictions. The characteristics of fabric-fabric self-friction in the LUFHES friction test were analysed theoretically and experimentally, as well as compared with that of the KES-F fabric-sensor friction/roughness test. It was found that fabric-fabric friction coefficients obtained in LUFHES were greater and in a wider range than those obtained in the KES-F fabric-sensor friction test, and the spectrum of LUFHES fabric-fabric friction profile has advantages in differentiating the main fabric characteristic structures.

In summary, the unique low-stress mechanical properties (shear and buckling) obtained in the LUFHES tests reveal insightful information of mechanical properties of fabric shell during biaxial deformations. The fabric-fabric friction was found to have advantages in discriminating fabric friction coefficient and fabric surface structures. Thus, the LUFHES has the potential to be used to sensitively evaluate fabric handle.

2.3.1.2	Compression buckling deformation	29
2.3.1.3	Shear properties	30
2.3.1.4	Tensile properties	33
2.3.2	Fabric Surface morphologies and properties.....	35
2.3.2.1	Fabric smoothness	35
2.3.2.1.1	Adhesion-shearing theory	36
2.3.2.1.2	Ploughing	37
2.3.2.1.3	Stick-Slip Phenomenon (SSP)	37
2.3.2.1.4	Spectral analysis of dynamic friction coefficients ...	38
2.3.2.2	Surface roughness.....	39
2.3.2.2.1	Fabric roughness	40
2.3.2.3	Relationship between fabric friction and geometrical roughness	41
2.3.2.4	Evaluation of fabric surface properties	41
2.4	Problems identified, objectives and proposed solutions	43
2.4.1	Problems	43
2.4.2	Objectives.....	44
2.4.3	Proposed solutions.....	44
Chapter 3 Methods for the characterisation of fabric mechanical properties and Experimental plan		46
3.1	Fabric materials used in the experiments	47
3.2	Equipment and methods for the characterisation of fabrics.....	50
3.2.1	Fabric Assurance by Simple Testing (FAST) (De Boos and Tester, 1994)	50
3.2.1.1	Shear modulus obtained in bias extension testing in the FAST-3 tester	50
3.2.1.2	Bending length and bending rigidity measured in the FAST- 2 tester.....	51
3.2.2	Kawabata Evaluation System for Fabric (KES-F).....	51
3.2.2.1	Shear modulus obtained in the KES-F1	51
3.2.2.2	Bending rigidity obtained in the KES-F2	52
3.2.2.3	Fabric surface friction coefficient and fabric roughness obtained in KES-F4.....	52
3.2.3	Universal tensile tester (Titan).....	52
3.2.4	Leeds University Fabric Handle Evaluation System (LUFHES).....	52
3.2.4.1	Shear modulus obtained in cyclic twisting test	53
3.2.4.2	Energies and compression buckling Young's modulus obtained in cyclic axial compression buckling test.....	53

3.2.4.3	Extension and friction test in LUFHES.....	53
3.3	Experimental design	54
Chapter 4 The influence of pre-tensions on energy consumption during cyclic axial compression processes.....		57
4.1	Materials and experiments.....	57
4.1.1	Fabric materials used in the experiments.....	57
4.1.2	Axial compression buckling deformation experiment	58
4.1.2.1	Levels of pre-tension forces applied on fabric shells	58
4.1.2.2	Approaches to study the effect of pre-tension forces on axial compression buckling of fabric shells	58
4.2	The influences of pre-tension forces on the energy consumed to deform undeformed fabric shells (A1cp1).....	62
4.2.1	Energy consumed to deform undeformed fabric shells (A1cp1).....	63
4.2.2	Compression buckling Young's modulus before undeformed fabric shell buckles (E1)	65
4.2.3	Relationship between modulus E1 and energy A1cp1	68
4.3	The influences of pre-tensions on energy consumed to deform recovered fabric shells (A1)	75
4.3.1	Energy consumed to deform recovered fabric shells (A1).....	75
4.3.2	Compression buckling Young's modulus before recovered fabric shell buckles (E2)	78
4.3.3	Relationship between modulus E2 and energy A1	81
4.4	The influences of pre-tensions on the energy consumed to self-recover deformed fabric shells (A2).....	84
4.5	The influences of pre-tensions on the energy consumed to forming permanent deformations in fabric shells (A3)	88
4.5.1	Energy consumed to form permanent deformations (A3).....	89
4.5.2	Compression buckling Young's modulus during forming permanent deformations (E4).....	91
4.5.3	Relationship between energy A3 and modulus E4.....	93
4.6	The influences of pre-tensions on the energy consumed to recover recoverable deformation of fabric shells (A4)	96
4.6.1	Energy consumed to recover the recoverable deformation (A4)	97
4.6.2	Compression buckling Young's modulus during recovering recoverable deformations of deformed fabric shells (E5).....	99
4.6.3	Relationship between energy A4 and modulus E5.....	100
4.7	Determination of suitable pre-tension of fabric shell buckling tests in the LUFHES.....	104

4.8	Summary	111
Chapter 5 Differences between shear modulus and shear rigidity obtained in unidirectional and biaxial deformation..... 113		
5.1	Fabric materials used in the research.....	113
5.2	Analysis of fabric shear modulus obtained in the three systems: FAST, KES-F and LUFHES	113
5.2.1	FAST testing system	113
5.2.1.1	Modelling the change of shear angles in the FAST bias extension test.....	114
5.2.1.2	Shear modulus obtained in the FAST bias extension test.....	116
5.2.2	KES-F testing system	117
5.2.3	LUFHES system	119
5.3	Differences of shear modulus obtained in the LUFHES, FAST and KES-F systems	125
5.3.1	Shear modulus obtained in the LUFHES and KES-F systems.....	128
5.3.1.1	G_{KESF} and G_{LUFHES} for woven fabrics	128
5.3.1.2	G_{KESF} and G_{LUFHES} for knitted fabrics	130
5.3.1.3	G_{KESF} and G_{LUFHES} for nonwoven fabrics.....	134
5.3.2	Shear modulus obtained in the KES-F, LUFHES and FAST systems	137
5.4	Differences of shear rigidity (SR) obtained in the LUFHES, FAST and KES-F shear tests.....	143
5.4.1	Differences of shear rigidity obtained in the LUFHES and the KES-F systems.....	146
5.4.1.1	Differences between shear rigidity obtained in the KES-F and LUFHES of woven fabrics.....	147
5.4.1.2	Differences between shear rigidity obtained in the KES-F and the LUFHES of knitted fabrics	147
5.4.1.3	Differences between shear rigidity obtained in the KES-F and the LUFHES of nonwoven fabrics.....	148
5.4.2	Differences of shear rigidities obtained in the FAST, LUFHES and KES-F tests	149
5.5	Summary	153
Chapter 6 Compression buckling force of fabric shells measured in the LUFHES and bending rigidities measured in the KES-F and the FAST systems..... 155		
6.1	Measurements of fabric compression buckling force and bending rigidity	155
6.1.1	Compression buckling force measured in the LUFHES	155
6.1.2	Bending rigidity obtained in the FAST system.....	157

6.1.3	Bending rigidity obtained in the KES-F system	158
6.2	Compression buckling force and bending rigidities	159
6.2.1	Differences of bending rigidities obtained in the KES-F and FAST systems	161
6.2.2	Correlation between compression buckling force and bending rigidity	166
6.3	Summary	169
Chapter 7 Fabric friction properties in relation to fabric structure and roughness.....		170
7.1	Analysis of fabric-fabric friction profile in the LUFHES	170
7.1.1	Theoretical analysis of fabric-fabric friction of a ripstop fabric.....	171
7.1.1.1	The fabric structure of a ripstop fabric	171
7.1.1.2	Models of the fabric surface of ripstop fabrics	173
7.1.1.3	Friction force between unit structures of ripstop fabric	176
7.1.1.3.1	Friction force when top fabric moves against bottom fabric of identical structure	177
7.1.1.3.2	Friction force when top fabric moves against bottom fabric of mirroring structure	177
7.1.2	Theoretical spectrum profile of friction coefficient	178
7.1.2.1	Theoretical friction coefficient profiles when top fabric moves against bottom fabric of identical structure.....	179
7.1.2.2	Theoretical friction coefficient profiles when top fabric moves against bottom fabric of mirroring structure.....	180
7.1.3	Fabric friction profile of the ripstop fabric in the LUFHES test.....	182
7.2	Analysis of fabric roughness profile in the KES-F system	184
7.2.1	Theoretical analysis of metal sensor-fabric friction in the KES-F system	184
7.2.1.1	Model of fabric friction when metal sensor moves against ripstop strip	185
7.2.1.2	Friction force produced by the KES-F roughness sensor and fabric surface	185
7.2.1.3	Friction coefficient profiles and spectrum of the ripstop fabric	186
7.2.2	Spectrum of the sensor-fabric roughness profile in the KES-F test.....	188
7.2.3	Spectrum of the sensor-fabric friction profile in the KES-F test	190
7.3	Comparison of the three spectra of the LUFHES fabric-fabric friction, the KES-F sensor- fabric friction and the KES-F sensor-fabric roughness profiles	193

7.4	The characteristic wavelengths in relation to fabric surface structural parameters.....	194
7.4.1	Ripstop fabric (W1).....	195
7.4.1.1	Fabric structure.....	195
7.4.1.2	Fabric surface spectrum of ripstop fabric in warp direction	195
7.4.2	Plain fabric (W4).....	198
7.4.2.1	Fabric structure.....	198
7.4.2.2	Fabric surface spectrum of the plain woven fabric (W4) in the warp direction	198
7.4.2.3	Fabric surface spectrum of the plain woven fabric (W4) in weft direction.....	200
7.4.3	Satin fabric (W7).....	203
7.4.3.1	Fabric structure.....	203
7.4.3.2	Fabric surface spectrum of the satin fabric (W7) in warp direction	203
7.4.3.3	Fabric surface spectrum of the satin fabric (W7) in weft direction	205
7.4.4	Twill fabric (W12).....	208
7.4.4.1	Fabric structure.....	208
7.4.4.2	Fabric surface spectrum of the twill fabric (W12) in warp direction	208
7.4.4.3	Fabric surface spectrum of the twill fabric (W12) in weft direction	211
7.4.5	Nonwoven (N1).....	213
7.4.5.1	Fabric structure.....	213
7.4.5.2	Fabric surface spectrum of the nonwoven fabric (N1) in machine direction.....	213
7.4.5.3	Fabric surface spectrum of the nonwoven fabric (N1) in cross direction.....	215
7.4.6	Fabric friction coefficients measured in the KES-F system and the LUFHES	217
7.4.7	Summary	219
7.5	Summary	220
	Chapter 8 Conclusions and future work	221
8.1	Conclusions	221
8.2	Future work.....	224
	List of References	226
	Appendix A Fabric material.....	A-1

Appendix B	Theoretical analysis of fabric friction profile between fabric and fabric surfaces of a ripstop fabric.....	B-1
Appendix C	Theoretical analysis of sensor-fabric friction profile of ripstop fabric in KES-F roughness test.....	C-1
Appendix D	Rectification of the fabric dynamic friction coefficient curves in LUFHES test	D-1

List of Figures

Figure 2.1 Skin (Purves et al., 2001).....	4
Figure 2.2 Discharge frequencies of a cold receptor, a warmth receptor and cold and hot pain nerve fibres a different temperatures (Guyton and Hall, 2000).....	5
Figure 2.3 The protocol of fabric hand evaluation used in the KES-F system (Kawabata, 1982).....	8
Figure 2.4 Measuring principles of the KES-F system (Hu, 2000)	9
Figure 2.5 Measuring principle of the FAST system (Hu, 2000)	13
Figure 2.6 Typical fabric extraction curve(Pan and Yen, 1992)	17
Figure 2.7 Feature parameters on the curve (Pan and Yen, 1992).....	18
Figure 2.8 The LUFHES system: (a) System with sample. (b) Sample holder	20
Figure 2.9 (a): Fabric deformation in the LUFHES twist buckling test. (b): A typical torque-angular displacement curve of the cyclic axial twist buckling-recovery process in the LUFHES	22
Figure 2.10 (a): Fabric deformation in the LUFHES compression buckling test. (b): A typical force-displacement curve of the cyclic axial compression buckling-recovery process	23
Figure 2.12 A typical force-displacement curve of extension-friction process	26
Figure 2.13 Bending of yarns with large friction between fibres (Behera and Hari, 2010)	28
Figure 2.14 Shearing curves for different materials (Lindberg et al., 1961) .	31
Figure 2.15 Model of a loop in weft knitted fabric.....	34
Figure 2.16 Models of stick-slip phenomenon in friction test. (a) Apparatus to measure friction between a plane surface and a rider. (b) Dynamic profile of friction forces	38
Figure 2.17 Mechanism of FFT analysis. (a) 3D graph of sine waves. (b) Time-domain view. (c) Frequency-domain view. (Craig, 2016).....	39
Figure 2.18 Roughness profile (Olympus, 2016).....	40
Figure 4.1 Influence of pre-tensions on the energy A1cp1 of woven fabric W11 in the warp direction	59
Figure 4.2 Influence of pre-tensions on the energy A1cp1 of knitted fabric K2 in the wale direction	60
Figure 4.3 Influence of the pre-tensions on energy A1cp1 of nonwoven fabric N8 in the MD	60
Figure 4.4 Data which does not follow the main trend appears in testing using five specimens in five tests	61
Figure 4.5 Force-displacement curve of the compression buckling deformation	62

Figure 4.6 The influences of pre-tensions on overall energy (A1cp1) consumed to produce deformations in fabric shells.....	64
Figure 4.7 The influences of pre-tensions on compression Young's modulus (E1) before buckling occurs in the first compression cycle	67
Figure 4.8 Relationship between pre-tensions and E1 of flash spun and thermally point bonded Tyvek nonwoven fabric, N7	68
Figure 4.9 Simplified ideal model of relationship between E1 and A1cp1....	70
Figure 4.10 Relationship between energy A1cp1 and modulus E1 for woven, knitted and nonwoven fabrics.....	72
Figure 4.11 Energy A1 and modulus E2 obtained in the 2 nd -5 th cycles compression buckling deformations	75
Figure 4.12 The influences of pre-tension on the energy consumed to deform recovered fabric shells (A1)	77
Figure 4.13 The influences of pre-tensions on modulus E2	80
Figure 4.14 Relationship between the modulus E2 and the energy A1 for woven, knitted and nonwoven fabrics	83
Figure 4.15 Energy A2 consumed to self-recover compression buckling deformations of fabric shell	85
Figure 4.16 The influences of pre-tensions on the energy consumed to self-recovery of deformed fabric shells	87
Figure 4.17 Energy A3 and modulus E4 obtained in the 2 nd -5 th cycle compression buckling deformation.....	89
Figure 4.18 The influences of pre-tension on the energy consumed in forming permanent deformations in fabric shells (A3).....	91
Figure 4.19 The influences of pre-tension on the modulus E4 of fabric shells in forming permanent deformations	92
Figure 4.20 Relationship between modulus E4 and energy A3 in fabric shell buckling-recovery deformation	94
Figure 4.21 The energy A4 in the cyclic compression buckling-recovery process of fabric shells.....	96
Figure 4.22 The influences of pre-tension on the energy A4 of woven, knitted and nonwoven fabrics	98
Figure 4.23 The influences of pre-tension on the modulus E5 during recovering recoverable deformations.....	100
Figure 4.24 Relationships between energy E5 and modulus A4.....	103
Figure 4.25 Changing rates of energy per unit pre-tension for woven, knitted and nonwoven fabrics with the increase of pre-tension	108
Figure 4.26 Changing rates per unit pre-tension of modulus for woven, knitted and nonwoven fabrics with the increase of pre-tension	110
Figure 5.1 Fabric shear deformation in the FAST bias extension test	114
Figure 5.2 Typical shear curve obtained in the KES-F system	117

Figure 5.3 Force analysis of fabric in the KES-F shear test 118

Figure 5.4 A typical torque (Nm)-twisting angle (degree) curve obtained in the LUFHES shear test 119

Figure 5.5 Force analysis of a fabric shell in the LUFHES shear test 120

Figure 5.6 Relation between shear stress (τ) and shear strain (γ) of a plain woven cotton fabric (W5) 122

Figure 5.7 Shear modulus of a plain woven cotton fabric in weft direction obtained in the LUFHES twisting test..... 122

Figure 5.8 Shear stress-shear strain relationship and shear modulus of long filament satin fabric (W7-weft)..... 123

Figure 5.9 Shear stress-shear strain relationship and shear modulus of Polypropylene spunbond nonwoven fabric (N11-CD) 123

Figure 5.10 Shear stress-shear strain relationship and shear modulus of single jersey cotton knitted fabric (K6-Course)..... 124

Figure 5.11 The relationship between G_{KESF} and G_{LUFHES} in the first cycle of shear test for seven knitted fabrics 130

Figure 5.12 Relationship between G_{KESF} and G_{FAST} of woven fabrics in warp direction..... 139

Figure 5.13 Relationship between arithmetical mean of $G_{LUFHES-Average}$ and G_{FAST} of woven fabrics..... 142

Figure 5.14 Relationship between arithmetical mean of $G_{LUFHES-Average}$ and G_{FAST} of knitted fabrics 143

Figure 5.15 Relationship between SR_{KESF} and SR_{LUFHES} (knitted fabrics without K3)..... 148

Figure 5.16 Relationship between SR_{KESF} and SR_{FAST} of woven fabrics ... 150

Figure 5.17 Relationship between SR_{FAST} and SR_{LUFHES} (1st cycle) for knitted fabrics without K3..... 150

Figure 6.1 Compression buckling curves of woven fabric W1 and knitted fabric K1..... 156

Figure 6.2 Determining compression buckling force in the LUFHES software 157

Figure 6.3 Fabric bending length obtained in the FAST cantilever bending test 158

Figure 6.4 Fabric pure bending curve in the KES-F system..... 159

Figure 6.5 Correlation between bending rigidities obtained in both the FAST and the KES-F systems for seven knitted fabrics 162

Figure 6.6 Correlation between bending rigidities obtained in the FAST and the KES-F systems for four nonwoven fabrics 162

Figure 6.7 Bending curve of K3-wale and K7-wale obtained in the KES-F bending test..... 163

Figure 6.8 Bending curve of K3-course and K7-course obtained in the KES-F bending test.....	163
Figure 6.9 Bending curve of N10-MD and N1-MD obtained in the KES-F bending length test.....	164
Figure 6.10 Relationship between critical compression buckling force and bending rigidity obtained in the KES-F systems (knitted fabrics)	167
Figure 6.11 Relationship between critical buckling force and bending rigidity measured in the FAST system (nonwoven fabrics)	167
Figure 7.1 The extension forces and dynamic friction force profile against relative displacement of the ripstop fabric in weft direction in the LUFHES	171
Figure 7.2 Ripstop fabric surface and cross-section structure	172
Figure 7.3 Symbols used to represent warp and weft yarn surface	173
Figure 7.4 Symbol of a weft yarn in R area	173
Figure 7.5 Symbol of a weft yarn in F area	174
Figure 7.6 Three weft yarns in ripstop strip R	174
Figure 7.7 Contact length of weft-weft and warp-weft yarn cross points when top fabric contact bottom fabric.	175
Figure 7.8 Two movements in fabric to fabric friction. (a) Top fabric moving against bottom fabric of identical structure. (b) Top fabric moving against bottom fabric of mirroring structure.	176
Figure 7.9 Theoretical friction coefficient profile when top fabric moves against identical fabric structures of bottom fabric.....	179
Figure 7.11 Theoretical friction coefficient profile when top fabric moves against bottom fabric of mirroring structure.	181
Figure 7.12 Spectrum of theoretical fabric-fabric friction coefficient when top fabric moves against bottom fabric of mirroring structure	182
Figure 7.13 Three spectra of the fabric-fabric friction profiles in LUFHES repeat tests.....	183
Figure 7.14 Spectrum of fabric-fabric friction profile of the ripstop fabric in the LUFHES system.....	183
Figure 7.15 Model of the KES-F roughness sensor moves against ripstop fabric	185
Figure 7.16 Theoretical friction coefficient profile of the ripstop fabric during the KES-F roughness test using a metal sensor	187
Figure 7.17 Theoretical spectrum of the metal sensor-fabric friction profile of the ripstop fabric during the KES-F roughness test	187
Figure 7.18 Vertical displacement profile of the sensor obtained in the KES-F roughness test of the ripstop fabric shown in Figure 7.2.....	189
Figure 7.19 Spectra of roughness profiles of the ripstop fabric in the KES-F roughness test.....	189

Figure 7.20 Average of the two spectra of the KES-F roughness tests shown in Figure 7.19	190
Figure 7.21 Friction profile of ripstop fabric in weft direction measured in the KES-F friction test	191
Figure 7.22 Spectra of friction profile of the ripstop fabric in the KES-F friction test	192
Figure 7.23 Average of two spectra of the KES-F friction tests shown in Figure 7.22	192
Figure 7.24 Surface structural parameters of plain woven fabric (W4) in both warp and weft directions	198
Figure 7.25 Structural parameters of Satin fabric (W7) in both warp and weft directions	203
Figure 7.26 Structural parameters of twill woven fabric (W12) in both warp and weft directions	208
Figure 7.27 Structural parameters of nonwoven fabric (N1) in both CD and MD	213
Figure 7.28 Relationship between friction coefficient obtained in the LUFHES and the KES-F friction tests	219

List of Tables

Table 2.1 Four types of mechanoreceptor (Pritchard and Alloway, 1999; Warwick et al., 2009).....	5
Table 2.2(1) Parameters measured by the KES-F system (Hu, 2000).....	10
Table 2.3 An example of constants in the KES-F conversion equations of winter suit fabrics (Kawabata, 1982).....	12
Table 3.1 (1) Specifications of woven fabrics.....	48
Table 3.2 Experiment for studying the effect of pre-tensions on the axial compression buckling of fabric shells.....	54
Table 3.3 Shear modulus measured in different systems (LUFHES, FAST and KES-F)	55
Table 3.4 Comparison of critical buckling force in the LUFHES buckling test and bending rigidity in the KES-F and FAST bending tests	55
Table 3.5 Characteristics and differences of fabric friction coefficients and roughness measured in the LUFHES and the KES-F	56
Table 4.1 Linear regression equations of relationship between pre-tension (N/m) and A1cp1 (mJ).....	65
Table 4.2 Structural changes with applied pre-tension for woven, knitted and nonwoven fabrics.	69
Table 4.4 Extension of fabrics in both direction under 2N/m.....	74
Table 4.5 (1) Linear regression equations of relationship between pre-tension (N/m) and A1 (mJ) of woven fabrics.....	77
Table 4.6 Linear regression equations of relationship between energy A1 and modulus E2	83
Table 4.7 (1) Linear regression equations of relationship between pre-tension (N/m) and A2 (mJ) for woven and knitted fabrics.....	87
Table 4.8 Quadratic regression equations of relationship between A3 and E495	
Table 4.9 (1) Quadratic regression equations between A4 and E5 for woven and knitted fabrics	103
Table 4.10 Three fabric groups based on fabric mass per unit area.....	106
Table 5.1 Fabrics used in the study of shear properties using unidirectional and biaxial testing systems	113
Table 5.3 Fabric shear modulus obtained in the FAST, KES-F and LUFHES systems	127
Table 5.4 Correlation between G_{KESF} and G_{LUFHES} for woven fabrics (Constant shear angle of $\pm 0.5^\circ$ - $\pm 2.5^\circ$ in the KES-F shear test and constant shear angle of 0.5° - 4.0° in the LUFHES shear test).....	128
Table 5.5 Extension force applied in perpendicular direction at the shear angle of 4° in the LUFHES test (elongation of 0.24%) and the elongation of fabric at extension force of 2N/m and 4.9N/m.....	129

Table 5.6 Correlation between G_{KESF} and G_{LUFHES} for knitted fabrics (Constant shear angle of $\pm 0.5^\circ$ - $\pm 2.5^\circ$ in the KES-F shear test and constant shear angle of 0.5° - 4.0° in the LUFHES shear test).....	130
Table 5.7 Correlation between G_{KESF} and G_{LUFHES} for the 6 knitted fabrics without fabric K3.....	131
Table 5.8 Shear modulus of knitted fabrics G_{KESF} and G_{LUFHES} when shear angles are between 0.5° and 2.5°	132
Table 5.9 Correlation between G_{KESF} and G_{LUFHES} for 7 knitted fabrics when fabrics have identical range of shear angles (0.5° - 2.5°).....	132
Table 5.10 Force applied to shear knitted fabrics to 4° in the KES-F and the LUFHES shear test	134
Table 5.11 Correlation between G_{KESF} and G_{LUFHES} for 4 nonwoven fabrics (Constant shear angle of $\pm 0.5^\circ$ - $\pm 2.5^\circ$ in the KES-F shear test and Constant shear angle of 0.5° - 4.0° in the LUFHES shear test).....	135
Table 5.12 G_{KESF} and G_{LUFHES} for 4 nonwoven fabrics obtained when shear angle is between 0.5° and 2.5°	135
Table 5.13 Force applied to shear nonwoven fabrics to 4° in the KES-F and the LUFHES shear tests	136
Table 5.14 Elongation of nonwoven fabric with 2N/m and 4.9N/m.....	137
Table 5.15 R^2 of linear regression equations between G_{FAST} and G_{KESF} as well as R^2 between G_{FAST} and G_{LUFHES}	138
Table 5.17 (1) Average of G_{LUFHES} in two directions obtained in LUFHES (woven fabrics).....	140
Table 5.18 R^2 of the linear regression equations between G_{FAST} and G_{LUFHES} (average of two directions).....	141
Table 5.19 (1) Shear rigidity (SR) obtained in the KES-F, LUFHES and FAST systems of knitted fabrics	144
Table 5.20 Linear relationship between SR_{KESF} and SR_{LUFHES}	146
Table 5.22 Average of shear rigidity at two directions obtained in LUFHES151	
Table 5.23 R^2 of the linear regression equations between SR_{FAST} and SR_{LUFHES} (average of two directions).....	152
Table 6.1 Fabric compression buckling force (P_{cr}) measured in the LUFHES and bending rigidity obtained in both the FAST and the KES-F systems (BR_{KES-F} and BR_{FAST}).....	160
Table 6.2 Correlation coefficients, R^2 , of linear regression equations between bending rigidities obtained in the FAST and the KES-F systems.....	161
Table 6.4 R^2 of linear regression equations between critical compression buckling force (P_{cr}) and bending rigidity obtained in the FAST and the KES-F systems	166
Table 7.1 Fabric structural lengths, A, B, C and D of the ripstop fabric shown in Figure 7.6	178

Table 7.3 Comparison of wavelengths of major peaks and their corresponding amplitude obtained in the spectra of LUFHES friction, the KES-F friction, and the KES-F roughness profiles	193
Table 7.4 Fabric surface spectra of the ripstop fabric (W1) in warp direction	196
Table 7.6 Fabric surface spectra of the plain woven fabric (W4) in warp direction.....	199
Table 7.7 Fabric surface spectra of the plain woven fabric (W4) in weft direction	201
Table 7.9 Fabric surface spectra of the satin fabric (W7) in warp direction	204
Table 7.10 Fabric surface spectra of the satin fabric (W7) in weft direction	206
Table 7.12 Fabric surface spectra of the twill woven fabric (W12) in warp direction.....	209
Table 7.13 Fabric surface spectra of the twill woven fabric (W12) in weft direction.....	211
Table 7.15 Fabric surface spectra of the nonwoven fabric (N1) in machine direction.....	214
Table 7.16 Fabric surface spectra of the nonwoven fabric (N1) in CD.....	216
Table 7.17 Friction coefficients of fabrics obtained in the LUFHES and the KES-F friction tests	218

List of Symbols

Symbols	Descriptions	Unit
Ac	Cross-section area	m ²
c	Bending length	mm
BR	Bending rigidity	Nm
E	Young's modulus	Pa (N/m ²)
F	Force	N
G	Shear modulus	Pa (N/m ²)
k	Bending curvature	cm ⁻¹
L	Sample length	m
ΔL	Displacement	m
M	Bending moment	Nm
M ₀	Frictional restraint couple	Nm
m	Fabric mass per unit area	g/m ²
N	Extension force	N
P _{cr}	Critical buckling force	N
P	Pressure	Pa
R	Radius	m
S	Displacement	m
SR	Shear rigidity	N/m
T	Torque	Nm
t	Thickness	m
W	Width of fabric	m
ρ	Radius of curvature	m
ν	Poisson's ratios	/
σ	Tensile stress	N/m ²
ε	Tensile strain	/
α	Twist angle	degree
θ	Shear angle	radian
μ	Friction coefficient	/
τ	Shear stress	N/m ²
γ	Shear strain	/
A	Length of weft yarn part on surface of ripstop fabric	mm

B	Length of warp yarn part on surface of ripstop fabric	mm
C	The structure difference between two adjacent weft yarns on surface of ripstop fabric	mm
D	The width of weft yarn of ripstop fabric in warp direction	mm
U	The length of metal sensor in KES-F roughness test in moving direction	mm

Chapter 1 Introduction

1.1 Background

Tactile comfort properties of woven, knitted and nonwoven fabrics used in suits and next-to-skin products such as sportswear, innerwear, lingerie, bedding liners, wipes, diaper and other hygiene products are primarily important functionalities for consumers, its evaluations and assessments are of great interests for both retailers and designer (Bertaux et al., 2007).

Tactile comfort of fabric refers to the human perception of the fabrics when it is touched with human skin (Chattopadhyay, 2008; Bishop, 1996). It is one of the main factors affecting consumers' purchasing decisions. Subjective assessment of fabric tactile comfort properties is usually done by using human hand when fabric is deformed by touching, stretching, rubbing and squeezing, etc. Objective assessment of the fabric tactile properties is always desirable, and it is usually evaluated through the measurement of the fabric low-stress mechanical properties such as friction, extension, compression, shear, bending and buckling properties (Behera and Hari, 1994).

Various methods for the objective measurements of fabric mechanical properties are developed for this purpose. The widely-used fabric objective measurement (FOM) systems include the Kawabata Evaluation System of Fabrics (KES-F) system (Kawabata, 1982), Fabric Assurance by Simple Testing (FAST) system (De Boos and Tester, 1994), PhabrOmeter system (Pan, 2006), Wool Comfort-Meter and Wool Handle-Meter (AWTA). However, all of the existing systems (KES-F, FAST, PhabrOmeter, etc.) rely on the relationship between subjective assessment of a limited number of standard fabrics and their individual mechanical properties measured during the processes of either unidirectional fabric deformations (e.g. FAST and KES-F) or uncontrolled complex deformations (e.g. PhabrOmeter and Wool Handle-Meter). Therefore conclusions from these systems have neither been objective nor represent the complex fabric deformations occurring during human hand evaluation (Mao, 2014). In order to avoid using standard fabrics and obtain 100% objective evaluation of fabric handle which is not possible in existing subjective and objective fabric handle assessment methods, the Leeds University Fabric Handle Evaluation System (LUFHES) (Mao and Taylor, 2012) was developed to evaluate fabric tactile properties objectively while mimicking fabric buckling deformation in subjective fabric hand evaluation process. In this system, the fabric mechanical properties

are measured while fabric shells are subjected to cyclic biaxial buckling deformations and the fabric surface properties are evaluated based on fabric-fabric self-friction. The human perception of fabric properties are linked with the fabric deformations, which is quantified by using the energies consumed to create or recover various types of fabric deformations (e.g., self-recovered deformations, recoverable deformations and permanent deformations, etc.). This research is thus intended to improve the understanding of low stress mechanical properties obtained in the LUFHES tests in relation to the objective evaluation of fabric handle. In addition, it is intended to determine how the fabric properties measured in the LUFHES are different from those measured in other popular systems (e.g., FAST and KES-F), and to determine if these testing systems have differences in discriminating various fabrics.

1.2 Structure of the thesis

In this thesis, a critical literature review is conducted regarding human tactile sensing system, how fabric mechanical properties are related to fabric tactile properties and existing subjective and objective testing methods used to evaluate fabric hand and fabric handle to identify gaps in existing research in using fabric buckling properties to evaluate fabric handle.

The suitable pre-tension for compression buckling test in LUFHES is determined by studying the influences of pre-tensions on fabric mechanical properties and energy consumptions. The fabric mechanical properties including shear modulus and critical buckling forces obtained in LUFHES biaxial deformations are analysed and compared with shear modulus and bending rigidity measured in unidirectional deformations in the KES-F and FAST systems to investigate if they are different in discriminating fabrics. Simplified models are established to show the theoretical characteristics of fabric-fabric friction profile obtained in the LUFHES and fabric-sensor roughness profile obtained in the KES-F system. The characteristics of fabric-fabric friction profiles and fabric-sensor roughness/friction profiles of some typical fabrics are analysed to investigate how they are affected by fabric surface structures. In addition, the differences between fabric-fabric friction and fabric-sensor friction are analysed.

Chapter 2 Literature Review

In this chapter, the human perception of fabric tactile properties, how fabric mechanical properties are related to the fabric tactile perceptions, and the existing subjective fabric hand and objective fabric handle evaluation methods are critically reviewed, and the knowledge gaps in using fabric buckling properties to evaluate fabric handle in the LUFHES method will be identified.

The concepts of 'fabric hand' or 'fabric handle' are commonly used interchangeably to refer to the fabric tactile properties (Bensaid et al., 2006). In this thesis, the terminology of fabric hand and fabric handle have different meanings (Mao and Taylor 2012). Fabric hand relates to the subjective perception of fabric tactile comfort made by individuals when fabrics are deformed and sensed by human hand, while fabric handle is related to the objective measurement of fabric mechanical properties in relation to tactile comfort (Mao and Taylor, 2012).

2.1 Fabric hand and subjective assessment of fabric tactile properties

Fabric hand is defined as: 'The total of the sensations expressed when a textile fabric is handled by touching, flexing of the fingers, smoothing and so on (Bishop, 1996). Fabric hand evaluation is a subjective way to evaluate fabric tactile properties by manipulating fabric with human hand and give a prediction of the feeling when it touches body. Fabric hand directly influences customers' perception of the usefulness of the fabric and indirectly affects the retailer's saleability (Behera et al., 2012), it is essential for textile designers, developers, manufacturers, and retailers to predict the customer's acceptance and maintain or improve the quality of existing products.

2.1.1 Human tactile sensation

Fabric hand is a result of human tactile sensation. Human fingers are used to doing the sensitive and discriminating assessment, and the brain is used to integrate and express the results (Ellis and Garnsworthy, 1980). Skin is the main organ of the haptic sensibility. It has two layers: epidermis on the top, and the dermal layer which contains nerves and blood vessels at the bottom as shown in Figure 2.1. Sensory receptors are mainly exist in dermal layer (Schacher et al., 2011).

Mechanoreceptors of Hairy Skin

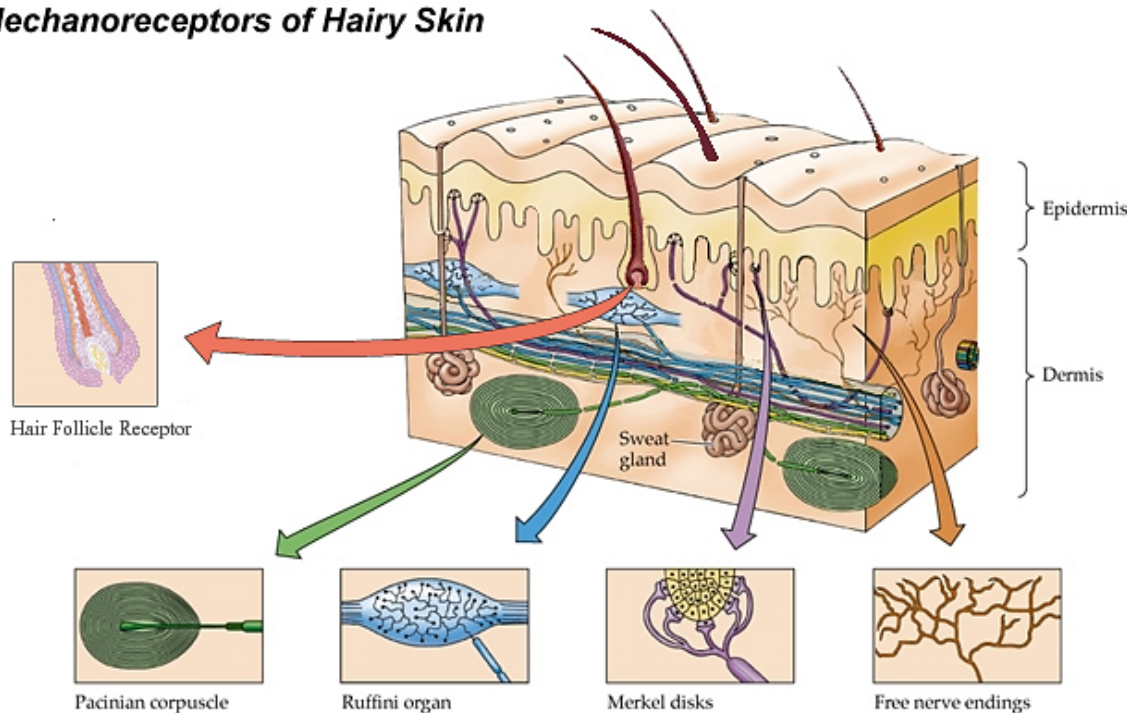


Figure 2.1 Skin (Purves et al., 2001)

Sensory information is collected from the somatic sensors within skin. Somatic sensors are divided into three groups (Behery, 2005):

1. Mechanoreceptors: stimulated by mechanical displacement of various tissues in the body;
2. Thermoreceptors: stimulated by temperature changes;
3. Nociceptors: representing the human pain sense.

Nociceptors respond to noxious stimuli that can produce tissue damage. There are two thermoreceptors: cold receptors and warm receptors, each of them is activated in a specific temperature range which is shown in Figure 2.2 (Costanzo, 2009; Guyton and Hall, 2000). Generally speaking, the number of cold thermoreceptors is about ten times more than that of warmth receptors, and cold receptors are located in shallower depth (0.15-0.17mm) than warmth receptors (0.3-0.6mm) relative to the skin surface. Thus humans are more sensitive to cold than to heat (Arens and Zhang, 2006). It was also found that the thermoreceptor is strongly stimulated when it is subjected to an abrupt change in temperature, however it responds to steady temperature states at lower rate (Arens and Zhang, 2006). Therefore, human will be sensitive to the cold feeling when skin touches a clothing surface which has a low temperature.

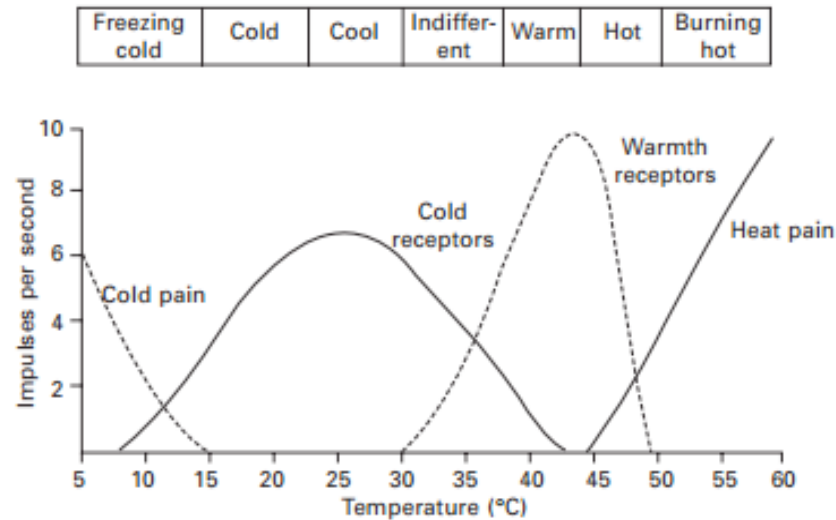


Figure 2.2 Discharge frequencies of a cold receptor, a warmth receptor and cold and hot pain nerve fibres at different temperatures (Guyton and Hall, 2000)

Mechanical sensations are detected by mechanoreceptors including four receptors: Meissner corpuscles, Merkel disks, Pacinian corpuscles and Ruffini endings. It is observed that different mechanoreceptors extract information about different aspects of mechanical deformation of skin (Pimenidis, 2009). The functions of these four mechanoreceptors are shown in Table 2.1.

Table 2.1 Four types of mechanoreceptor (Pritchard and Alloway, 1999; Warwick et al., 2009)

Mechanoreceptor	Function	Responsive to
Pacinian corpuscles	Very sensitive to skin deformations of a few microns, so they could respond to small vibrations transmitted through subcutaneous tissue.	Vibration 100-300 Hz
Meissner corpuscles	Sensitive to low frequency vibrations and important for discriminating texture of objects moves across fingertips.	Vibration 5-40 Hz
Ruffini endings	Respond to external or internal stimulation generated by muscle contraction.	Skin Stretch
Merkel disks	Slowly adapting responses to punctate indentations of the skin and mediate sensations of light pressure required to code local form, edges and other surface features of objects.	Pressure

Subjective sensing is a combination of various receptors responsible for feeling textures, pressure, stretching, temperature, dynamic deformation and vibration (Behery, 2005). When fabric is touched by hand, receptors on the skin select and

translate the stimuli into electric signals which are transported to the nervous centres and being processed into the different information by cerebral regions to generate a response (Schacher et al., 2011). The response to the action of touching fabric is usually psychological. According to the properties of the touched fabric, the feeling could be smooth, soft, thick, warm, or stiff, and this is people's perception of fabric hand (Schacher et al., 2011).

As shown in Table 2.1, Pacinian corpuscles and Meissner corpuscles are responsible for feeling vibrations, thus the vibrations produced by the relative movement between fabric surface and fingertips could be detected and affects human perception. Therefore evaluating the fabric surface properties (e.g. fabric roughness, fabric smoothness) is important to predict fabric tactile properties.

In addition, Ruffini endings and Merkel disks are responsible for feeling skin stretch and pressure. Fingertips are also deformed when the fabric is manipulated (e.g. stretched, bent, buckled, twisted) by human hand. The skin deformation and pressure are related to the force or energy required to deform the fabric, therefore evaluating the fabric mechanical properties plays important role in predicting fabric tactile properties.

2.1.2 Subjective Evaluation of Fabric Hand

The studies on subjective assessment of tactile properties of fabric were firstly studied by Binns in 1926 (Sular and Okur, 2008). Subjective evaluation of fabric hand is affected by several factors, including the assessors (e.g. the gender, age, culture background and personal preference) and testing conditions (e.g., quantification methods, and analysis methods), etc. It is highly based on people's subjective opinions and preferences. The same fabric, when evaluated subjectively by different people with different backgrounds, may mean different things to them and in extreme cases, even the opposite (Pan.N. et al., 1988). Peirce noted that 'the judgement of fabric hand depends on time and place, on seasons, fashions, and personal and racial predilections. In order to overcome the limitations of subjective assessment, efforts were made to develop instruments which could provide objective measurements of fabric tactile properties (Peirce, 1930). The key elements in the subjective evaluation are summarized as below (Bishop, 1996; Kawabata, 1982):

- 1) Judges: trained experts or normal customers without specific background;
- 2) Criteria of judgement: the choice of descriptors for fabric attributes;
- 3) Assessment technique: free or specified fabric-manipulation technique assessment of given attributes;
- 4) Method of the assessment: scale or rank order;

5) Analysis of results.

Choosing and using appropriate descriptors was crucial for the subjective assessment of fabric hand (Wauer, 1965), the difference between vocabularies of experts and untrained judges or consumers was significant enough to interfere with communication between experts and consumers (Brand, 1964). 'Bipolar descriptors' for the subjective evaluation of fabric hand are usually used in the fabric hand evaluation, examples of seven bipolar pairs of descriptors identified to have good correlations including coarse-fine, stiff-pliable, rough-smooth, harsh-soft, cool-warm, hard-soft, and rustling-quiet (David et al., 1985). However, it was found (Bishop, 1996) that the use of bipolar descriptors might only represent positive and negative fabric attributes in judges' mind, and thus further reduced the objectivity of subjective evaluations.

Fabric hand could be evaluated in pairs of fabric (Howorth and Oliver, 1958; Howorth, 1964), in which judges were asked to state reasons for accepting or rejecting a fabric from a pair. All descriptive terms used in the judgement were recorded and the frequency of their occurrence were calculated, and a set of seven descriptors frequently used in fabric evaluations were identified, they were smoothness, softness, coarseness, thickness, weight, warmth and stiffness. Among these descriptors, smoothness and stiffness are found to be of primary importance and would be applied to any type of fabric (Howorth, 1964).

2.2 Fabric objective measurement (FOM) of fabric handle

Fabric handle refers to the objective evaluation of fabric tactile properties through fabric objective measurement (FOM) and quantitatively evaluate fabric tactile properties. The quantitative fabric handle results could overcome the problem of descriptive language associated with definition of fabric handle descriptors and establish an objective basis for communication between researchers and industries (Bishop, 1996). Fabric handle measurement could provide quick and reliable results to respond quickly to the changing needs of customers. Their repeatable results also benefit the control of quality or innovation of new products.

Peirce pioneered to evaluate fabric handle according to the physical measurement of the fabric properties (Peirce, 1930). Since then, several systems including the KES-F and FAST systems, PhabrOmeter system, Wool Handle-Meter, FTT system and LUFHES systems were developed for the similar purpose.

2.2.1 Conventional testing system (the KES-F and FAST systems)

2.2.1.1 Kawabata Evaluation System for fabric (KES-F)

The KES-F system was designed in 1970s to study the fabric mechanical properties under low stress or deformation conditions which are similar to what happen when the fabrics are handled or when they are worn or shaped (Hu, 2000; Minazio, 1995). The KES-F system was developed to assess the correlation between physical characteristics and subjective sensations. The KES-F system is accepted as a commercially viable method, so many researchers used it to evaluate fabric surface properties (Lord et al., 1988) or show the capability of their presented devices by comparing their results with the KES-F results (Bertaux et al., 2007).

In subjective assessment, the method each expert used for evaluating the fabric hand was analysed by Kawabata, and similar method was used in the KES-F system to evaluate fabric handle properties (Kawabata, 1982). The method was summarized as below.

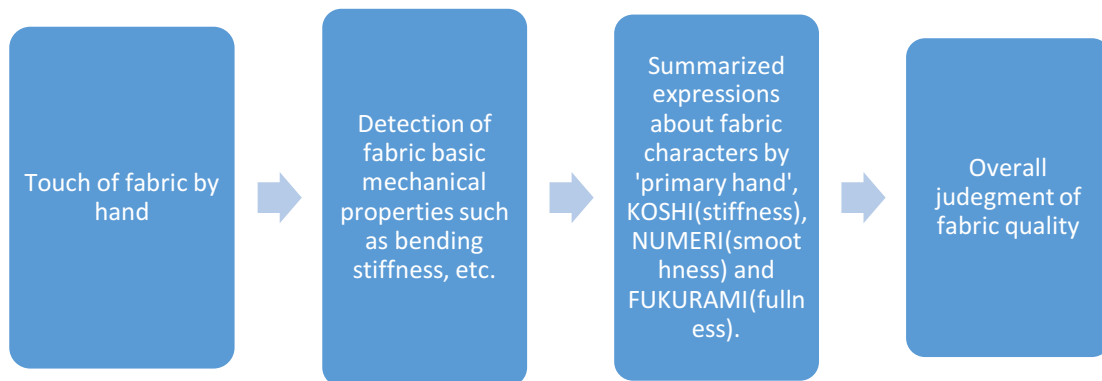


Figure 2.3 The protocol of fabric hand evaluation used in the KES-F system (Kawabata, 1982)

2.2.1.1.1 Measuring of fabric mechanical properties and thermal properties

Kawabata chose 7 fabric mechanical properties which he found important in evaluating fabric hand. They were tensile, shear, bending, compression, surface properties, weight and thickness (Kawabata, 1982). Four testers were designed to measure the fabric mechanical properties; the measuring principles are shown in Figure 2.4. Besides fabric mechanical properties, the sensation of coldness or warmth when skin touches a fabric is also an important factor affecting fabric comfort. Thus the peak heat flux, thermal conductivity and heat retention properties are also measured by using KES-F7 (Thermo-Labo) (KatoTech, 2016).

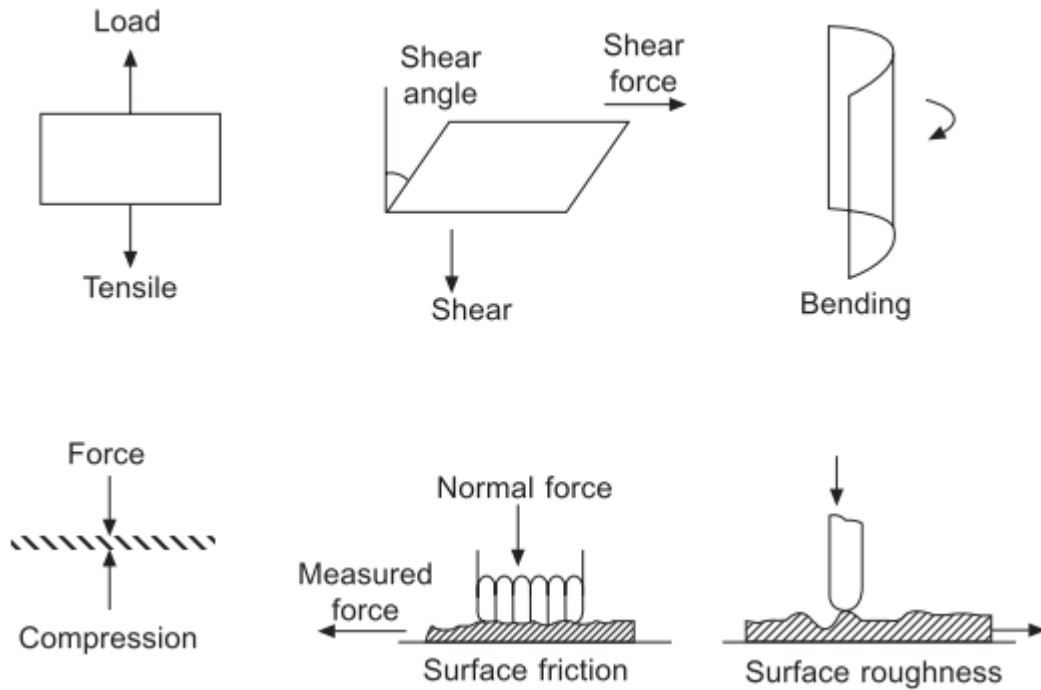


Figure 2.4 Measuring principles of the KES-F system (Hu, 2000)

(1) Tensile and shear tester (Hu, 2000; Kawabata, 1982)

With this tester, both tensile and shear properties are evaluated. A sample with 5cm x 20cm size are tested. Tensile properties are obtained by applying an extension force to the sample held by two chucks. The force is released when it reaches maximum 490N/m, and the sample is allowed to recover to the origin position. To obtain the shear properties, the sample is subjected to a constant force to reach pre-set shear deformation of $\pm 8^\circ$ shear angle. During the shear test, a constant vertical force is applied on fabric to delay the onset of fabric buckling (Wang et al., 2008);

(2) Pure bending tester (Hu, 2000; Kawabata, 1982)

Sample is held by two chucks, one is fixed and the other chuck is movable to apply pure bending force to the sample. During the test, the sample is bent with a constant curvature rate. The bending moment and bending curvature are recorded and their relationship is studied to obtain the sample bending properties;

(3) Compression tester (Hu, 2000; Kawabata, 1982)

In the compression test, a standard area of fabric is subjected to a compression force applied by a movable plunger. The plunger moves downwards with a constant rate of 0.02mm/s until the compressive force reaches 50 gf/cm². It then moves upwards to allow the fabric to recover. The relationship between compressional stress and strain is studied to obtain the compressive properties of sample;

(4) Surface tester (Hu, 2000; Kawabata, 1982)

In the surface test, fabric is placed horizontally, and two contactors are contacted with the fabric with constant normal forces. The fabric friction coefficient and the mean deviation of the friction coefficient are detected by friction contactor. The geometrical surface roughness is detected by the roughness contactor.

(5) Thermal properties tester (KatoTech, 2016)

The thermal conductivity was measured based on the ease at which heat is transmitted from a heat plate with a constant temperature (30°C) through a sample to a heat plate with a constant temperature (20°C). In the measurement of heat retention properties, the sample was set on a heat plate with a constant temperature (room temperature + 10°C) and was left in contact with the air. A constant wind was then applied continuously to the sample surface. The amount of heat lost through the sample was then measured to calculate the heat retention rate (%).

16 mechanical parameters are measured by the four separated apparatus shown in Figure 2.4.

Table 2.2(1) Parameters measured by the KES-F system (Hu, 2000)

Fabric property	Parameter measured	Unit
Tensile	Extensibility, the strain at 490N/m	%
	Linearity of tensile load-extension curve	
	Tensile energy per unit area	gf·cm/cm ²
	Tensile resilience, the ability of recovering from tensile deformation	%
Shear	Shear rigidity, the average slope of the linear regions of the shear hysteresis curve to ±2.5° shear angle	gf/cm·degree
	Hysteresis of shear force at ±0.5° shear angle	gf/cm
	Hysteresis of shear force at ±5° shear angle	gf/cm
Bending	Bending rigidity, the average slope of the linear regions of the bending hysteresis curve to ±1.5cm ⁻¹ curvature	gf·cm
	Bending hysteresis, the average width of the bending hysteresis loop at ±0.5cm ⁻¹ curvature	gf·cm/cm

Table 2.2(2) Parameters measured by the KES-F system (Hu, 2000)

Compression	Linearity of compression-thickness curve	
	Compressional energy per unit area	gf·cm/cm ²
	Compressional resilience, the ability of recovering from compressional deformation	%
Surface properties	Coefficient of friction	
	Mean deviation of coefficient of friction	
	Geometrical roughness	mm
Fabric construction	Fabric weight per unit area	mg/cm ²
	Fabric thickness	mm

2.2.1.1.2 Link objective mechanical properties with subjective assessment results

According to the measurement of fabric basic mechanical properties, eight essential expressions of primary hand were generated and selected: KOSHI (stiffness), NUMERI (Smoothness), FUKURAMI (fullness and softness), SHARI (crispness), HARI (anti-drape stiffness), SHINAYAKASA (flexibility), KISHIMI (scrooping feeling), and SOFUTOSA (soft touch) (Kawabata, 1982).

The primary hand value of a group of fabrics, such as 214 samples for men’s winter suiting, was rated from 0-10 by the Japanese experts and then linked with mechanical data by using a series of regression conversion equations shown below (Kawabata, 1982):

$$Y = C_0 + \sum_{i=1}^{16} C_i x_i \dots\dots\dots (2.1)$$

Where Y is hand value which is evaluated by experts by hand; C_0 and C_i are constants; variables x_i are mechanical properties normalised by mean and standard deviation value:

$$x_i = \frac{X_i - \bar{X}_i}{\sigma_i} \dots\dots\dots (2.2)$$

Where X_i is the value of i^{th} mechanical property or its logarithm; \bar{X}_i is mean of X_i ; σ_i is standard deviation of X_i .

The total hand value is graded from 0(not useful) to 5(excellent) by the experts, and related to the primary hand value and the total hand value.

$$THV = C_0 + \sum_{i=1}^3 Z_i \dots\dots\dots (2.3)$$

$$Z_i = C_{i1}(Y_i - M_{i1})/\sigma_{i1} + C_{i2}(Y_i^2 - M_{i2})/\sigma_{i2} \dots\dots\dots (2.4)$$

Where Y_i is the i^{th} primary hand value. Different products use different primary hand values. C , M , σ are constants. An example of winter suit fabric is shown in Table 2.3.

Table 2.3 An example of constants in the KES-F conversion equations of winter suit fabrics (Kawabata, 1982)

i	Y_i	C_{i1}	C_{i2}	M_{i1}	M_{i2}	σ_{i1}	σ_{i2}
1	KOSHI	0.6750	-0.5341	5.7093	33.9032	1.1434	12.1127
2	NUMERI	-0.1887	0.8041	4.7537	25.0295	1.5594	15.5621
3	FUKURAMI	0.9312	-0.7703	4.9798	26.9720	1.4741	15.2341

2.2.1.2 Fabric Assurance by Simple Testing (FAST)

The FAST system was developed by CSIRO to provide the industry with a relatively simple and robust system to predict the properties of wool and wool blended fabric that their tailoring performance and appearance of tailored garments in wear, and it is frequently used as an alternative to the KES-F system (Hu, 2000; Tokmak et al., 2010). The FAST system contains three instruments and one testing method (De Boos and Tester, 1994). 14 parameters are measured or calculated. The measuring principles of the FAST system are shown in Figure 2.5.

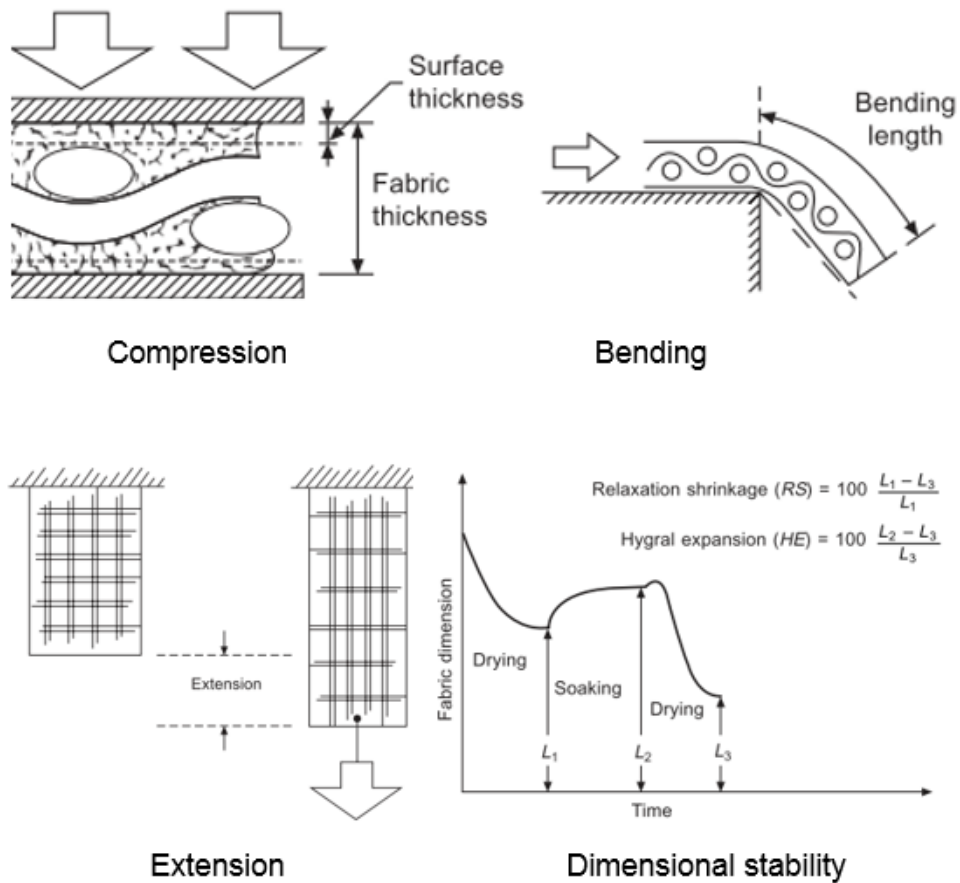


Figure 2.5 Measuring principle of the FAST system (Hu, 2000)

(1) Compression meter (Hu, 2000; De Boos and Tester, 1994)

This tester enables the measurement of both fabric thickness and surface thickness with two pre-set weights, 2 gf/cm² and 100 gf/cm². The surface thickness is defined as the difference between thicknesses under these two loads, it could be a measure of fabric compressibility. Higher surface thickness suggests higher fabric compressibility;

(2) Bending meter (Hu, 2000; De Boos and Tester, 1994)

This instrument is used to measure bending length. It is designed based on the cantilever bending principle. From this measurement, the bending rigidity of fabric could be calculated by:

$$\text{Bending rigidity} = \text{Weight} \times (\text{Bending length})^3 \times 9.807 \times 10^{-6} \dots (2.5)$$

(3) Extension meter (Hu, 2000; De Boos and Tester, 1994)

The instrument is designed based on simple lever principle. The elongation of fabric is measured at three different loads (4.9N/m, 19.8N/m and 98N/m) by removing weights from counterbalancing beam.

It is normal to measure the fabric elongation in warp, weft and bias directions. All three loads are applied on samples in warp and weft direction, but only 4.9N/m is applied on bias samples. Three fabric properties are calculated with these measurements:

$$\text{Formability} = \text{Bending Rigidity} \times \frac{\text{Extension (19N/m)} - \text{Extension (4.9N/m)}}{14.7} \dots\dots\dots (2.6)$$

$$\text{Shear rigidity} = \frac{123}{\text{Bias extensibility(4.9N/m)}} \dots\dots\dots (2.7)$$

$$\text{Extensibility} = \text{extension (98N/m)} \dots\dots\dots (2.8)$$

(4) Dimensional stability test (Hu, 2000; De Boos and Tester, 1994)

The dimensional stability test in the FAST system aims to measure the hygral expansion and relaxation shrinkage of fabric. It involves the measurements of fabric dimensional changes before and after a wet relaxation process.

2.2.1.3 Comparison between the KES-F and FAST systems

Both the KES-F and FAST systems are designed to measure the fabric mechanical properties in low-stress but rely on different testing principles. For example, pure bending is measured in the KES-F bending tester, the bending length is measured in the FAST bending tester based on a cantilever mechanism. Shear modulus of a fabric plate is measured in the KES-F system, while bias extension of fabric strips measured in the FAST-3 tester is used to estimate fabric shear rigidity. Dynamic fabric shear/bending deformations could be obtained in the KES-F system (Hu, 2000). It was found that the results obtained in these two systems were highly correlated with each other (Ly et al., 1991; Hu, 2000).

Leaf and Lloyd challenged the inherent limitations of the KES-F system and the validity to draw any conclusion about a fabric when primary or total hand values were computed using equations obtained from experiments based on a completely different class of fabrics (Lloyd and Leaf, 1990). The primary hand values established in KES-F system were regarded as being points in coordinate spaces defined by base vectors consisting of certain mechanical properties, this is based on the assumption that the fabric mechanical properties are linearly independent. However, the measured mechanical properties typically exhibit some degree of linear dependent (Lloyd and Leaf, 1990). The numerical scales associated with the primary hand values were thus essentially arbitrary and not

necessarily linear, so it is difficult to compare fabrics numerically with total hand values because of the relevancy and sensitivity of the numerical values of hand.

Although the initial purpose of developing this testing system was to replace subjective assessment of fabric hand by objective testing methods, the determination of objective hand characteristics relied heavily on subjective scaling results. The KES-F system linked the 16 mechanical properties of fabric directly to Japanese hand preference by using multivariate statistical regression analysis, it thus could not provide an appropriate solution for fabric hand assessment in countries other than Japan (Pan et al., 1993). For example, it was found in Kawabata's research that there was no correlation between the judgements of Japan and Australia for summer suiting (Kawabata, 1982).

Another concern of the KES-F system is the regression equations linking the objective mechanical properties with subjective assessment results are not suitable for all fabric ranges. For example, the constants given in Table 2.3 are obtained in objective and subjective evaluations of fabrics for men's winter suiting, so they are not suitable to predict the fabric handle of fabrics for men's summer suiting. Because of the huge varieties of fabric, huge amount of experiments and efforts are required to build up the standards for all kinds of fabrics. In addition, it is also concerned that whether the standard remains as the same after 30 years, while the technology and fashion trend have

been moving forward rapidly every day, it would require enormous amount of experimental work and labour to build up a new standard, which create difficulties for its practical application (Kawabata, 1982). In addition, the KES-F system has high-price and uses complex and time-consuming methods to evaluate fabrics.

The FAST system was developed to evaluate tailoring properties of wool fabrics, so conclusions made by using the FAST system might not be suitable for fabric made from other materials. It is also based on the correlations between a number of subjectively assessed fabric properties like the KES-F system (Kim and Slaten, 1999), so it could not objectively evaluate fabric handle.

While the two systems are supposed to measure fabric properties in low stress, the extension forces exerted on fabrics during testing are huge. For example, fabric extensibility in the KES-F and FAST systems are obtained under 490N/m and 98N/m, respectively. Some kinds of fabrics (e.g. knitted fabric and nonwoven fabric) might be extended remarkably under such large extension forces.

2.2.2 Integrated testing systems

Limitations of conventional fabric objective measurements inspire researchers to develop new testing systems based on new mechanisms which have higher

accuracy, reproducibility and ease. Several new integrated testing systems were developed to meet the increasing needs of current textile market.

2.2.2.1 Ring, Nozzle, Slot and Funnel methods

Ring method was developed based on the inspiration by lady's method to choose scarfs via pulling a scarf through a ring to learn about the behaviour. In this process, the scarf has several deformations: extension, shear, bending, and friction with ring. In 1978, Alley developed an instrument evaluating the fabric handle by measuring the forces required to draw a piece of fabric through an orifice/nozzle and analysing its force-displacement curve (Alley, 1978). A quantity termed 'handle modulus' was calculated from the force-displacement data, geometric considerations of nozzle, extraction force and the dimension of fabric sample. Grover et al (Grover et al., 1993) also developed a hand measurement device similar to Alley's, but used a simpler ring shape to replace the nozzle.

Recently several machines were developed to evaluate fabric handle by using nozzle, slot and funnel methods. Both PhabrOmeter (Pan, 2006; *Phabrometer*) system and Wool Handle-Meter (AWTA) were developed based on the nozzle extraction method. Handle-o-Meter were developed based on a slot test. During the test, fabric is forced into the slot by a penetrator beam. Combined effects of flexibility and surface friction of material are measured to evaluate fabric handle. Elmogahzy-Kilinc handle measurement system (Kilinc-Balci, 2011) was developed to evaluate fabric handle by pulling fabric through a flexible light funnel. The developer stated that the funnel could provide multiple configurations of fabric hand and closely simulate the various aspects of the fabric hand property, and the funnel media could allow both constrained and unconstrained fabric folding or unfolding. All these testing systems provide integrated parameters of fabric handle.

Several studies (Behery, 1986; Pan and Yen, 1992; Grover et al., 1993; Kim and Slaten, 1999) had compared the extraction measurement techniques with other measurement methods. Behery et al. compared the results of extraction method and the KES-F system, and found that there was a fairly good agreement between two results (Behery, 1986). Grover et al. compared the withdraw force required to extract six shirting fabric pass through a ring by using a tensile tester with the KES-F data showed that the withdraw force correlated with fabric weight (W), and bending properties (B and $2HB$) (Grover et al., 1993). The withdraw force on these functionally finished fabric correlated with the coefficient of friction (MIU), work of compression (WC), and fabric weight (W).

Compared with the KES-F system, the handle force technique did not fully inform about the various individual aspects of fabric handle that would be useful in more fundamental research. It was stated that the fabric handle determined by the extraction method was influenced by various physical and surface properties, such as drapability, flexural rigidity, and static friction resistance (Kim and Slaten, 1999). In other words, fabric handle values measured by using this method represent fabric hand are overall fabric hand determined by a combination of various physical properties.

It was found that fabrics were deformed under a very complex yet low stress state including tensile, shearing, and bending as well as frictional actions during the extraction process (Pan and Yen, 1992). Consequently, all the information corresponding to this complex stress state contributed to the load-displacement extraction curve and there was no direct method available to derive the information into well-defined physical parameters or to identify the specific characteristics on the curve corresponding to known fabric properties. Thus, several indirect attempts to give the physical interpretations of the typical extraction curve, as shown in Figure 2.6, were made. The correlation coefficients between features extracted in the curve and sixteen measured KES-F properties were studied. The results showed that the peak B resulting from fabric folding prior to entering the nozzle was correlated with fabric bending stiffness, weight and thickness. The peak A of the curve was related to tensile energy, shear hysteresis, bending rigidity, weight and thickness, which suggested that the tensile and shear stresses become significant at this point. The initial slope C of the curve was related to fabric compressional linearity, compressional resilience, surface geometrical roughness and weight. The slope D which is the slope prior to the principal peak A was found related to tensile energy, the thickness, weight and shear hysteresis (Pan and Yen, 1992).

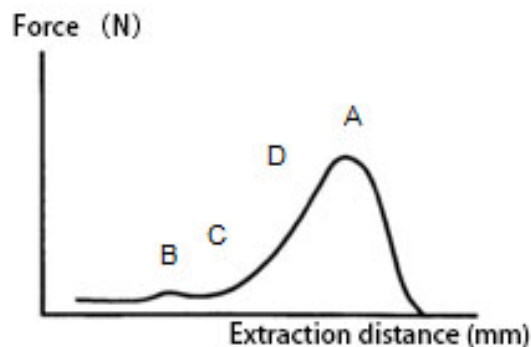


Figure 2.6 Typical fabric extraction curve(Pan and Yen, 1992)

Five characteristics of the curve illustrated in Figure 2.7 are Peak location ($L(\text{mm})$), Peak force ($P(\text{N})$), Width at $P/2$ ($W(\text{mm})$), Area under curve ($A(\text{N}\cdot\text{mm})$) and Nominal slope ($S(\text{N}/\text{mm})$) (Pan and Yen, 1992).

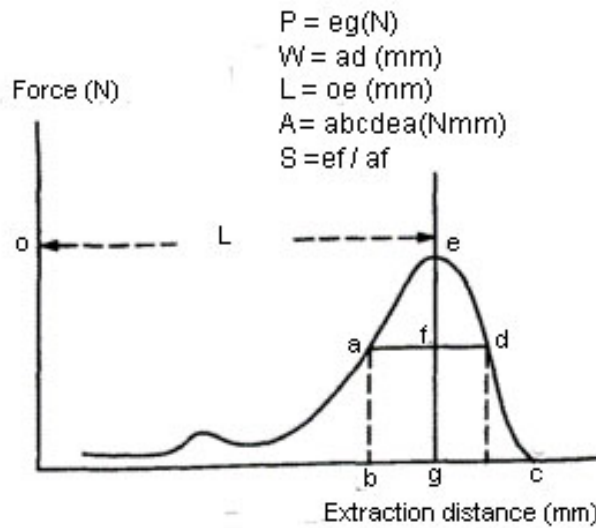


Figure 2.7 Feature parameters on the curve (Pan and Yen, 1992)

Because of the complex interactions of these five features and fabric properties, there were still tremendous difficulties in interpreting the force-displacement curve, and their conclusions are subjective because of the standard fabrics used to explain meanings of extraction curves (Mao and Taylor, 2012). In summary, the ring, nozzle, slot and funnel extraction methods used in PhabrOmeter system, Wool Handle-Meter system, Handle-o-Meter and Elmogahzy-Kilinc handle measurement system involve a series of complicated, non-reproducible mechanical deformation behaviour of fabrics and thus are difficult to be interpreted in relation to the fabric handle properties, this restricts its applications.

2.2.2.2 Tissue Softness Analyser (TSA)

The TSA was developed to evaluate softness, smoothness, roughness, stiffness, elasticity, compressibility of tissues and fabrics (Gruener, 2011). The developer stated that the test of softness is not only evaluated by sense of touch, other sensory organs are also important, such as the effect of sound. A primary hand value in KES-F is also related to sound. It is called SHARI which means crisp, dry and sharp sound made by rubbing the fabric surface with itself and is used to describe a feeling of a crisp and rough surface of fabric (Kawabata, 1980).

During the TSA test, a scraper is lowered on the sample. The scraper twists for 360° while it applies pressure on the sample. The displacement of sample is measured to calculate sample's elasticity. The sound arising from the turn is received and recorded with a vibration sensor in a specified measurement time

interval. Then the sound is evaluated based on the sound spectrum or the frequency band, and the performance parameter is computed and used to predict sample softness.

It is reported that TSA has a good performance in tissue area (*The TSA and its triumph in the tissue industry*, 2012). Compared with tissues, textiles have more complicated surface structures and could be produced by more types of materials. Woven and knitted fabrics have periodic patterns on surface which are formed by interlacing of yarns. Therefore the sound produced by scraper and fabric might be highly affected by these patterns. Besides, sound depends on two touched materials, moving the scraper on cotton and polyester might produce different sounds. Are the results comparable between textiles made of different materials? Limited results were found about the textile test. Therefore it is doubted that if the TSA is suitable to evaluate fabric handle properties.

2.2.2.3 Fabric Touch Tester (FTT) system

Li Y. et al. argued that the existing fabric handle evaluation systems mainly concentrated on the judgement of mechanical properties, while the thermal-wet property is also important for overall comfort perception (Li, 2001). The Fabric Touch Tester (FTT) system was developed to measure both the mechanical and thermal sensory properties of fabrics. The FTT system (Li et al., 2003) has a thin film heat flux sensor to measure the heat flow through a fabric sample held between two testing plates. At the same time, other mechanical properties including multi-dimension bending properties, compression properties, and friction properties were measured. The software takes all the data and converts it into objective measurements and graphs, and the information can be used to communicate hand requirements through the supply chain. FTT system was used by Hu J. Y. et al. to evaluate the thermal-mechanical properties of the fabric (Hu, J.Y. et al., 2006). They found that the sensations of fabric-skin touch under non-sweating conditions like smoothness, softness, prickliness, warmth and dampness could be predicted using the measurements of the system. However, the FTT system does not provide a proper measurement of shear properties and thus fails to show the full picture of fabric tactile properties.

2.2.3 Leeds University Fabric Handle Evaluation System (LUFHES)

The characteristics of axial compression buckling of different fabrics are distinctively different and are thought to be related to fabric handle properties (Lindberg et al., 1961). Based on this finding, a new fabric handle evaluation system, Leeds University Fabric Handle Evaluation System (LUFHES) (Mao and

Taylor, 2012) was developed to discriminate fabric handle in a pure objective, reproducible and controllable manner.

The LUFHES system is shown in Figure 2.8, a fabric cylindrical shell of 80mm in diameter, 110mm in length and 50mm in gauge length is used in the LUFHES tests.

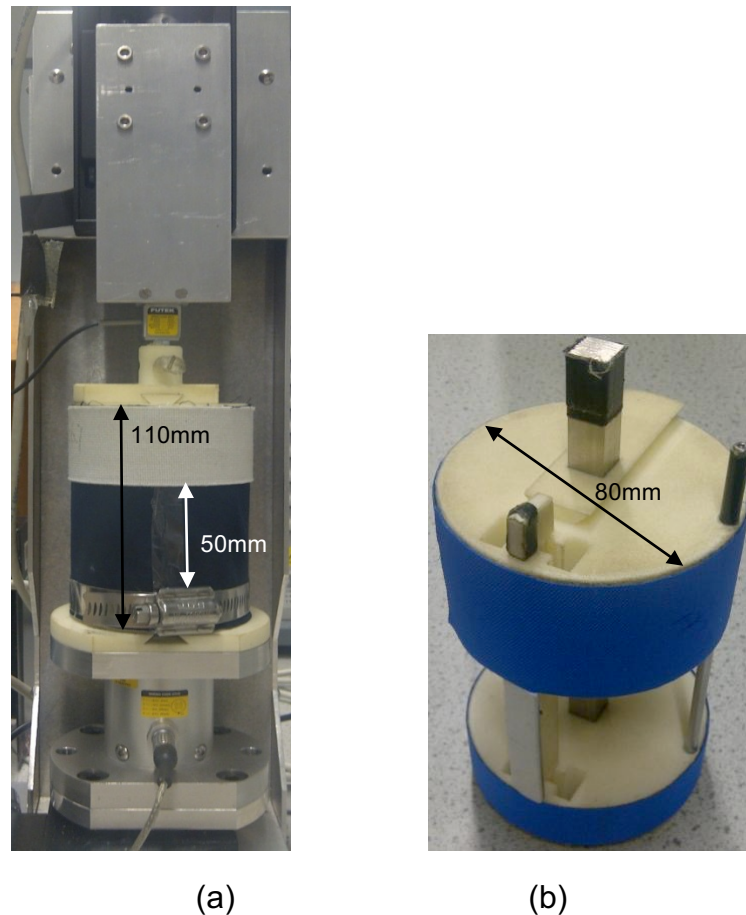


Figure 2.8 The LUFHES system: (a) System with sample. (b) Sample holder

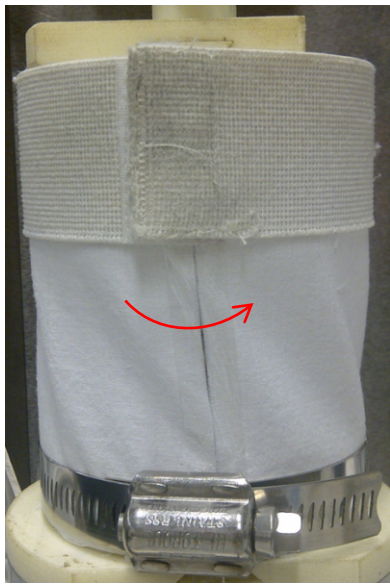
The tests in the LUFHES system contain two kinds of movement: the vertical movement of the upper sample holder is responsible for the axial compression buckling deformation of fabric shells and fabric friction tests, while the rotation of the bottom sample holder is responsible for the shear test. The upper sample holder attached a strip of fabric for conducting fabric self-friction test is shown in the Figure 2.8(b). The fabric specimen to be tested, which is identical to the fabric strip attached on the upper sample holder, is rolled up to the outer side of the fabric sample holder to form a cylindrical shell (see Figure 2.8 (a)), then a strip of ultrathin (20 μ m) and soft adhesive tape is used to join the two edges of the fabric shell together. The upper end of the fabric shell is fixed on the surface of the upper sample holder using an elastic band of a fixed length, and the bottom end

of the fabric shell is fixed onto the bottom sample holder using a metal fastener, the assembly of the fabric shell is mounted onto the LUFHES system as shown in Figure 2.8 (a) (Mao and Taylor, 2012).

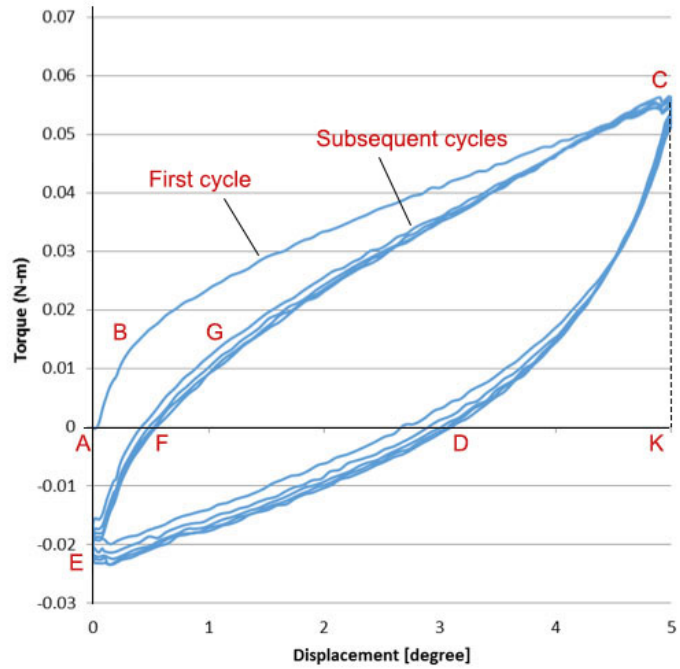
A complete measurement in the system for a fabric shell contains a cyclic twisting test, a cyclic axial compression buckling test, and an extension and friction test. According to the dynamic force-displacement curve in compression buckling test and the torque-angular displacement curve in twisting test, energies consumed to form different types of deformations in fabric shells are obtained. Based on these energies, five fabric handle indices related to fabric handle are defined: sponginess, crispiness, flexibility, stiffness and softness. According to the fabric-fabric friction force-displacement curve, another fabric handle index, smoothness is defined (Mao 2014; Mao & Taylor 2012). In addition, according to the fabric shell cyclic twisting, compression and extension test results, the Young's modulus and shear modulus of fabric cylindrical shell, buckling forces, and fabric roughness during biaxial deformation processes are obtained.

2.2.3.1 The characteristics of fabric deformations and the displacement curves of the cyclic twist and compression buckling-recovery processes

An example of fabric deformation in twist buckling test and a typical torque-degree curve of cyclic twist-recovery processes is shown in Figure 2.9.



(a)



(b)

Figure 2.9 (a): Fabric deformation in the LUFHES twist buckling test. (b): A typical torque-angular displacement curve of the cyclic axial twist buckling-recovery process in the LUFHES

In each cycle of the LUFHES twist buckling-recovery process, the fabric shell's bottom end is twisted gradually to reach a small twist angle and then twisted back to its original angular position as shown in Figure 2.9(a). The same process is repeated 4 times to evaluate shear properties of fabric shell which is recovered from deformations in first cycle. During the twist buckling-recovery process, the torque required to twist and recover fabric shell is recorded, and a typical torque-angle curve is shown in Figure 2.9(b).

An example of fabric deformation in compression buckling test and a typical force-displacement curve of cyclic compression-recovery processes is shown in Figure 2.10.

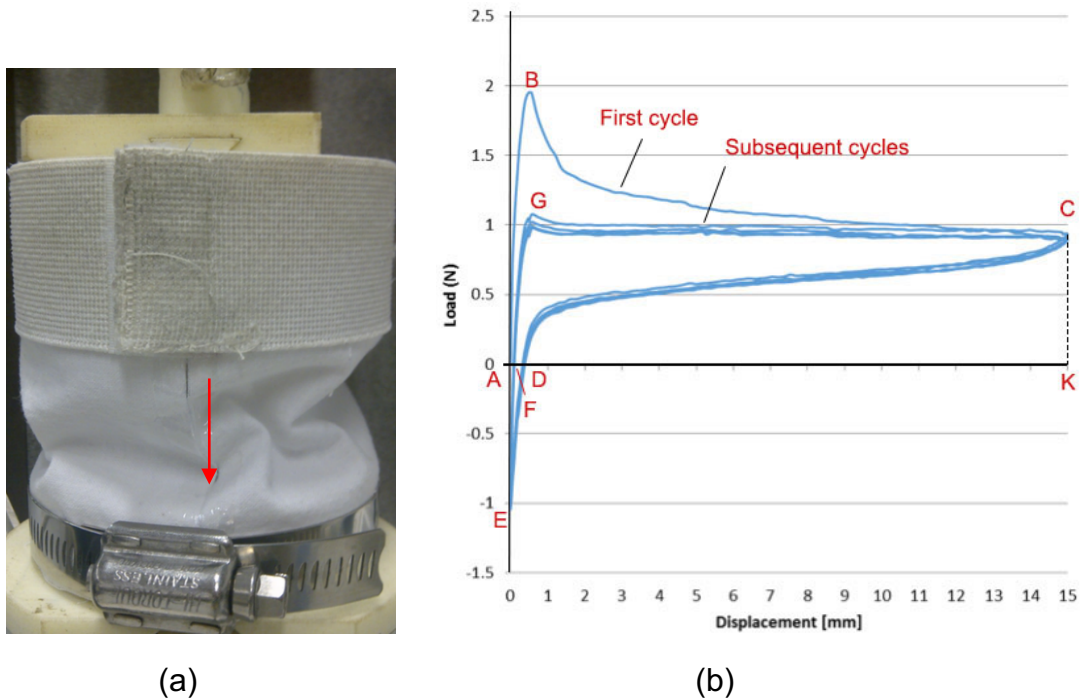


Figure 2.10 (a): Fabric deformation in the LUFHES compression buckling test.
 (b): A typical force-displacement curve of the cyclic axial compression buckling-recovery process

In each cycle of the LUFHES compression buckling-recovery process, the top end of the fabric shell is compressed gradually and recovered back to its original shell length as shown in Figure 2.10(a). The same process is repeated 4 times to evaluate the compression buckling and recover properties of the fabric shell which is recovered from deformations in first cycle. During compression buckling-recovery process, the force required to compress and recover fabric shell is recorded, and a typical force-displacement curve is shown in Figure 2.10(b).

In both twist and compression buckling process (first twist/compression-recovery cycle), there are a twist/compression phase and a recovery phase. At the beginning of the twist/compression deformation (starting point A), fabric shell is gradually twisted/compressed by an external torque/force and the torque/force increased as the sample is deformed gradually. The twist/compression phase of the first twist/compression-recovery cycle is represented by the line ABC (see Figure 2.9(b)/Figure 2.10(b)) when the fabric reaches to the point C which corresponds to the maximum twist angle/compression displacement (point K in the X-axis) before its recovery.

In the recovery phase of the twist/compression-recovery process, the deformed fabric shell starts to return towards its original position from the maximum displacement point C, and the strain energy stored in the deformed fabric is released to produce an elastic force to help the fabric recover to a certain displacement point D (shown as line CD in Figure 2.9(b)/Figure 2.10(b)). While

the deformed fabric shell does not recover completely to its original position by this elastic force, an external torque/force is applied from point D to recover the deformed fabric back to its original position at point E which corresponds to the zero twist angle/compression displacement. The recovery phase of the first twist/compression-recovery cycle is represented by the line CDE in Figure 2.9(b)/Figure 2.10(b).

In the twist/compression phase of the second twist/compression-recovery cycle, the recovered fabric shell being stretched at point E is gradually twisted/compressed to a state of zero torque/force at point F (shown as line EF in Figure 2.9(b)/Figure 2.10(b)). Because the deformed fabric shell is not returned to the original angular/length position when the torque/force of the fabric shell is zero, this means that part of the deformation of the deformed fabric shell cannot be recovered by the external torque/force. With further twist/compression of the recovered fabric shell in the second cycle from point F, the twist/compression of the fabric shell in the second cycle terminates at point C when the twist angle/compression displacement reaches to its maximum (shown as line FC in Figure 2.9(b)/Figure 2.10(b)). At this moment, the torque/force applied to twist/compress the fabric shell reaches to its peak.

In the recovery phase of the second twist/compression-recovery cycle, the twisted/compressed fabric shell starts to recover from the point C towards its original angular/length position. The twist/compression recovery phase in the second (and other consecutive) cycles have small differences to the twist/compression recovery phase in the first cycle, so they are also represented by the line CDE in Figure 2.9(b)/Figure 2.10(b).

Even though the twist/compression and recovery phases of the subsequent cyclic twist/compression-recovery cycles are slightly different from the corresponding phases of the second cycle, the differences are relatively small for most of textile fabrics in this research, they are thus represented by the lines EFC and CDE in Figure 2.9(b)/Figure 2.10(b), respectively.

As indicated in previous research (Mao and Taylor, 2012; Mao, 2014), the areas under the torque-degrees curves and compression-displacement curves represent the energies consumed to deform the fabric shell, to recover the deformation of the deformed fabric shell and to form the unrecoverable fabric deformations during the twist/compression buckling-recovery processes. They are summarised as follows (Mao and Taylor, 2012; Mao, 2014):

- Area ABCKA is the energy consumed to deform the undeformed fabric shell in the first cycle of twist/compression buckling process, and denoted as A_{1cp1} ;

- Area FGCKF is the energy consumed to deform the recovered fabric shell in the second and subsequent cyclic twist/compression cycles, denoted as A1;
- Area DCKD is the work done by the elastic force produced by the deformed fabric to self-recover the twist/compression deformation, denoted as A2;
- Area AFEA is the energy consumed to recover permanently deformed fabric, denoted as A3;
- Area DEFD is the energy consumed to recover the recoverable deformation through stretching and extension, denoted as A4.

2.2.3.2 The characteristics of fabric shell deformations in the extension-friction test in LUFHES

The friction test in LUFHES measures fabric to fabric friction. The primary hand value SHARI in KES-F is also based on the sound the fabric makes when it rubs against itself (Kawabata, 1980). A model of the extension-friction test in LUFHES is shown in Figure 2.11. The LUFHES friction test set contains two parts, one is an upper sample holder which is covered by a piece of fabric outside, and another part is the fabric shell. The upper sample holder is covered by the fabric shell and a calibrated elastic band is placed at the outside of two fabrics to provide pressure. During the LUFHES friction test, the upper sample holder is dragged upwards at a constant speed to produce relative movement between two fabrics and the friction between fabric and fabric is measured. The external force applied to initiate and keep relative moment is recorded. A typical force-displacement curve in extension-friction test is shown in Figure 2.12.

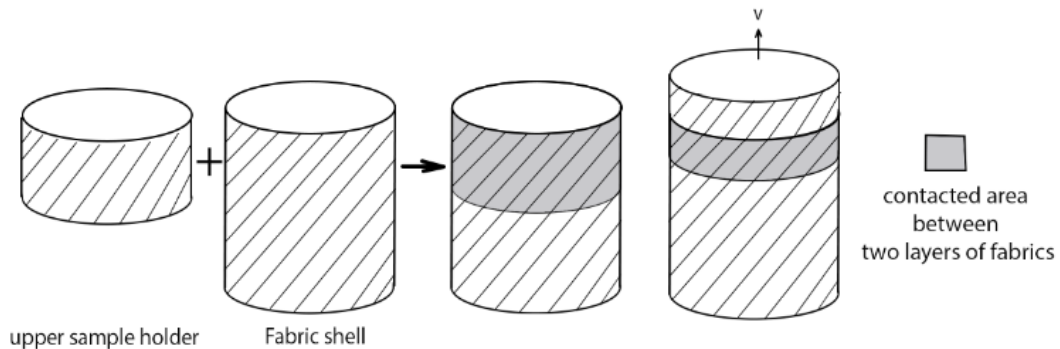


Figure 2.11 Model of the LUFHES friction test

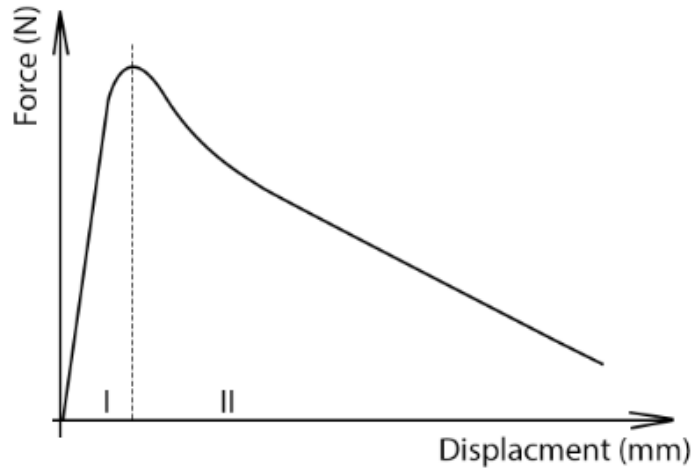


Figure 2.12 A typical force-displacement curve of extension-friction process

In Figure 2.12, the force-displacement curve is separated into two sections.

External force is applied on fabric shell, so fabric is extended at the beginning as shown in section I that force increases quickly within a small displacement. When static friction force between two fabric shells are overcome by external force, the relative movement between fabric and fabric starts and the dynamic friction force measured decreases due to both the smaller dynamic friction coefficient and the gradual reduction of contacted area between two fabrics with the increase of fabric shell linear displacement.

The shear, compression buckling, extension and friction properties of the fabric shell are measured in sequence in the LUFHES. This not only has the advantage of saving the time in preparing the number of fabric specimens, but also the shear, buckling and friction properties of the target fabrics are obtained in the same fabric specimen. Fabric deformations measured in the LUFHES mimic the fabric deformation in subjective handle assessment process and they are quantified by using energy methods. However, there are still some fundamental questions about the LUFHES unanswered. For example, could the mechanical properties obtained in compression buckling deformations and twisting deformations in LUFHES discriminate different fabrics? And why? What are the differences of the fabric properties measured between the LUFHES, KES-F and FAST systems? Thus, further research is needed to improve understanding of the mechanism of this system.

2.3 Fabric mechanical and surface properties

Several mechanical properties of fabric were found to be related to fabric tactile properties, they are bending, shearing, tensile, buckling, and fabric surface

properties (Behery, 2005). The influencing factors and the measurement methods of these properties are reviewed in this section.

2.3.1 Mechanical properties

2.3.1.1 Bending properties

Bending of a slender structural element characterizes its behaviour subjected to an external load applied perpendicular to a longitudinal axis of the element (Chandramouli, 2012). It was found that the bending resistance of woven fabrics had three components (Grosberg, 1966): (1) the bending resistance of the threads lying in the direction of bending; (2) interaction between the threads; and (3) a frictional restraint. Similarly, in the research of Abbott, it was also confirmed that the bending resistance of a fabric was due to both frictional and elastic forces (Abbott et al., 1973). Excluding the initial non-linear region of a fabric bending, the bending rigidity, bending moment and the radius of bending curvature have the following relationship (Grosberg, 1966):

$$M - M_0 = \frac{BR}{\rho} \dots\dots\dots (2.9)$$

Where M is the applied bending moment (Nm), M_0 is the frictional restraint couple (Nm), BR is the bending rigidity of the cloth (Nm²), and ρ is the resulting radius of curvature (m). This equation only applies when $M > M_0$. If $M < M_0$, no bending takes place

Grosberg (1966) found that the internal frictional restraint of most fabrics during fabric bending raised from the relative rubbing movement between individual fibres inner and between the yarns. The frictional forces produced by the pressures were mainly from both the intra-yarn pressure in yarn twists and the inter-yarn pressure acting at the crossover regions in woven fabric. It was also found that the final bending resistance of fabric was always greater than the sum of the bending resistance of the yarns in the fabric (Grosberg, 1966).

An example of the movement of fibres during bending of yarns is shown in Figure 2.13 when large friction forces exist between fibres (Behera and Hari, 2010). In the yarns, if the freedom of movement of fibres is completely hindered, fibres tend to move towards the neutral plane of the deformation as shown in Figure 2.13. In order to relieve the strain, fibres have to adjust themselves around the bending position, as shown in Figure 2.13. It is noted that fabric buckling involves fabric bending (Grosberg and Swani, 1966a), it is thus anticipated that there might be similar effect of pre-tension on the fabric buckling, however, there is no such study on fabric buckling reported.

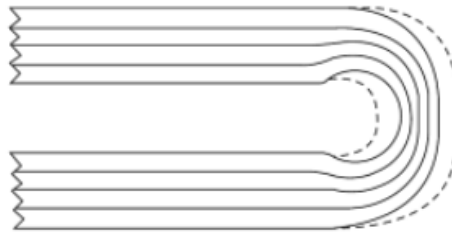


Figure 2.13 Bending of yarns with large friction between fibres (Behera and Hari, 2010)

Three methods are often used to test fabric bending properties: cantilever test, hanging loop test and pure bending test (Wang et al., 2008):

1. Cantilever test: A fabric strip of rectangular shape with one end clamped and supported on a horizontal platform while the rest of the strip is allowed to overhang and bend under its own weight. The bending length is obtained when the free end of the fabric strip reaches a plane inclined at 41.5°. Fabric bending rigidity based on the bending length measured in cantilever test can be calculated in equation 2.10 (Peirce, 1930),

$$BR = m \cdot c^3 \cdot 9.8 \times 10^{-12} \dots\dots\dots (2.10)$$

In which *BR* is fabric bending rigidity per unit width (Nm), *m* is fabric mass per unit area (g/m²); *c* is bending length (mm);

2. Hanging loop method: this method may be used when fabrics are too flexible or limp. Fabric loops of different shapes (pear, ring and heart) are formed when one end of a fabric strip is brought against the other end by bending through angles of 180° (pear), 360° (ring) and 540° (heart) and joined together and hanged vertically under its own weight. The length of this loop is called hanging length, which is inversely related to bending stiffness;
3. Pure bending test: this approach is used in the KES-F bending tester. A fabric strip is mounted on two clamps and then is bent at a constant rate of bending curvature by moving one of the clamps. Relation between bending moment (*M*) and bending curvature (*k*) is obtained as below (Gürdal et al., 1999):

$$M = BR \cdot k \dots\dots\dots (2.11)$$

Where *BR* is the bending rigidity which refers to the moment per unit length per unit of curvature.

Bending rigidity is also found be related to Young’s modulus *E* and area moment of inertia *I* (Bueno, M. et al., 2008):

$$BR = EI \dots\dots\dots (2.12)$$

In addition, Bending rigidity *BR* is also found be related to Young's modulus (*E*), Poisson's ratio *ν* and cube of the elastic thickness (*t*) (Vinson, 1989):

$$BR = \frac{Et^3}{12(1-\nu^2)} \dots\dots\dots (2.13)$$

The cantilever bending test is adopted in the FAST system and pure bending test is adopted in the KES-F system to evaluate fabric bending properties. But there is

little knowledge about their differences for different kinds of fabrics and which one is more suitable to be used to predict fabric handle. In addition, the fabric always has a curvature in a subjective test, but both the cantilever bending test and pure bending test evaluate the bending properties of fabric plate. Thus, it is also wondering if the bending property of fabric plate could predict the behaviour of fabric shell in subjective assessment.

2.3.1.2 Compression buckling deformation

Compression buckling is characterized as a sudden failure of a structural component which is subject to an axial compressive load (Leckie and Dal Bello, 2009). During fabric buckling process, yarns in the woven fabric are moved and bent, and they have three possible motions (Brenner and Chen, 1964): one motion occurs in the compressive stage when the yarns parallel to the loading direction increase their crimp amplitude and the cross yarns are forced closer to one another. The second motion begins when this compression releases the normal forces at yarn crossover points making it easier for yarns to move. The third motion happens in the post-buckling stage, when yarn is deformed by bending.

It was found that both plate buckling and shell buckling of woven fabrics have the following four characteristics (Lindberg et al., 1961):

- (1) A pronounced maximum force was always obtained at the buckling point and this buckling point was usually more pronounced in shell buckling than in plate buckling. This force at which buckling happens is usually called the critical buckling force. It is an important characteristic of buckling. In buckling, when the external force is below the critical buckling load, only axial deformation exists in the structure;
- (2) The second buckling cycle does not generally give the same buckling curve as in the first cycle, and there is a difference between the first and the second curve, denoted as noncyclical energy loss. This means that the fibres will never return to their original position even if the fabric appears smooth. This energy loss was thought to be related to the frictional restraint from the inter-yarn pressure in the fabric (Grosberg and Swani, 1966a). It was demonstrated by Lindberg that if the frictional force between yarns is very small, a small permanent deformation could be obtained; but if the frictional force is very large, for example, if the fibres are spot-welded together, there will be no slippage and no friction-dependent permanent deformation (Lindberg et al., 1961). This means that there are two minima for the permanent deformation at extreme values, and there ought to be an intermediate value where the permanent deformation has a maximum value;

(3) The third and subsequent compression buckling cycles show very small additional deviations. It was also noted that the values obtained for the recovered energy must have a noticeable influence on the dynamic properties of fabric (Lindberg et al., 1961).

Buckling and bending are two different deformations. In bending, a lateral deformation is produced by a bending stress parallel to the lateral direction. In compression buckling, when the external force is below the critical buckling force, only axial deformation exists in the structure, no lateral deformation (e.g., curvature) takes places (Siddiqi, 2014). However, at the moment of buckling, curvature occurs and resisting bending moment is generated to balance the bending moment. Therefore when axial compression force equals to the critical compression buckling force (P_{cr}), the fabric buckles and the fabric buckling force is related to the bending moments in post buckling status.

The compression buckling force in a plate buckling is related to bending rigidity as given in equation 2.14. It was also found that critical buckling force of fabric plate has good linear relationship with fabric bending rigidity (Lindberg et al., 1961).

$$P_{cr} = \frac{4\pi^2 \cdot BR}{L^2} \dots\dots\dots (2.14)$$

Where P_{cr} is the critical buckling force (N), BR is the bending rigidity (N·m) and L is the sample length (m).

It was stated that very often a textile fabric is not in a form of a plane plate when it is subjected to compression forces, such as the buckling of sleeve, and the testing handle by squeezing the fabric in the hand, fabric already has a curvature perpendicular to the direction of compressive force (Dahlberg, 1961). Lindberg (1961) also stated that the shell buckling load was more closely related to the handle of a fabric than plate buckling. However, for the compression buckling deformation of fabric cylindrical shells, there was no theory and model available to show whether and how their compression buckling forces are related to the fabric bending rigidity measured from fabric plates.

2.3.1.3 Shear properties

Shear deformation of a material refers to parallel internal surfaces sliding past one another (Behera and Hari, 2010). Shear modulus G is defined to describe the shear properties of a material based on the shear stress applied and its corresponding shear strain incurred. It is defined as the ratio of shear stress to the shear strain per unit length of materials studied (Lee, S.M., 1995).

Fabric shear deformations are involved in various fabric deformation such as bending, draping, buckling, pliability, and fabric handle evaluations. It was found

that there were two factors determining fabric shear behaviour: friction coefficient and elastic bending forces (Lindberg et al., 1961). Frictional forces were produced when the intersecting yarns had any relative movement between each other. Elastic forces were produced when the yarn system approached jamming. For a tightly woven fabric, its yarns were already jammed, the elastic forces were then very rapidly built up, and there would be no sliding of yarns (i.e., little friction effect) over each other at the intersections.

In the research of Lindberg et al.(1961), the shear properties of 66 commercial fabrics covering a wide range were evaluated and four types of shear behaviour curves for different materials shown in Figure 2.14 were discussed.

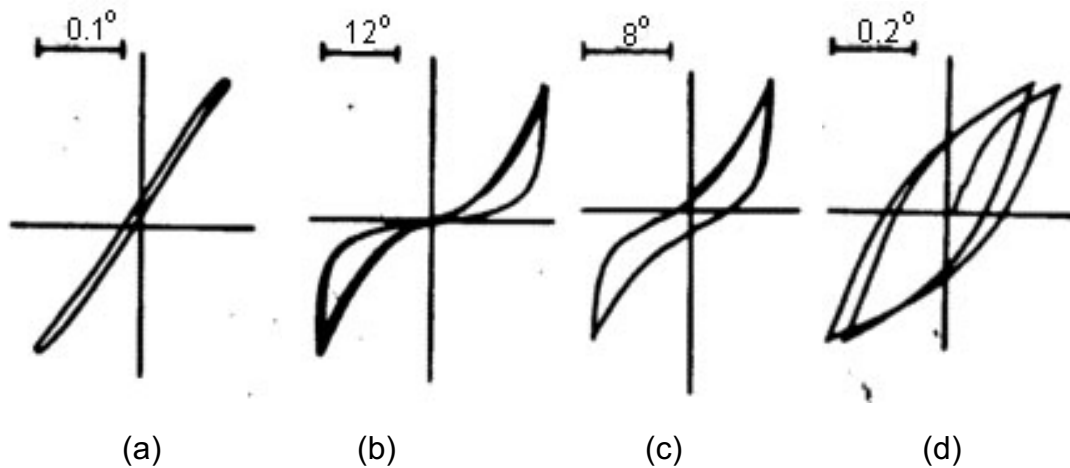


Figure 2.14 Shearing curves for different materials (Lindberg et al., 1961)

When a fabric is either very tightly woven or has a high frictional resistance at yarn intersections, its shearing curve is more or less completely linear with very little hysteresis (Figure 2.14(a)). If the fabric is loosely woven (low cover factor) and the friction is very low, curves of this type would be similar to Figure 2.14(b), in which the load rapidly increases as jamming is approached. In comparison with the Figure 2.14(b), if the friction is increased while the same cover factor is maintained, an S-shaped curve is obtained like Figure 2.14(c). If the load at first increased rapidly due to static friction, then the yarn slipping at yarn intersections begins and the system slide just before the maximum force, the curves shown in Figure 2.14(d) is obtained. The shearing hysteresis shown in this case is noted as a result of the yarn slippage at the yarn intersections in the fabric.

Fabric shear deformations is grouped into four stages in terms of the mechanism of the frictional slippage (Grosberg and Park, 1966): (1) deformation due to rigid intersections when the shear is too small to overcome the friction; (2) yarn slippage at the intersection; (3) an elastic deformation when slipping is complete;

(4) jamming in the structure. Therefore fabric shear properties are greatly affected by fabric structures.

It was found that pre-tension affects the shear properties of polyurethane-coated nylon fabric and material behaviour during the initial buckling deformation region, the post-buckling diagonal fold region, and also the final state and cumulative damage (Glaser and Caccese, 2014).

Some authors have reported the shear deformation is related to bending, because shear stress applied on fabric produce bending moments in the yarns/fibres to bend them (Leaf and Sheta, 1984; Hu, 2000).

Fabric shear modulus of a flat fabric plate could be measured directly as described in Kawabata Evaluation System for Fabrics (KES-F), in which a rectangular fabric sample is subjected to a pair of equal and opposite stresses F which are acting parallel to its edges (Hu, 2000).

Fabric shear modulus could also be measured by using a unidirectional bias extension method such as described in the FAST system (De Boos and Tester, 1994). In the research of Kilby, a simple trellis model was used to study the relationship between Young's modulus in bias direction and the shear modulus of plain woven fabric (Kilby, 1963). When a woven fabric is extended in a direction making an angle, Φ , with the warp threads, the Young's modulus in extension deformation in that direction, E_Φ , was given in equation 2.15 (Kilby, 1963; Leaf and Sheta, 1984):

$$\frac{1}{E_\Phi} = \frac{\cos^4\Phi}{E_1} + \left(\frac{1}{G} - \frac{\nu_1}{E_2} - \frac{\nu_2}{E_1}\right) \sin^2\Phi \cos^2\Phi + \frac{\sin^4\Phi}{E_2} \dots\dots\dots (2.15)$$

Where E_1 and E_2 are the Young's modulus in the warp and weft directions, and ν_1 and ν_2 are the fabric Poisson's ratios. when $\Phi = 45^\circ$, equation 2.15 is simplified to equation 2.16 below (Kilby, 1963; Leaf and Sheta, 1984):

$$\frac{1}{G} = \frac{4}{E_{45}} - \frac{(1-\sigma_2)}{E_1} - \frac{(1-\sigma_1)}{E_2} \dots\dots\dots (2.16)$$

For anisotropic woven fabrics, when Young's modulus of warp and weft direction is much greater than shear modulus ($E_1, E_2 \gg G$), the relationship between Young's modulus in bias direction and shear modulus is simplified as below:

$$\frac{1}{G} \approx \frac{4}{E_{45}} \dots\dots\dots (2.17)$$

Usually when bias extension method is used, greater E_1 and E_2 are implied. Because this implied assumption on E_1 and E_2 as well as other assumptions that threads are inextensible in theoretical analysis made in this testing method, inconsistencies of the testing results were found from fabric to fabric (Wang et al.,

2008), although this method is comparatively easy to carry out. In addition, whether this method is applicable to various knitted and nonwoven fabric is still unclear.

The LUFHES shear test evaluates shear property of a thin cylindrical shell. Shear modulus of a thin cylindrical shell in a biaxial deformation could be measured in a twisting test and this is modelled in the equation 2.18 below (Young and Budynas, 2002):

$$G = \frac{90 * T * L}{\theta * \pi^2 R^3 t} \dots \dots \dots (2.18)$$

Where G is shear modulus (Pa), T is torque (Nm), L is length of cylindrical shell (m), R is inner radius of cylindrical shell (m), t is thickness of the cylindrical shell (m), and θ is the angle displacement (degree).

The KES-F, FAST and LUFHES systems use different mechanisms to evaluate fabric shear properties. There is little knowledge about the differences or relationship between the shear properties obtained in these three testing mechanisms, and some questions need to be answered, such as do their results agree well with each other for all kinds of fabrics, and which testing mechanism is more suitable to be used to predict fabric handle.

2.3.1.4 Tensile properties

Fabric tensile properties indicate how fabrics react to extension forces applied (Behera and Hari, 2010), and woven, knitted and nonwoven fabrics react to the applied forces differently.

When a woven fabric is extended by a force on its longitudinal direction, yarns aligned in this direction are slightly straightened and their crimps are reduced (Afroz and Siddika, 2014); alignments of fibres in these yarns are reoriented towards the direction of the force applied. In contrast, the yarns aligned on the direction perpendicular to the applied force might be further bent and the wave amplitude of their crimps are increased, and the fibres in those yarns are compacted due to the increases of the yarn crimps (Afroz and Siddika, 2014).

Knitted fabric is built up with loops as shown in Figure 2.15, it contains loop head, loop leg and loop foot. Different knitted fabrics have different structural change when force is applied. The structural changes of three widely used knitted fabrics, plain jersey fabric, interlock fabric and 1x1 rib fabric, under applied extension forces are summarised as below (Bueno, M. et al., 2008; Zahidul, 2011).

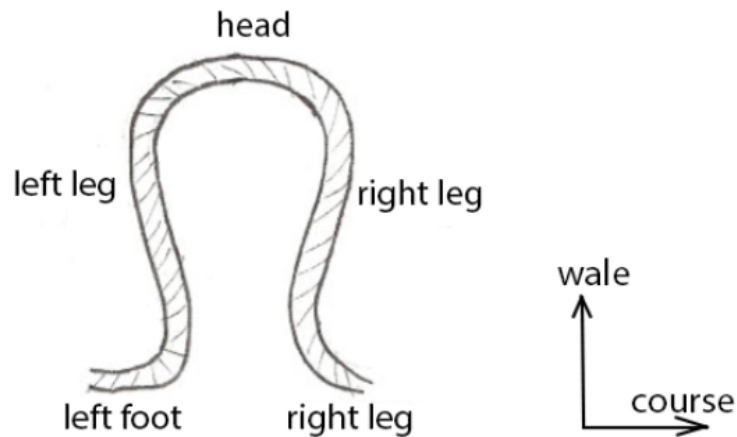


Figure 2.15 Model of a loop in weft knitted fabric

Plain jersey fabric might have two steps to rearrange structure when a force is applied (Bueno, M. et al., 2008). The first step is the decrease of stitch bending in the thickness direction, bending of yarns are involved. The second step varies between course-wise tension and wale-wise tension. The loop head and loop feet come closer when force is applied in course direction. The loop legs come close when force is applied in wale direction. Yarn to yarn friction forces are involved in the second step. The above structure rearrangements are followed by yarn extension and yarn compression at contact area.

Interlock fabric is a kind of two sided fabric. Both sides of interlock fabric has an appearance of the face side of the plain jersey fabric. The elongation of interlock fabric in both wale-wise and course-wise is approximately the same as plain jersey (Zahidul, 2011), so the structure change in interlock fabric caused by an applied force might be similar to that in jersey fabric. Followed by the structure rearrangement, yarn is stretched and also compressed at contact area.

Different from plain jersey and interlock fabric which have the same stitches in course direction, a 1x1 rib fabric is made of one column of face stitch adjacent to one column of reverse stitch. The effect in the course direction is a combination of the curling effect from columns of face stitch groups against the same effect but in the opposite direction from columns of reverse stitch groups (Bueno, M. et al., 2008). Thus the extension behaviour of a rib fabric in wale direction is similar to what plain jersey fabric has in the wale-wise, and there are four mechanisms occur during the course-wise tension of rib fabric: (a) the rotation of the float yarn segment between two stitches of different types (face and reverse); (b) their uncurling; (c) stitch elongation occurs with bending and yarn to yarn friction; and finally, (d) yarn stretching (Bueno, M. et al., 2008).

Nonwovens are complex fibrous assemblies. When an extension force is applied on, fibres in the nonwovens will undergo a structure reorientation before they are

strained. When force is applied in cross direction (CD, 90° to its initially preferred fibre orientation), fibres might reorient significantly and the dominant orientation angle changes from its initially preferred machine direction (MD) towards loading direction. While when the force is applied in MD, the preferences of original fibre orientation increase (Bueno, M. et al., 2008). The fibre reorientation is due to the bent fibres at their interfaces with the bonds are straightened by tensions, and this would lead to highly localized stress concentrations at bonding places, in other words, the contact areas between fibres and the compression force at contact areas will be increased and result in an increased friction between fibres.

For textile fabrics, both Poisson's ratio and Young's modulus are two characteristic properties to describe the fabric tensile deformation behaviours (Hu, 2000). Fabric Poisson effect describes the fabric contraction in the direction perpendicular to the direction a fabric is elongated, Poisson's ratio is the ratio of the relative transverse contraction strain to the related extension strain in the direction of the applied load. Young's modulus is the description of a fabric elastic deformation under applied forces, and it is defined as the slope of its stress-strain curve in the elastic deformation region (Zhou et al., 2010).

It is shown that woven, knitted and nonwoven fabrics have different extension deformations. In the fabric test, a pre-tension is always applied on fabric to remove surface wrinkles before measurement, so the pre-tension applied on fabric might produce different deformations in woven, knitted and nonwoven fabrics and affect the testing results. For the LUFHES test, it is unknown how pre-tension affects fabric biaxial deformation, and how much pre-tension is suitable for woven, knitted and nonwoven fabrics in the LUFHES tests. It is also unknown that how the KES-F, FAST and LUFHES results are affected by the different extension forces applied on fabric.

2.3.2 Fabric Surface morphologies and properties

2.3.2.1 Fabric smoothness

Fabric smoothness is a fabric frictional property and is related to static/dynamic friction coefficients of the fabrics (Ajayi, 1992b). Friction is the force resisting the relative motion between two contacted surfaces. The causes of friction are diverse, one suggestion is given by Amonton in 1699 that the friction is due to the force needed to lift one surface over the asperities of the other (Gupta, 2008). The other suggestions include that the friction is due to the attractive forces between the atoms on two surfaces, or to electrostatic forces (Gupta, 2008). These two theories assume that the surfaces remained separate. Bowden, Tabor and their colleges (Bowden and Tabor, 1954; Bowden and Tabor, 1973; Howell et al.,

1959) suggested that the predominant effects during friction are an actual union or welding of the two surfaces at the points of contact, and the friction force is the result of the effort needed to shear these junctions in order to initiate sliding. This led to the most successful concept of friction, adhesion-shearing theory, which applies to metals and many other materials (Gupta, 2008). For plastics and fibres sliding on themselves or on other materials, it was observed that the transfer of material from one to the other and this proves the operation of adhesion mechanism (Gupta, 2008).

2.3.2.1.1 Adhesion-shearing theory

For plastic and elastic materials such as polymers and metals, two friction surfaces only contact at the tips of asperities and the normal force applied on the points exerts a pressure that is higher than the yield pressure of the materials. Deformations happen at the tips of the asperities because of this pressure until the contact area has increased and the pressure decreases to the point that the force can be supported elastically. In order to initiate a relative sliding between the two surfaces, the junctions between them are ruptured by shearing. The shear strength of junctions is defined as S (N/m^2), therefore the friction force (F) needed to rupture the junction is shown in equation 2.19 (Gupta, 2008):

$$F = SA \dots\dots\dots (2.19)$$

Where A is the real contact area and it is dependent on the extent of deformation, and we have,

$$A = \frac{N}{P_y} \dots\dots\dots (2.20)$$

Where N is the normal force (N), and P_y is the yield pressure of material (Pa).

Thus the friction force (F) is obtained in 2.21 (Gupta, 2008):

$$F = \left(\frac{S}{P_y}\right) N = \mu N \dots\dots\dots (2.21)$$

Because both S and P_y are constant for a certain material, the friction coefficient μ is a material property.

However, it is found that equation 2.21 is not applicable to viscoelastic materials, for example fibres and textile materials, and μ is a function of both normal force and geometric area of contact for such viscoelastic materials (Carr et al., 1988). It is suggested that friction force F has a non-linear relationship with normal force for most polymeric materials as shown, for example, in the empirical equation 2.22 (Howell, 1953; Lincoln, 1952),

$$F = aN^n \dots\dots\dots (2.22)$$

Where a and n are empirical constants.

Equation 2.22 assumes that friction arose from adhesion at the points of real contact and the junctions had a constant shear strength S . It was found that a and n varied with types of fibre, and their results clearly support the validity of the adhesion-shearing mechanism of friction in fibres and polymers (Howell, 1953; Lincoln, 1952). This might be especially true for polymer to polymer frictions.

When interest is in characterizing the frictional behaviour of a material, friction forces under various normal forces are needed in friction tests to obtain a and n values in equation 2.22.

2.3.2.1.2 Ploughing

When a rough hard surface slides over a soft surface, the roughness of the harder surface will groove or plough out the surface of the softer body. In equation 2.19, a term representing the ploughing force (P) is usually added (Gupta, 2008):

$$F = SA + P \dots\dots\dots (2.23)$$

For textiles, a typical example of this type of friction is the metal to polymer surfaces, and the ploughing effect won't happen in textiles to textiles frictions (Gupta, 2008).

2.3.2.1.3 Stick-Slip Phenomenon (SSP)

A classic model to represent stick-slip phenomenon (SSP) (Gupta, 2008) is shown in Figure 2.16(a) and the curve of tension force F against time is shown in Figure 2.16(b). In a friction process, it usually takes a greater force to initiate the sliding of one object against another than to maintain sliding after motion has commenced. Because of the different coefficients of friction, the friction trace is intermittent to form Stick-Slip Phenomenon (SSP) in fabric friction test. As shown in Figure 2.16, kinetic friction force (F_K) is usually smaller than static friction force (F_S). The rider slips and accelerates back until the tension of spring drops to F_K . Then, due to inertia, rider continues to move but decelerates until the tension force $F < F_K$ and rest again. It then moves along the platform until F reaches F_S . There are two reasons for the occurrence of stick-slip phenomenon (SSP). The first reason is the growth in junctions (such as contact area) due to creep and/or application of a tangential stress; the second reason is the strengthening of junctions due to inter-diffusion of surface atoms across the interface. Therefore the two conditions to form Stick-Slip Phenomenon (SSP) are summarised as follows (Gupta, 2008):

1. Coefficient of friction is variable, i.e. $\mu_s > \mu_k$ (μ_s : static, μ_k : kinetic);
2. The system is flexible enough to enable a change in the speed of the sliding body.

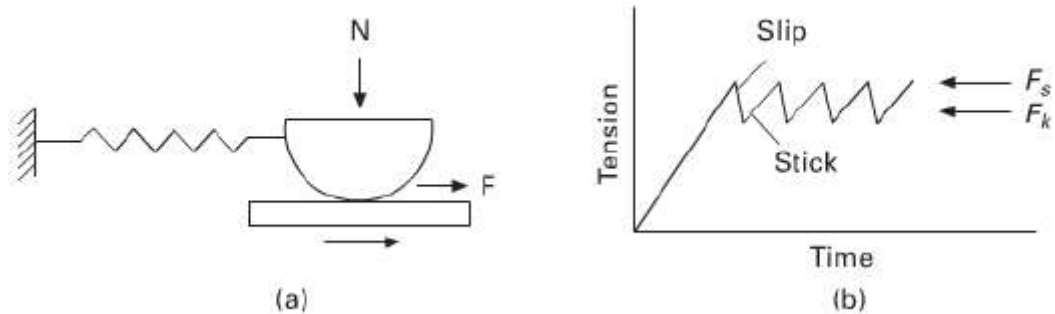


Figure 2.16 Models of stick-slip phenomenon in friction test. (a) Apparatus to measure friction between a plane surface and a rider. (b) Dynamic profile of friction forces

The magnitude of stick-slip is affected by many factors, such as viscoelastic properties of two materials, the speed, and the viscoelastic nature of the electro-mechanical system used.

2.3.2.1.4 Spectral analysis of dynamic friction coefficients

Woven and knitted fabrics are composed of basic structural element, which leads to periodical changes in surface geometry. It was found that the number of peaks in the force-time curve of fabric-fabric friction test and amplitude of resistance are well correlated with some pertinent fabric properties, such as yarn set and structural protuberances, respectively (Ajayi, 1992a; Ajayi, 1992b). Therefore the frequency of dynamic friction forces is considered to correspond to that of the threads in the woven and the knitted fabrics.

Fast Fourier Transform (FFT) method could break down the original signal into a sum of sine waves, and it is frequently used to extract spectrum of dynamic friction frequency-amplitude characteristics (see Figure 2.17).

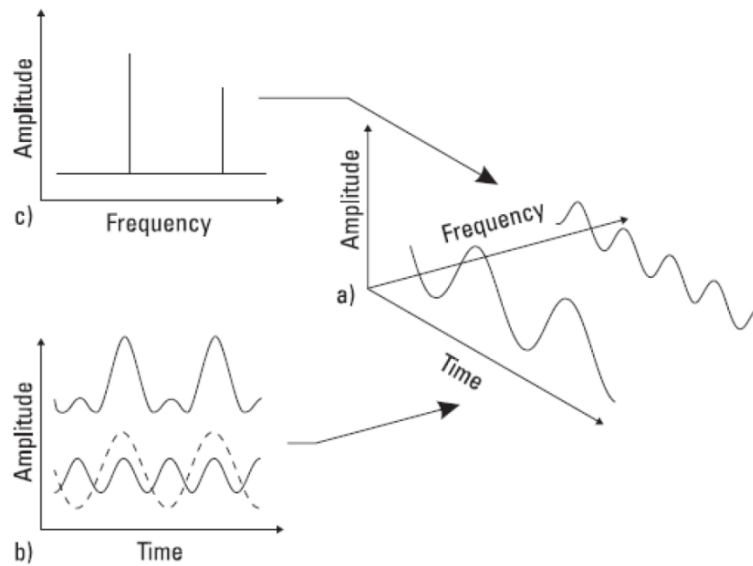


Figure 2.17 Mechanism of FFT analysis. (a) 3D graph of sine waves. (b) Time-domain view. (c) Frequency-domain view. (Craig, 2016)

The influences of fabric structure on the stick-slip motion of kinetic friction force were studied by using spectral analysis (Hosseini Ravandi et al., 1994). The friction tests were conducted between a Perspex sled and five cotton plain-weave fabrics in warp and weft directions. It was found that the stick-slip motion in fabric friction process is strongly affected by fabric construction, for example, the warp and weft density and reed space, yarns protruding from the fabric surface. The main resistance against the movement of sled is corresponding to the ridges of warp or weft yarns on fabric surface. Therefore spectrum analysis of fabric dynamic friction characteristic could lead to reveal the fabric surface structural characteristics, i.e., fabric surface roughness.

2.3.2.2 Surface roughness

Surface roughness is a measure of the texture of a surface and it is quantified by the vertical deviations of a surface from its ideal form. If the deviations are large, the surface is rough, vice versa (Akgun, 2014). Physically, any surface is generally composed of three components: form, waviness and roughness in accordance with wavelength or frequency, and roughness corresponds to the high frequency or small wavelength component (Mooneghi et al., 2014) .

The amplitude parameters of roughness focus on surface height information. Four frequently used roughness parameters are introduced below:

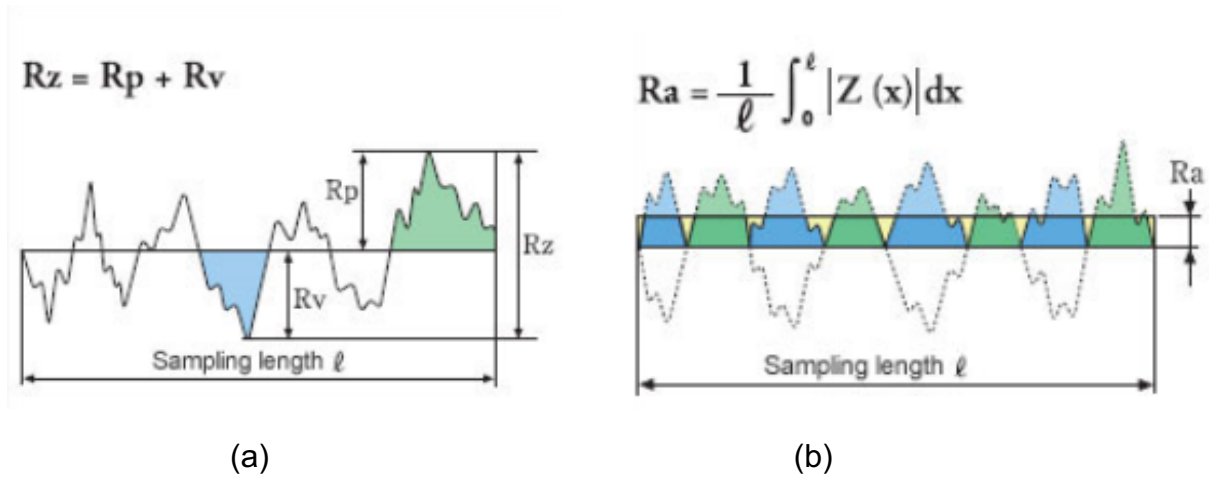


Figure 2.18 Roughness profile (Olympus, 2016)

Two roughness profiles in sampling length are shown in Figure 2.18. A mean line is drawn in both profiles and acts as a reference line to do various calculations. Usually, the mean line is placed where the sum of areas above it is equal to the sum of areas below it (Mooneghi et al., 2014). Sampling length is the length in x direction which is used to identify irregularities of surface roughness. The ordinate value ($Z(x)$) is the height of the profile in x position from the mean line. Four parameters were defined as below:

R_p : maximum value of peak height on the profile curve in a sampling length.

R_v : maximum value of valley depth on the profile curve, in a sampling length.

R_z : sum of the maximum value of profile peak height and the maximum value of profile valley depth in a sampling length.

R_a : arithmetical mean of the absolute values of $Z(x)$ in a sampling length.

Among the above four parameters, R_a is the most useful and common parameter in surface roughness analysis and quality control. In textiles, mean absolute deviation (MAD) is also commonly used, it is defined as below (Mooneghi et al., 2014):

$$MAD = \frac{1}{\ell} \int_0^{\ell} |Z(x) - R_a| dx \dots\dots\dots (2.24)$$

2.3.2.2.1 Fabric roughness

Fabric surface has periodic variations due to regular interlaced patterns of yarns. The geometric roughness measurement is an element of global objective measurement.

Fabric surface roughness is affected by several fabric and yarn construction parameters such as yarn twist, ply number, fabric cover, fabric thickness and yarn crimp variations (Akgun, 2014), it was found that there is a strong linkage between

the fabric structural characterization of woven and knitted fabrics and surface roughness data measured in the KES-F system by using FFT spectral analysis (Vassiliadis and Provatidis, 2004).

Both spectral analysis of Perspex-fabric friction profile and surface roughness profile were claimed to be related to fabric texture, but there is limited knowledge about the differences or relationship between their amplitudes or wavelengths obtained in spectral analysis. In addition, the peaks in fabric-fabric force-time curve were also found related to fabric structure, but it is not clear if the spectrum of fabric-fabric friction profile could also provide information of fabric structural parameter. It is also curious about which kind of surface test (e.g. fabric-fabric friction, sensor-fabric) is more suitable to be used to study fabric surface properties.

2.3.2.3 Relationship between fabric friction and geometrical roughness

Both fabric friction and roughness are related to surface texture. According to the adhesion-shearing theory, fabric friction is produced by shearing the probes fabric surface. Fabric roughness is related to the dimensions and spatial variations of surface probes. Therefore fabric friction and roughness affects each other.

Studies have shown that surface roughness has a dominant influence on friction coefficient between dry fingertip skin and surfaces of smaller roughness. For fine textures, the smaller the amplitude of the probe surface roughness, the higher the friction coefficient (Hendriks and Franklin, 2009). For example, friction coefficients of dry fingers against a glass of smaller roughness is 2.18 ± 1.09 , but friction coefficients on a rough glass surface is about 0.53 ± 0.22 (Derler et al., 2009). In contrast, the coefficient of friction increases with the increase of surface roughness for very rough surfaces, this is due to the effect of friction ridges and ploughing (Tomlinson et al., 2009).

However, it is unknown that if analysing the fabric friction property (e.g. friction force-displacement curve) could quantify or discriminate fabric roughness or not. Thus, more research is necessary to investigate the relation between fabric friction and geometrical roughness.

2.3.2.4 Evaluation of fabric surface properties

Because of the importance of fabric surface properties, efforts have been made to evaluate the fabric friction and roughness properties. First techniques used were subjective methods. Stockbridge et al. evaluated the roughness of woven and knitted fabric by groups of people (Stockbridge et al., 1957). It was shown that there was a significant degree of consistence between groups.

In order to quantify the fabric surface properties, several objective methods have been developed. They could be divided into two kinds: contact methods and non-contact methods.

Contact methods are able to applying pressure on fabric surface by contactor. Kawabata evaluation system of fabric (KES-F) (Kawabata, 1982) measures fabric friction coefficient and roughness by moving sensors on fabric surface. Ajayi used the universal tensile tester (Instron) equipped with a friction assembly to measure the friction of woven, knitted and nonwoven fabrics (Ajayi, 1992b). The results measured by contact methods depend on the type and size of contactor.

Therefore these methods could evaluate fabric surface properties erroneously. For example, Ramgulam stated that the KES-F roughness test results of a towel is not realistic (Ramgulam et al., 1993). Because the contactor dug in and became trapped, this stopped the relative movement of fabric and resulted in unrealistic results.

In the non-contact methods, there is no contact between fabric surface and sensor. This methods could be further divided into two groups: optical methods (Bueno, Marie Ange et al., 2000; Bueno, M.A. et al., 1999; Bueno, M. A. et al., 2000; Ishizawa et al., 2002; Ramgulam et al., 1993) and image analysis and fractal methods (Hu, J.L. et al., 2002; Sul et al., 2006). It was found that non-contact methods could physically describe fabric roughness and texture. But subjective assessment of fabric surface properties consists of applying pressure on fabric surface. Because of this fact, some researchers believe that results obtained in contact results are more compatible with subjective methods (Mooneghi et al., 2014). In order to apply this pressure, a clear glass is suggested to apply on fabric surface during the non-contact measurements. The non-contact methods could physically describe fabric roughness and texture. However, it is also doubted that if it is sufficient to quantify fabric tactile sensations. In subjective fabric surface assessment, vibrations generated by frictions between human skin and the fabric surface in the process of a human finger sliding over a fabric surface. The static and dynamic stress state of skin are transduced into electrical impulses to activate mechanoreceptors in skin to allow brain to perceive tactile information about fabric surface roughness and smoothness (Mao et al., 2016). Human fingertip and palm skin are covered with ridges, the interaction between skin ridges and fabric surface cannot be simulated by noncontact methods. In addition, because finger skin is viscoelastic, friction between fabric and skin cannot be simulated by test between fabric and metal surface. Mao stated that fabric-fabric self-friction test might be a potential method to mimic the vibration between finger and fabric (Mao et al., 2016). Ajayi, J. O. compared the friction

coefficients of three different sled surfaces: fabric-fabric, rubber-fabric, and Perspex-fabric (Ajayi, 1992b). According to the comparison, he stated that fabric-fabric friction test provides the most sensitive surface and the best discrimination. A possible reason is when similar fabrics are tested against themselves, the surface protuberances such as yarn crown, twill, ribs and cords fit better together. But the characteristics of friction and vibration process are still not clear.

2.4 Problems identified, objectives and proposed solutions

2.4.1 Problems

Because fabric tactile property is an important factor in product design and could affect consumer's purchasing, great efforts were made to evaluate fabric tactile properties both subjectively and objectively. However, each of the existing fabric hand and fabric handle measurement systems has limitations in evaluating fabric tactile properties. Subjective assessment result is highly based on people's subjective opinions and preferences, so it lacks reliability and repeatability. Objective measurement systems rely on the relationship between subjective assessment of limited standard fabrics and their individual mechanical properties measured during the processes of either unidirectional fabric deformations (e.g. the FAST and KES-F systems) or uncontrolled complex deformations (e.g. PhabrOmeter and Wool Handle-Meter). Therefore conclusions from these systems have neither been objective nor represent the complex deformation during human hand evaluation.

The LUFHES system was invented to discriminate fabrics in terms of fabric handle properties based on biaxial fabric buckling properties, which is a mimic of the fabric deformation in subjective assessment of fabric hand but in a controlled manner. However, it was found that:

- (1) Little is known about how the testing conditions such as pre-tensions applied on fabric cylindrical shell affect the fabric buckling deformation;
- (2) Little is known about the characteristics of fabric mechanical properties obtained in cyclic buckling deformations in LUFHES;
- (3) Little is known about the differences and relationships of the fabric mechanical properties between unidirectional and biaxial deformations;
- (4) Little is known about the characteristics of friction and vibration in fabric-fabric self-friction test;
- (5) Little is known about if fabric-fabric self-friction test could discriminate fabric roughness properties.

2.4.2 Objectives

The two objectives of this project are as follows:

1. To improve the understanding of mechanical properties measured in axial compression buckling and circumferential torsion buckling of fabric shells and their roles in objective evaluation and discrimination of fabrics;
2. To improve the understanding of mechanisms and characteristics of fabric-fabric self-friction and its relationship with fabric surface characteristics, such as fabric structure and roughness.

In order to achieve above two objectives, following measurements and analysis will be conducted:

- To analyse the characteristics of mechanical properties (e.g. shear modulus and critical buckling force) obtained in the LUFHES test;
- To investigate the differences between mechanical properties measured in biaxial buckling deformations and unidirectional deformations;
- To investigate the influence of pre-tensions on fabric mechanical properties during compression buckling deformation;
- To investigate the mechanism and characteristics of fabric-fabric self-friction and its relationship with fabric surface structure and roughness.

2.4.3 Proposed solutions

Fabric properties of selected woven, knitted and nonwoven fabrics having different thickness, weight per unit area and structures are studied in this project. Woven and knitted fabrics commonly used in apparels direct contact with human skin are of our interests, as their tactile properties are especially important for both wearer and designer (Bertaux et al., 2007). Nonwoven fabrics widely used in next-to-skin hygiene products such as wipes and diapers are also selected in in this project.

In this project, characteristics of fabric properties (e.g. shear modulus) measured in biaxial buckling deformations in LUFHES will be analysed and compared with those obtained in other existing fabric objective measurement (FOM) systems such as the FAST and KES-F systems. Small strain-stress mechanical properties obtained in both the FAST and KES-F systems are conventionally considered to be related to the fabric tactile properties, the comparison of these properties with the properties obtained in the LUFHES system are hoped to give an indication

about the mechanical properties obtained in LUFHES and the differences between these systems in fabric measurements and discriminating fabrics.

The characteristic of fabric-fabric friction profile obtained in the LUFHES friction test will be analysed theoretically and experimentally, and compared with those of the sensor-fabric friction/roughness profiles obtained in the KES-F friction/roughness test. Spectral analysis (FFT) will be used to obtain the spectra of these friction/roughness profiles. The comparison between these three spectra and the comparison between wavelength/amplitude in spectra and fabric surface structure are hoped to improve the understanding about the characteristics of fabric-fabric friction and its relationship with fabric structures.

Chapter 3 Methods for the characterisation of fabric mechanical properties and Experimental plan

In this chapter, fabric materials, equipment, testing methods used in the experiments of this research are described, and the experimental plan and the objectives to be achieved are elaborated and explained.

It is known from the literature review in chapter 2 that the fabric tactile property is affected by fabric mechanical properties in small strain deformations including bending, tensile, shearing, compression, friction, and buckling properties (Behera and Hari, 1994). However, it is noticed that these fabric mechanical properties obtained in each of the existing fabric handle evaluation methods are different (Hu, 2000; Pan, 2006; AWTA). For example, fabric properties measured in the conventional fabric handle evaluation methods such as universal tensile tester (e.g., Titan made by James Heal Ltd, UK), the KES-F and FAST systems are from unidirectional fabric deformations; while fabric properties obtained in the ring and extraction methods such as PhabrOmeter and Wool Handle-Meter are from fabric multidirectional deformations which are similar to the fabric deformations in subjective assessment of fabric hand properties. In contrast to the fabric deformations in ring and nozzle extraction method in which fabric deformations are not controllable and their results are thus difficult to be reproduced, fabric properties measured in the LUFHES for the evaluation of fabric handle are from controlled cyclic biaxial fabric buckling deformations (compression buckling, twist buckling and extension) of fabric cylindrical shells. Therefore three key questions to be answered are: (1) how to understand the mechanical properties obtained in LUFHES tests? (2) what's relationships of fabric properties measured from different fabric deformations? (3) The fabric properties measured from which type of fabric deformations would be better used to describe fabric handle?

Fabric handle is claimed to be related to fabric mechanical properties of fabrics under small strain (Bishop, 1996). However, fabric mechanical properties measured rely on fabric deformation processes during testing, in which fabrics could be deformed in unidirectional, biaxial and multiaxial directions. It is known that subjective fabric hand evaluations are in multiaxial deformation processes, there is little research to investigate if there is any difference between the fabric properties measured in different fabric deformations in the FAST, KES-F and LUFHES tests. Therefore the relationship between fabric mechanical properties (e.g., shear modulus, critical buckling force and bending rigidity) in buckling biaxial deformation and unidirectional deformation are studied in this research.

Besides fabric mechanical properties, fabric surface properties are also important in evaluating fabric tactile properties. In the KES-F system, fabric surface properties are measured by moving metal sensors on fabric surface, while in the ring or nozzle extraction methods, fabric surface properties are evaluated by evaluating friction between fabric and the inside wall of metal ring or nozzle. However, none of these methods could mimic the interaction between fabric and fingers which have viscoelastic ridges on surface. Fabric-fabric self-friction is one of the methods frequently used to evaluate fabric smoothness and roughness in subjective fabric hand assessment process, the characteristics of friction coefficient and roughness obtained in fabric to fabric self-friction process in LUFHES are thus analysed and compared with those obtained in the metal-fabric friction coefficient and roughness measured in the KES-F system, and its relationship with fabric roughness is investigated.

It is hoped that this research could improve the understanding of fabric mechanical properties measured in buckling deformations and their applications in discrimination and fingerprinting of fabrics.

3.1 Fabric materials used in the experiments

To make the conclusions obtained from this study based on a wider fabric choices, the mechanical properties of fabrics having different fabric types and structures (fibre compositions, fabric weaves, mass per unit area and thickness) were investigated in the LUFHES system. Three types of fabric (woven, knitted and nonwoven) frequently used in clothing and next-to-skin textile products are studied in the experiments of this research. Woven and knitted fabrics are traditional fabric choices to produce clothing, and nonwoven fabrics are widely used to produce healthcare products such as diapers and wipes. 29 fabrics are selected for this project in total including 12 woven fabrics, 7 knitted fabrics and 10 nonwoven fabrics.

The twelve woven fabrics cover ripstop, plain, twill and satin woven structures, their mass per unit area is from 58g/m^2 to 427g/m^2 , and the thickness ranges from 0.1mm to 1.1mm. The seven knitted fabrics include single jersey, interlock and 1x1 rib knitted structures, and their mass per unit area is from 145g/m^2 to 404g/m^2 , and thickness is from 0.7mm to 1.8mm. The ten nonwoven fabrics for topsheet and wipes are spunbond, thermal point bonded, and through-air thermal bond technics, their fibre diameters are around 13.3 - 27.4 μm , mass per unit area is from 18g/m^2 to 89g/m^2 , and fabric thickness ranges from 0.2mm to 1.9mm.

All of the 29 fabrics are made from different fibres including cotton, wool, synthetic fibres and their blends.

Table 3.1 (1) Specifications of woven fabrics

Woven fabric	Fabric structure	Fibre materials	Thickness (mm) (under 200Pa)	Mass per unit area (g/m ²)	Count (number/10cm)		Linear density (tex)	
					warp	Weft	warp	weft
W1	Ripstop	Polyamide	0.10	57.8	435	760	5	5
W2	Plain	Cotton	0.38	135.1	350	320	19	19
W3	Plain	Cotton	0.61	303.6	353	267	23	41
W4	Plain	Wool	0.62	211.3	175	130	60	72
W5	Plain	Cotton/PET	0.33	118.5	480	310	13	13
W6	Broken Satin	Cotton	0.76	255.6	530	270	23	27
W7	Satin(5/3)	Synthetic	0.16	114.7	785	285	8	14.7
W8	Broken Satin	Cotton	0.51	218.7	313	316	23.3	18.7
W9	Twill (1/2)	Synthetic	0.65	221.8	300	240	33.3	36.7
W10	Twill (1/2)	Wool	1.08	263.5	183	130	68	66
W11	Twill (2/2)	Wool/viscose	0.99	358.0	250	280	61	61
W12	Twill (3/1)	Cotton	1.10	426.7	260	160	100	80

Table 3.1 (2) Specifications of nonwoven fabrics

Nonwoven fabrics	Bonding structures	Fibre materials	Fabric thickness (mm)	Fibre diameter (μm)	Apparent mass per unit area* (g/m^2)	Apparent density* (kg/m^3)
N1	Thermal bonded	Polypropylene	0.23	27.4	18.43	80.0
N2	Hydroentangled	Cotton	0.48	18.5	44.37	92.5
N3	Hydroentangled	Polypropylene	1.91	21.8	89.45	46.9
N4	Hydroentangled	Cotton	0.69	21.0/ 13.3	58.37	84.6
N5	Hydroentangled	Cotton/Polypropylene	0.58	18.9/ 12.6	34.11	58.8
N6	Hydroentangled	Cotton/Polypropylene	0.49	21.8/ 18.6	22.95	46.9
N7	Flash spun (Tyvek)	Polyethylene	0.21	/	42.30	201.4
N8	Spunbond	Polypropylene	0.32	19.8	25.11	78.5
N10	through-air thermal bond	Polypropylene (Staple fibre)	0.41	19.2	22.55	55.0
N11	Spunbond	Polypropylene	0.36	19.8	25.92	72.0
Aperture hydroentangled nonwovens	Size of aperture (mm^2)	Number of aperture per square centimetres		Real mass per unit area [‡] (g/m^2)	Real bulk density [‡] (g/m^3)	
N4	0.48	40		72.24	104.69	
N5	0.47	40		42.00	72.42	
N6	0.62	36		29.54	60.29	

* Apparent mass per unit area and apparent bulk density were calculated by using the fabric area including the area and volume of apertures;

‡ Real mass per unit area and real bulk density were calculated by using the fabric area excluding the area and volume of apertures.

Table 3.1 (3) Specifications of knitted fabrics

Knitted fabric	Knitting structure	Fibre materials	Thickness (mm) (under 200Pa)	Mass per unit area (g/m ²)	Count (Loop/10cm)		Linear density (tex)
					Wale	Course	
K1	Interlock	Synthetic	1.05	241.9	14	10.2	27.3
K2	Interlock	Wool/PET	1.27	248.8	10	12.2	29.3
K3	1x1 rib	Wool/PET	1.75	404.4	16	10.8	28.7x2
K4	Interlock	Synthetic	1.16	298.9	17.2	10	26.7
K5	Interlock	Cotton	0.75	177.6	15.2	11	16.7
K6	Jersey	Cotton	0.68	144.9	15	19.4	17.3
K7	1x1 rib	Viscose	1.46	324	15.4	12	25.3

3.2 Equipment and methods for the characterisation of fabrics

In this project, all the fabric tests were conducted in a conditioned environment with temperature around 20 °C and humidity around 65%. The force and pre-tension were in a unit of N/m, which means the force applied on fabric in a unit width (or the force applied on fabric in a unit circumference length for a fabric shell).

3.2.1 Fabric Assurance by Simple Testing (FAST) (De Boos and Tester, 1994)

The FAST tensile tester (FAST-3) is used to obtain the fabric shear properties by extending fabric strips cut in bias directions under a fixed extension force of 4.9N/m. Besides, the FAST bending tester (FAST-2) is used to evaluate fabric bending length and rigidity.

3.2.1.1 Shear modulus obtained in bias extension testing in the FAST-3 tester

Fabric specimens cut in bias directions (both 45° and 135°) and having an effective test area of 50mm in width and 100mm in length are extended under the load force of 4.9N/m, the corresponding extensions are used to calculate the fabric shear modulus according to the relationship between Young's modulus in bias direction and the shear modulus shown in equation 5.14 in section 5.2.1.2

For each fabric, tensile elongations of three specimens in each of the two orthogonal directions are measured, and the average shear modulus is obtained.

3.2.1.2 Bending length and bending rigidity measured in the FAST-2 tester

Fabric bending length measured in the FAST bending tester, FAST-2, follows cantilever bending principle. Bending lengths of three fabric specimens having a size of 50mm in width and 200mm in length for each of the two orthogonal directions of each fabric are measured. During bending length test, a fabric specimen is placed on a flat platform with an aluminium plate placed on the top of the fabric without covering the leading edge. The fabric strip is slowly moved until the leading edge block a light beam generated by instrument, and the fabric bending length at this moment is recorded. This process is repeated for another side of the same fabric end; two sides of the other fabric end are also tested. Therefore four readings are obtained for each fabric specimen, and average bending length of three specimens of each direction of a fabric are obtained and it is used to calculate the fabric bending rigidity according to the equation 6.3 shown in section 6.1.2 .

3.2.2 Kawabata Evaluation System for Fabric (KES-F)

There are four testers in the KES-F system to measure fabric mechanical properties: tensile & shear tester (KES-F1), bending tester (KES-F2), compression tester (KES-F3) and surface tester (KES-F4). In this project, fabric shear modulus is measured in the KES-F1, and bending rigidity is measured in the KES-F2 and fabric roughness and friction coefficient are measured in the KES-F4. Three specimens are tested in each of the two orthogonal fabric directions; each fabric specimen has a size of 200mm x 200mm for all the tests conducted in the KES-F system. Average of three specimens in each direction are obtained (KES-F Manual).

3.2.2.1 Shear modulus obtained in the KES-F1

In the KES-F shear testing, a fabric specimen is held by two chucks having a gauge length of 50mm, and an extension force 4.9N/m is applied vertically onto fabric. A shear force is applied onto the fabric forwards and backwards within a maximum angle of 8°. A shear force (N/m)-shear angle (degree) curve is obtained in this process In the KES-F system (Hu, 2000), average slope of force-degree curve between $\pm 0.5^\circ$ and $\pm 2.5^\circ$ is used to evaluate fabric shear rigidity. In this study, this slope is used to calculate shear modulus and shear rigidity according to equation 5.20 in section 5.2.2.

3.2.2.2 Bending rigidity obtained in the KES-F2

Fabric pure bending property is measured in the bending tester (KES-F2). A fabric specimen is mounted on two fabric clamps with a gap of 10mm between them. The fabric specimen is bent at a constant bending deformation rate of $5 \text{ mm}^{-1}/\text{s}$ by moving one of the clamps, and a bending moment – curvature curve is obtained. In the KES-F system, the average slope of the bending moment-curvature curve between 0.5cm^{-1} and 1.5cm^{-1} is used to evaluate fabric bending rigidity (Hu, 2000). In this project, bending rigidity obtained in the KES-F system is calculated according to the equation 6.5 in section 6.1.3.

3.2.2.3 Fabric surface friction coefficient and fabric roughness obtained in KES-F4

In the surface tester KES-F4, a fabric specimen is mounted on the equipment horizontally with one fabric end being fixed at a winding drum and the other end being connected to a tension device of 400g (19.8N/m). Two metal sensors contact the fabric surface with the following constant normal forces: 50g for the friction sensor and 10g for the roughness sensor. During the rotation of the drum moving the fabric at a speed of 1mm/s, the fabric friction coefficient and its mean deviation is detected by friction sensor, and the geometrical surface roughness is detected by the roughness sensor.

3.2.3 Universal tensile tester (Titan)

Fabric elongations in unidirectional deformation under small extension force (2N/m and 4.9N/m) are obtained in a universal tensile tester, Titan, which is developed by James Heal Ltd, UK in this project. A fabric specimen with a width of 50mm is mounted on two fabric clamps with a gauge length of 50mm. The fabric specimen is extended at a constant speed of 0.2mm/s, and the fabric elongations when extension force is 2N/m and 4.9N/m are obtained in the force-extension curve recorded in Titan extension test.

3.2.4 Leeds University Fabric Handle Evaluation System (LUFHES)

The LUFHES system described in section 2.2.3 is used to evaluate the shear modulus and buckling property (e.g. critical buckling force) of fabric cylindrical shell in biaxial deformation processes, as well as the fabric-fabric self-friction properties (Mao and Taylor, 2012).

Each fabric is tested in two directions: warp/wale/MD and weft/course/CD for woven, knitted and nonwoven fabrics, respectively. For each direction, three fabric specimens are evaluated. Woven, knitted and nonwoven fabrics tested in each direction are denoted with a different initial letter. For example, woven fabric W1 in

warp direction is denoted as W1-p and in weft direction as W1-t; knitted fabric K2 in wale direction is labelled as K2-w and in course direction as K2-c; nonwoven fabric N1 in machine direction is denoted as N1-m and in cross direction as N1-c.

Before each test, usually a pre-tension of 2N/m is applied on fabric shells in their axial direction unless it is explicitly stated.

3.2.4.1 Shear modulus obtained in cyclic twisting test

In each fabric shell twisting test, each specimen is deformed in five twisting cycles. In each cycle of the twisting buckling process, the bottom end of the fabric shell is twisted to 5° at the speed of $0.5^\circ/\text{s}$ and then return back to the starting position while its upper end is fixed.

During the cyclic twisting test, the torques required to twist fabric shell and recover deformed fabric shell are measured and corresponding torque-degree curve is obtained. The twisting torque measured is employed to obtain the shear modulus of fabric (equation 5.35 in section 5.2.3). In addition, various energies consumed to deform the fabrics during the fabric deformation process are obtained (see section 2.2.3.1).

3.2.4.2 Energies and compression buckling Young's modulus obtained in cyclic axial compression buckling test

During each cyclic compression buckling test, each fabric shell specimen is deformed and recovered for five cycles. In each cycle of the compression buckling test, the upper end of the fabric shell is moved downwards to compress the fabric shell for 15mm at the speed of 1mm/s and then return back to its starting position while the bottom end is fixed. Fabric shells are deformed to have identical displacement (15mm) in each compression buckling-recovery cycle, dynamic forces required to compress the fabric shells and recover the deformed fabric shells in the compression buckling process are measured to obtain the corresponding force-displacement curves. The fabric critical buckling force (see section 6.1.1) and various energies consumed during the fabric buckling-recovery process (see section 2.2.3.1) are calculated from these compression buckling force-displacement curves.

3.2.4.3 Extension and friction test in LUFHES

In the extension and friction test, the upper end of fabric shell is pressed on the fabric surface of the fabric strip attached on upper sample holder by a strip of elastic band of fixed length. During the extension and friction test, the upper sample holder with the fabric strip attached on is dragged out of the inner surface of the fabric shell at a speed of 1mm/s for 20mm. When the extension force

equals to or greater than the static friction force existed between the two fabric surfaces, the relative movement between them takes place in the axial direction and the fabric to fabric self-friction force between the two pieces of identical fabric specimens is measured, the dynamic friction force-displacement curve is thus obtained to calculate the dynamic friction coefficient and fabric roughness accordingly.

3.3 Experimental design

The experiments to study the effect of pre-tensions on the compression buckling of fabric shells, the shear modulus, critical buckling force and fabric-fabric self-friction obtained in the LUFHES tests, and the comparison between mechanical properties obtained in LUFHES and those measured in the KES-F and FAST systems are shown in Table 3.2 to Table 3.5, respectively.

Table 3.2 Experiment for studying the effect of pre-tensions on the axial compression buckling of fabric shells

Purpose	To investigate the influence of pre-tension on energy consumption and fabric shell modulus during fabric compression buckling deformation; To determine suitable pre-tension in the LUFHES test.
Material	Six woven fabrics: W1, W4, W5, W10, W11 and W12 Five knitted fabrics: K2, K3, K5, K6 and K7 Eight nonwoven fabrics: N1, N2, N3, N4, N5, N6, N7 and N8
Instrument	LUFHES
Testing conditions	Five levels of pre-tension forces are used in this test: 0.8N/m, 1.2N/m, 1.6N/m, 2N/m and 4N/m.
Properties measured	Energies consumed to deform and recover fabric shells and compression Young's modulus of fabric shells during their deformation and recovery processes are obtained.

Table 3.3 Shear modulus measured in different systems (LUFHES, FAST and KES-F)

Purpose	To analyse the shear modulus obtained in the LUFHES shear test; To show the differences of the three systems (FAST, KES-F and LUFHES) in measuring fabric shear modulus, and their differences in discriminating fabrics in terms of shear rigidity.
Fabrics	Eleven woven fabrics: W1, W2, W3, W4, W6, W7, W8, W9, W10, W11 and W12 Seven knitted fabrics: K1, K2, K3, K4, K5, K6, K7 Four nonwoven fabrics: N1, N8, N10, N11
Instrument	LUFHES, FAST and KES-F
Properties measured	Shear modulus and shear rigidity

Table 3.4 Comparison of critical buckling force in the LUFHES buckling test and bending rigidity in the KES-F and FAST bending tests

Purpose	To determine if fabric critical buckling force measured in the LUFHES test and bending rigidity measured in the KES-F/FAST test in agreement in evaluation fabric stiffness.
Material	Eleven woven fabrics: W1, W2, W3, W4, W6, W7, W8, W9, W10, W11 and W12 Seven knitted fabrics: K1, K2, K3, K4, K5, K6, K7 Four nonwoven fabrics: N1, N8, N10, N11
Instrument	LUFHES, FAST and KES-F.
Properties measured	Critical buckling force of fabric is measured in axial compression buckling test in LUFHES; Bending rigidity of fabric is measured in standard bending test of the FAST and KES-F systems.

Table 3.5 Characteristics and differences of fabric friction coefficients and roughness measured in the LUFHES and the KES-F

Purpose	<p>To investigate the characteristics of fabric-fabric self-friction;</p> <p>To study the relationship of vibration in fabric-fabric self-friction curve with fabric surface structure and fabric roughness;</p> <p>To investigate the differences between fabric-fabric friction and fabric-sensor friction.</p>
Material	W1, W4, W7, W12, and N1
Instrument	LUFHES, and KES-F
Properties measured	Fabric friction coefficient and roughness are measured in the LUFHES and the KES-F system

Chapter 4 The influence of pre-tensions on energy consumption during cyclic axial compression processes

The energies consumed to form and recover specific types of fabric deformations in the compression buckling-recovery process of fabric cylindrical shells are used to quantify the deformations produced in the fabric shells during compression buckling-recovery processes (Mao and Taylor, 2012). The energy consumption in the compression buckling-recovery process depends on fabric structures which could be shown in fabric mechanical properties such as modulus. Textile fabrics are soft materials and its intrinsic structures and mechanical properties (e.g., fabric modulus) are affected by its initial states such as pre-tensions applied. Currently there is little research reported on how fabric mechanical properties and the energy consumption in its compression processes are influenced by pre-tensions applied.

In order to establish suitable pre-tensions applied on fabric shell in the LUFHES compression buckling tests, the influences of the pre-tensions on both the fabric structure changes which is represented by the fabric modulus and the amount of fabric deformations created which is represented by the energy consumed to generate specific deformations are studied in this chapter. The influences of pre-tensions on both the fabric structure changes (i.e., the compression buckling modulus of the fabric shells) and the amount of various deformations (represented by energy consumptions in corresponding deformations) of fabric cylindrical shells made from nineteen fabrics including woven fabrics, knitted fabrics and nonwovens are studied. The pre-tensions suitable for compression buckling measurement in LUFHES are discussed.

4.1 Materials and experiments

4.1.1 Fabric materials used in the experiments

Nineteen fabrics including six woven fabrics (W1, W4, W5, W10, W11 and W12), five knitted fabrics (K2, K3, K5, K6, K7) and eight nonwovens (N1-N8) are studied in this chapter, and their specifications are shown in Table 3.1. These fabrics have different fabric structures and have a wide range of mass per unit area and fabric thickness. Six woven fabrics have ripstop, plain weave and twill weave structures, their mass per unit area ranges from 58g/m² to 430g/m², thickness ranges from 0.1mm to 1.1mm. Five knitted fabrics have jersey, interlock and 1x1 rib structures; their mass per unit area is from 145g/m² to 400g/m², thickness from 0.7mm to 1.8mm. Eight nonwoven fabrics are produced from different technical processes including thermal bonding, hydroentanglement and spunbond technologies, their

mass per unit area ranges from 18g/m^2 to 90g/m^2 , thickness from 0.2mm to 1.9mm.

4.1.2 Axial compression buckling deformation experiment

The axial compression buckling deformation of fabric cylindrical shell made from the fabrics introduced in the section 4.1.1 is performed in LUFHES. The effect of pre-tension is analysed based on the energy consumed to generate and recover each type of buckling deformations. The energy consumption is calculated from compression force-displacement curves under different pre-tensions (Mao and Taylor, 2012).

In compression buckling process, fabric shell is deformed to have identical displacement (15mm) in each compression buckling-recovery cycle, the energy is stored in deformed yarns/fibres during compression process and is released to produce self-recovery in recovery process, and fabric shell is returned back to its original length by external force.

4.1.2.1 Levels of pre-tension forces applied on fabric shells

It is known that large pre-tension forces applied onto a fabric shell might permanently change the fabric structure, and small pre-tension forces, such as 0.4N/m (pre-tension force per unit circumference length of the fabric shell), will not straighten fabric shells having wrinkles. Therefore the smallest pre-tension force used in this study is 0.8N/m , and the five levels of pre-tension forces used in this research are, 0.8N/m , 1.2N/m , 1.6N/m , 2.0N/m and 4.0N/m . It is hoped that suitable pre-tensions applied on fabric shells in LUFHES tests are determined based on the study of the effect of pre-tensions on the fabric mechanical properties and energy consumed in the compression buckling-recovery deformation processes.

4.1.2.2 Approaches to study the effect of pre-tension forces on axial compression buckling of fabric shells

Two possible approaches could be adopted to design the experiment for studying the effect of pre-tensions on fabric shells:

1. First approach: Five compression buckling deformation tests are conducted by using five undeformed fabric specimens applied with five different pre-tension forces, respectively. This approach has the advantage of eliminating the accumulated effects of pre-tensions on fabric shells but possibly introduces errors incurred from the differences of the five fabric specimens such as different amount of unevenness, uniformity and undetectable defects;
2. Second approach: Five compression buckling deformation tests are conducted by using one fabric specimen but applied with five levels of pre-tension forces consecutively in five tests. Each of the five pre-tensions is applied on the buckling deformation test of the

same fabric shell in an order from the smallest to greatest pre-tensions. This approach uses one fabric specimen throughout the five tests, thus the errors incurred from the possible difference of fabric properties between different specimens in the five tests are minimized. However, this approach might have the problem of accumulated fabric structural changes due to both the consecutive pre-tensions applied on the fabric shell and accumulated fabric deformations generated in prior tests.

In order to determine which of the above two approaches is better for this study, a preliminary experiment of comparing the effect of the two approaches is conducted using one woven fabric (W11 in warp direction, W11-p), one knitted fabric (K2 in wale direction, K2-w) and one nonwoven fabric (N8 in MD, N8-m). The effect of pre-tension forces on the total energy consumption (A1cp1) in these three fabrics are shown in Figure 4.1 to Figure 4.3.

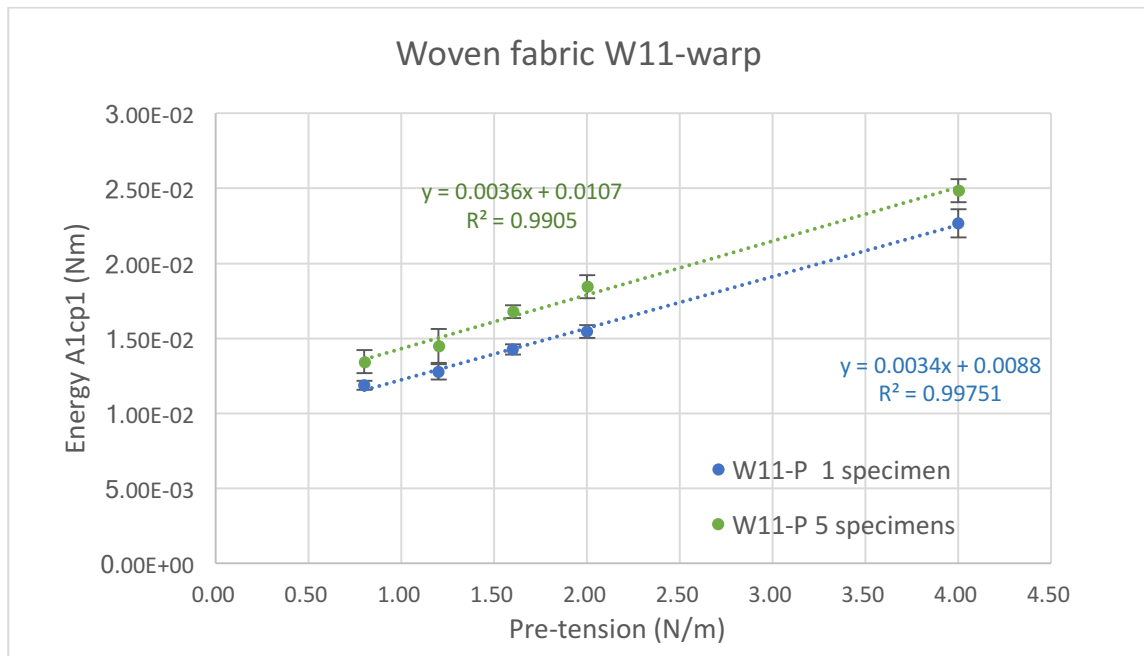


Figure 4.1 Influence of pre-tensions on the energy A1cp1 of woven fabric W11 in the warp direction

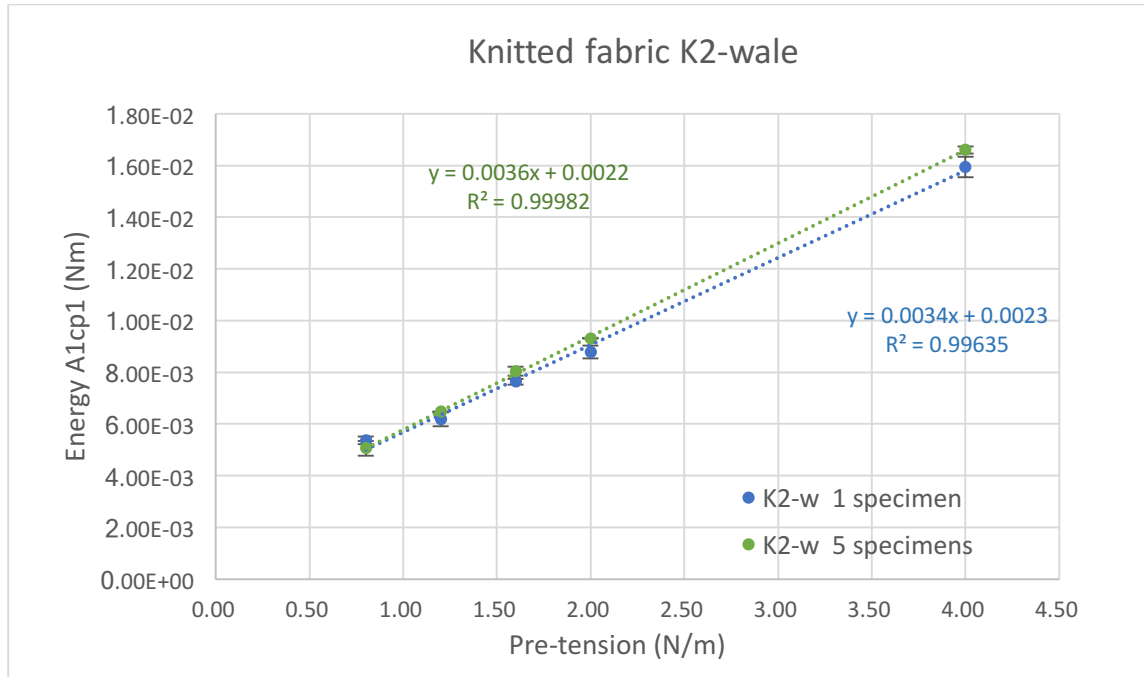


Figure 4.2 Influence of pre-tensions on the energy A1cp1 of knitted fabric K2 in the wale direction

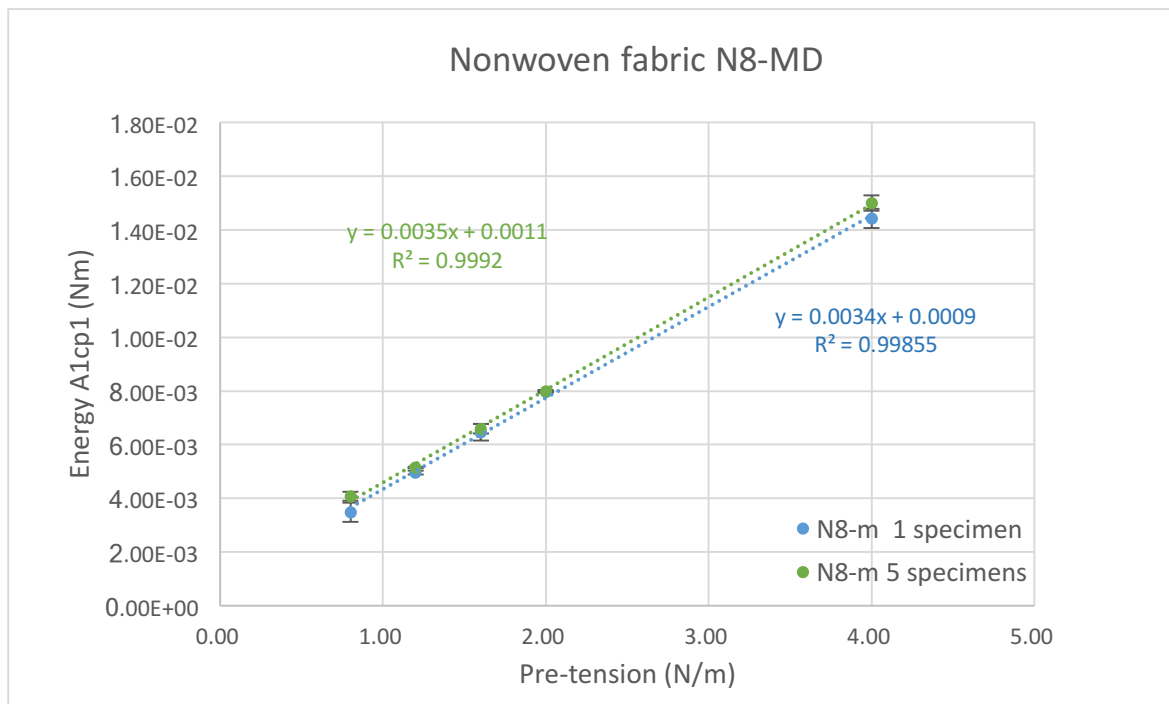


Figure 4.3 Influence of the pre-tensions on energy A1cp1 of nonwoven fabric N8 in the MD

It is shown that, for both nonwoven and knitted fabrics, the difference of energy consumptions in each of the applied pre-tension forces between the two approaches are small, while the differences of the energy consumptions of the woven fabrics in each of the applied pre-tension forces between the two

approaches are relatively greater. A possible reason is the accumulation of structural changes (e.g. permanent deformation or wrinkle) during compression buckling test has greater effect on woven fabric than on knitted or nonwoven fabrics. However, the trends of the energy A_{1cp1} increasing with the increase of pre-tension are almost identical for the two approaches for the three fabrics. For example, the slopes of the trendlines for two approaches of the three fabrics are nearly the same (0.0034 and 0.0036 for W11-warp, 0.0034 and 0.0036 for K2-wale, 0.0034 and 0.0035 for N8-MD).

However, data which strays away from the main trend (marked in the red circle in Figure 4.4) of the energy consumption appears when using the first approach (using five fabric specimens in the tests), while such error hardly appears when the second approach (one fabric specimen is used throughout the five tests) is used.



Figure 4.4 Data which does not follow the main trend appears in testing using five specimens in five tests

As shown in Figure 4.4, data which does not follow the main trend appears in the test of a W11-p specimen having pre-tension of 1.2N/m. In a repeat test of using another undeformed fabric specimen, the data obtained appears to be the same as shown in Figure 4.1. It is believed that the reason of this data strays away from the correct trendline is due to either the difference between fabric specimens or the differences in preparation of fabric shells. Therefore the second approach of using one fabric shell specimen throughout five tests having different pre-tensions is adopted in this study to avoid the errors produced due to using different

specimens (i.e., the first approach). In addition, as shown in Figure 4.1-Figure 4.3, the standard deviations for woven, knitted and nonwoven samples are very small which means the LUFHES results have good reproducibility. Thus, one specimen for each direction of fabric is used to study the influence of pre-tensions on energy consumption during cyclic axial compression processes.

4.2 The influences of pre-tension forces on the energy consumed to deform undeformed fabric shells (A1cp1)

The force-displacement curve of the compression buckling deformation of a fabric shell is shown in Figure 4.5. The compression force increases with the compression displacement rapidly before buckling occurs, then decreases gradually in the post-buckling stage. As discussed in section 2.2.3.1, the area A1cp1 (shaded area in Figure 4.5) represents the overall energy consumed to deform an undeformed fabric shell in the first cycle of cyclic compression buckling processes (Mao and Taylor, 2012).

The modulus of fabric shells in the first compression buckling cycle before buckling point during compression buckling process, denoted as E_1 , is defined as the compression force required to compress unit area of fabric to unit strain (line AB in Figure 4.5) (LUFHES Software).

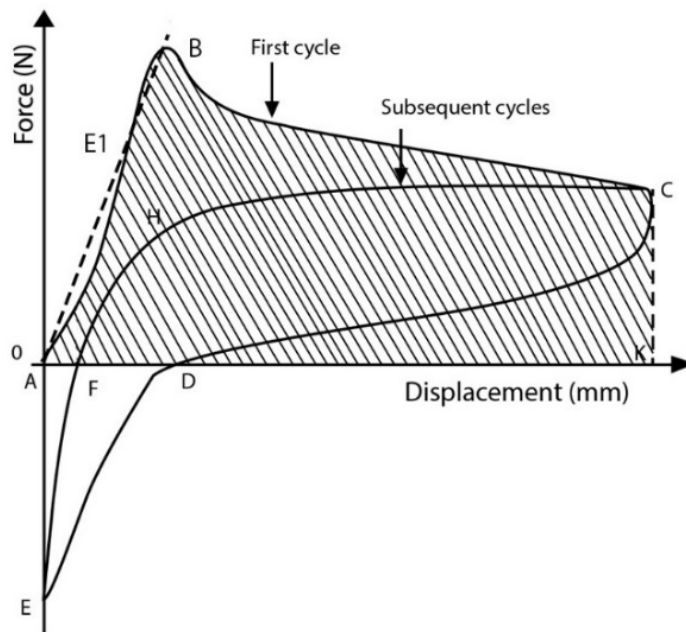


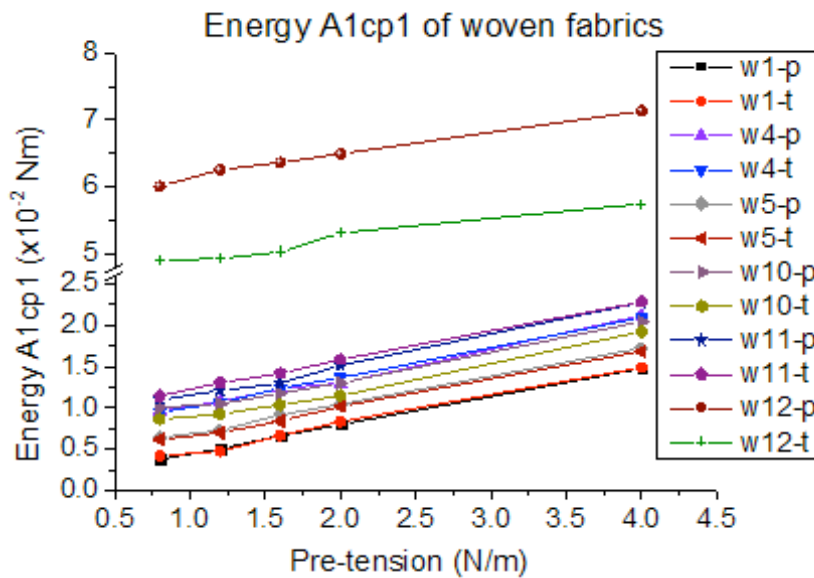
Figure 4.5 Force-displacement curve of the compression buckling deformation

4.2.1 Energy consumed to deform undeformed fabric shells (A1cp1)

The influences of pre-tensions on A1cp1 of woven fabrics, knitted fabrics and nonwoven fabrics are shown in Figure 4.6 (a), (b) and (c), respectively, and the linear regression equations between pre-tensions and the energy A1cp1 are shown in Table 4.1.

It is found from Figure 4.6 and Table 4.1 that energy consumed to deform undeformed fabric shells (A1cp1) increases linearly with the increase of the pre-tensions. This indicates that the energy consumed to deform undeformed fabric shells increases linearly with the increase of pre-tension applied on fabrics.

The slope of linear regressions equations shown in Table 4.1 represents the relationship between energy A1cp1 and pre-tension, greater slope means energy A1cp1 increases rapidly with the increase of pre-tension. It is shown that the slopes of linear regression equations are between 2.5 and 3.7 for woven, knitted and nonwoven fabrics. This suggests that the energy A1cp1 increases at similar rates with the increase of pre-tension for woven, knitted and nonwoven fabrics.



(a)

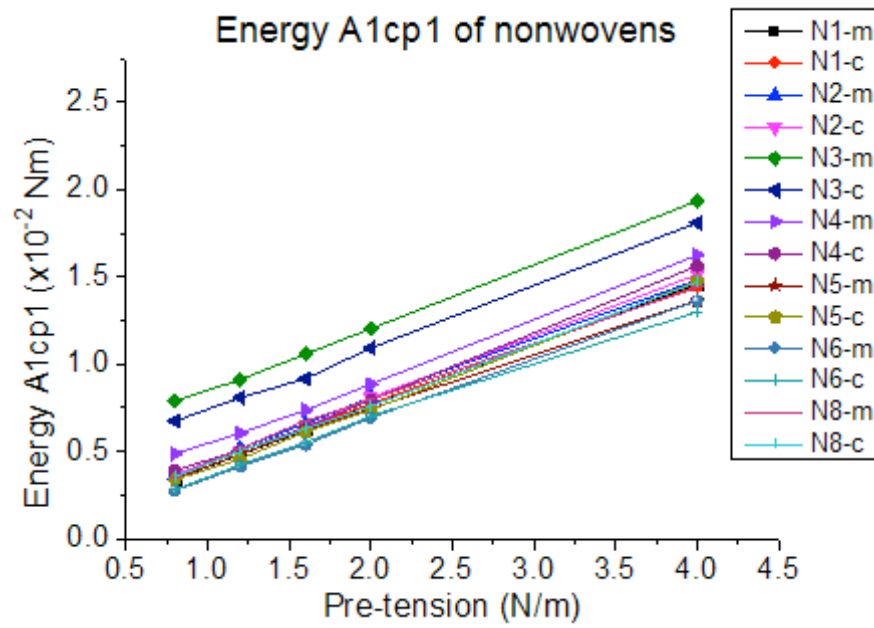
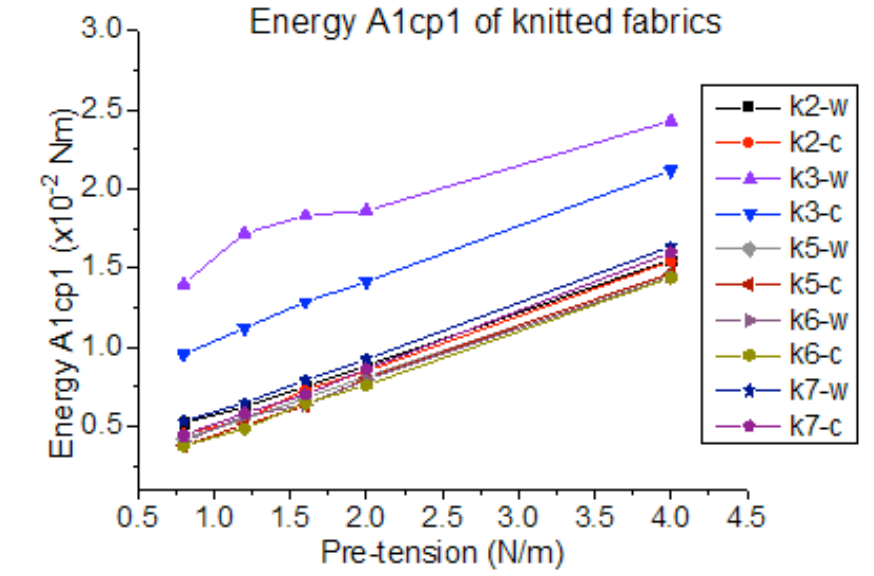


Figure 4.6 The influences of pre-tensions on overall energy (A1cp1) consumed to produce deformations in fabric shells

Table 4.1 Linear regression equations of relationship between pre-tension (N/m) and A1cp1 (mJ)

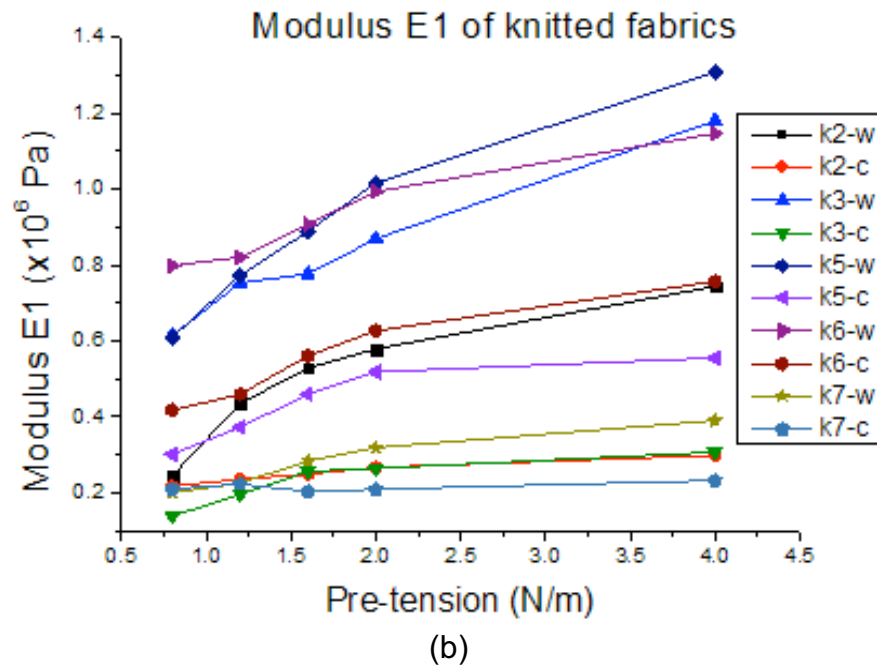
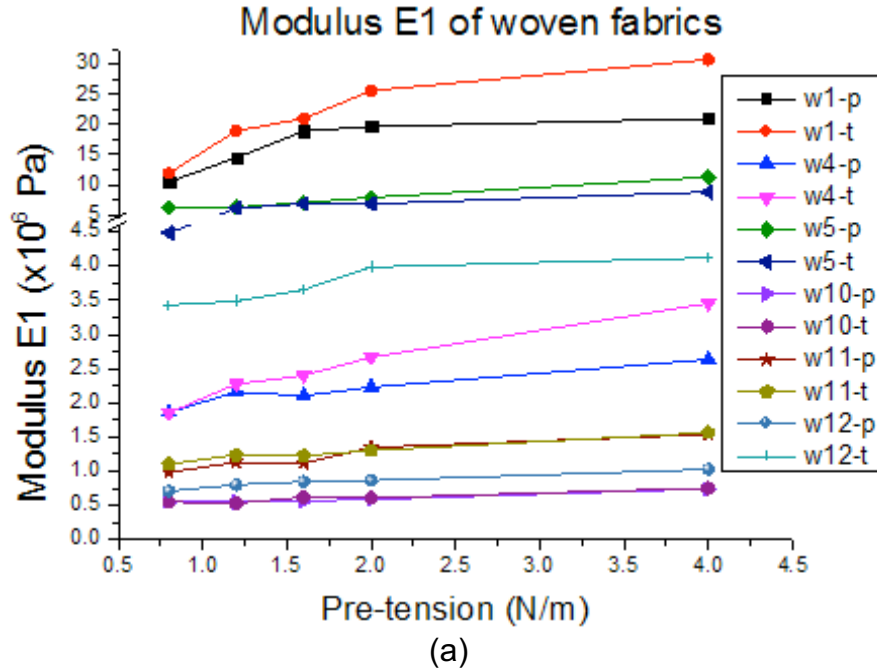
Fabric	Warp/wale/MD		Weft/Course/CD	
	Linear regression equation	R ²	Linear regression equation	R ²
W1	Y= 2.91X +1.73	0.99	Y= 3.44X +1.15	0.99
W4	Y= 3.62X +6.41	0.99	Y= 3.59X +6.50	1.00
W5	Y= 3.43X +3.52	1.00	Y= 3.41X +3.15	0.98
W10	Y= 3.37X + 6.66	0.99	Y= 3.42X +5.2	0.99
W11	Y= 3.77X +7.55	0.99	Y= 3.54X + 8.67	1.00
W12	Y= 3.35X + 58.09	0.99	Y= 2.78X + 46.58	0.96
K2	Y= 3.26X + 2.40	1.00	Y= 3.46X +1.58	0.91
K3	Y= 2.92X +12.88	0.95	Y= 3.59X + 6.88	1.00
K5	Y= 3.25X +1.59	1.00	Y= 3.42X +1.01	0.86
K6	Y= 3.22X +1.49	1.00	Y= 3.34X +0.99	0.94
K7	Y= 3.48X +2.39	1.00	Y= 3.62X +1.41	1.00
N1	Y= 3.48X +0.66	1.00	Y= 3.39X +0.91	1.00
N2	Y= 3.47X +1.01	1.00	Y= 3.59X +0.78	1.00
N3	Y= 3.62X + 4.85	1.00	Y= 2.57X + 3.74	1.00
N4	Y= 3.60X + 1.77	1.00	Y= 3.72X +0.66	1.00
N5	Y= 3.16X +1.06	0.99	Y= 3.58X +0.37	1.00
N6	Y= 3.40X +0.04	1.00	Y= 3.15X +0.47	1.00
N8	Y= 3.34X +1.15	1.00	Y= 3.48X +0.76	1.00

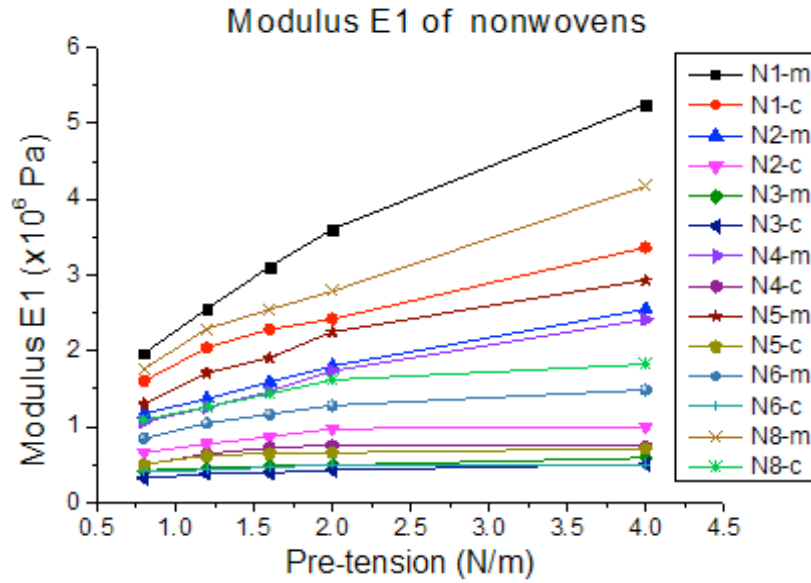
4.2.2 Compression buckling Young's modulus before undeformed fabric shell buckles (E1)

Energy consumption during fabric deformations relies on the fabric structures. Hearle and Shanahan (Hearle and Shanahan, 1978; Shanahan and Hearle, 1978) found that the energy consumed in fabric deformations was related to fabric structural parameters such as yarn diameter, crimp height and thread spacing, and the state of fabric under imposed external forces can be determined by using minimum energy method. It is known that pre-tension exerted on fabrics could change their micro-structures, e.g., crimp of woven fabrics, loop structure of knitted fabrics, and fibre orientation of nonwoven fabrics (Bueno, M. et al., 2008; Afroz and Siddika, 2014), but it is difficult to directly measure those fabric structural changes under pre-tensions. Young's modulus is a parameter to represent the intrinsic structural changes of a solid material, the relationships between pre-tensions and compression buckling Young's modulus of undeformed

fabric shells (E1) during compression buckling process are investigated in this section to show the fabric structural changes under different pre-tensions.

The influences of pre-tensions on E1 of woven, knitted and nonwoven fabrics are shown in Figure 4.7(a) (b) (c), respectively.





(c)

Figure 4.7 The influences of pre-tensions on compression Young's modulus (E1) before buckling occurs in the first compression cycle

It is shown in Figure 4.7 that, regardless of fabric types, compression buckling Young's modulus E1 gradually increases with the increase of the pre-tension applied on fabric. This indicates that pre-tensions have changed fabric internal structure and have stiffened the fabrics.

It was noticed that fabrics having smaller thickness (for example, woven fabrics W1 and W5, knitted fabrics K6 and K5, and nonwoven fabric N1) always have greater E1 than thicker fabrics in both directions, this is on contrast with the influences of pre-tensions on energy consumed to compress fabric shells, where thicker and heavier fabrics (fabrics W12, K3 and N3) consume more energy than other fabrics.

It was also noticed that, for fabric already having permanent creases and wrinkles, the linear relationship between pre-tensions and modulus E1 was not observed. The influence of pre-tensions on E1 of a flash spun and thermally point bonded Tyvek nonwoven fabric (N7) is shown in Figure 4.8. The creases formed on this Tyvek fabric cannot be eliminated even under greater pre-tensions in the test, so five fabric specimens were used in the tests.

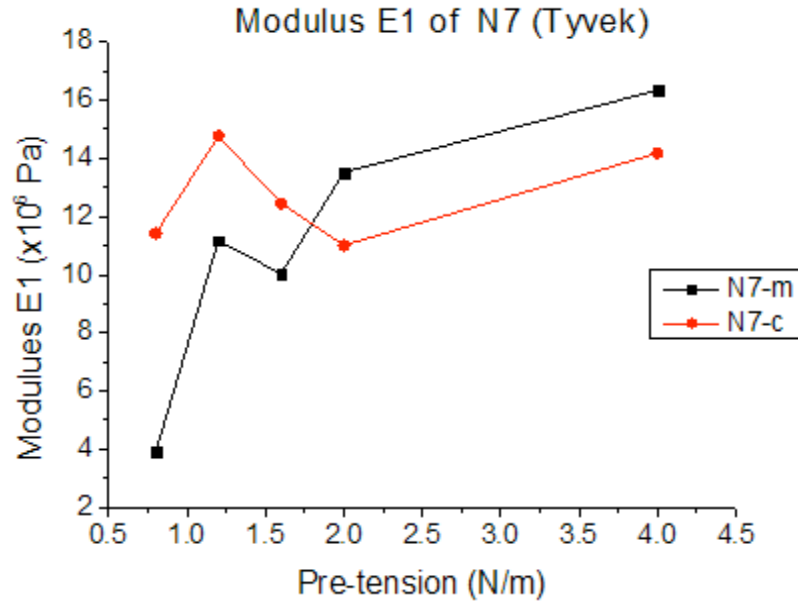


Figure 4.8 Relationship between pre-tensions and E1 of flash spun and thermally point bonded Tyvek nonwoven fabric, N7

It was shown in Figure 4.8 that E1 of the fabric shell made from this creased Tyvek fabric varied with the increase of pre-tension without a clear linear trend against the increase of pre-tension which was in contrast that observed with the other nonwoven fabrics. It was concluded that the pre-tension applied cannot remove all of the fabric creases and fabrics having different levels of creasing could lead to misleading conclusions; therefore, fabric having such stubborn creases should not be used in the testing.

4.2.3 Relationship between modulus E1 and energy A1cp1

It is known that pre-tensions applied on fabrics change fabric structures and result in increased friction between yarns/fibres and increased yarn/fibre orientation in the loaded directions (Afroz and Siddika, 2014; Bueno, M. et al., 2008). It is also shown in the sections 4.2.1 and 4.2.2 that both modulus E1 and energy A1cp1 increase with the increase of pre-tension, it is thus reasonable to make the hypothesis that the increase of energy consumed to buckle undeformed fabric shells is due to the changes of fabric micro-structure (represented by changes of modulus E1) with the increase of pre-tension. Therefore the relationship between modulus E1 and energy A1cp1 is investigated to show how the changes of modulus E1 link with the change of energy A1cp1.

The effect of pre-tension on the fabric structural changes varies with fabric types (woven, knitted and nonwoven fabrics) and are summarised in the Table 4.2.

Table 4.2 Structural changes with applied pre-tension for woven, knitted and nonwoven fabrics.

Fabric type	Effect of pre-tension on fabric structure
Woven fabric	<ul style="list-style-type: none"> • Yarns along loaded direction are slightly straightened; • Crimp of yarn along loaded direction is reduced. The yarns are compacted due to change of crimp, so both compression force and contact area increase at contact point between yarns/fibres and friction resistant is increased (Afroz and Siddika, 2014).
Knitted fabric	<ul style="list-style-type: none"> • Decrease of stitch bending in the thickness direction, bending of yarn decrease and both compression force and contact area increase at contact point between yarns and friction resistant is increased (Bueno, M. et al., 2008). • For weft knitted fabrics, loop legs come close when tension is along wale direction, loop and yarn orientation increase along loaded direction (Bueno, M. et al., 2008). Yarn orientation at loop head increases when tension is applied along course direction.
Nonwoven fabric	<ul style="list-style-type: none"> • Fibres reorient with applied tension and increase the preference of fibres towards loading direction (Bueno, M. et al., 2008). Reorientation is due to bent fibres being straightened by pre-tensions, therefore the contact areas between fibres and the compression force at contact areas will increase and result in an increased friction between fibres.

During the axial compression buckling process of a fabric with pre-tension applied, there is one specific position that the pre-tension of the fabric shell is zero. However, due to the viscoplastic nature of textile fabrics, there are residual structural changes induced by the pre-tensions still remain in the fabric. The residual structural changes maintain the additional compressive forces induced by the pre-tensions at the contact points between yarns/fibres and the increased yarn/fibre orientation.

It is known that yarns/fibres in fabrics are moved and bent (Brenner and Chen, 1964) during buckling of fabric. In pre-buckling process, external force is smaller than critical buckling force, only axial deformation exists in fabric structure and yarns/fibres are moved without bending deformation. Because of the increased friction between yarns/fibres induced by the pre-tensions, greater external force is required to move and bend them. In addition, greater external force is required to buckle fabric due to the increased orientation preference of yarns/fibres in longitudinal direction under greater pre-tensions and this leads to greater critical buckling force. Therefore a steeper force-displacement curve is obtained before buckling occurs, and a greater E_1 is obtained.

Fabric deformations in post-buckling process is similar to fabric bending, and both bending and buckling involve bending rigidity (Wright, 2005). As mentioned above, greater pre-tensions result in greater internal friction forces which increase the resistance to fabric bending (Grosberg and Swani, 1966b). Thus, it is anticipated that greater pre-tensions would lead to greater bending rigidity as well as greater buckling forces, and greater energy (A_{1cp1}) would be consumed in post-buckling process to deform fabric shell.

The theoretical relationship between $E1$ and A_{1cp1} can be obtained when the axial compression buckling force-displacement curve is simplified as a trapezoid area as shown in Figure 4.9.

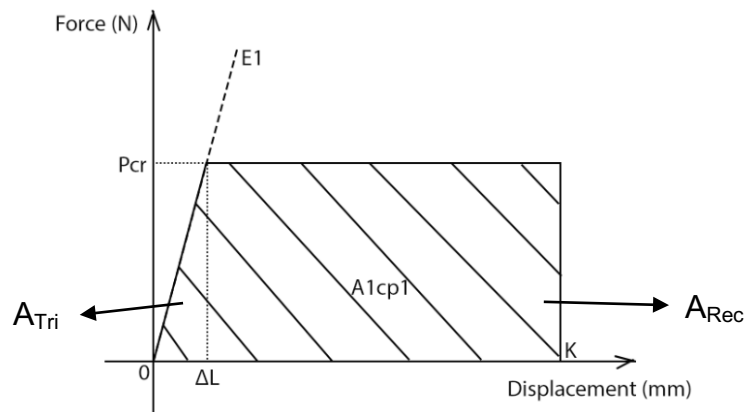


Figure 4.9 Simplified ideal model of relationship between $E1$ and A_{1cp1}

In Figure 4.9, A_{1cp1} equals to the trapezoid area including a triangular area (A_{Tri}) and a rectangular area (A_{Rec}). $E1$ is calculated, according to its definition in section 4.2.1, by using the area of triangular (A_{Tri}).

$$E1 = \frac{\sigma}{\epsilon} = \frac{\frac{P_{cr}}{2\pi Rt}}{\frac{\Delta L}{L}} = \frac{P_{cr} \cdot L}{\Delta L \cdot 2\pi Rt} = \frac{L}{2\pi Rt} \cdot \frac{P_{cr} \cdot \Delta L}{\Delta L^2} = \frac{L}{2\pi Rt} \cdot \frac{2A_{Tri}}{\Delta L^2} = \frac{L \cdot A_{Tri}}{\pi Rt \Delta L^2} \dots\dots (4.1)$$

$$A_{Tri} = A_{1cp1} - A_{Rec} = A_{1cp1} - (OK - \Delta L)P_{cr} \dots\dots\dots (4.2)$$

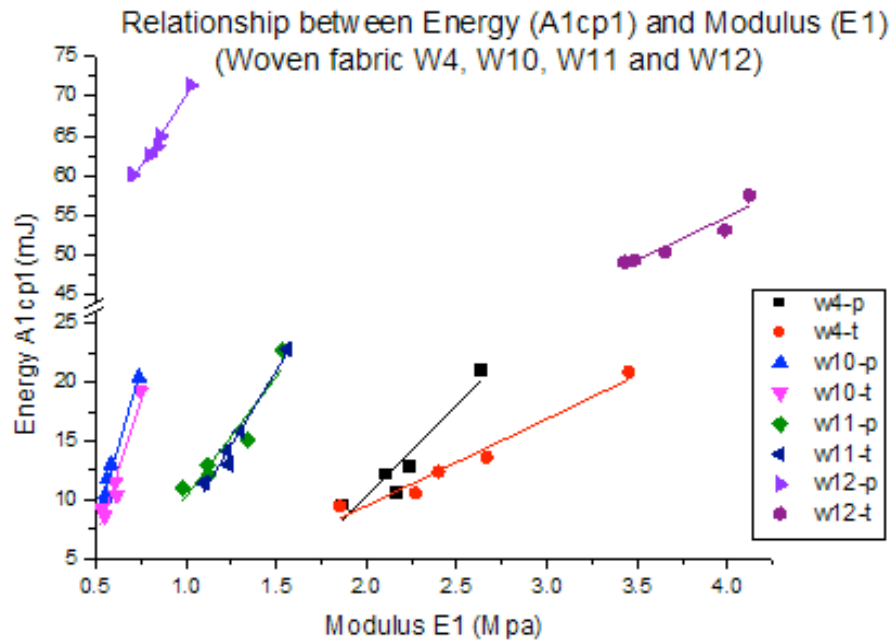
Therefore,

$$E1 = \frac{L \cdot [A_{1cp1} - (OK - \Delta L)P_{cr}]}{\pi Rt \Delta L^2} \dots\dots\dots (4.3)$$

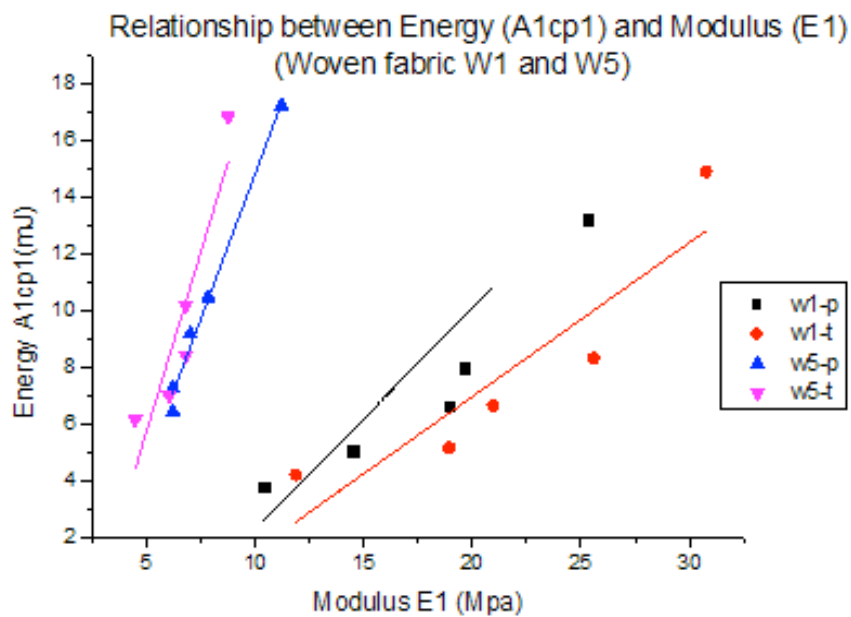
Where L and R are the original length and radius of fabric cylindrical shell, respectively; OK is the maximum compression displacement in compression buckling test. They are known constants in the fabric shell axial compression test, t is the fabric thickness. P_{cr} and ΔL are the fabric critical buckling force and corresponding displacement, respectively, and will be determined in the compression buckling measurement.

It is apparent in equation 4.3 that the compression buckling Young's modulus E_1 is proportional to A_1cp_1 , the energy consumed to deform the fabric shell.

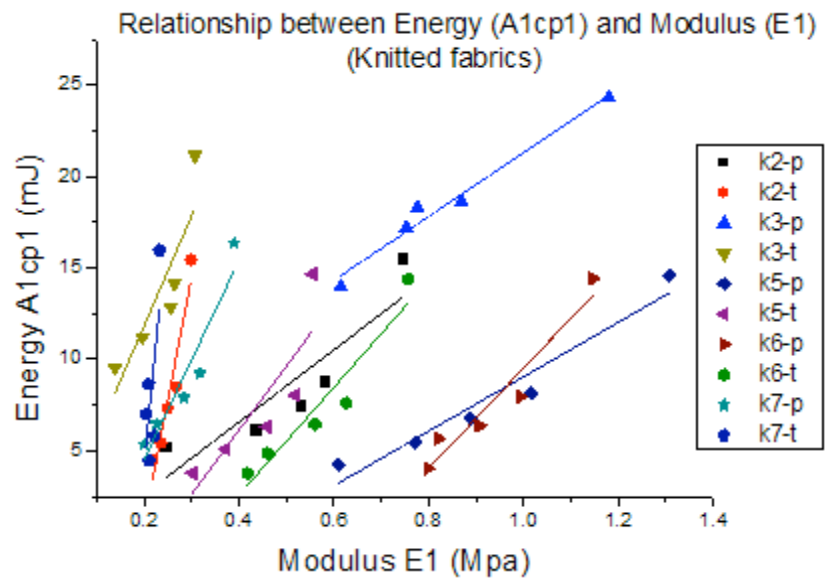
For the fabric shells made from the 19 fabrics described in the section 4.1.1, the relationship between axial compression modulus E_1 and corresponding compression energy, A_1cp_1 , measured during compression buckling tests are shown in Figure 4.10(a) (b) (c) (d).



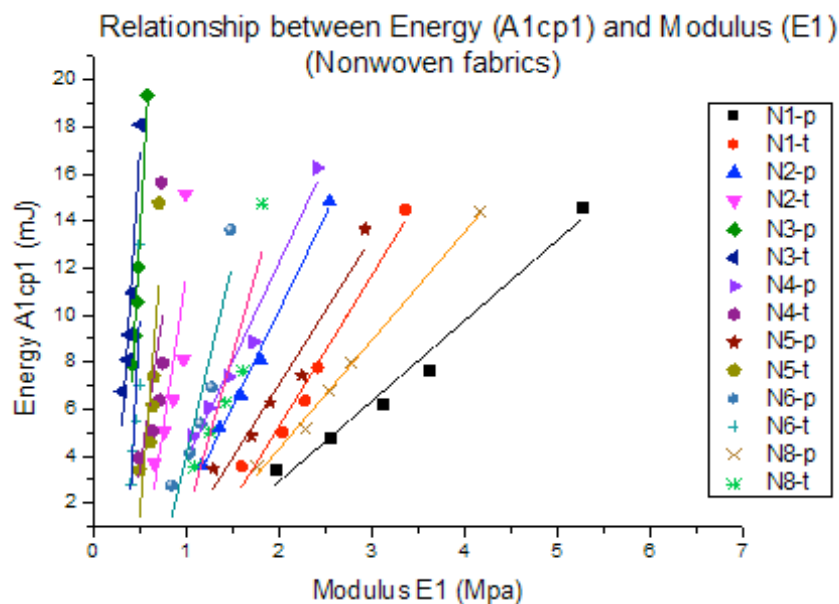
(a)



(b)



(c)



(d)

Figure 4.10 Relationship between energy A1cp1 and modulus E1 for woven, knitted and nonwoven fabrics

It is shown in Figure 4.10 that, energy A1cp1 increases almost linearly with the increase of modulus E1 for all of woven, knitted and nonwoven fabrics tested. We have three observations below:

- (1) Greater pre-tensions stiffen fabrics and lead to both greater compression modulus of fabric shells and greater energy consumed to deform the fabric shells;

- (2) The compression Young's modulus are linearly correlated to the energy consumed to deform the fabric shells measured during compression buckling tests, the linear regression equations and R^2 shown in Table 4.3 are between 0.80 and 0.99 for all woven fabrics, between 0.70 and 0.98 for knitted fabrics (except K7-c), between 0.65 and 1.0 for nonwoven fabrics (except N4-CD);
- (3) The slope of linear equation shown in Table 4.3 represents the increasing rate of A1cp1 against the increase of modulus E1. As shown in Table 4.3, slopes of regression equations vary in a wide range from 0.55 (W1-weft) to 264.29 (K7-course). Greater slope suggests A1cp1 increases rapidly with the increase of E1, which means the energy A1cp1 is sensitive to the change of fabric structures.

Table 4.3 Linear regression equation of relationship between A1cp1 (mJ) and E1 (MPa)

Fabrics	Warp/wale/MD		Weft/Course/CD	
	Linear regression equation	R^2	Linear regression equation	R^2
W1	$Y = 0.62X - 3.65$	0.91	$Y = 0.55X - 4.11$	0.82
W4	$Y = 15.32X - 20.26$	0.90	$Y = 7.40X - 5.32$	0.96
W5	$Y = 2.04X - 5.65$	0.99	$Y = 2.53X - 6.96$	0.85
W10	$Y = 52.98X - 18.70$	0.98	$Y = 47.87X - 17.51$	0.93
W11	$Y = 20.40X - 10.13$	0.90	$Y = 25.51X - 17.32$	0.97
W12	$Y = 35.74X + 34.26$	0.98	$Y = 10.98X + 10.94$	0.90
K2	$Y = 19.77X - 1.35$	0.80	$Y = 134.04X - 25.77$	0.93
K3	$Y = 17.45X + 3.85$	0.98	$Y = 59.88X - 0.15$	0.77
K5	$Y = 14.90X - 5.88$	0.94	$Y = 35.10X - 7.93$	0.73
K6	$Y = 27.37X - 17.87$	0.94	$Y = 29.40X - 9.18$	0.92
K7	$Y = 54.37X - 6.37$	0.90	$Y = 264.29X - 48.60$	<u>0.47</u>
			$Y = 31142X^2 - 13325X + 1430.3$	0.83
N1	$Y = 3.43X - 3.95$	0.98	$Y = 6.43X - 7.62$	0.97
N2	$Y = 8.12X - 6.10$	1.00	$Y = 26.41X - 14.89$	0.69
N3	$Y = 70.27X - 22.37$	0.99	$Y = 61.37X - 14.13$	0.93
N4	$Y = 8.42X - 4.66$	0.98	$Y = 26.83X - 10.19$	<u>0.39</u>
			$Y = 161.84X^2 - 174.72X + 50.70$	<u>0.44</u>
N5	$Y = 6.25X - 5.48$	0.96	$Y = 47.50X - 22.55$	0.67
N6	$Y = 16.46X - 12.57$	0.87	$Y = 76.26X - 28.69$	0.66
N8	$Y = 4.62X - 4.95$	1.00	$Y = 13.87X - 12.59$	0.85

Table 4.4 Extension of fabrics in both direction under 2N/m

Fabric	Extension (%) under 2N/m	
	Wale/MD	Course/CD
K2	1.34	3.52
K3	0.15	0.89
K7	1.21	7.64
N4	1.37	5.13
N5	2.61	12.01
N6	4.24	38.3

It is noticed in Table 4.3 that some knitted fabrics and nonwoven fabrics have huge differences between the slopes of linear regression equations at two fabric directions, such as the slopes of knitted fabric K2, K3 and K7 (K3 and K7 are 1x1 rib knitted fabrics) and thin aperture hydroentangled nonwoven fabric N5 and N6. Their slopes in the course/CD direction are much greater than the slopes in the wale/MD direction. A common characteristic of these fabrics is that all of them have greater extensibility in course/CD direction than that in wale/MD direction as shown in Table 4.4.

It is also noticed that correlation coefficient, R^2 , of linear equation for fabric K7 in course direction is significantly smaller ($R^2=0.47$) than that of quadratic equation ($R^2=0.83$); while nonwoven fabric N4 in CD has small R^2 in both linear equation ($R^2=0.39$) and quadratic equation ($R^2=0.44$). The common characteristic of these two fabrics is their greater extensibility (see Table 4.4).

As a summary, it is thus concluded that, for fabrics having greater extensibility, the energy consumption during their fabric shell compression buckling process is very sensitive to their fabric structural changes, and might not have linear relationship between energy consumption ($A1cp1$) and modulus ($E1$) with the increase of pre-tension. In addition, applying pre-tension leads to the change of fabric internal structure which is indicated by the increase of fabric compression modulus and this corresponds to the increase of the energy consumed to deform fabrics.

4.3 The influences of pre-tensions on energy consumed to deform recovered fabric shells (A1)

Fabric shell is deformed and recovered in the first cycle of buckling-recovery process, but only part of the deformations could be recovered in the recovery phase. Permanent deformations remained in the fabric shells affect consecutive fabric deformations in the 2nd-5th cycles, and lead to less energy consumed to deform recovered fabric shells in 2nd-5th cycles which is represented by A1 (shaded area in Figure 4.11) (Mao and Taylor, 2012).

The Young's modulus of fabric shell in the 2nd-5th compression buckling cycle before buckling point (H) is denoted as E2, it is defined as the compression force required to compress unit area of fabric to unit strain in the 2nd-5th cycle (line FH in Figure 4.11) (LUFHES Software).

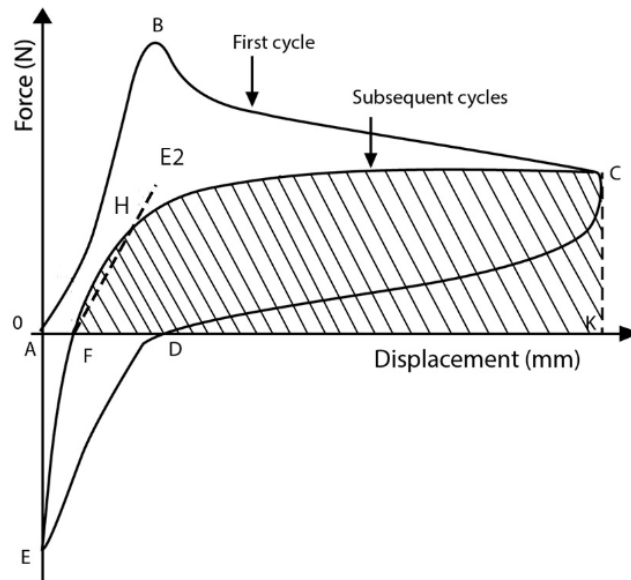
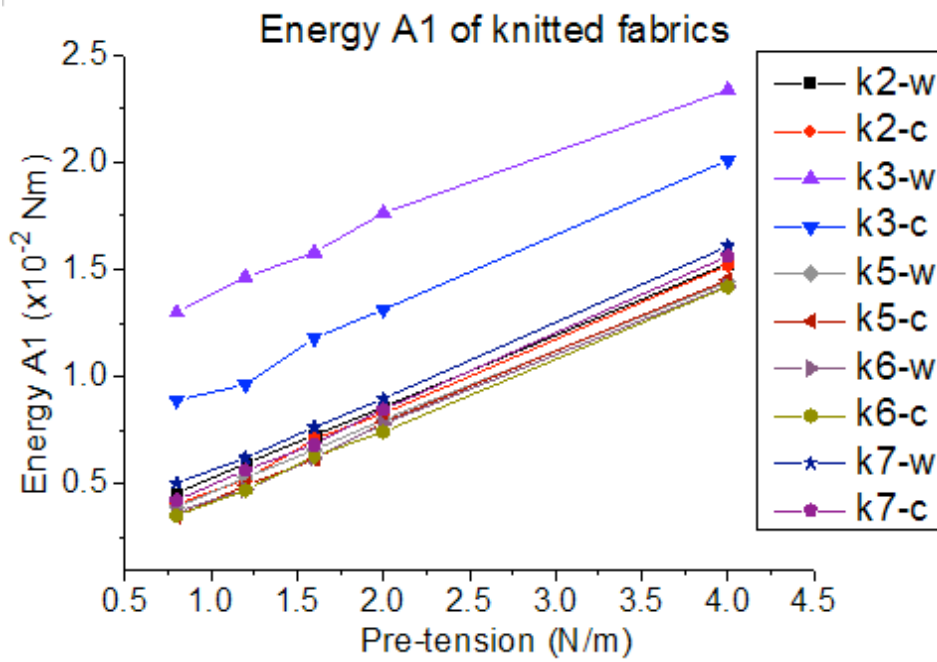
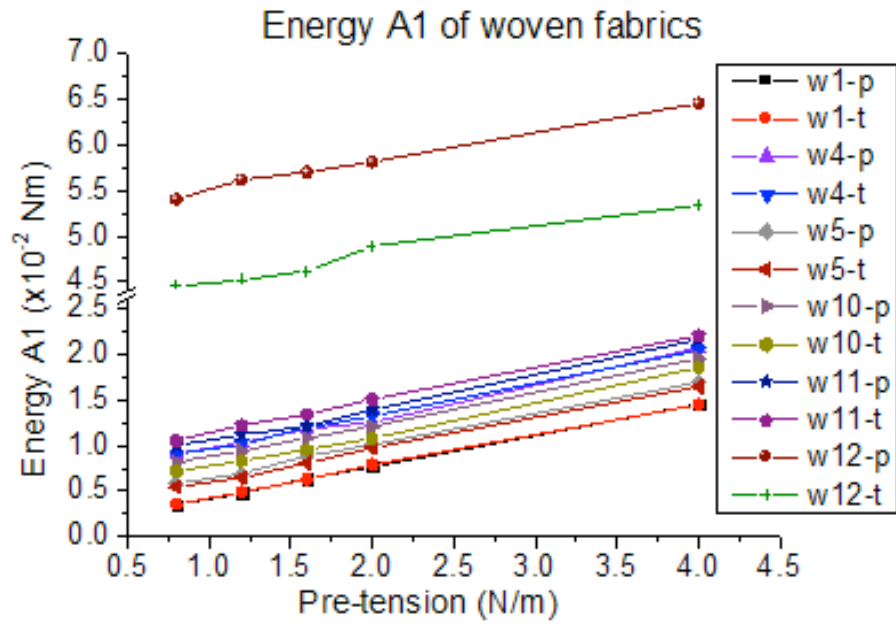
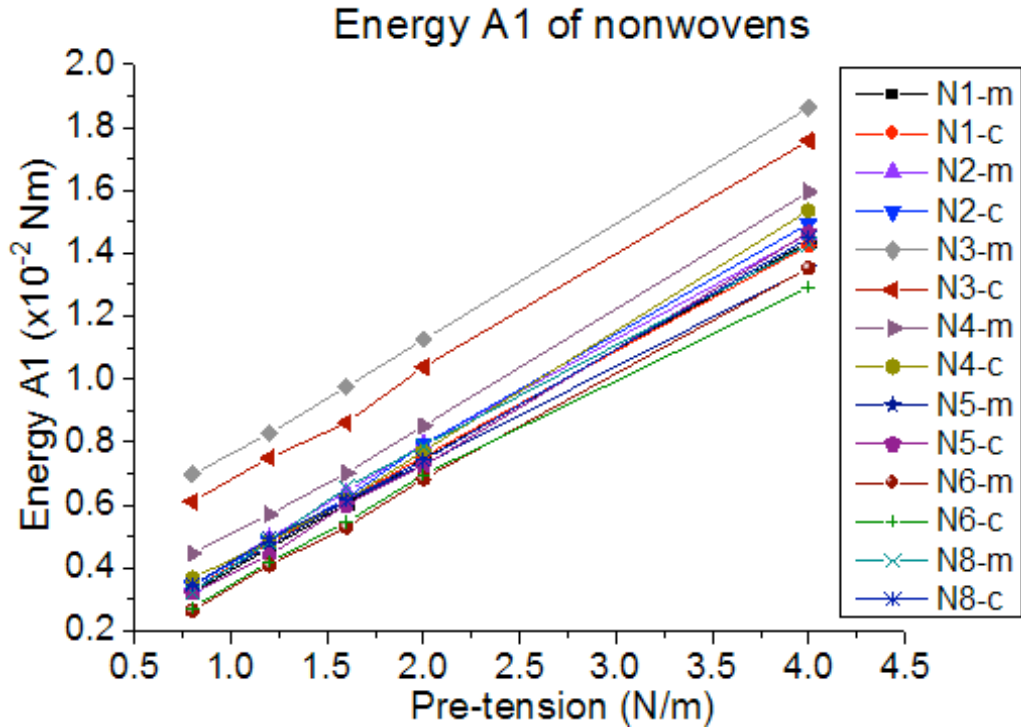


Figure 4.11 Energy A1 and modulus E2 obtained in the 2nd-5th cycles compression buckling deformations

4.3.1 Energy consumed to deform recovered fabric shells (A1)

The influences of pre-tensions on A1 for woven, knitted and nonwoven fabrics are shown in Figure 4.12 (a), (b) and (c), respectively. Similar to A1cp1, the energy A1 increases linearly with the increase of pre-tension (see Table 4.5), and greater pre-tension leads to greater energy consumed to deform recovered fabrics.





(c)

Figure 4.12 The influences of pre-tension on the energy consumed to deform recovered fabric shells (A1)

It is shown in Table 4.5 that the slopes of linear regression equations are between 2.8 and 3.8, and do not have significant difference between woven, knitted and nonwoven fabrics. These slopes represent the increasing rate of energy A1 with the increase of pre-tension, it thus suggests that the energy A1 increases at similar rates with the increase of pre-tension for woven, knitted and nonwoven fabrics.

Table 4.5 (1) Linear regression equations of relationship between pre-tension (N/m) and A1 (mJ) of woven fabrics

Fabric	Warp/wale/MD		Weft/Course/CD	
	Linear regression equation	R ²	Linear regression equation	R ²
W1	Y= 3.44X + 0.77	1.00	Y= 3.41X + 0.87	1.00
W4	Y= 3.64X + 5.88	0.99	Y= 3.59X +6.06	1.00
W5	Y= 3.48X +3.03	1.00	Y= 3.48X + 2.55	1.00
W10	Y= 3.57X + 5.14	1.00	Y= 3.60X +3.96	1.00
W11	Y= 3.68X + 6.68	0.99	Y= 3.56X + 7.80	1.00
W12	Y= 3.17X + 51.86	0.99	Y= 2.86X + 42.13	0.97

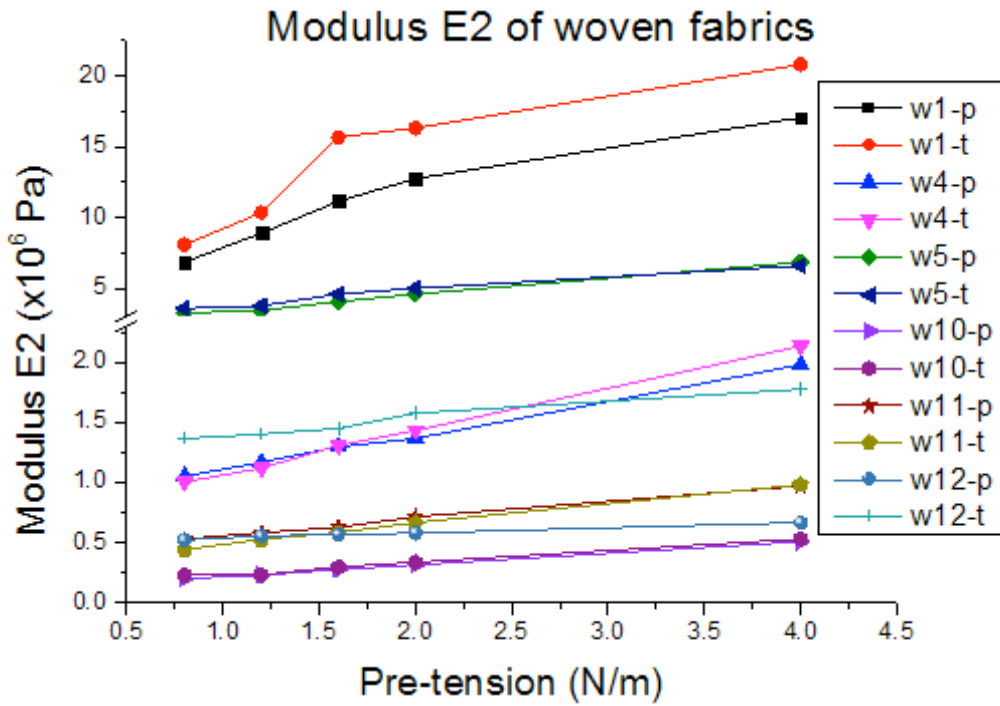
Table 4.5 (2) Linear regression equations of relationship between pre-tension (N/m) and A1 (mJ) of knitted and nonwoven fabrics

K2	$Y = 3.34X + 1.91$	1.00	$Y = 3.50X + 1.23$	1.00
K3	$Y = 3.20X + 10.73$	0.99	$Y = 3.57X + 5.84$	1.00
K5	$Y = 3.28X + 1.34$	1.00	$Y = 3.45X + 0.75$	1.00
K6	$Y = 3.33X + 0.92$	1.00	$Y = 3.35X + 0.79$	1.00
K7	$Y = 3.48X + 2.09$	1.00	$Y = 3.57X + 1.29$	1.00
N1	$Y = 3.48X + 0.46$	1.00	$Y = 3.40X + 0.67$	1.00
N2	$Y = 3.47X + 0.81$	1.00	$Y = 3.60X + 0.56$	1.00
N3	$Y = 3.66X + 3.94$	1.00	$Y = 3.60X + 3.11$	1.00
N4	$Y = 3.63X + 1.37$	1.00	$Y = 3.70X + 0.44$	1.00
N5	$Y = 3.17X + 0.91$	0.99	$Y = 3.61X + 0.18$	1.00
N6	$Y = 3.40X + 0.04$	1.00	$Y = 3.16X + 0.39$	1.00
N8	$Y = 3.40X + 0.82$	1.00	$Y = 3.43X + 0.69$	1.00

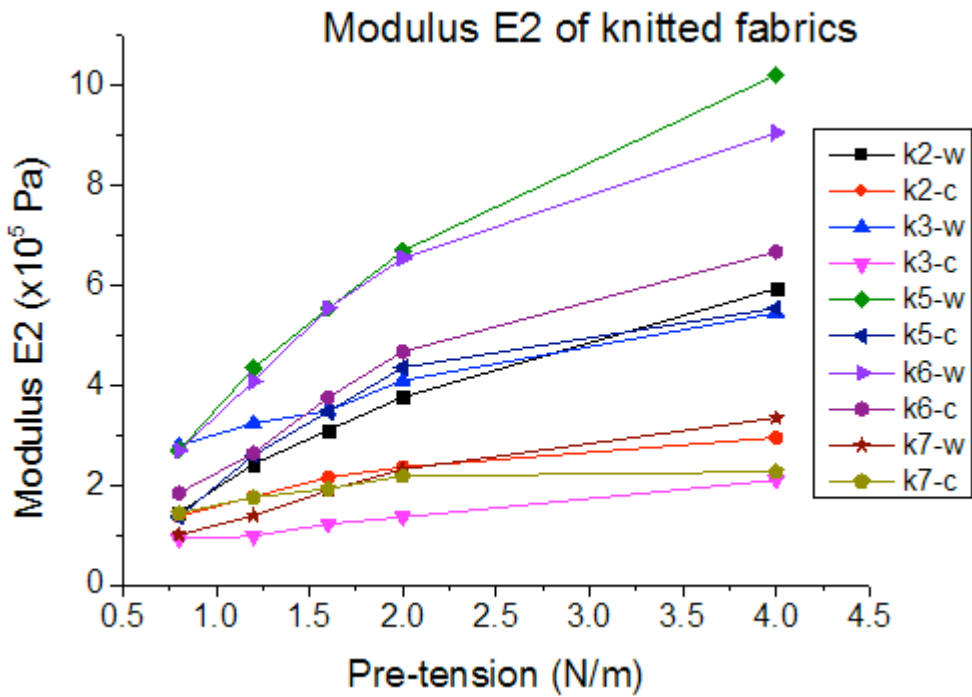
It is found that heaviest and thickest fabrics, W12, K3 and N3, require more energy to be deformed in the 2nd – 5th cycles than other fabrics, while thinner and lighter fabrics such as W1, K6 and N6, require less energy to be deformed. This indicates that more energy is likely to be consumed to deform recovered fabric shell of woven, knitted and nonwoven fabrics which have thicker thickness or greater mass per unit area.

4.3.2 Compression buckling Young's modulus before recovered fabric shell buckles (E2)

As discussed in section 4.2, pre-tensions affect fabric structure and modulus is an intrinsic fabric property depending on fabric structures, the influences of pre-tension on fabric modulus before recovered fabric shell buckles (E2, see Figure 4.11) are investigated to show the influences of pre-tension on woven, knitted and nonwoven fabric structural changes as shown in Figure 4.13(a) (b) (c).



(a)



(b)

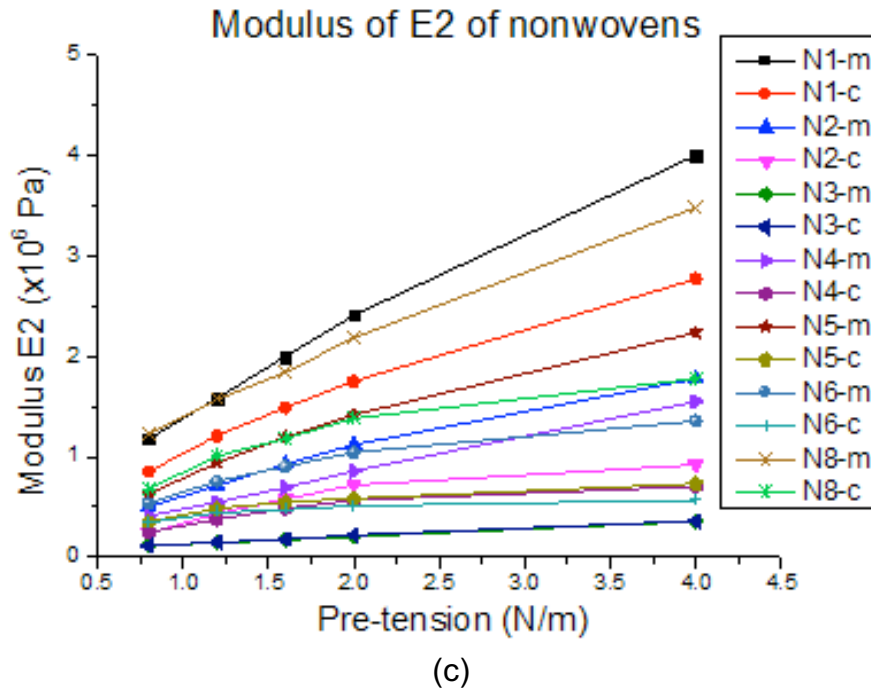


Figure 4.13 The influences of pre-tensions on modulus E2

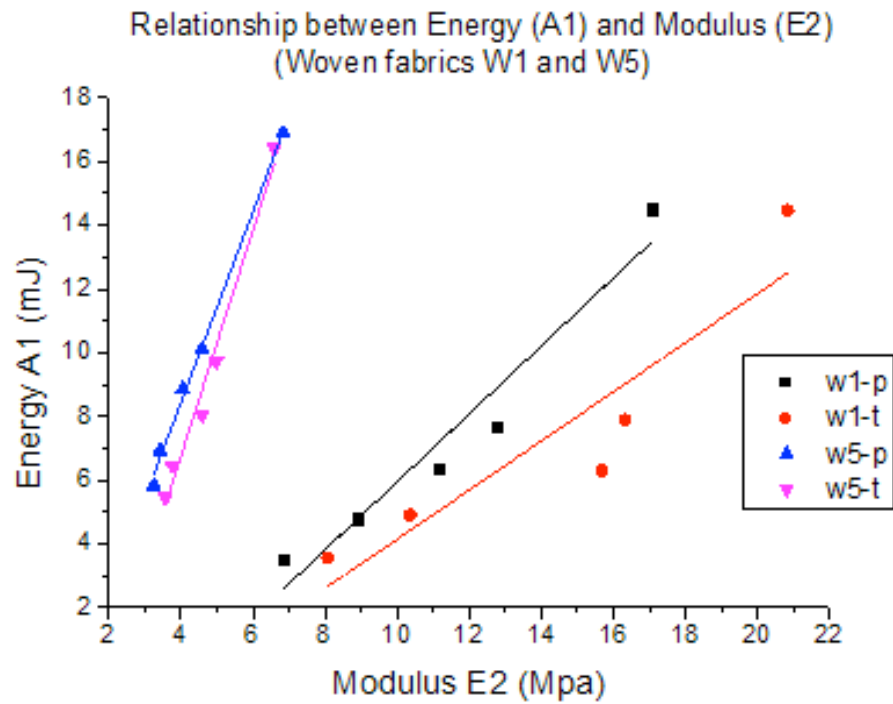
Similar to E1 in the section 4.2, modulus E2 increases with the increase of pre-tension for most of fabrics. This indicates that pre-tensions still have noticeable effects on the structure of recovered fabrics in the 2nd-5th cycles.

In comparison with the fact that level of pre-tensions hardly change the ranking of the energy consumed, A1, for different fabrics, level of pre-tensions could change the ranking of the modulus E2 for different fabrics. For example, usually lighter and thinner fabrics have greater modulus E2 than heavier and thicker fabrics under greater pre-tensions, but different levels of pre-tension change the relative ranking of E2 for fabric W12 in both directions, K3 in wale, K7 in course, N6 in MD and N8 in CD among the nineteen fabrics.

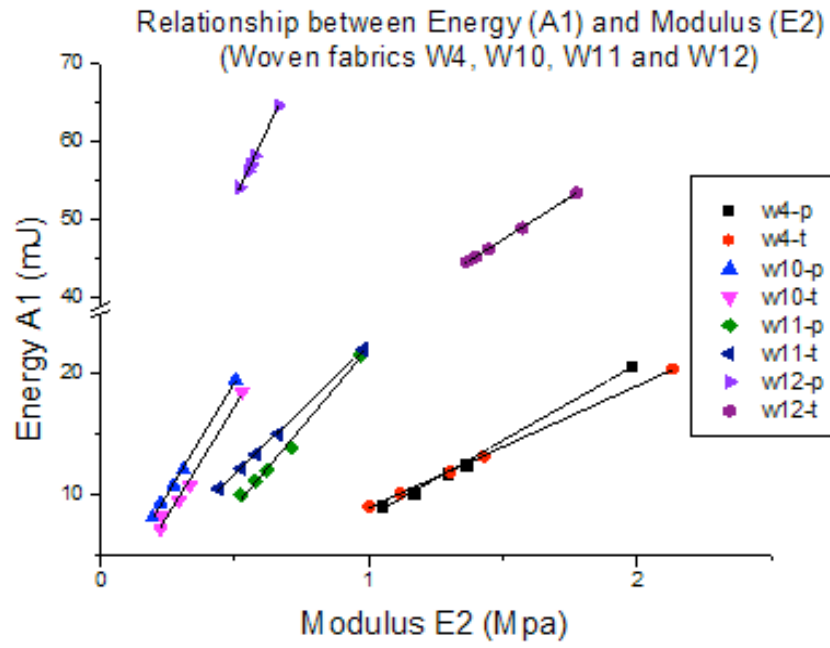
It was noticed that knitted fabrics usually have a greater modulus E2 in the wale direction than in the course direction (e.g., knitted fabrics K5 and K6), and that nonwoven fabrics usually have greater modulus E2 in the MD than in the CD (nonwoven fabrics N1 and N8). This might imply that the fabric modulus E2 is highly related to the orientations of constituent yarns and fibres in knitted and nonwoven fabrics. It was also noticed that woven fabric W1 made from polyamide filaments has a greater modulus E2 than other woven fabrics, this indicates that the fabric modulus E2 might also be significantly influenced by the mechanical properties of constituent fibres.

4.3.3 Relationship between modulus E2 and energy A1

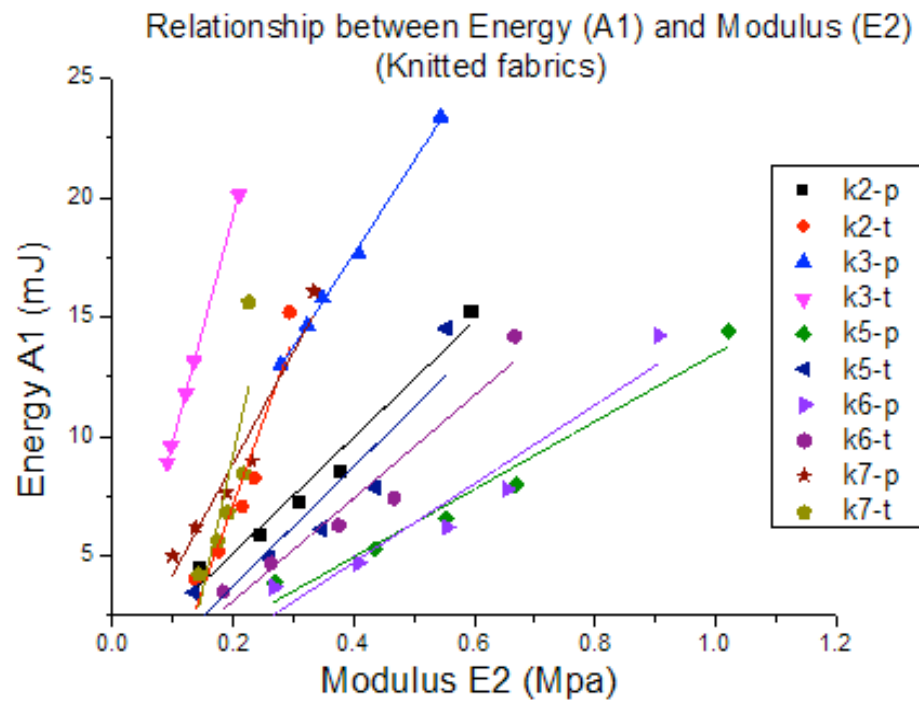
As indicated above in section 4.3.1 and 4.3.2, both the modulus E2 and energy A1 increase with the increase of pre-tension. The relationship between modulus E2 and corresponding energy A1 are shown in Figure 4.14. It is shown that energy A1 increases with the increase of modulus E2 and they have very strong linear relationships for almost all woven, knitted and nonwoven fabrics measured. The linear regression equations and R^2 of the relationship between the modulus E2 and energy A1 are shown in Table 4.6.



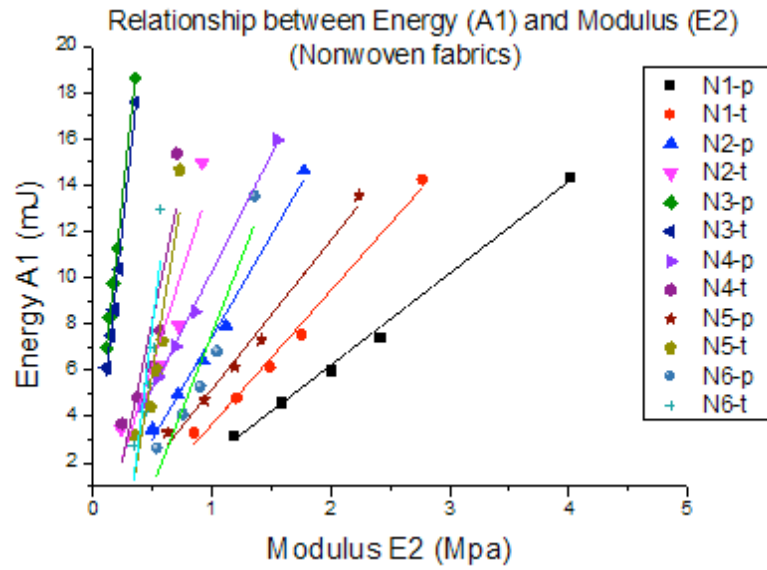
(a)



(b)



(c)



(d)

Figure 4.14 Relationship between the modulus E2 and the energy A1 for woven, knitted and nonwoven fabrics

Table 4.6 Linear regression equations of relationship between energy A1 and modulus E2

Fabric	Warp/wale/MD		Weft/Course/CD	
	Linear regression equation	R ²	Linear regression equation	R ²
W1	Y= 1.07X – 4.73	0.94	Y= 0.77X – 3.58	0.85
W4	Y= 12.59X – 4.37	1.00	Y= 10.07X – 1.13	1.00
W5	Y= 3.00X – 3.58	1.00	Y= 3.55X – 7.47	0.98
W10	Y= 36.73X + 0.95	1.00	Y= 36.00X – 0.67	0.99
W11	Y= 26.28X – 4.13	0.99	Y= 21.33X + 1.07	1.00
W12	Y= 73.02X + 16.11	1.00	Y= 21.58X + 15.00	1.00
K2	Y= 24.27X + 0.24	0.97	Y= 70.03X – 6.88	0.91
K3	Y= 38.88X + 2.07	1.00	Y= 94.23X + 0.34	1.00
K5	Y= 14.20X – 0.74	0.97	Y= 24.89X – 1.24	0.86
K6	Y= 16.45X – 1.86	0.93	Y= 21.51X – 1.20	0.94
K7	Y= 46.58X – 0.46	0.95	Y= 111.75X – 13.18	0.70
N1	Y= 3.97X - 1.72	1.00	Y= 5.78X – 2.13	0.99
N2	Y= 8.81X – 1.40	0.99	Y= 16.00X – 1.75	0.86
N3	Y= 48.80X + 1.31	1.00	Y= 46.78X + 0.54	1.00
N4	Y= 10.14X + 0.11	1.00	Y= 23.98X – 3.85	0.83
N5	Y= 6.44X – 1.27	0.99	Y= 30.17X – 9.15	0.87
N6	Y= 13.17X – 5.61	0.92	Y= 42.56X – 13.38	0.81
N8	Y= 4.88X-2.71	1.00	Y= 9.84X – 4.57	0.89

As shown in Table 4.6, slopes of the linear regression equations between the modulus E2 and energy A1 vary in a wide range from 0.77 (fabric W1 in weft direction) to 111.75 (fabric K7 in course direction). It indicates that there are noticeable differences of the relationship between E2 and A1 for different fabrics, and there are smaller differences of slopes between two directions for the same fabric.

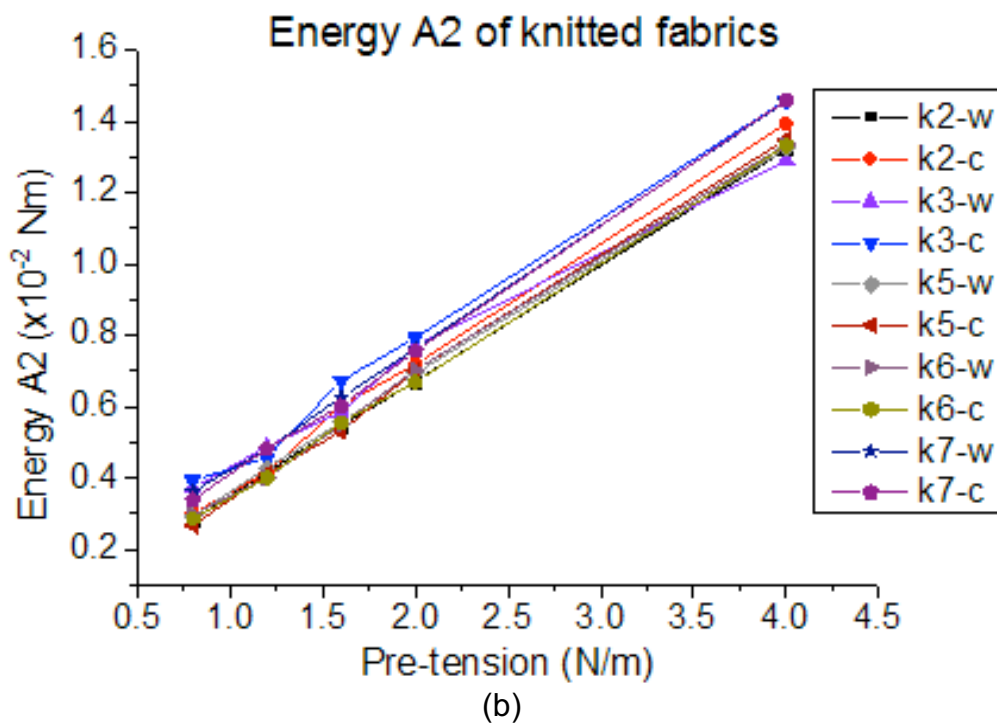
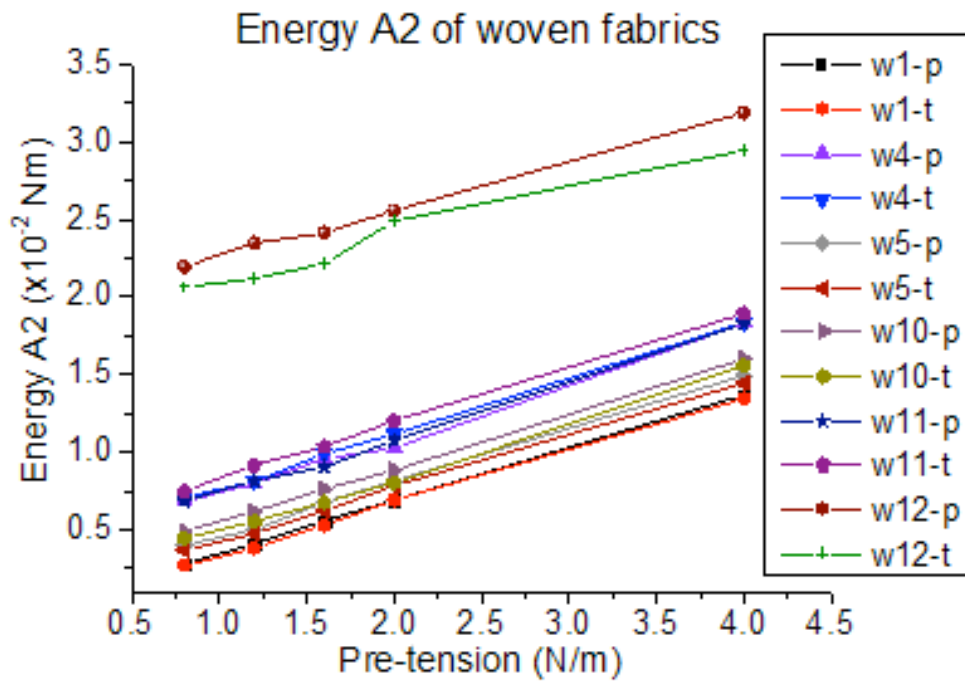
In contrast to the relationship between A1cp1 and E1, in which some fabrics having large extensibility (e.g., fabric K7 in course direction and N4 in CD) have poor linear relationship between A1cp1 and E1, the modulus E2 and energy A1 for all fabrics have very good linear relationship, all of their R^2 in Table 4.6 are more than 0.70 and 2/3 of them are greater than 0.9. These R^2 are much greater than R^2 for the relationship between A1cp1 and E1 (see section 4.2.3), and such differences might be due to the differences of fabric deformation in the first cycle and the 2nd-5th cycles.

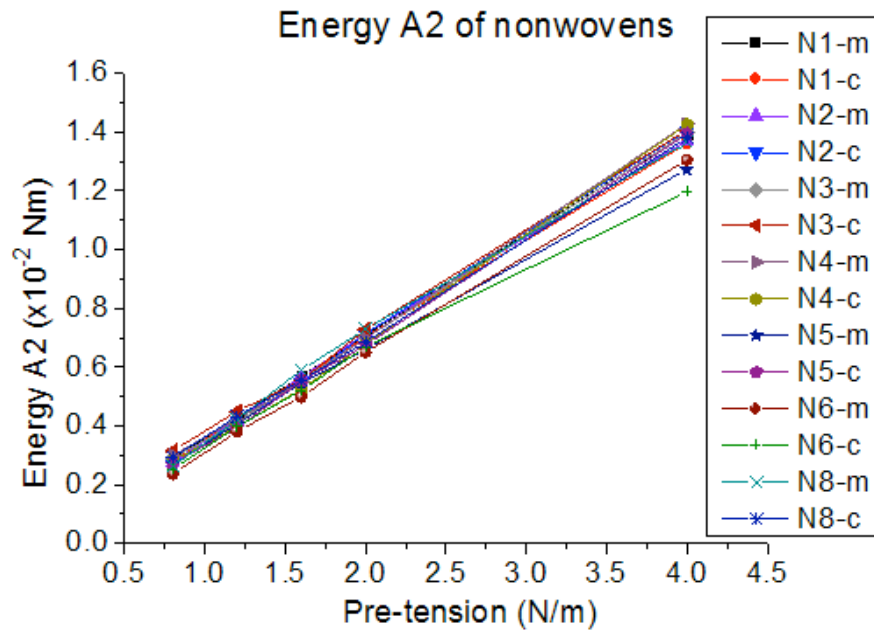
The difference between fabric deformations in the first cycle and the 2nd-5th cycles is that fabric deforms in the 2nd-5th cycles tracking the wrinkles produced in the first cycle. While the energy consumption A1cp1 could be affected by fabric structure influenced by the pre-tensions in the first cycle, the fabric deforms in 2nd-5th cycles tracking the wrinkles on the fabric which would be less affected by pre-tensions, thus the energy consumption A1 has better linear relationship with modulus E2.

Similar to modulus E1 and energy A1cp1, it is believed that the increase of E2 and A1 is related to the increase of friction between yarns/fibres and re-orientation of yarns/fibres in the loaded direction of pre-tensions.

4.4 The influences of pre-tensions on the energy consumed to self-recover deformed fabric shells (A2)

In fabric shell compression buckling-recovery process, the energy consumed to self-recover deformations, A2, is shown as the shaded area in Figure 4.15 (Mao and Taylor, 2012). The influences of pre-tension on the energy A2 of woven, knitted and nonwoven fabrics are shown in Figure 4.16(a) (b) (c), respectively.





(c)

Figure 4.16 The influences of pre-tensions on the energy consumed to self-recovery of deformed fabric shells

As shown in Figure 4.16, woven fabrics have greater A2 to self-recover their deformations than both knitted and nonwoven fabrics do. However, it is noticed that slopes of the linear regression equations between E2 and A2 are all between 2.8 and 3.7 as shown in Table 4.7(1)(2). This means the increasing rates of A2 with the increase of pre-tension do not have noticeable differences between woven, knitted and nonwoven fabrics.

Table 4.7 (1) Linear regression equations of relationship between pre-tension (N/m) and A2 (mJ) for woven and knitted fabrics

Fabric	Warp/wale/MD		Weft/Course/CD	
	Linear regression equation	R ²	Linear regression equation	R ²
W1	Y= 3.41X + 0.05	1.00	Y= 3.40X -0.11	1.00
W4	Y= 3.62X + 3.636	0.99	Y= 3.56X + 4.07	1.00
W5	Y= 3.46X + 1.12	1.00	Y= 3.41X + 0.83	1.00
W10	Y= 3.49X + 1.99	1.00	Y= 3.53X + 1.28	1.00
W11	Y= 3.61X + 3.68	1.00	Y= 3.55X + 4.76	1.00
W12	Y= 3.08X + 19.49	1.00	Y= 2.87X + 18.15	0.97
K2	Y= 3.24X +0.27	1.00	Y= 3.42X + 0.29	1.00
K3	Y= 2.88X +1.48	0.99	Y= 3.40X + 1.01	0.99
K5	Y= 3.21X +0.42	1.00	Y= 3.38X + 0.04	1.00
K6	Y= 3.28X +0.28	1.00	Y= 3.28X +0.19	1.00
K7	Y= 3.44X +0.77	1.00	Y= 3.50X + 0.55	1.00

Table 4.7 (2) Linear regression equations of relationship between pre-tension (N/m) and A2 (mJ) for nonwoven fabrics

Fabric	Warp/wale/MD		Weft/Course/CD	
	Linear regression equation	R ²	Linear regression equation	R ²
N1	Y= 3.46X +0.13	1.00	Y= 3.36X +0.20	1.00
N2	Y= 3.40X +0.16	1.00	Y= 3.56X -0.13	1.00
N3	Y= 3.49X + 0.01	1.00	Y= 3.43X + 0.32	1.00
N4	Y= 3.56X -0.04	1.00	Y= 3.62X -0.34	1.00
N5	Y= 3.11X + 0.34	1.00	Y= 3.52X -0.19	1.00
N6	Y= 3.33X -0.26	1.00	Y= 2.91X +0.48	1.00
N8	Y= 3.40X +0.20	1.00	Y= 3.40X +0.17	1.00

The influences of pre-tension on the energy A2 also depend on fabric types and fabric structures. For woven fabrics, W12 which has the greatest mass per unit area has the greatest A2 than other woven fabrics. However, for knitted and nonwoven fabrics, the energy A2 increases mainly with the increase of pre-tension and the influences of fabric mass per unit area and thickness are not significant (see Figure 4.16).

4.5 The influences of pre-tensions on the energy consumed to forming permanent deformations in fabric shells (A3)

A complete cycle of axial compression buckling deformation of fabric shell includes two processes: buckling process and recovery process. Fabric shells are deformed in the buckling process and recovered to its original gauge length in the recovery process. The recovery process contains two steps: the fabric deformations are partially self-recovered by the strain energy stored inside deformed fabric (A2) in the first step. and the deformations remained on fabric shells are recovered in the second step by the work done by the external force applied. The residue strains after one cycle are almost wholly determined by the friction resistant which arises in the fabric due to inter-yarn pressure (Grosberg and Swani, 1966a), part of deformations are remained when external forces are withdrawn as shown in Figure 4.17. The corresponding energy (A3 as the shaded area in Figure 4.17) is used to quantify how much permanent deformation is produced in fabric shell during compression buckling deformations.

As pre-tension affects fabric structure and modulus is an intrinsic fabric property representing fabric structures, the relationships between pre-tensions and fabric modulus are also investigated. Modulus E4 of fabric shell during forming

permanent deformations (the slope of the line EF from starting point (E) of the 2nd-5th cycles to point (F) at which no force is applied on fabric shells) is calculated and analysed (LUFHES Software).

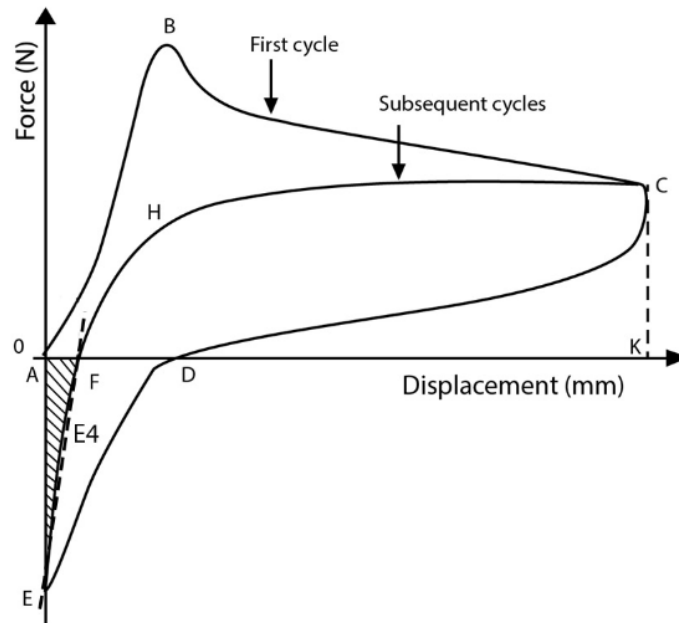


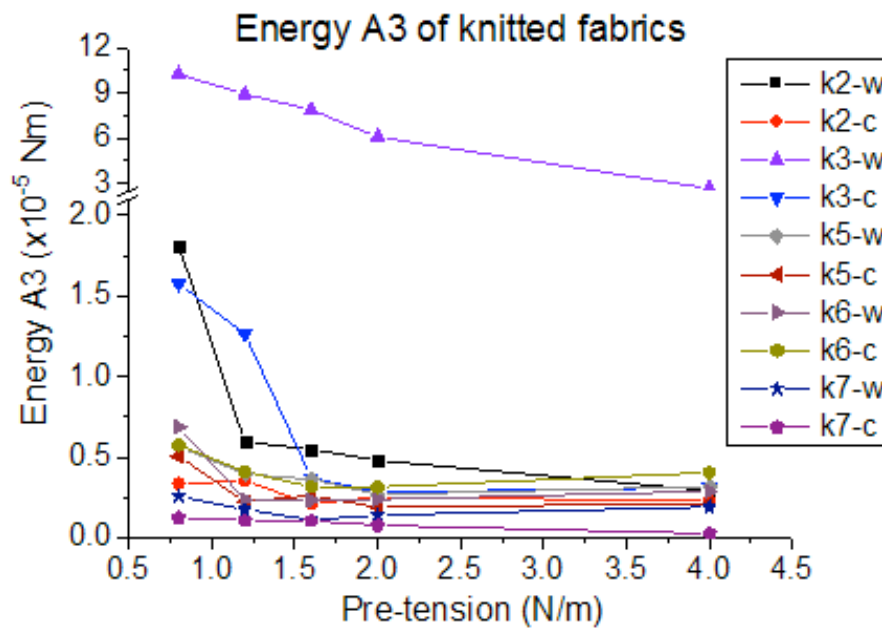
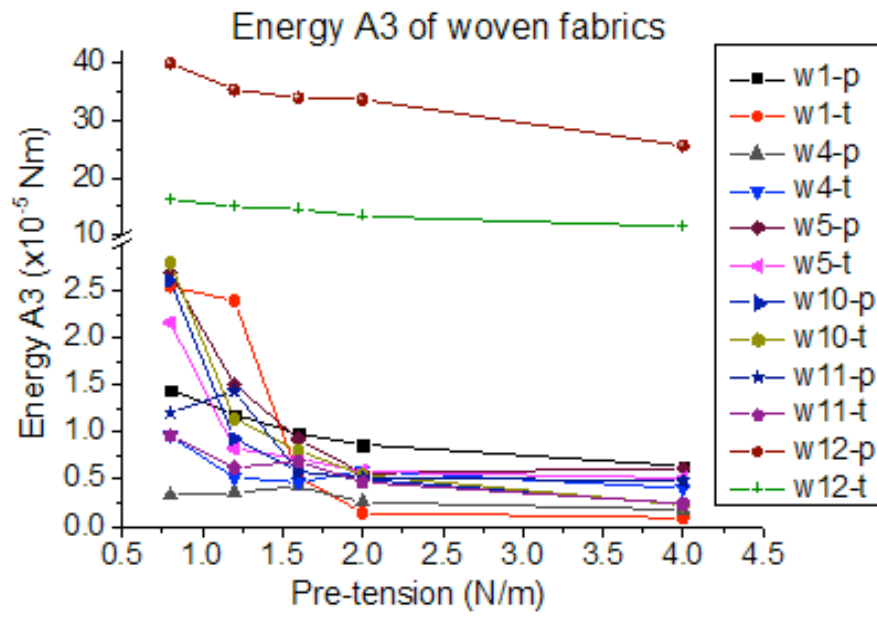
Figure 4.17 Energy A3 and modulus E4 obtained in the 2nd-5th cycle compression buckling deformation

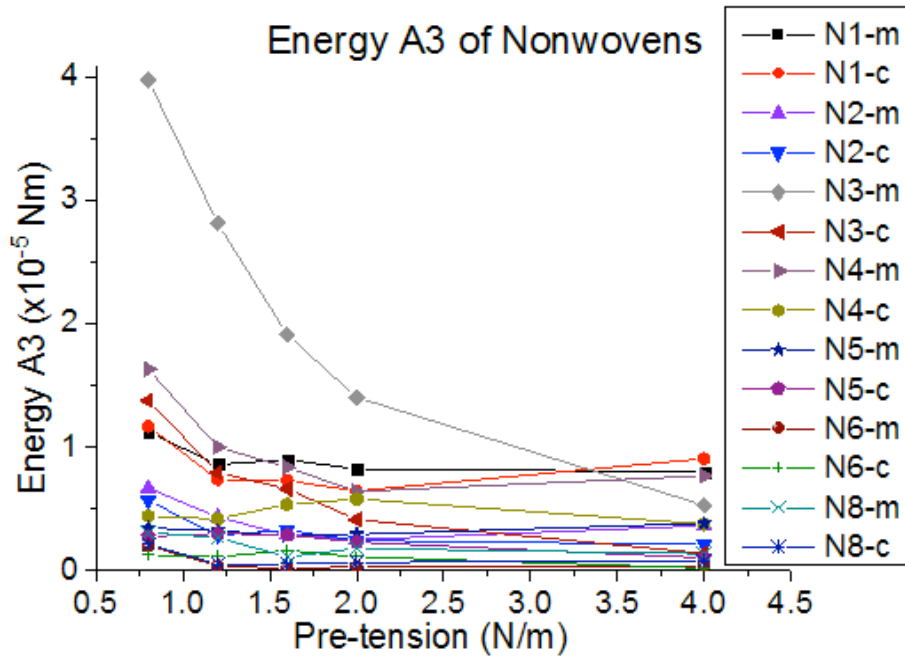
4.5.1 Energy consumed to form permanent deformations (A3)

The influences of pre-tension on the energy A3 for woven, knitted and nonwoven fabrics are shown in Figure 4.18(a), (b) and (c).

Generally speaking, energy A3 decreases with the increase of pre-tension, this means less permanent deformation is formed with greater pre-tensions. The relative ranking of energy A3 in different fabrics has a small magnitude and randomly varies with different level of pre-tensions, this means that the energy consumed to form permanent fabric deformations appears to fluctuate markedly, which might be due to the effects of some uncontrollable factors (e.g., the uncertain deformations formed in previous buckling deformation cycles).

Among woven fabrics (see Figure 4.18(a)), W12 has the largest mass per unit area and thickness and it consumes the largest amount of energy to form permanent deformations. Similar trend is also found in knitted and nonwoven fabrics: K3 and N3 have the greatest mass per unit area and thickness among knitted and nonwoven fabrics, respectively, and they consume the relatively greatest amount of energy A3 to form permanent deformations.



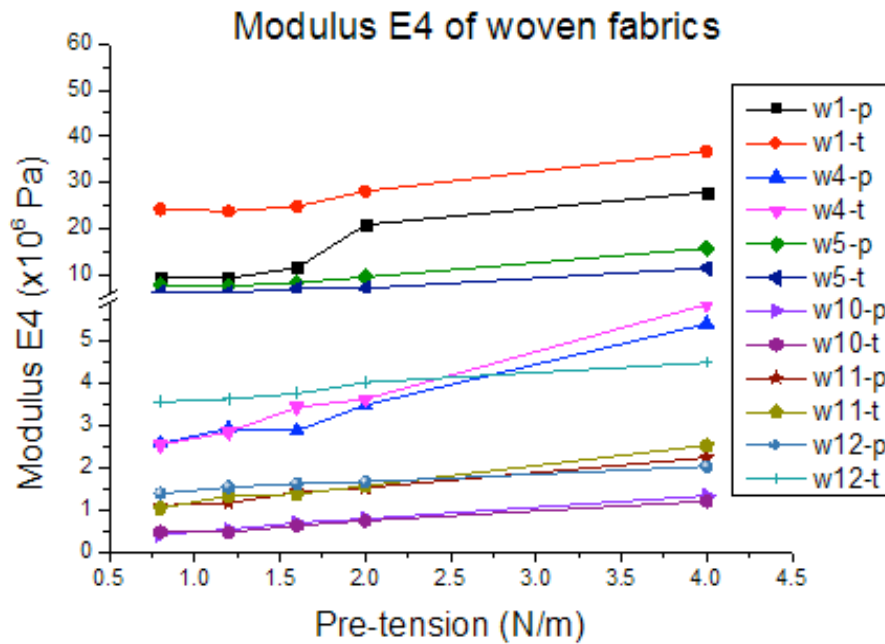


(c)

Figure 4.18 The influences of pre-tension on the energy consumed in forming permanent deformations in fabric shells (A3)

4.5.2 Compression buckling Young’s modulus during forming permanent deformations (E4)

The influences of pre-tensions on modulus E4 for woven, knitted and nonwoven fabrics are shown in Figure 4.19(a), (b) and (c), respectively.



(a)

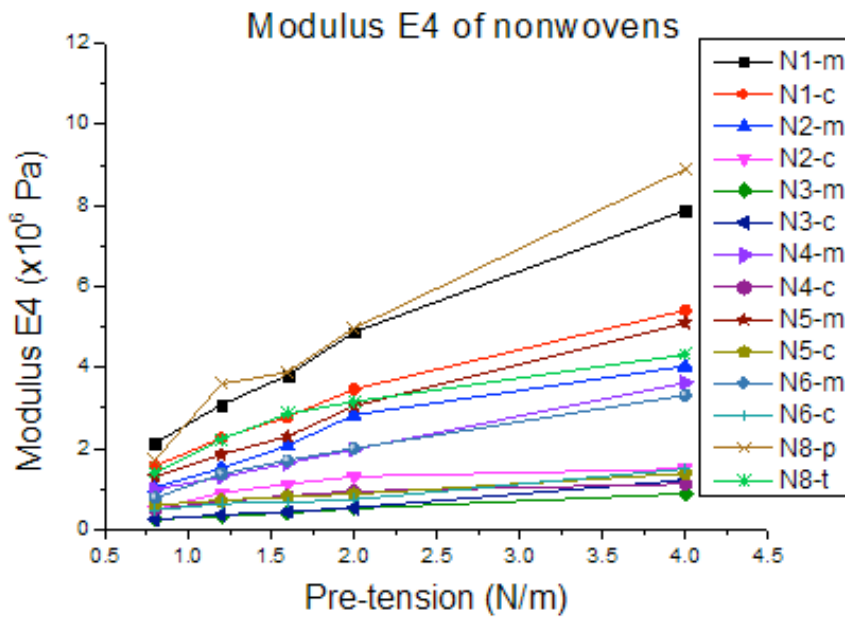
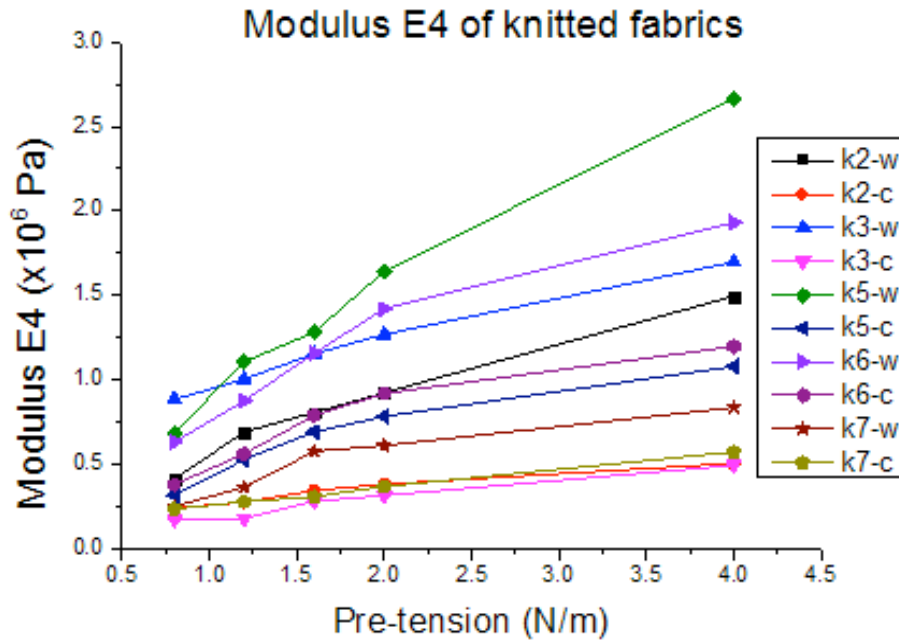
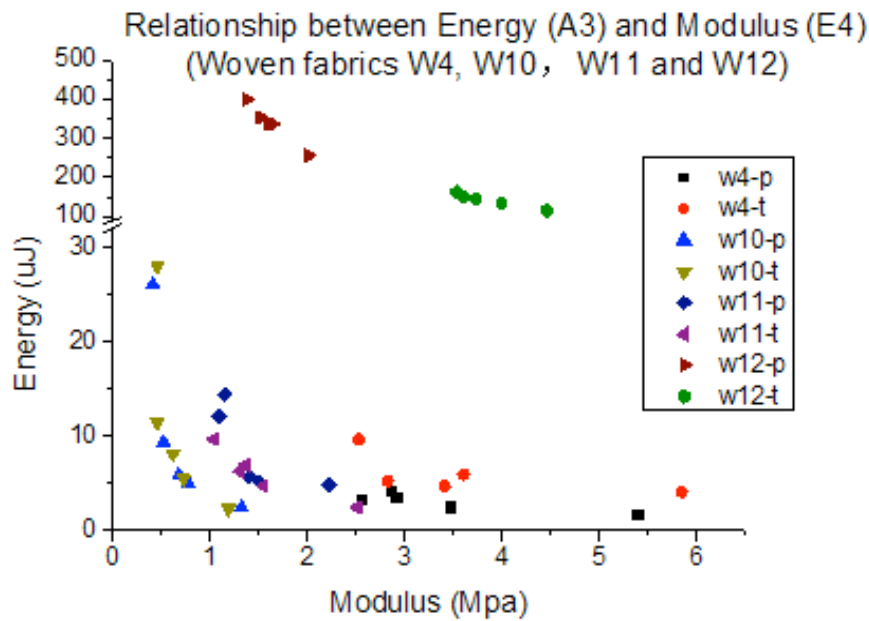


Figure 4.19 The influences of pre-tension on the modulus E4 of fabric shells in forming permanent deformations

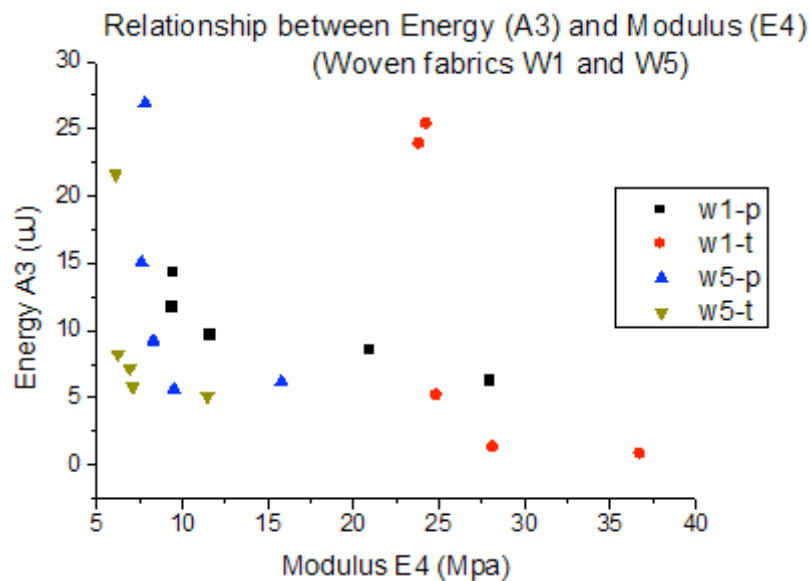
Generally speaking, modulus E4 increases with the increase of pre-tension for fabrics measured. It is also noticed that fabrics with thinner thickness always have greater E4 than thicker fabrics have. W1 and W5 are the first and second thinnest thickness among woven fabrics, and they have the first and second greatest E4 among woven fabrics. Similarly, thinnest knitted fabric K6 and K5 as well as nonwoven fabric N1 also have greatest modulus E4.

4.5.3 Relationship between energy A3 and modulus E4

In comparison with the influences of pre-tensions on the energy A3, the influences of pre-tensions on modulus E4 are much clearer. While energy A3 decreases with the increase of pre-tension, modulus E4 increases with the increase of pre-tension, thus the decrease of energy A3 consumed to form permanent fabric deformations is related to the fabric structures represented by modulus E4 under different pre-tensions. Relationships between modulus E4 and corresponding energy A3 are shown in Figure 4.20, and the quadratic equations between A3 and E4 for woven, knitted and nonwoven fabrics are shown in Table 4.8.



(a)



(b)

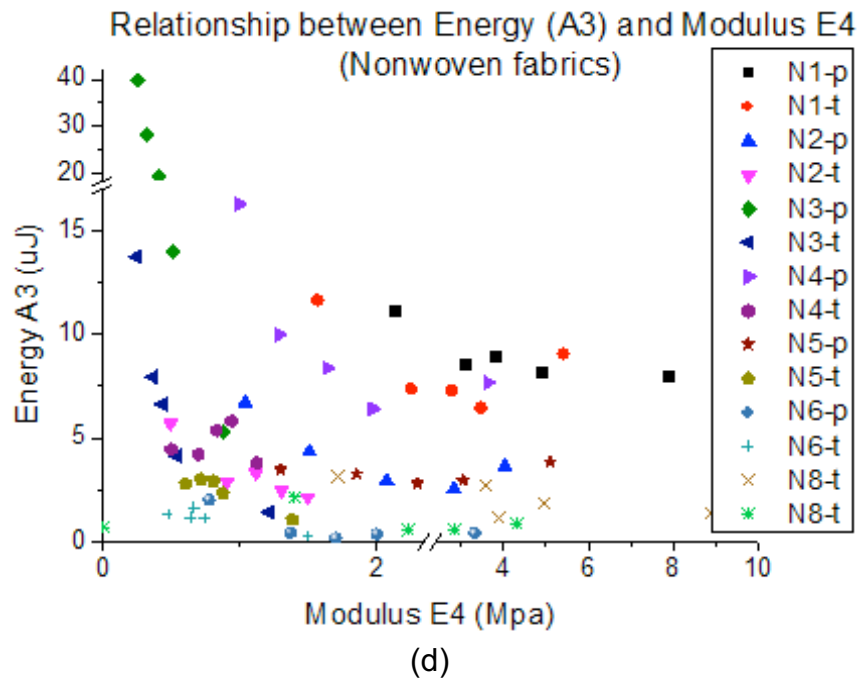
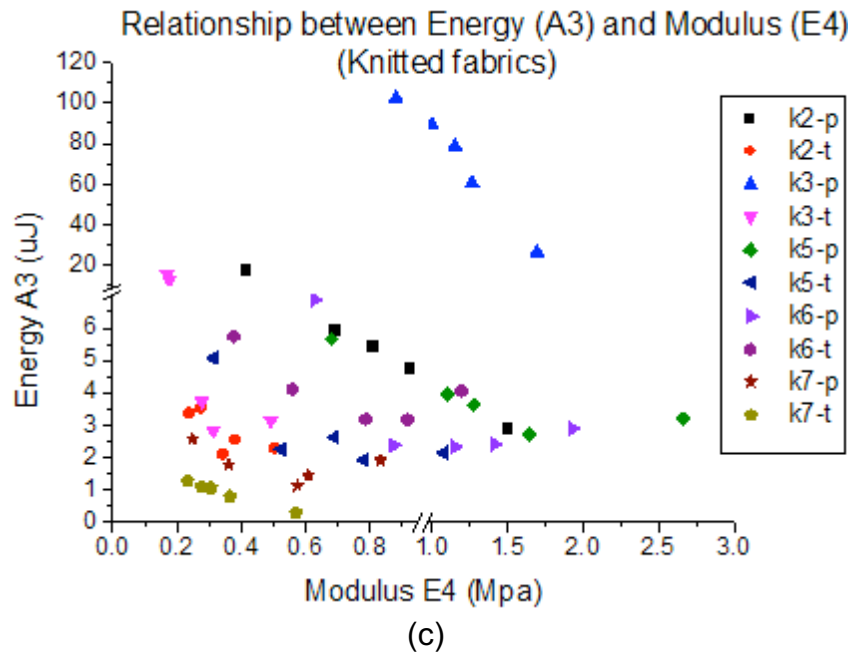


Figure 4.20 Relationship between modulus E4 and energy A3 in fabric shell buckling-recovery deformation

Table 4.8 Quadratic regression equations of relationship between A3 and E4

Fabric	Warp/wale/MD		Weft/Course/CD	
	Regression equation	R ²	Regression equation	R ²
W1	$Y = 0.01X^2 - 0.75X + 18.60$	0.80	$Y = 0.44X^2 - 28.06X + 442.57$	0.85
W4	$Y = 0.10X^2 - 1.55X + 7.08$	0.72	$Y = 0.91X^2 - 8.91X + 24.97$	0.63
W5	$Y = 1.00X^2 - 25.20X + 153.68$	0.60	$Y = 2.05X^2 - 38.06X + 172.10$	0.62
W10	$Y = 62.33X^2 - 129.91X + 65.50$	0.86	$Y = 67.02X^2 - 133.32X + 66.12$	0.64
W11	$Y = 18.52X^2 - 69.23X + 67.20$	0.89	$Y = 4.61X^2 - 21.20X + 26.60$	0.98
W12	$Y = 61.25X^2 - 426.63X + 866.45$	0.99	$Y = 26.65X^2 - 260.36X + 746.39$	0.97
K2	$Y = 25.32X^2 - 61.41X + 38.36$	0.95	$Y = 31.66X^2 - 28.24X + 8.48$	0.74
K3	$Y = 17.06X^2 - 138X + 211.22$	0.99	$Y = 281.93X^2 - 221.8X + 44.08$	0.98
K5	$Y = 1.71X^2 - 7.00X + 9.64$	0.99	$Y = 9.96X^2 - 17.29X + 9.28$	0.88
K6	$Y = 6.68X^2 - 19.35X + 15.63$	0.78	$Y = 10.20X^2 - 18.04X + 11.06$	1.00
K7	$Y = 11.26X^2 - 13.19X + 5.10$	0.96	$Y = 2.27X^2 - 4.75X + 2.24$	0.99
N1	$Y = 0.19X^2 - 2.34X + 14.92$	0.83	$Y = 1.11X^2 - 8.29X + 21.46$	0.91
N2	$Y = 1.21X^2 - 7.07X + 12.52$	0.98	$Y = 3.18X^2 - 9.62X + 9.53$	0.92
N3	$Y = 132.92X^2 - 203.72X + 81.79$	0.98	$Y = 30.36X^2 - 56.74X + 25.52$	0.99
N4	$Y = 4.13X^2 - 21.96X + 33.09$	0.93	$Y = -11.44X^2 + 18.57X - 2.30$	0.43
N5	$Y = 0.22X^2 - 1.28X + 4.78$	0.93	$Y = -2.48X^2 + 2.52X + 2.29$	0.94
N6	$Y = 0.72X^2 - 3.53X + 4.1786$	0.90	$Y = -1.20X^2 + 1.29X + 0.97$	0.85
N8	$Y = 0.059X^2 - 0.86X + 4.40$	0.61	$Y = 0.44X^2 - 2.91X + 5.19$	0.87

It is shown in Figure 4.20 and Table 4.8 that modulus E4 and energy A3 have non-linear relationships for most of woven, knitted and nonwoven fabrics. Energy consumed to produce permanent deformation, A3, decreases rapidly with the increases of fabric modulus E4 initially, but when modulus E4 reaches a specific value, energy A3 decreases slightly with the associated increase in the modulus E4.

According to Table 4.8, the energy A3 of nonwoven fabrics N4, N5 and N6 in the CD have an inverted-U relationship with E4, and it shows that the energy A3 does not change apparently at the beginning, but decreases significantly when E4 becomes great. All these three nonwovens are aperture nonwovens, and they are easily stretched in cross direction as shown in Table 4.4. Therefore, the special

relationships between E4 and A3 for fabrics N4, N5 and N6 might be due to their large extensibility in the CD.

4.6 The influences of pre-tensions on the energy consumed to recover recoverable deformation of fabric shells (A4)

In the second step of recovery process, external forces are applied to recover remaining deformations which are not recovered by the energy A2 in self-recovery process. The energy consumed to recover recoverable deformations, A4, in the recovery process of buckling-recovery cycles are shown as shaded area in Figure 4.21 (Mao and Taylor, 2012).

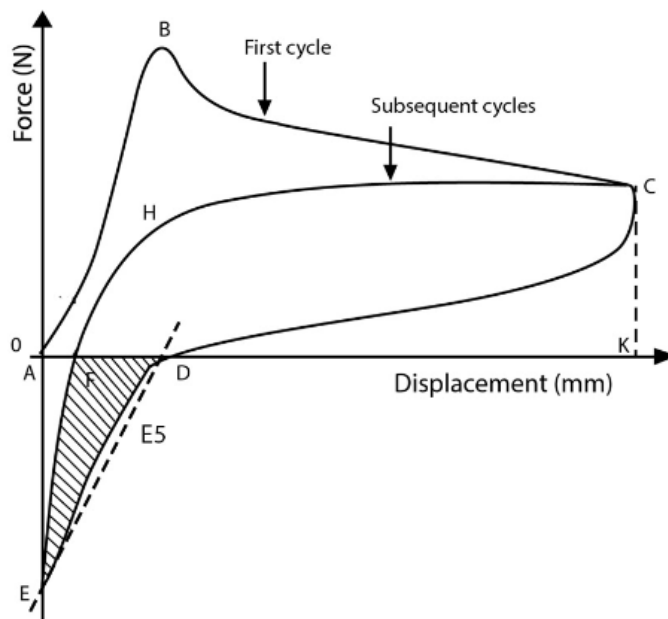
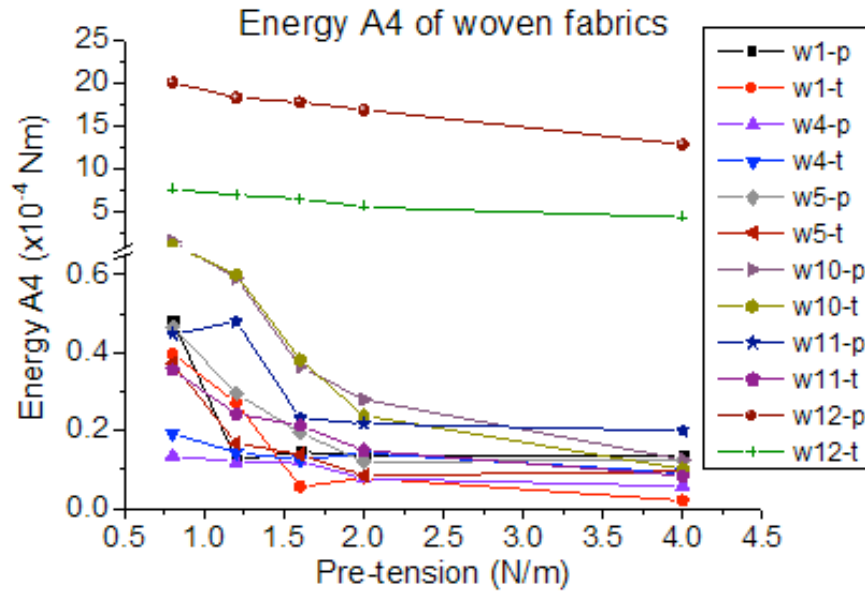


Figure 4.21 The energy A4 in the cyclic compression buckling-recovery process of fabric shells

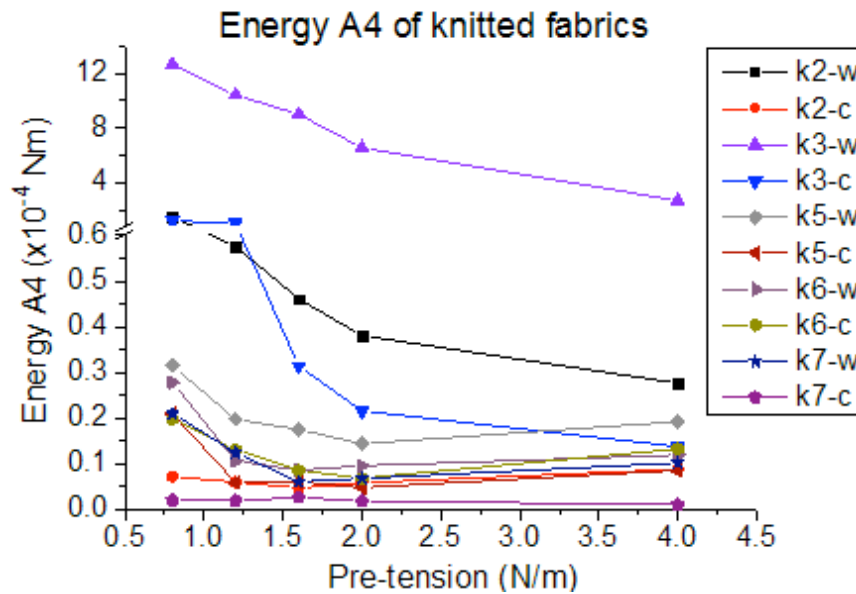
The Young's modulus for fabric shell to recover recoverable deformation, E5, is obtained in the force-displacement curve from point D at which no external force is applied on fabric to point E at which fabric shell is recovered to its original length (Figure 4.21) (LUFHES Software).

4.6.1 Energy consumed to recover the recoverable deformation (A4)

The influences of pre-tension on the energy A4 for woven, knitted and nonwoven fabrics are shown in Figure 4.22(a), (b) and (c).



(a)



(b)

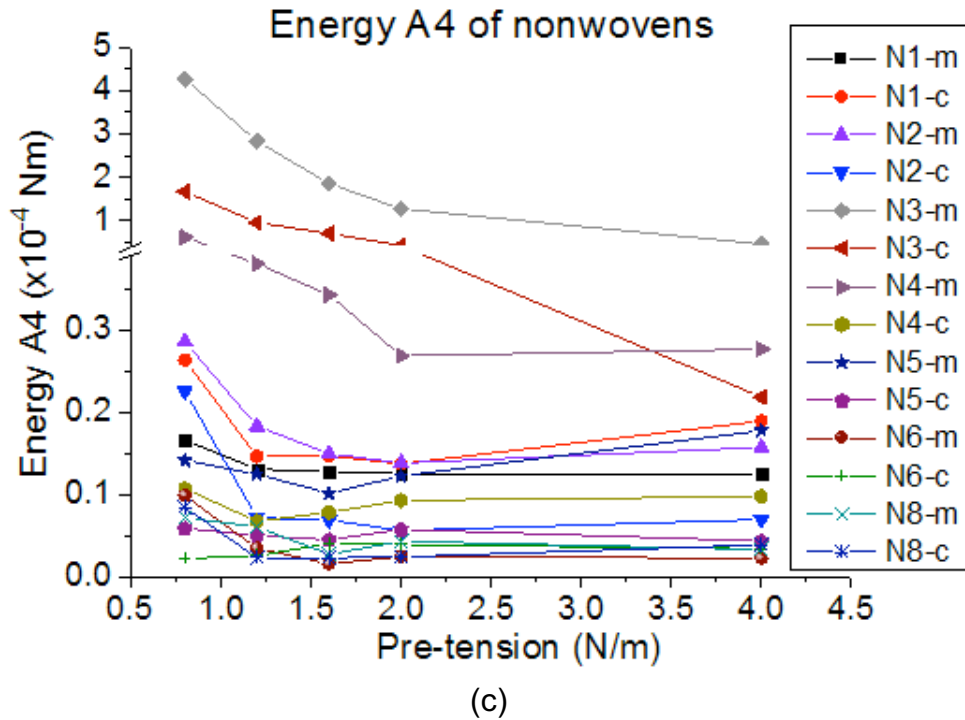


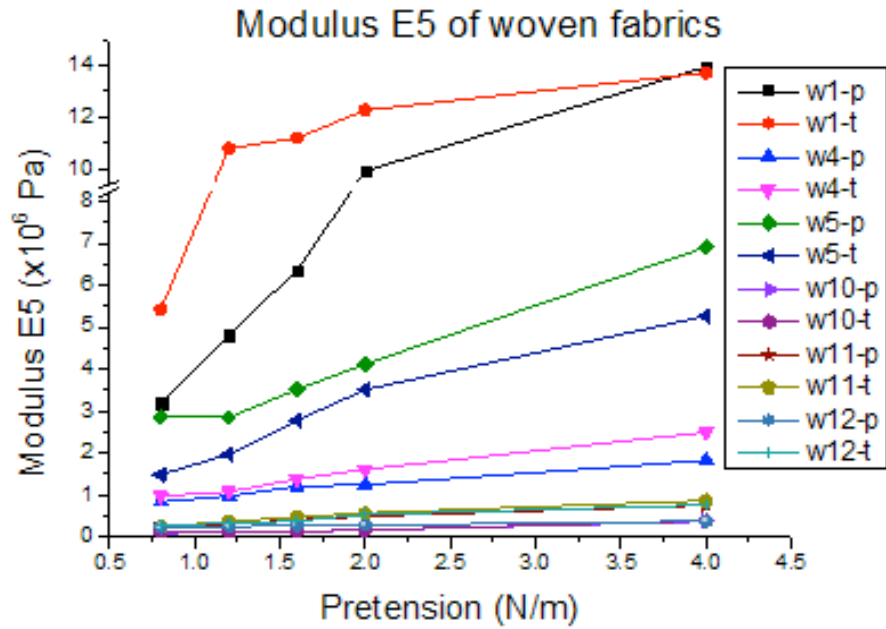
Figure 4.22 The influences of pre-tension on the energy A4 of woven, knitted and nonwoven fabrics

Similar to the influences of pre-tension on the energy A3, the energy A4 decreases with the increase of pre-tension, this means that less recoverable deformations are formed with greater pre-tensions. However, energy A4 is easily affected by many other factors and frequently fluctuates with the increase of pre-tension due to its small magnitude in comparison with A1cp1, A1 and A2 (about one tens of the energy A1 and A2).

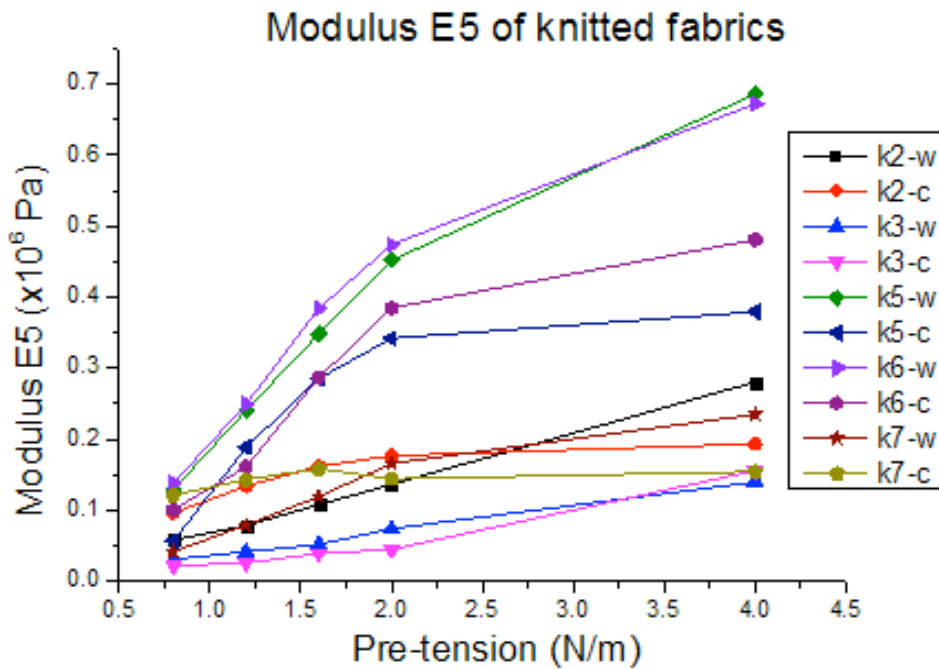
It is also found in Figure 4.22 that fabric W12, K3 and N3 which has the greatest mass per unit area and thickness in each group of woven, knitted and nonwoven fabrics consumes the greatest amount of energy to recover recoverable deformations in their groups.

4.6.2 Compression buckling Young's modulus during recovering recoverable deformations of deformed fabric shells (E5)

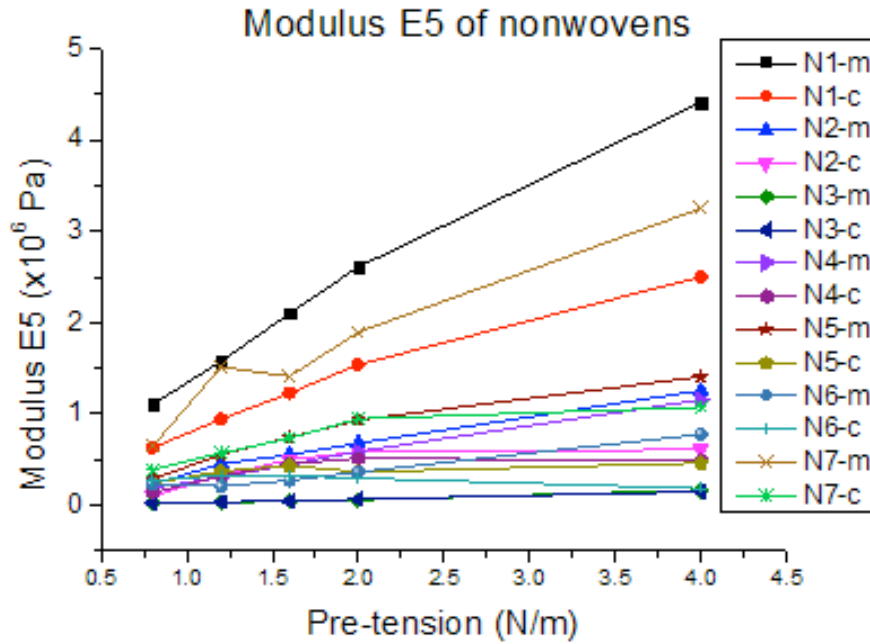
The influences of pre-tension on the energy E5 for woven, knitted and nonwoven fabrics are shown in Figure 4.23(a) (b) (c), respectively.



(a)



(b)



(c)

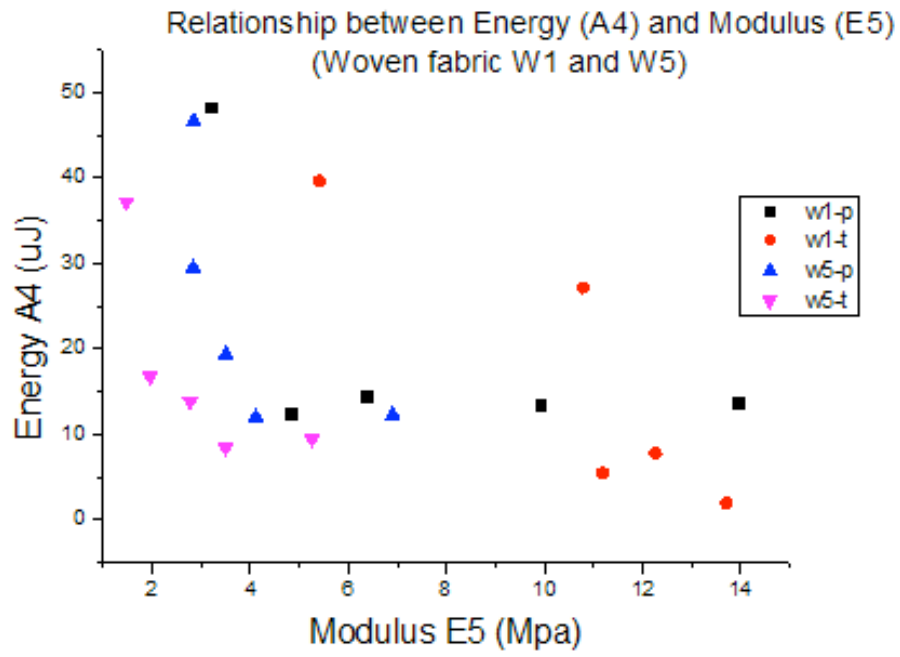
Figure 4.23 The influences of pre-tension on the modulus E5 during recovering recoverable deformations

It appears in Figure 4.23 that modulus E5 increases with the increase of pre-tension for all of the fabrics. This indicates that the pre-tension has stiffening effect on fabrics.

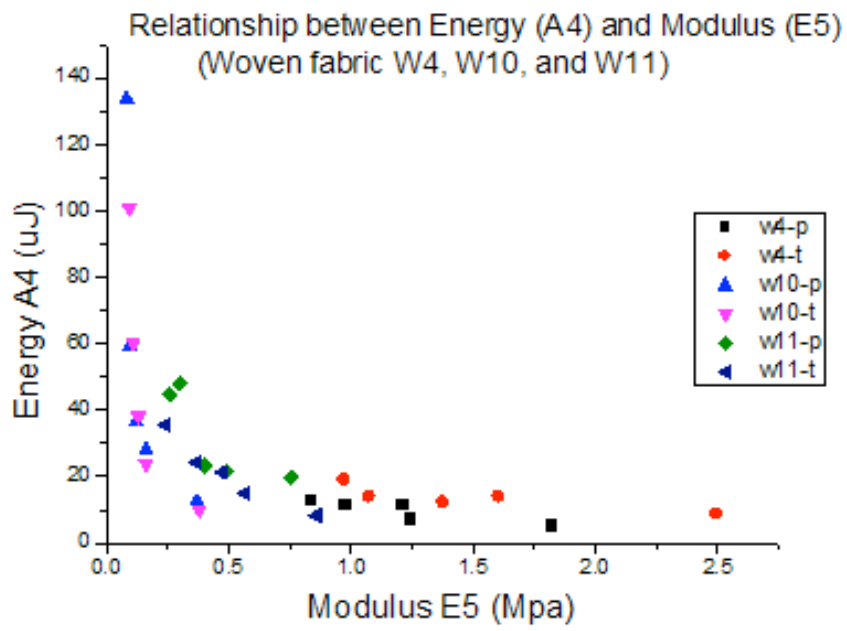
Similar to the influences of pre-tensions on other modulus, it is noticed that fabrics having smaller thickness always have greater E5 in comparison with thicker fabrics. For example, thinner woven fabrics W1 and W5, knitted fabric K6 and K5 as well as nonwoven fabric N1 have relatively greater E5 than other fabrics.

4.6.3 Relationship between energy A4 and modulus E5

As shown in the discussions above, the energy A4 decreases with the increase of pre-tension while the modulus E5 increases with the increase of pre-tension, it is thus suspected that the decrease of A4, the energy consumed to recover recoverable deformation of fabric shells was related to the fabric structure changes (such as the yarns/fibres in deformed fabrics are moved to their original positions by external force) which are represented by modulus E5. The relationship between E5 (MPa) and corresponding A4 (μJ) obtained in buckling-recovery processes of fabric shells are shown in Figure 4.24 and Table 4.9 (1) (2).



(a)



(b)

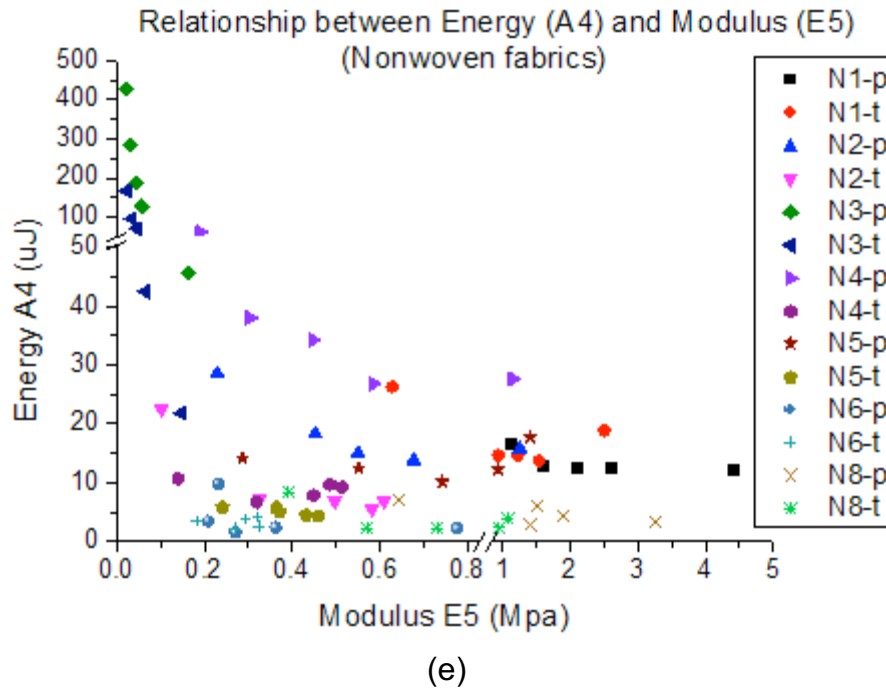


Figure 4.24 Relationships between energy E5 and modulus A4

Table 4.9 (1) Quadratic regression equations between A4 and E5 for woven and knitted fabrics

Fabric	Warp/wale/MD		Weft/Course/CD	
	Regression equation	R ²	Regression equation	R ²
W1	$Y = 0.72X^2 - 14.54X + 78.67$	0.68	$Y = -0.19X^2 - 1.17X + 51.846$	0.82
W4	$Y = 2.67X^2 - 15.05X + 24.16$	0.81	$Y = 2.58X^2 - 14.17X + 28.52$	0.75
W5	$Y = 5.34X^2 - 58.32X + 160.39$	0.81	$Y = 3.94X^2 - 32.64X + 72.57$	0.87
W10	$Y = 4137.1X^2 - 2188.2X + 257.31$	0.78	$Y = 3680.3X^2 - 2013.8X + 245.01$	0.94
W11	$Y = 246.36X^2 - 306.94X + 111.22$	0.89	$Y = 60.17X^2 - 109.54X + 58.05$	0.99
W12	$Y = 12623X^2 - 12272X + 4099.4$	1.00	$Y = 641.63X^2 - 1315.2X + 1052.7$	0.99
K2	$Y = 6183.9X^2 - 2523.3X + 250.61$	0.79	$Y = 1225.4X^2 - 346.1X + 29.35$	0.75
K3	$Y = 77801X^2 - 22132X + 1841.6$	1.00	$Y = 33591X^2 - 6720.1X + 247.2$	0.99
K5	$Y = 132.35X^2 - 128.02X + 44.92$	0.96	$Y = 350.81X^2 - 191.32X + 30.40$	0.97
K6	$Y = 161.63X^2 - 154.42X + 43.65$	0.86	$Y = 244.8X^2 - 159.67X + 33.08$	0.97
K7	$Y = 1033.5X^2 - 336.75X + 32.72$	0.97	$Y = 1203.4X^2 - 337.08X + 25.27$	<u>0.13</u>

Table 4.9 (2) Quadratic regression equations between A4 and E5 for nonwoven fabrics

Fabric	Warp/wale/MD		Weft/Course/CD	
	Regression equation	R ²	Regression equation	R ²
N1	$Y = 0.90X^2 - 6.01X + 21.42$	0.82	$Y = 11.20X^2 - 37.88X + 43.86$	0.83
N2	$Y = 38.33X^2 - 69.05X + 42.06$	0.99	$Y = 118.04X^2 - 114.08X + 32.74$	0.98
N3	$Y = 52450X^2 - 12190X + 637.04$	0.98	$Y = 22269X^2 - 4833.6X + 251.81$	0.95
N4	$Y = 92.17X^2 - 154.54X + 83.68$	0.91	$Y = 97.24X^2 - 65.88X + 17.94$	0.90
N5	$Y = 14.96X^2 - 22.19X + 19.40$	0.94	$Y = -35.42X^2 + 17.34X + 3.73$	0.86
N6	$Y = 44.06X^2 - 49.85X + 14.36$	<u>0.26</u>	$Y = 97.69X^2 - 49.11X + 9.01$	<u>0.07</u>
N8	$Y = 0.78X^2 - 4.38X + 9.38$	0.52	$Y = 38.73X^2 - 62.32X + 26.39$	0.92

As the energy A4 is always in smaller magnitude as discussed before, it is easily affected by other factors and thus lead to poor correlations between A4 and E5 (see Table 4.9). Similar to the relationship between A3 and E4, the energy A4 generally decreases with the increase of E5. It is shown in Figure 4.24 and Table 4.9 (1) (2) that relationship between E5 and A4 can be described by quadratic regression equations for most of fabrics except knitted fabric K7 and nonwoven fabrics N6 and N8. It is noticed that fabrics K7 and N6 have larger extensibility and usually have loose structures; their structures could have noticeable changes under relatively small pre-tensions. It is believed that fabrics having larger extensibilities have special characteristics under pre-tension and need further investigation.

4.7 Determination of suitable pre-tension of fabric shell buckling tests in the LUFHES

Pre-tensions applied on fabric shell could minimize its creases or wrinkles and lead to the fabrics being deformed in comparable testing conditions in order to improve the repeatability of fabric shell compression buckling processes. In many standard mechanical property measurements such as the tensile test of fabrics (BS EN ISO 13934-1:2013), pre-tensions applied on the fabrics depend on the fabric mass per unit area, heavier fabrics usually require greater pre-tensions. However, there is little knowledge about how much pre-tension is suitable for woven, knitted and nonwoven fabrics in the fabric shell compression buckling test in LUFHES.

Suitable pre-tensions for compression buckling of fabric shell tests should be:

- (1) Pre-tensions should be able to remove creases/wrinkles on fabrics;
- (2) Pre-tensions applied should not significantly change fabric structures and mechanical properties;
- (3) Pre-tensions applied on different fabrics should not significantly change the relative magnitudes of their mechanical properties.

It is concluded in this chapter that greater pre-tensions alter fabric structures which is represented by compression buckling Young's modulus (e.g. E_1). It will lead to greater energy consumptions to form/recover fabric deformations (e.g., A1cp1, A1 and A2) and smaller energy consumptions to form recoverable and permanent deformations (e.g., A3 and A4) during fabric shell cyclic compression buckling-recovery processes.

However, it is also found that the influences of pre-tensions on both energy consumptions (A1cp1, A1, A2, and A3) and fabric structural changes (e.g., E1) vary with different fabric types, fabric thickness, mass per unit area and extensibility.

In order to determine suitable pre-tension in fabric shell buckling deformation measurements, the changing rate of energy and modulus with the increase of pre-tension is studied. The changing rates of energy and modulus per unit pre-tension are defined as below:

$$\text{Changing rate of } A(P_i) = \frac{A(P_i) - A(0.8)}{A(0.8) \times (P_i - 0.8)} \times 100\% \dots\dots\dots (4.4)$$

$$\text{Changing rate of } E(P_i) = \frac{E(P_i) - E(0.8)}{E(0.8) \times (P_i - 0.8)} \times 100\% \dots\dots\dots (4.5)$$

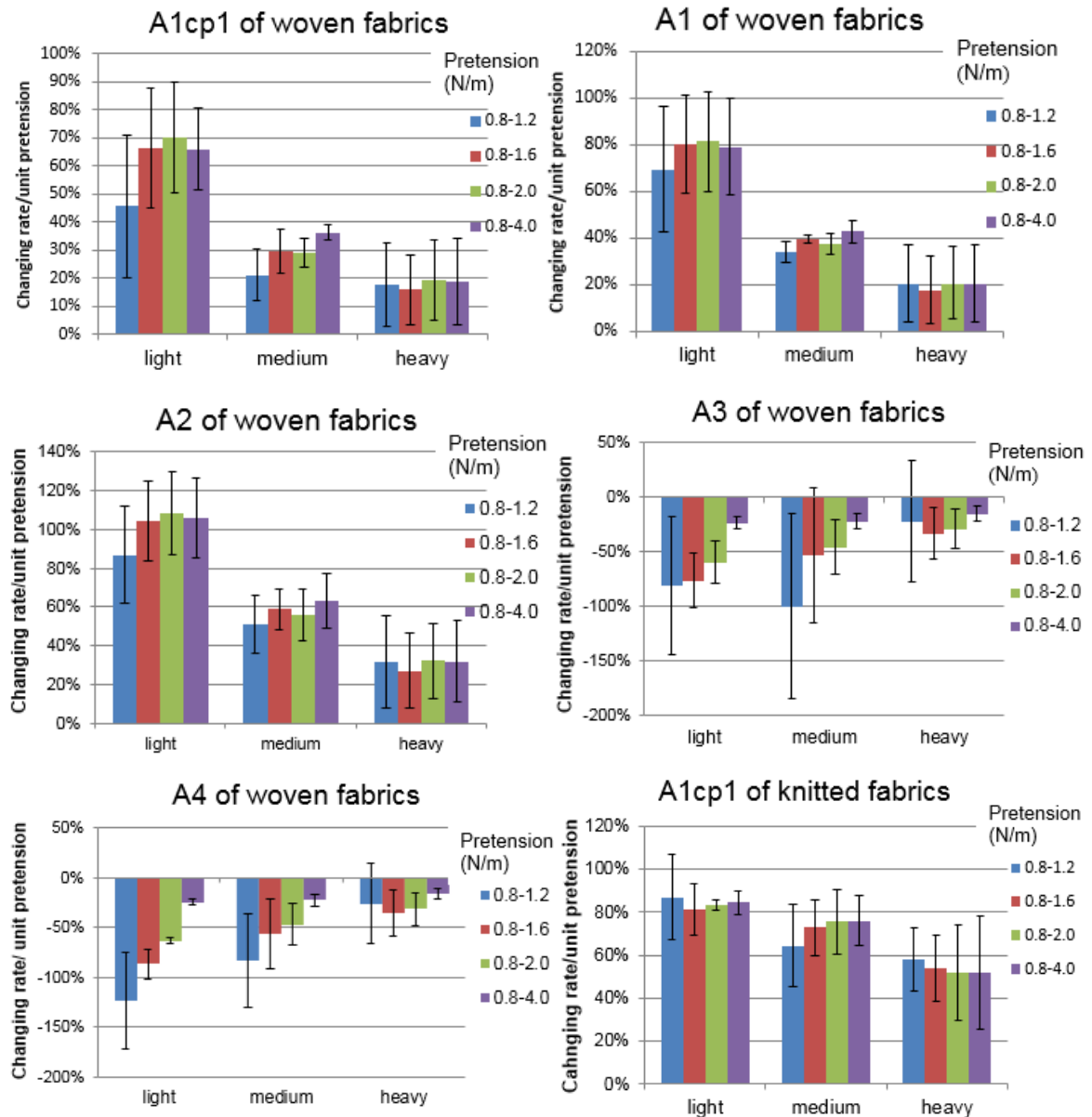
Where $E(P_i)$ and $A(P_i)$ are the modulus and energy consumed under the external pre-tension P_i ($P_i = 1.2; 1.6; 2.0; 4.0 \text{ N/m}$), respectively. As explained in section 4.1.2.1, the pre-tension of 0.4 N/m (i.e., the pre-tension force of 0.1 N applied on fabric shell having perimeter of 0.25 m) applied was not sufficient to straighten the fabric shell having wrinkles, so the pre-tension force of 0.8 N/m was the smallest pre-tension force used in this study. $E(0.8)$ and $A(0.8)$ are the modulus and energy consumed for each fabric under pre-tension of 0.8 N/m and they are used as references to evaluate the changing rate of energy and modulus with the increase of pre-tension.

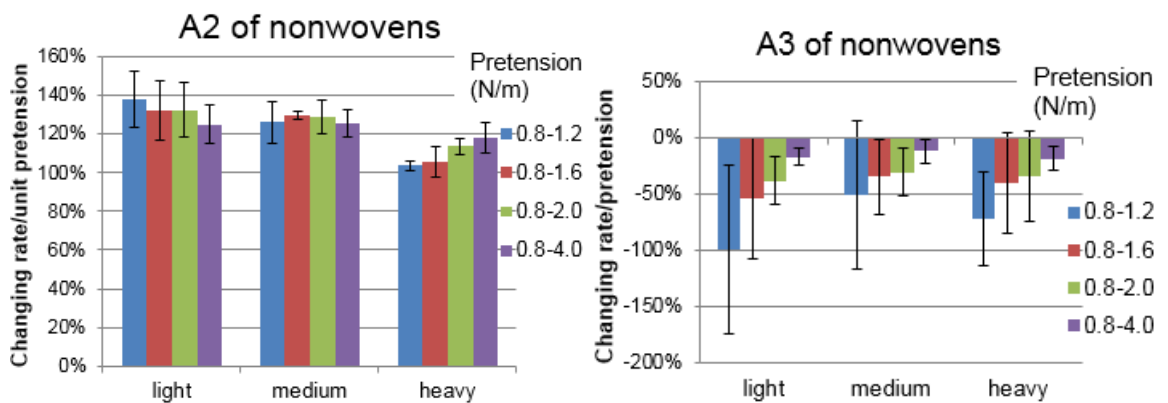
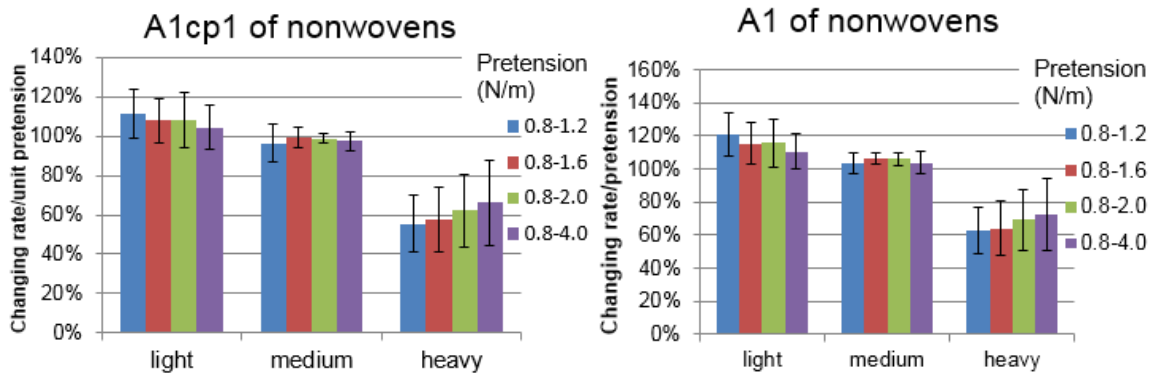
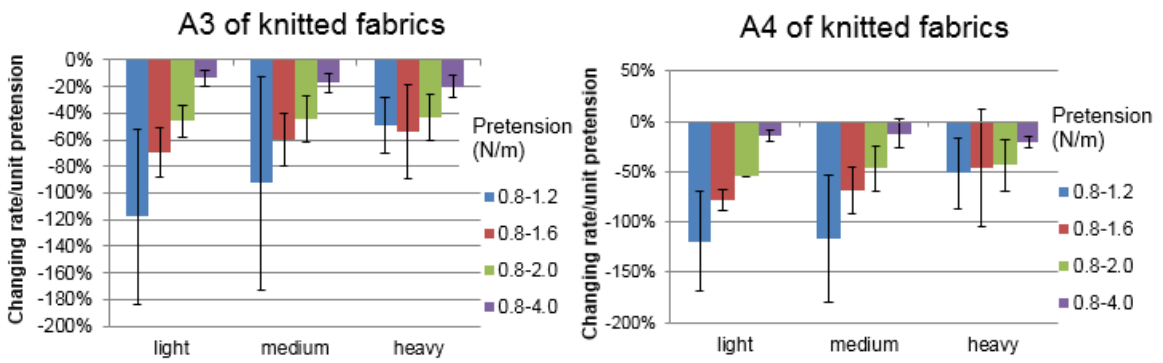
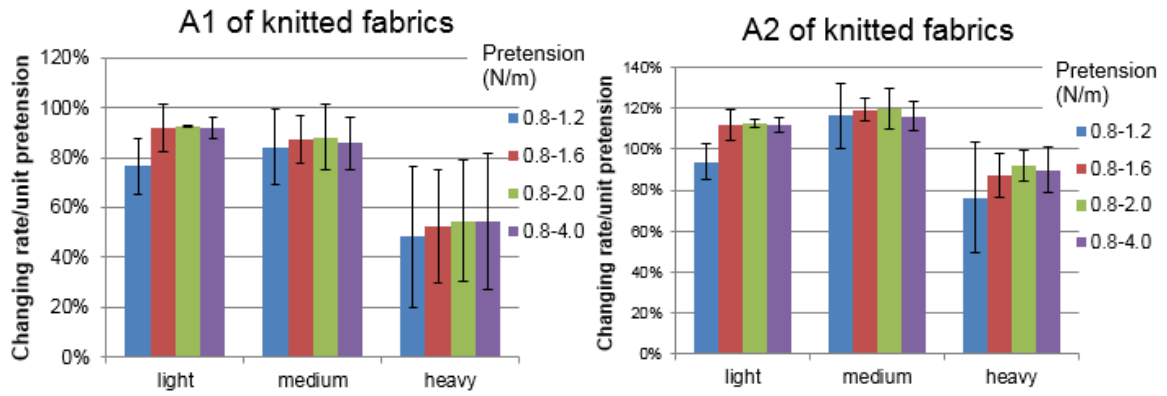
Because it was found that energies consumed to deform and recover fabric shells (e.g. A1cp1, A1 and A2) are affected by fabric mass per unit area, fabrics are grouped into three groups: light, medium and heavy fabric groups according to their fabric mass per unit area (see Table 4.10).

Table 4.10 Three fabric groups based on fabric mass per unit area

Fabric groups	Mass per unit area of fabrics (g/m ²)		
	Woven fabrics	Knitted fabrics	Nonwoven fabrics
Light	<200 (W1, W5)	<150 (K6)	<30 (N1, N6, N8)
Medium	200-300 (W4, W10)	150-300 (K2, K5)	30-50 (N2, N5)
Heavy	>300 (W11, W12)	>300 (K3, K7)	>50 (N3, N4)

The changing rates of both energy consumption and modulus together with their standard deviations when the pre-tension increases from 0.8 to 1.2N/m, 0.8 to 1.6N/m, 0.8 to 2.0N/m, and 0.8 to 4.0N/m are shown in Figure 4.25 and Figure 4.26, respectively.





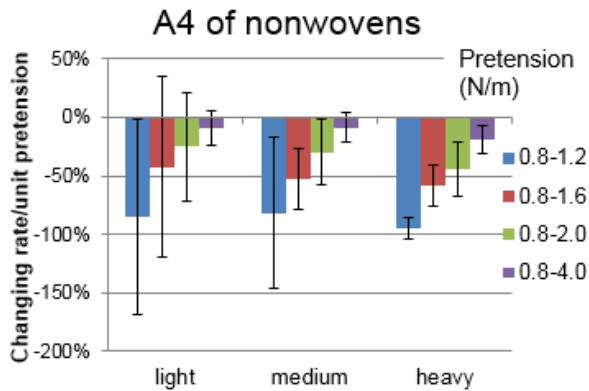


Figure 4.25 Changing rates of energy per unit pre-tension for woven, knitted and nonwoven fabrics with the increase of pre-tension

For heavy woven fabrics, the changing rates of energy consumed (A1cp1, A1 and A2) hardly have abrupt change within the range of pre-tensions used in this research (i.e., less than 4.0N/m). For most heavy knitted and nonwoven fabrics, the changing rates of energy consumed (A1cp1, A1 and A2) constantly increase with the increase of pre-tension within the range of pre-tensions used in this research (i.e., less than 4.0N/m).

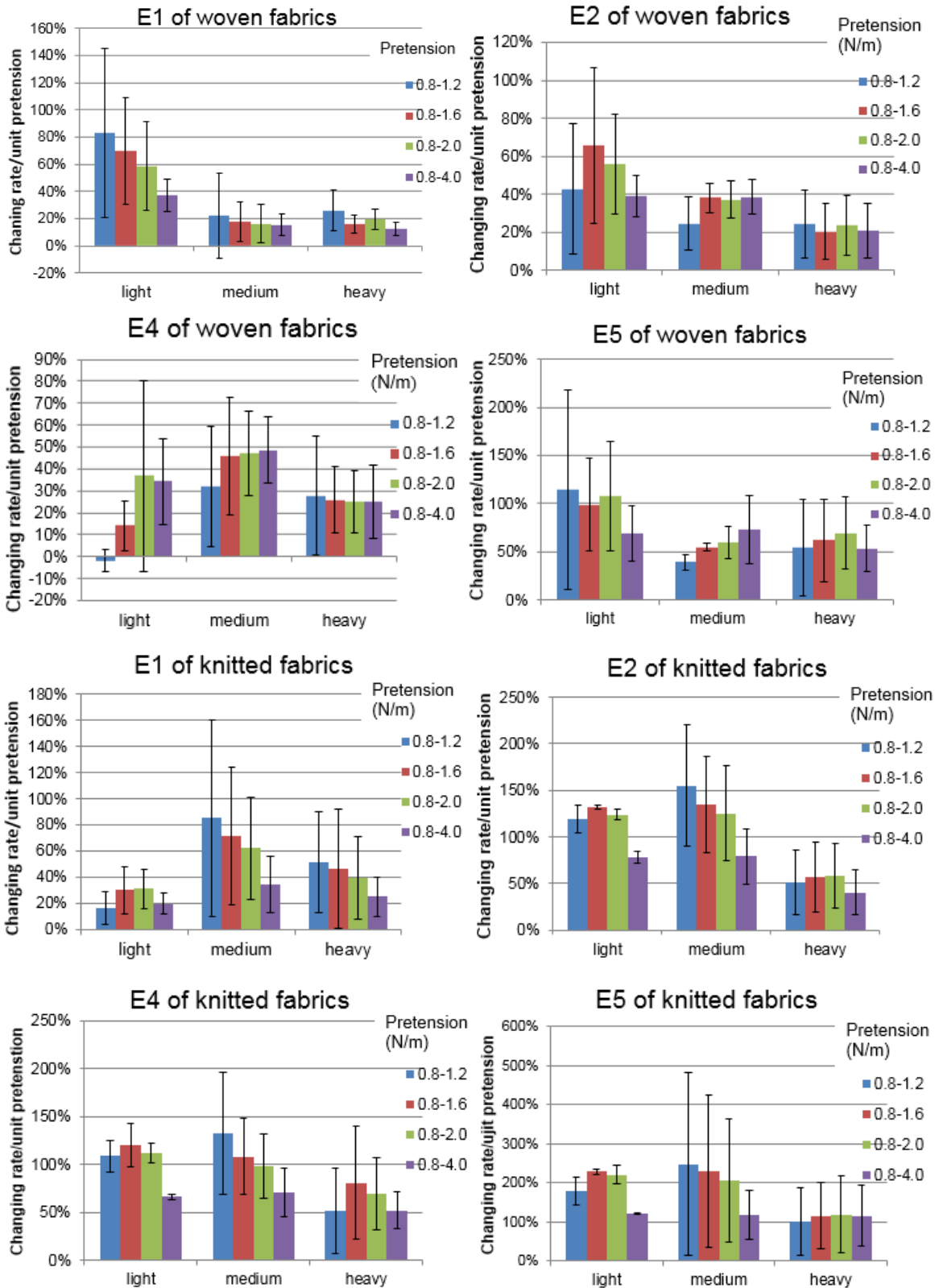
For medium weight woven, knitted and nonwoven fabrics, the changing rates of energy consumed (A1cp1, A1 and A2) hardly have abrupt change with the increase of pre-tension within the range of pre-tensions used in this research.

For light weight woven fabrics, the changing rates of energy consumed (A1cp1, A1 and A2) have constant increases when the pre-tension is less than 2.0N/m and have a small abrupt decrease when the pre-tension is greater than 2.0N/m. For light weight knitted fabrics, the changing rates of energy consumed (A1cp1, A1 and A2) have an abrupt increase when the pre-tension is greater than 1.2N/m, then have hardly any change when pre-tension increases from 1.2N/m to 4.0N/m. For light weight nonwoven fabrics, the changing rates of energy consumed (A1cp1, A1 and A2) constantly decrease with the increase of pre-tension within the range of pre-tensions used in this research (i.e., smaller than 4.0N/m).

For all of these fabrics, the changing rates of energy consumed to form permanent and recoverable deformations (A3 and A4) constantly decrease with the increase of pre-tension within the range of pre-tensions used in this research (i.e., smaller than 4.0N/m). But changing rates always have significant decreases when pre-tension is greater than 2.0N/m.

Any constant and abrupt changes of the changing rates of energies consumed (A1cp1, A1 and A2) indicate the excess fabric structure changes. For these woven, knitted and nonwoven fabrics studied, most of their abrupt increases happen when the pre-tension is greater than 1.2N/m, and either abrupt increases

or decreases of them happen when pre-tension is greater than 2.0N/m. Therefore the pre-tension applied on these fabric shells is suggested to be greater than 1.2N/m and less than 2.0N/m.



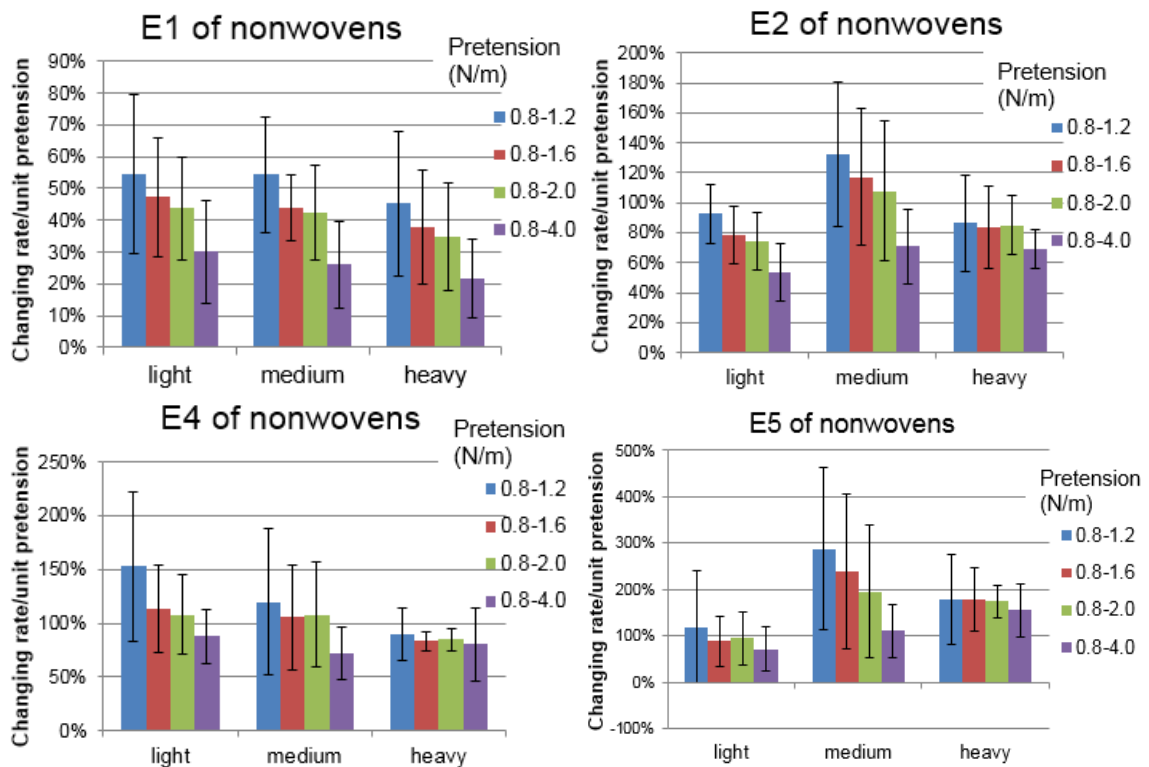


Figure 4.26 Changing rates per unit pre-tension of modulus for woven, knitted and nonwoven fabrics with the increase of pre-tension

Regarding compression buckling Young's modulus, the changing rates of modulus (E1, E2, E4 and E5) have abrupt changes (either increases or decreases) when pre-tension is greater than 2.0N/m for light weigh woven fabrics, and light and medium weight knitted and nonwoven fabrics.

For heavy weight woven fabrics, there is hardly apparent abrupt change in the changing rates of modulus (E1, E2, E4 and E5) within the pre-tensions applied. For medium weight woven fabrics, there is hardly apparent abrupt change in the changing rate of modulus (E1, E2, E4 and E4) when pre-tension is greater than 1.2N/m. For heavy weight knitted and nonwoven fabrics, there is an apparent abrupt decrease of the changing rates of modulus E1 and E2 when pre-tension is greater than 2.0N/m.

Since changes of modulus represent the intrinsic structural changes of fabrics, any abrupt changes of fabric structures due to the pre-tensions applied should be avoided, it is thus concluded that pre-tension which is greater than 1.2N/m and smaller than 2.0N/m is suitable for the fabric shell compression buckling test in LUFHES for those woven, knitted and nonwoven fabrics.

As a summary of the conclusions from both energy consumed and modulus changes, and with the consideration of the possible influences of creases and wrinkles on the fabric deformations (see Figure 4.8), a pre-tension of 2.0N/m is

suggested to be applied on all of the fabric testing in the LUFHES tests throughout this research.

4.8 Summary

The main findings of this chapter are summarized as below:

1. Pre-tensions applied on fabric shells during cyclic biaxial compression buckling deformation process stiffened fabrics;
2. Fabric structural changes due to pre-tensions exerted were quantified by using the changes of compression buckling Young's modulus during compression buckling process. For most of woven, knitted and nonwoven fabrics, compression buckling Young's modulus (E1, E2, E4 and E5) increased linearly with the increase of pre-tension;
3. Greater pre-tensions lead to greater energy consumption to deform fabric shells in fabric compression buckling (A1cp1 and A1) and greater strain energy released from deformed fabric (A2) to self-recover the elastic compression buckling deformations. These energies increased linearly with the increase of pre-tension;
4. Greater pre-tensions applied on fabric shells also lead to smaller energy consumption to form recoverable (A4) and permanent (A3) fabric deformations during fabric shell buckling-recovery process;
5. In comparison with lightweight and thin woven, knitted and nonwoven fabrics, corresponding heavyweight and thick fabrics usually required greater energy to be deformed in compression buckling process, to form permanent deformations and to recover recoverable deformations. However, only heavy and thick woven fabrics usually released greater strain energy to self-recover deformed fabrics;
6. In comparison with thick fabrics, thin woven, knitted and nonwoven fabrics usually have greater compression buckling Young's modulus (E1, E2, E4 and E5) before undeformed/recovered fabric buckles (E1/E2), during forming permanent deformation (E4) and recovering recoverable deformation (E5);
7. The changes of energy consumptions with the fabric structural change were shown in the relationship between energy consumptions and compression buckling Young's modulus. For all the woven fabrics, most knitted fabrics and nonwoven fabrics tested, energy consumed to deform fabric shells in fabric compression buckling (A1cp1 and A1) increased linearly with the increase of compression buckling Young's modulus (E1 and E2). While energy consumed to form permanent deformation (A3) and energy consumed to recover recoverable deformation (A4) decreased initially with the increases of the compression buckling Young's modulus (E4 and E5), when modulus reached a specific value, A3 and A4 either decreased slowly with the increase modulus or hardly had significant change.

8. Suitable pre-tensions for the fabric shell compression buckling tests for a wide range of woven, knitted and nonwoven fabrics were found in the range of 1.2N/m to 2.0N/m.

Chapter 5 Differences between shear modulus and shear rigidity obtained in unidirectional and biaxial deformation

In this chapter, a model is built to calculate the shear modulus obtained in LUFHES and its characteristics are analysed. In addition, the differences of the fabric shear modulus obtained in unidirectional deformations (e.g., in the FAST and the KES-F systems) and biaxial deformations (e.g., in the LUFHES) are compared to determine if there is any difference between these three systems in objectively evaluating fabric shear properties. Differences of corresponding fabric shear rigidities obtained in the three systems are compared to identify their differences in discriminating fabrics.

5.1 Fabric materials used in the research

Shear modulus (and shear rigidity) of 22 fabrics listed in Table 5.1 are obtained in the LUFHES, FAST and KES-F shear tests. These 22 fabrics include 11 woven fabrics, 7 knitted fabrics and 4 nonwoven top sheet fabrics, and their specifications are introduced in Table 3.1.

Table 5.1 Fabrics used in the study of shear properties using unidirectional and biaxial testing systems

Woven fabrics	W1, W2, W3, W4, W6, W7, W8, W9, W10, W11, W12
Knitted fabrics	K1, K2, K3, K4, K5, K6, K7
Nonwoven fabrics	N1, N8 [‡] , N10, N11 [‡]

[‡]Fabrics which had only two repeats in the KES-F test due to limited amount of fabrics available.

5.2 Analysis of fabric shear modulus obtained in the three systems: FAST, KES-F and LUFHES

In this section, theoretical analysis of fabric shear modulus based on the analysis of the fabric shear deformation process in the FAST, KES-F and LUFHES are given.

5.2.1 FAST testing system

Fabric shear rigidity are obtained in the FAST system by measuring the extensibility, $\varepsilon(\%)$, of a fabric strip in bias direction under a constant extension force of 4.9N/m. Six specimens including three in 45° and three in 135° directions are evaluated, and the average of the six extensibility obtained is used to calculate the fabric shear rigidity (De Boos and Tester, 1994). However, the

previous analysis of the fabric shear rigidity is based on the assumption that fabric extension in bias direction is solely due to fabric shear displacement without fabric yarn elongation during the shear test.

With consideration of possible large extension of fibres/yarns in some woven, knitted and nonwoven fabrics used in this research, a modified shear modulus model based on the analysis of the fabric shear deformation process is given below.

5.2.1.1 Modelling the change of shear angles in the FAST bias extension test

A constant force (4.9N/m) was applied on the fabric strip in the FAST bias extension test, so the shear angle of different fabrics varies with the fabric bias extensions. A model for the analysis of fabric shear deformation in the FAST bias extension testing process is shown in Figure 5.1 (a).

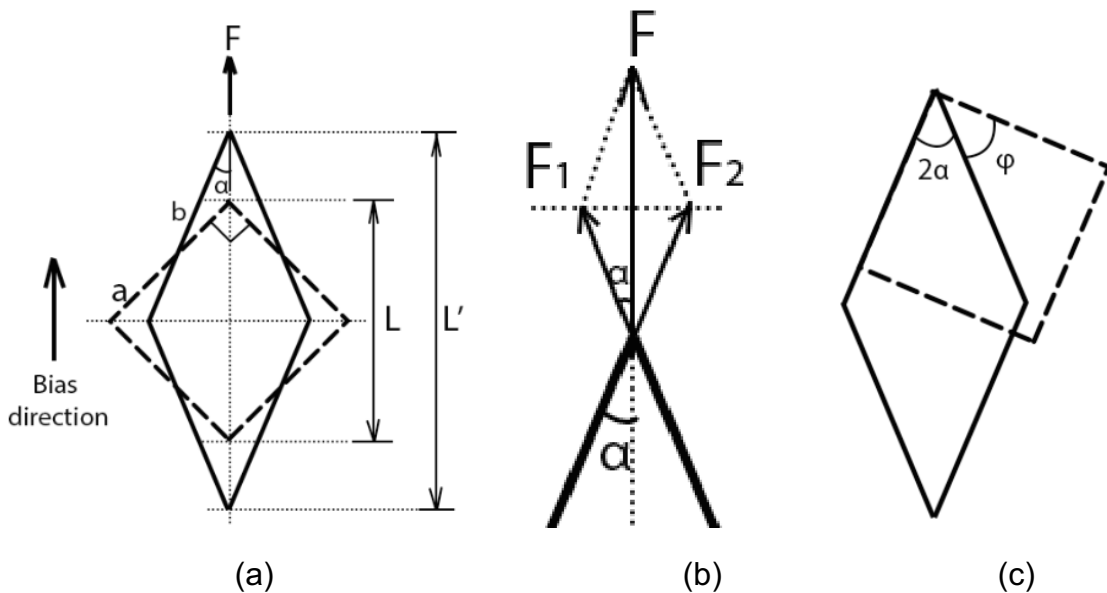


Figure 5.1 Fabric shear deformation in the FAST bias extension test

It is assumed that the fabric studied is homogenous and elastic; it has identical Young’s modulus (E) in its two principal orthogonal directions (e.g., warp/weft directions for woven fabric, wale/course direction for knitted fabric, and MD/CD for nonwoven fabric). A square having side length, a , on the fabric surface plane before extension (Figure 5.1 (a)) is considered in the analysis. The four sides of the square are parallel to the fabric two principal orthogonal directions (e.g., weft/warp, wale/course and MD/CD), respectively. Thus, its diagonal length, L , is:

$$L = \sqrt{2}a \dots \dots \dots (5.1)$$

When an extension force, F , is applied onto the fabric strip in its bias direction, the shape of square is deformed with the extension of the fabric strip. When the fabric

reaches a new stable status (Figure 5.1 (a)) under the force F , the shape of the square turns into a parallelogram having a side length of b and an acute angle of 2α (see Figure 5.1 (a)), we have,

$$b = a + \Delta a \dots\dots\dots (5.2)$$

$$\cos\alpha = \frac{\frac{L'}{2}}{b} \dots\dots\dots (5.3)$$

Where Δa is the fabric extension in the two orthogonal side length directions.

The diagonal length of the parallelogram, L' , is different from the original diagonal length, L , due to both the fabric extension under the applied force, F , in the fabric diagonal direction, and the shear deformation of the fabric.

The total strain along the fabric bias direction, ϵ , is known in the FAST bias extension test, we thus have,

$$L' = L \times (1 + \epsilon) \dots\dots\dots (5.4)$$

The change of the side length from a in the square into b in the parallelogram is due to the fabric extension under the applied force F , whose component forces along the side length of the parallelogram, F_1 and F_2 , are shown in Figure 5.1 (b). Thus, we have,

$$F_1 = F_2 = \frac{F}{2\cos\alpha} \dots\dots\dots (5.5)$$

Also, the fabric unidirectional Young's modulus in the two orthogonal directions (e.g., warp and weft), E , are defined in the equation 5.6,

$$E = \frac{F_1 \cdot a}{A_c' \cdot \Delta a} \dots\dots\dots (5.6)$$

Where A_c' is the cross-section area of fabric in two orthogonal directions of the square, we have,

$$A_c' = \sqrt{2}A_c \dots\dots\dots (5.7)$$

Where A_c is the cross-section area of fabric strip in bias direction.

Substituting equation 5.5 and 5.7 into 5.6 and rearrange equation 5.6, we have,

$$\Delta a = \frac{F}{2\sqrt{2}\cos\alpha} \cdot \frac{a}{A_c \cdot E} \dots\dots\dots (5.8)$$

Substitute equations 5.1, 5.2, 5.4 and 5.8 into equation 5.3, we have,

$$\cos\alpha = \frac{\sqrt{2}(1+\epsilon)}{2 + \frac{F}{\sqrt{2}A \cdot E \cdot \cos\alpha}} \dots\dots\dots (5.9)$$

Rearrange equation 5.9, we have,

$$\cos\alpha = \frac{\sqrt{2}}{2} \left[(1 + \varepsilon) - \frac{F}{2AE} \right] \dots\dots\dots (5.10)$$

Shear angle, φ , is thus shown in equation 5.11 below,

$$\varphi = 90^\circ - 2\alpha = 90^\circ - 2 \times \arccos \left(\frac{\sqrt{2}}{2} \left[(1 + \varepsilon) - \frac{F}{2AE} \right] \right) \dots\dots\dots (5.11)$$

Based on equation 5.11, the fabric shear angle during the FAST test does not only depend on fabric extension obtained and the force applied (F), but also vary with the fabric Young’s modulus, this means that the fabric extensions obtained in the FAST test could have greater error if they are used to represent the changes of fabric shear angles when fabrics have relatively smaller Young’s modulus (E) in orthogonal directions (warp/weft direction of woven fabric, wale/course direction of knitted fabric and MD/CD of nonwoven fabric); such error could be much reduced when fabrics have greater Young’s modulus (E) in both two orthogonal directions.

5.2.1.2 Shear modulus obtained in the FAST bias extension test

For woven fabrics, the relationship between Young’s modulus in bias direction and shear modulus is shown in equation 5.12 below (Kilby, 1963),

$$E_{45} = 4G \dots\dots\dots (5.12)$$

In the standard FAST bias extension test, the extension of a fabric strip in bias direction (ε (%)) is measured when a constant force of 4.9N/m is applied on the fabric strip having a thickness t (m) in the bias direction. Young’s modulus of the fabric strip in bias direction, E_{45} (Pa), is thus calculated in equation 5.13,

$$E_{45} = \frac{\sigma}{\varepsilon} = \frac{\frac{F}{A_c}}{\frac{\varepsilon(\%)}{100}} = \frac{\frac{4.9}{t}}{\frac{\varepsilon(\%)}{100}} = \frac{490}{\varepsilon(\%) \cdot t} \dots\dots\dots (5.13)$$

Substitute equation 5.13 into equation 5.12, the fabric shear modulus obtained in the FAST test, G_{FAST} , is thus given in equation 5.14,

$$G_{FAST} = \frac{122.5}{\varepsilon(\%) \cdot t} \dots\dots\dots (5.14)$$

Thus the shear rigidity obtained in the FAST, SR_{FAST} , is given in equation 5.15 (De Boos and Tester, 1994):

$$SR_{FAST} = G_{FAST} \times t = \frac{122.5}{\varepsilon(\%)} \dots\dots\dots (5.15)$$

According to the FAST manual, the equation 5.15 (*shear rigidity* = $\frac{123}{\varepsilon(\%)}$) used to evaluate fabric shear property was based on the equation 5.12 for homogenous and symmetric plain woven fabrics. Thus the FAST bias extension test might not suitable to measure shear rigidity and shear modulus of fabric structures other

than plain woven fabrics (e.g., twill woven fabrics, satin woven fabrics, knitted fabrics, nonwoven fabrics and composite fabrics).

5.2.2 KES-F testing system

In the KES-F shear test process, the two ends of a piece of fabric are fixed by using two chucks, its effective test area is 50mm x 200mm (length x width). During the shear test, one chuck is stationary, and the other one moves leftwards and rightwards to up to 8°. Force required to increase the shear angle is measured. An extensional force of 100g (4.9N/m) is applied on the fabric of 200mm in width by using a bottom clamp during shear test.

A typical shear curve obtained in the KES-F shear test is shown in Figure 5.2.

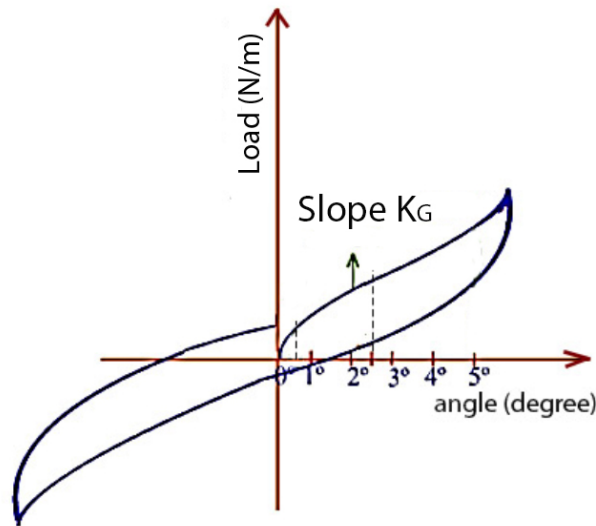


Figure 5.2 Typical shear curve obtained in the KES-F system

Two slopes of shear curve between ±0.5° and ±2.5° are calculated by the KES-F software, and the average of these two slopes is used to evaluate fabric shear property by the KES-F system (Hu, 2000). This slope is marked as K_G in this study, and equations are developed to calculate fabric shear modulus and shear rigidity obtained in the KES-F by using K_G .

Shear modulus G is defined as (Behera and Hari, 2010):

$$G = \frac{d\tau}{d\gamma} \dots\dots\dots (5.16)$$

In which τ is shear stress and γ is shear strain. Shear stress τ is:

$$\tau = \frac{F}{A} = \frac{F_{KESF} \times W}{W \cdot t} = \frac{F_{KESF}}{t} \dots\dots\dots (5.17)$$

Where F_{KESF} is the force applied to shear fabric (N/m) (y-axis of curve in Figure 5.2); W is the width of specimen (m); t is the thickness of fabric (m).

Shear strain, γ , is thus given in equation 5.18:

$$\gamma = \tan\theta \dots\dots\dots (5.18)$$

Where θ is the shear angle of the fabric in degree (x-axis of curve in Figure 5.2);

When θ is small (between 0.5° and 2.5°), the shear strain approximately equals to radian of θ :

$$\gamma = \frac{\theta \times \pi}{180} \dots\dots\dots (5.19)$$

Substitute equations 5.17 and 5.19 into 5.16, we have the shear modulus obtained in the KES-F shear test, G_{KESF} , shown in equation 5.20,

$$G_{KESF} = \frac{d\left(\frac{F_{KESF}}{t}\right)}{d\left(\frac{\theta \times \pi}{180}\right)} = K_G \cdot \frac{180}{\pi t} \dots\dots\dots (5.20)$$

Where $K_G = \frac{dF_{KESF}}{d\theta}$ is the slope of the force-degree curve measured in the KES-F shear test.

It is noticed that G_{KES-F} could have significant errors when K_G for a piece of fabric is not linear during the shear deformation process.

It is realised that there is an extension force, $N=4.9N/m$, applied on the fabric perpendicular to the shear movement direction during the KES-F shear test and this extension force might lead to greater G_{KES-F} . The force applied on fabric during the KES-F shear test when shear angle is θ is shown in Figure 5.3.

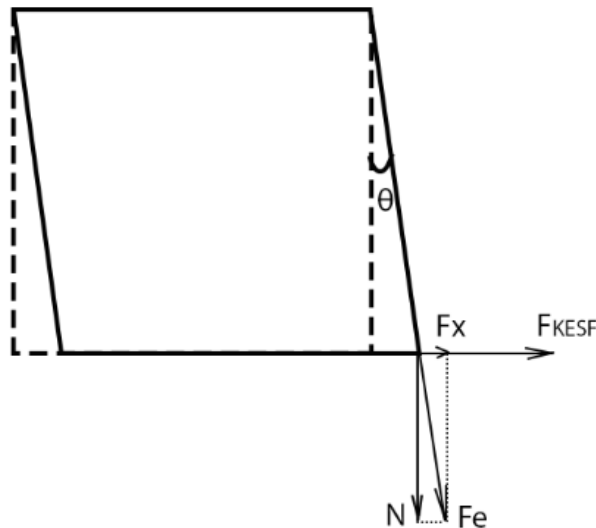


Figure 5.3 Force analysis of fabric in the KES-F shear test

Due to the vertical extension force N , fabric is extended during the KES-F shear test. The force applied to extend the fabric is denoted as F_e , which has a component force F_x in transverse direction as shown in Figure 5.3. According to the relationship between F_x and N , we have,

$$F_x = N \cdot \tan\theta \dots\dots\dots (5.21)$$

Therefore the actual effective shear force F applied on fabric in the KES-F shear test is (Wang et al., 2008):

$$F = F_{KESF} - F_x = F_{KESF} - N \cdot \tan\theta \dots\dots\dots (5.22)$$

Where F_{KESF} is the force measured in the KES-F; θ is the fabric shear angle.

Then the normalized shear modulus of fabric obtained in the KES-F shear test excluding the effect of the extension force N is deduced as below:

$$\tau = \frac{F \cdot W}{t \cdot W} = \frac{F}{t} = \frac{F_{KESF} - N \cdot \tan\theta}{t} \dots\dots\dots (5.23)$$

$$\gamma = \tan\theta \dots\dots\dots (5.24)$$

Where τ is shear stress; γ is shear strain; W is the width of fabric plate; and t is fabric thickness.

Substitute equation 5.23, 5.24 into equation 5.16, we have,

$$G_{KESF-Norm} = \frac{d\tau}{d\gamma} = \frac{d\left(\frac{F_{KESF} - N \cdot \tan\theta}{t}\right)}{d(\tan\theta)} = G_{KESF} - \frac{N}{t} \dots\dots\dots (5.25)$$

5.2.3 LUFHES system

Fabric shear modulus obtained in the LUFHES shear test is based the biaxial torsion deformation process of a fabric shell, which is different from the fabric shear deformation in both the KES-F and FAST tests. During the LUFHES shear test, the top end of fabric shell is fixed, and the bottom end of the fabric shell is twisted up to 5° and then returned back to its original position. The dynamic changes of the torque required to form shear deformation in the fabric shell against the twisting angle (degree) is obtained as shown in Figure 5.4.

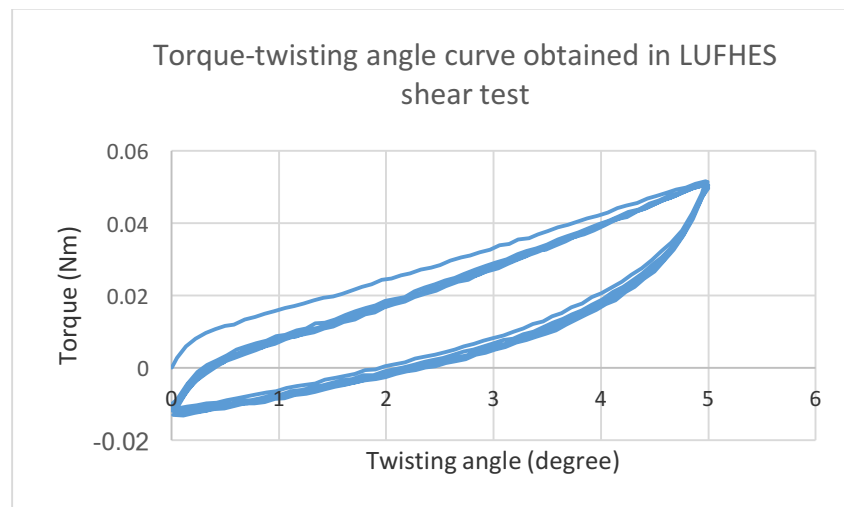


Figure 5.4 A typical torque (Nm)-twisting angle (degree) curve obtained in the LUFHES shear test

The models used to obtain fabric shear modulus and shear rigidity from the relationship between torque and twist degree are established below.

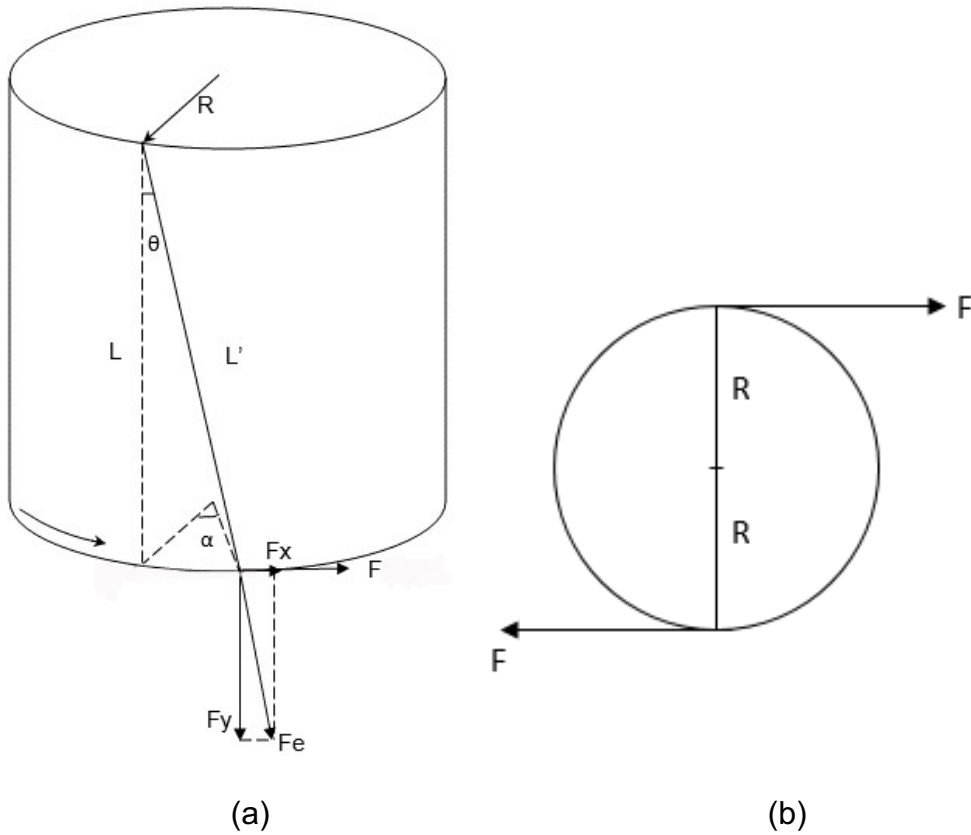


Figure 5.5 Force analysis of a fabric shell in the LUFHES shear test

The force applied on the fabric shell during the LUFHES shear test is shown in Figure 5.5. During the fabric shell shear deformation, a pair of torque forces F - F (Figure 5.5(b)) is applied on the circumference of the bottom end of the fabric cylindrical shell, which has a diameter of $2R$ and length of L . When the bottom end of the fabric shell is twisted in an angle of α (degree), the shear angle of the fabric shell, θ (radian), is shown in Figure 5.5(a). The relationship between shear angle θ and the twisting angle α is shown in equation 5.26 below,

$$\theta = \frac{\pi R \alpha}{180 \cdot L} \dots \dots \dots (5.26)$$

As the gauge length between top and bottom sample holder is fixed, which is the same as the effective length of the fabric shell, L , the length of the yarns aligned in the fabric shell longitudinal direction is extended to L' during this shear deformation process. The force applied to extend the fabric shell is denoted as F_e , which has a component force F_x in transverse direction. For the force applied to shear fabric, F_{shear} , we have,

$$F = F_{shear} + F_x \dots \dots \dots (5.27)$$

The twist of fabric shell is a force couple system as shown in Figure 5.5(b). So,

$$F = \frac{T}{2R} \dots\dots\dots (5.28)$$

Where T (Nm) is the torque applied to shear fabric; R (m) is radius of fabric cylindrical shell.

The vertical force F_Y , which is the component of F_e in fabric shell longitudinal direction, is known in the LUFHES shear test. According to the relationship between F_X and F_Y in Figure 5.5(a), we have

$$F_X = F_Y \cdot \tan\theta \dots\dots\dots (5.29)$$

Substitute equations 5.28 and 5.29 into 5.27, we have,

$$F_{shear} = \frac{T}{2R} - F_Y \cdot \tan\theta \dots\dots\dots (5.30)$$

Thus we have shear stress τ and shear strain γ ,

$$\tau = \frac{F_{shear}}{A'} = \frac{F_{shear}}{\pi R t} \dots\dots\dots (5.31)$$

$$\gamma = \tan\theta \dots\dots\dots (5.32)$$

Where A' is the cross-section area of semicircle on which F_{shear} acts; R is the radius of the fabric cylindrical shell and t is the fabric thickness.

Substitute equations 5.26 and 5.30 into 5.31, we have,

$$\tau = \frac{T}{2\pi R^2 t} - \frac{F_Y \cdot \tan\theta}{\pi R t} = \frac{T}{2\pi R^2 t} - \frac{F_Y \cdot \tan\frac{\pi R \alpha}{180 \cdot L}}{\pi R t} \dots\dots\dots (5.33)$$

Substitute equation 5.26 into 5.32, we have,

$$\gamma = \tan\theta = \tan\frac{\pi R \alpha}{180 \cdot L} \dots\dots\dots (5.34)$$

Substitute equations 5.33 and 5.34 into equation 5.16, we have

$$G_{LUFHES} = \frac{d\left(\frac{T}{2\pi R^2 t} - \frac{F_Y \cdot \tan\frac{\pi R \alpha}{180 \cdot L}}{2\pi R t}\right)}{d\left(\tan\frac{\pi R \alpha}{180 \cdot L}\right)} \dots\dots\dots (5.35)$$

An example of the relationship between shear stress τ and shear strain γ during fabric shear deformation is shown in Figure 5.6 , and the shear modulus of some typical fabrics in different twisting angles in the LUFHES cyclic shear tests are shown in Figure 5.7- Figure 5.10. Because there are hardly noticeable differences between the shear stress-strain curves in the 2nd-5th cycles in the cyclic shear test, the average of shear modulus in the 2nd-5th cycles are shown.

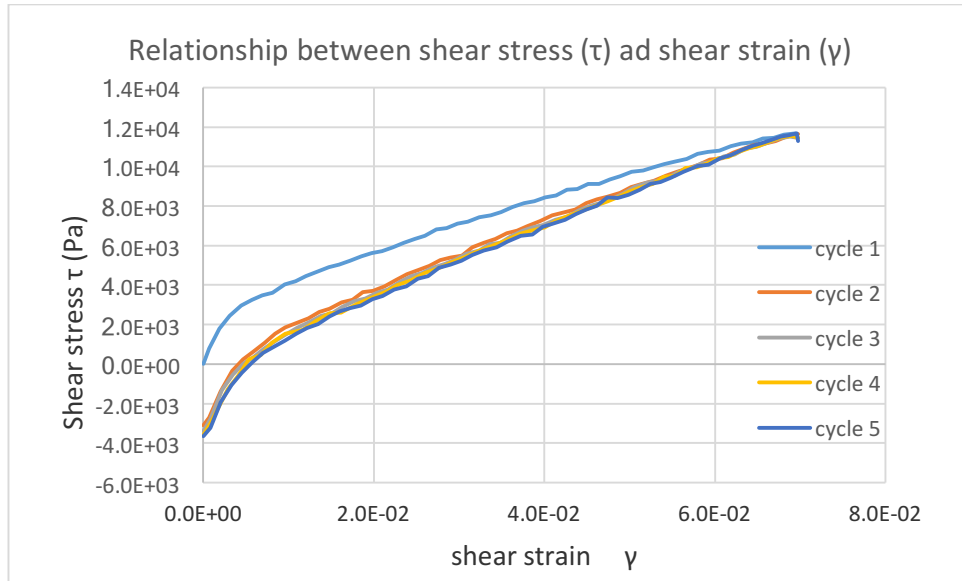


Figure 5.6 Relation between shear stress (τ) and shear strain (γ) of a plain woven cotton fabric (W5)

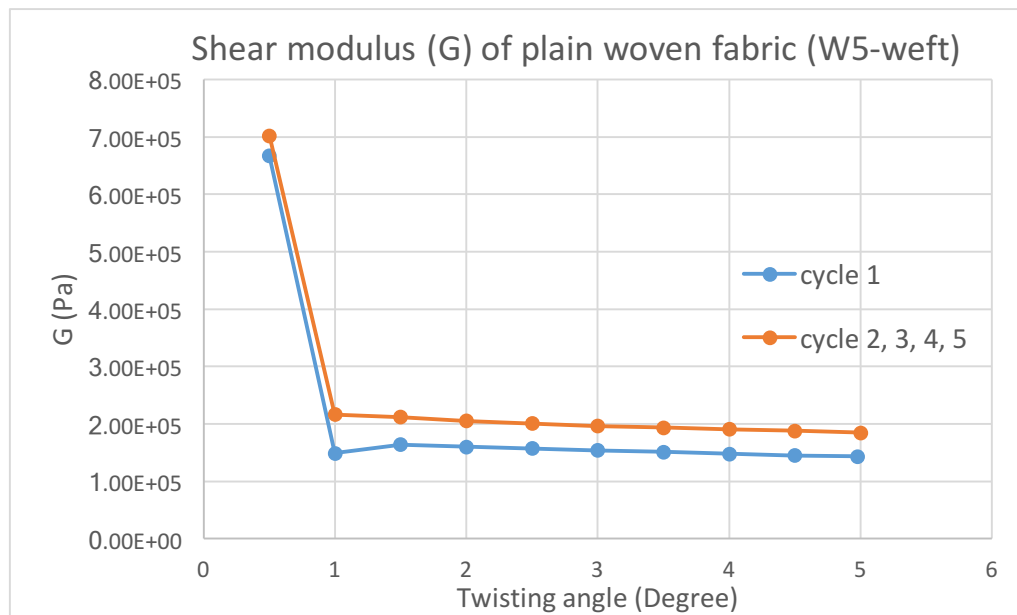


Figure 5.7 Shear modulus of a plain woven cotton fabric in weft direction obtained in the LUFHES twisting test

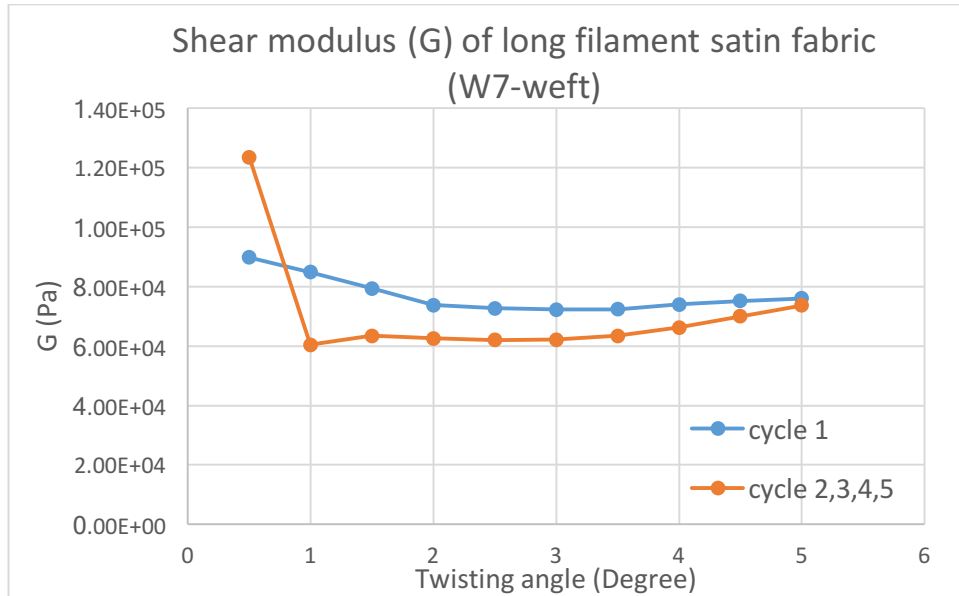


Figure 5.8 Shear stress-shear strain relationship and shear modulus of long filament satin fabric (W7-weft)

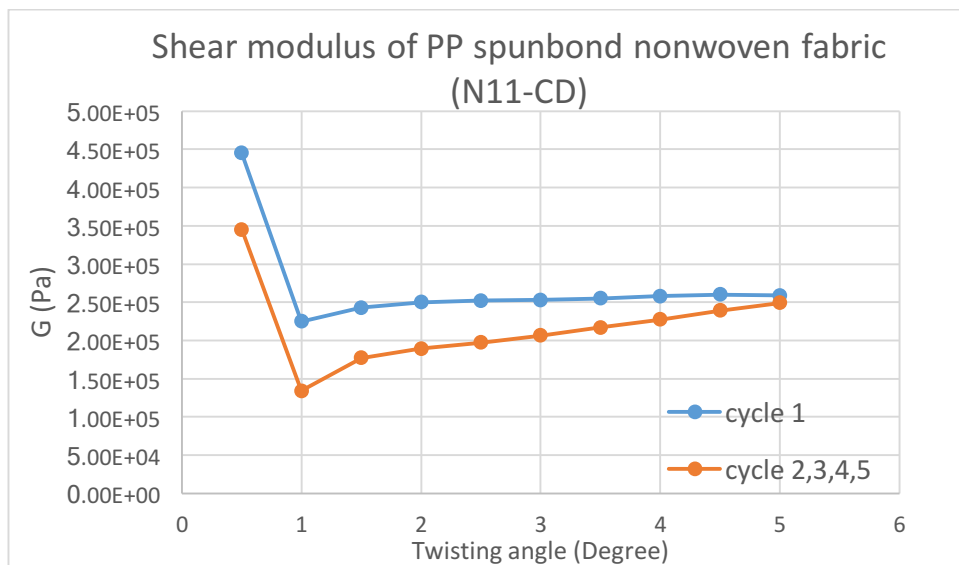


Figure 5.9 Shear stress-shear strain relationship and shear modulus of Polypropylene spunbond nonwoven fabric (N11-CD)

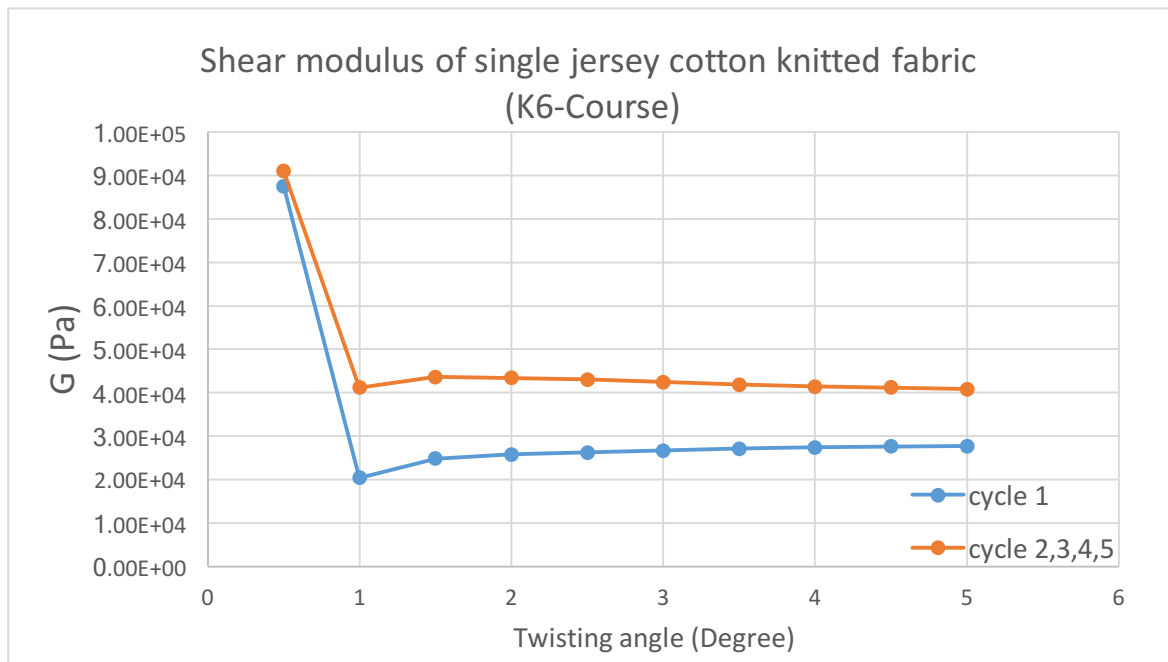


Figure 5.10 Shear stress-shear strain relationship and shear modulus of single jersey cotton knitted fabric (K6-Course)

It is found that the shear stress (τ) increases linearly with the increases of twisting angles when the twisting angle is greater than 0.5° but varies differently when the twisting angle is less than 0.5° . It is shown that shear modulus of the three fabrics W5, N11 and K6 is much greater when the twisting angle is between 0 and 0.5° in the first cycle of shear testing, then decreases significantly and becomes constant between 0.5° and 5° . However, shear modulus of satin fabric W7 in $0-0.5^\circ$ does not have significant differences with shear modulus in $0.5^\circ-5^\circ$. It is noticed that the shear modulus in $0-0.5^\circ$ of all the four fabrics, W5, N11, K6 and W7, in the 2nd – 5th cycles are much greater than the shear modulus in $0.5^\circ-5^\circ$.

Leaf and Sheta (1984) stated that frictional resistance in the yarn/fibre intersection regions have to be overcome to generate movement in the initial stage of shear deformation. Lindberg (1964) also found that the shear stress increases rapidly at first due to frictional forces are produced when yarns move relatively at intersections. Therefore high initial shear modulus in $0-0.5^\circ$ of W5, N11 and K6 might be due to greater frictional resistance.

It is found that shear modulus of fabric W7 and N11 increase slightly with the increase of shear angle. It was believed in previous research (Gibson and Postle, 1978; Lindberg et al., 1961) that the increases of shear modulus with the increases of shear angles is a result of jamming. However, Gibson and Postle (1978) believed that buckling occurs when fabric is jammed and fabric buckling could lead to a drop of the shear modulus. This might imply that the yarns/fibres in

satin fabric W7 and nonwoven fabric N11 are relatively easy to be jammed when fabrics have greater angle deformation.

The differences of shear modulus of the satin fabric W7 between the first cycle and the 2nd – 5th cycles might imply that external forces applied would overcome friction between yarns/fibres to shear fabric in the initial of the first cycle, but would resist recovery of fabric's permanent deformation formed in the initial twisting of the 2nd – 5th cycles.

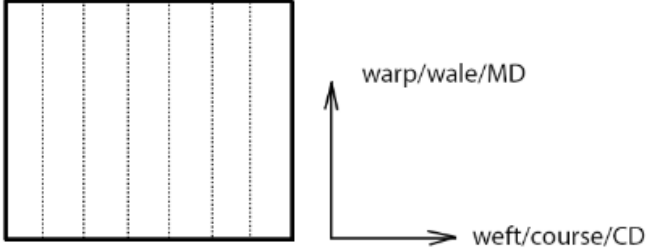
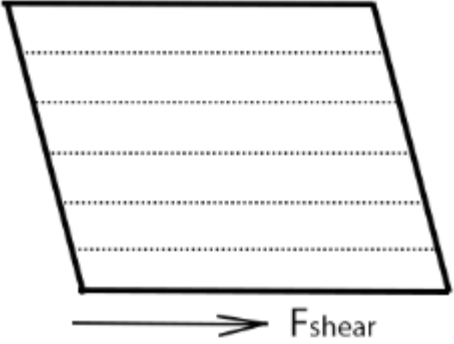
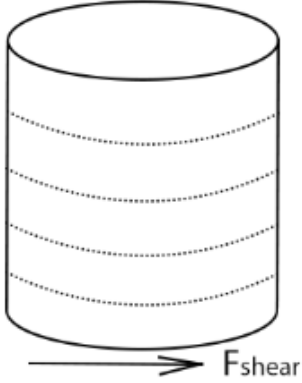
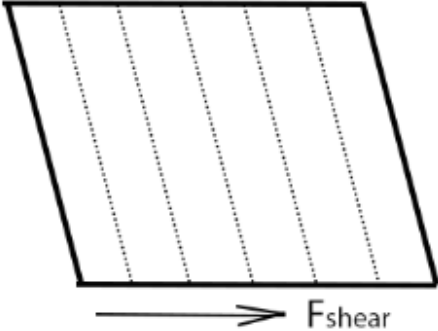
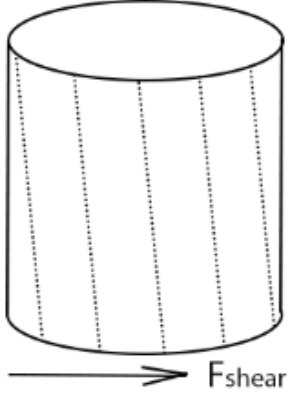
It is also found that the shear modulus of both tightly plain woven fabric W5 and dense knitted fabric K6, in the 2nd-5th cycles is greater than that in the first cycle, while the two loosely bonded fabrics, satin woven fabric W7 and nonwoven fabric N11, have greater shear modulus in the first cycle than in the 2nd-5th cycles. The reason for these trends is unclear and would need further investigation.

5.3 Differences of shear modulus obtained in the LUFHES, FAST and KES-F systems

Differences of shear modulus of the 22 fabrics obtained in the LUFHES, FAST and KES-F systems are compared in Table 5.3. Shear modulus of each fabric in two directions are obtained in both the KES-F and LUFHES systems, while only one shear modulus is obtained in the FAST system.

The shear modulus of fabric in warp/wale/MD direction is obtained when a shear force is applied on fabric in warp/wale/MD direction in the KES-F and LUFHES tests as shown in Table 5.2. The shear modulus of fabric in weft/course/CD direction is obtained when a shear force is applied in weft/course/CD direction in the KES-F and LUFHES shear tests.

Table 5.2 Shear test of fabric in two directions in the KES-F and the LUFHES systems

Fabric		
	KES-F shear test	LUFHES shear test
Shear in warp/wale/MD		
Shear in weft/course/CD		

Both shear modulus, G_{KESF} , and the normalized shear modulus, $G_{KESF-Norm}$, in the KES-F shear test are given in Table 5.3. It is shown that $G_{KESF-Norm}$ is smaller than G_{KESF} and the effect of the extension force (4.9N/m) has greater impact on the shear modulus of thin fabrics, such as woven fabrics W1 and W7.

Table 5.3 Fabric shear modulus obtained in the FAST, KES-F and LUFHES systems

Fabric		$G_{KESF} / G_{KESF-Norm}$ (Pa)		G_{LUFHES} (Pa)		G_{FAST} (Pa)* Constant extension force of 4.9 N/m
		Constant shear angle of $\pm 0.5^\circ - \pm 2.5^\circ$		Constant shear angle of $0.5^\circ - 4.0^\circ$		
		Original shear modulus	Normalized shear modulus	First cycle	2 nd -5 th cycle	
W1	Warp	2.35E+05	1.86E+05	2.46E+05	2.55E+05	2.37E+05
	Weft	2.48E+05	1.99E+05	2.06E+05	2.50E+05	
W2	Warp	2.85E+05	2.72E+05	1.62E+05	1.67E+05	2.80E+05
	Weft	2.79E+05	2.66E+05	1.55E+05	1.61E+05	
W3	Warp	6.56E+05	6.48E+05	4.63E+05	4.67E+05	4.00E+06
	Weft	6.35E+05	6.27E+05	3.83E+05	4.00E+05	
W4	Warp	5.13E+04	4.33E+04	4.16E+04	4.92E+04	5.00E+04
	Weft	5.59E+04	4.80E+04	5.27E+04	6.14E+04	
W6	Warp	1.11E+05	1.05E+05	8.07E+04	1.22E+05	3.11E+05
	Weft	1.15E+05	1.09E+05	1.03E+05	1.54E+05	
W7	Warp	8.36E+04	5.30E+04	8.29E+04	8.01E+04	1.68E+05
	Weft	9.67E+04	6.61E+04	6.51E+04	6.95E+04	
W8	Warp	2.24E+05	2.14E+05	1.57E+05	2.18E+05	1.30E+06
	Weft	2.22E+05	2.12E+05	1.30E+05	1.75E+05	
W9	Warp	4.59E+04	3.84E+04	3.78E+04	4.59E+04	4.37E+04
	Weft	5.55E+04	4.80E+04	5.03E+04	5.71E+04	
W10	Warp	3.72E+04	3.26E+04	3.07E+04	4.18E+04	2.60E+04
	Weft	3.67E+04	3.21E+04	2.62E+04	3.73E+04	
W11	Warp	4.98E+04	4.48E+04	4.00E+04	4.69E+04	4.66E+04
	Weft	5.23E+04	4.74E+04	4.04E+04	4.63E+04	
W12	Warp	2.66E+05	2.62E+05	2.05E+05	2.34E+05	7.42E+05
	Weft	3.05E+05	3.01E+05	2.12E+05	2.49E+05	
K1	Wale	6.52E+04	6.05E+04	3.45E+04	4.04E+04	4.79E+04
	Course	6.33E+04	5.87E+04	3.85E+04	4.61E+04	
K2	Wale	2.80E+04	2.41E+04	1.34E+04	1.92E+04	1.24E+04
	Course	2.90E+04	2.52E+04	1.42E+04	2.06E+04	
K3	Wale	1.98E+04	1.70E+04	2.92E+04	4.67E+04	1.44E+04
	Course	2.88E+04	2.60E+04	3.07E+04	4.97E+04	
K4	Wale	6.89E+04	6.46E+04	3.52E+04	4.76E+04	3.99E+04
	Course	6.59E+04	6.17E+04	3.62E+04	4.93E+04	
K5	Wale	4.94E+04	4.29E+04	1.92E+04	2.64E+04	2.55E+04
	Course	5.20E+04	4.54E+04	3.00E+04	3.86E+04	
K6	Wale	4.92E+04	4.20E+04	2.14E+04	3.07E+04	2.99E+04
	Course	5.06E+04	4.34E+04	2.86E+04	4.16E+04	
K7	Wale	1.39E+04	1.05E+04	8.81E+03	1.20E+04	8.04E+03
	Course	1.94E+04	1.60E+04	1.11E+04	1.50E+04	
N1	MD	8.90E+05	8.68E+05	2.63E+05	2.78E+05	5.89E+05
	CD	5.76E+05	5.54E+05	3.98E+05	4.08E+05	
N8	MD	6.92E+05	6.76E+05	1.14E+05	1.24E+05	3.80E+05
	CD	3.56E+05	3.41E+05	2.25E+05	1.91E+05	
N10	MD	1.73E+05	1.61E+05	4.75E+04	5.47E+04	1.34E+05
	CD	1.55E+05	1.43E+05	1.21E+05	1.26E+05	
N11	MD	6.94E+05	6.80E+05	1.32E+05	1.48E+05	5.61E+05
	CD	3.64E+05	3.50E+05	2.92E+05	2.66E+05	

$$*G_{FAST} = \frac{122.5}{\varepsilon(\%)}$$

5.3.1 Shear modulus obtained in the LUFHES and KES-F systems

It is shown in Table 5.3 that G_{LUFHES} and G_{KESF} have similar magnitude, and G_{KESF} is greater than G_{LUFHES} in most cases. It is also found that G_{FAST} of W3, W8 and W12 are much greater than their corresponding G_{KESF} and G_{LUFHES} . The correlation between G_{KESF} and G_{LUFHES} are discussed for woven, knitted and nonwoven fabrics, respectively below.

5.3.1.1 G_{KESF} and G_{LUFHES} for woven fabrics

The linear relationship between shear modulus obtained in the KES-F and the LUFHES of 11 woven fabrics and their R^2 are given in Table 5.4.

Table 5.4 Correlation between G_{KESF} and G_{LUFHES} for woven fabrics (Constant shear angle of $\pm 0.5^\circ$ - $\pm 2.5^\circ$ in the KES-F shear test and constant shear angle of 0.5° - 4.0° in the LUFHES shear test)

R^2		G_{KESF}	G_{LUFHES}	
			1 st cycle	2 nd – 5 th cycle
G_{KESF}		1.0	/	/
G_{LUFHES}	1 st cycle	0.95	1.0	/
	2 nd – 5 th cycle	0.92	0.98	1.0

As shown in Table 5.4, for the 11 woven fabrics, G_{KESF} has strong linear relationship with G_{LUFHES} in both the first cycle and the 2nd-5th cycles, R^2 between each of them are more than 0.90. Such excellent linear correlations suggest that the comparison of woven fabrics in terms of shear modulus in the KES-F system is likely to be identical to the comparison done by using the LUFHES system.

It is noticed in Table 5.5 that the extension forces applied onto fabrics during shear test in LUFHES vary with fabrics from 3.6N/m to 23.7N/m, which are different from the extension force of 4.9N/m applied in the KES-F system. The good linear relationship between G_{KESF} and G_{LUFHES} implies that the different extension forces hardly affect woven fabric shear modulus obtained in these two systems. This is probably because the difference between woven fabrics elongations under 2N/m and 4.9N/m is small (see Table 5.5), which means woven fabrics do not have significant structural differences before shear deformation takes place in the LUFHES and KES-F tests.

Table 5.5 Extension force applied in perpendicular direction at the shear angle of 4° in the LUFHES test (elongation of 0.24%) and the elongation of fabric at extension force of 2N/m and 4.9N/m

Fabric		Extension force (N/m) applied in perpendicular direction at the shear angle of 4° in the LUFHES test (elongation of 0.24%)	Elongation (%) in unidirectional shear test (obtained in the Titan tensile test)	
			2N/m	4.9N/m
W1	Warp	12.3	0.70	0.87
	Weft	9.4	0.42	0.49
W2	Warp	9.7	0.44	0.56
	Weft	13.2	0.77	0.95
W3	Warp	23.7	0.43	0.64
	Weft	21.2	0.19	0.35
W4	Warp	8.3	1.07	1.29
	Weft	7.6	0.70	0.87
W6	Warp	7.3	0.61	0.89
	Weft	13.1	1.05	1.32
W7	Warp	14.3	0.32	0.40
	Weft	10.7	0.23	0.28
W8	Warp	13.3	0.71	0.86
	Weft	13.3	0.65	0.84
W9	Warp	4.0	0.15	0.36
	Weft	5.5	0.17	0.56
W10	Warp	5.2	0.45	1.15
	Weft	4.5	0.46	1.41
W11	Warp	3.6	0.18	0.37
	Weft	4.6	0.19	0.39
W12	Warp	12.2	0.57	1.00
	Weft	16.0	0.54	0.78

It is also noticed that, for woven fabrics, G_{KESF} and G_{LUFHES} in the first cycle have slightly better linear relationship than that of G_{KESF} and G_{LUFHES} in the 2nd-5th cycles. It is indicated that the shear modulus of undeformed fabric obtained in both the KES-F test and the first cycle of the LUFHES test agree well and the shear modulus might be affected by the permanent shear deformation (or

potential unrecovered extension deformations) produced in the first cycle of LUFHES shear test.

5.3.1.2 G_{KESF} and G_{LUFHES} for knitted fabrics

R^2 of the linear regression equations between G_{KESF} and G_{LUFHES} of seven knitted fabrics are given in Table 5.6 and Figure 5.11 below.

Table 5.6 Correlation between G_{KESF} and G_{LUFHES} for knitted fabrics (Constant shear angle of $\pm 0.5^\circ$ - $\pm 2.5^\circ$ in the KES-F shear test and constant shear angle of 0.5° - 4.0° in the LUFHES shear test)

R^2		G_{KESF}	G_{LUFHES}	
			1 st cycle	2 nd – 5 th cycle
G_{KESF}		1.0	/	/
G_{LUFHES}	1 st cycle	0.59	1.0	/
	2 nd – 5 th cycle	0.38	0.92	1.0

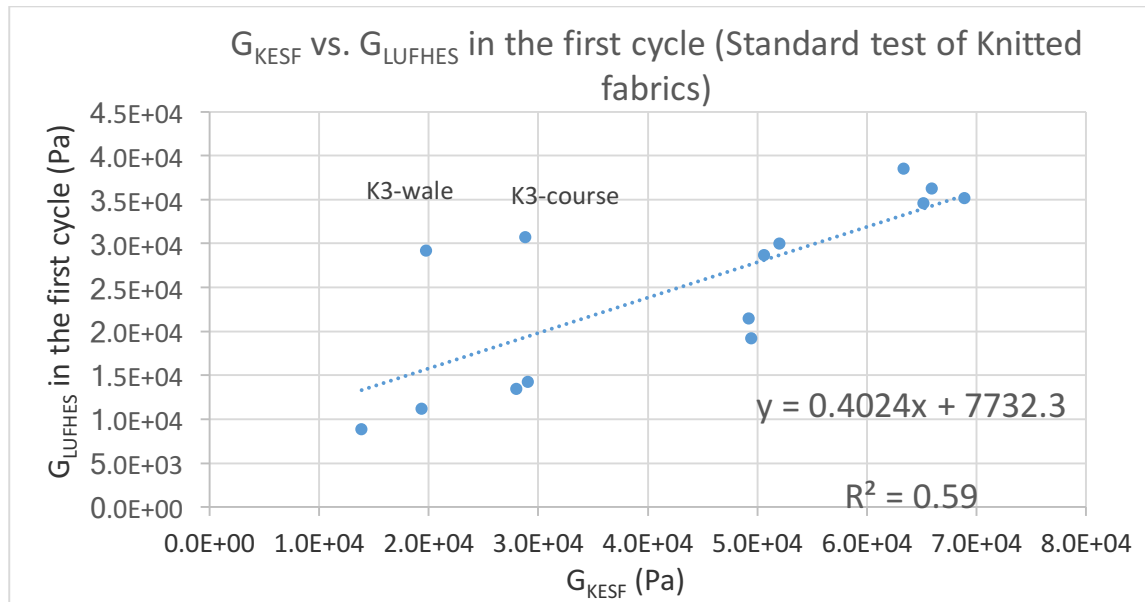


Figure 5.11 The relationship between G_{KESF} and G_{LUFHES} in the first cycle of shear test for seven knitted fabrics

For knitted fabrics, G_{KESF} does not show good linear relationship with G_{LUFHES} . It is noticed in Figure 5.11 that shear modulus of K3 in both wale and course directions stray away from the trend line of knitted fabrics. After excluding fabric K3 from this group of knitted fabrics, the linear regression coefficients R^2 increase to around 0.9 (see Table 5.7), this suggests that shear modulus obtained in both the KES-F and LUFHES shear tests agree well for all of the knitted fabrics tested except fabric K3. Knitted fabric K3 is a 1x1 rib knitted fabric knitted by using two yarns as shown in Appendix A. This special structure of knitted fabric K3 might be a reason for its different shear modulus from other knitted fabrics.

Table 5.7 Correlation between G_{KESF} and G_{LUFHES} for the 6 knitted fabrics without fabric K3

G obtained in the standard KES-F and LUFHES shear tests as in the manual		
R^2		G_{KESF}
G_{LUFHES}	1 st cycle	0.91
	2 nd – 5 th cycle	0.91

With consideration of the different testing conditions adopted in both the KES-F and LUFHES testing systems, there are two possible causes for the differences of shear modulus between G_{KESF} and G_{LUFHES} for the fabric K3: different shear angles and different extension forces exerted on fabrics when measuring the shear modulus in the two systems.

Firstly, it is noticed that G_{KESF} and G_{LUFHES} were obtained under different shear angles in the two testing systems (i.e., G_{KESF} was measured when the shear angle is in the range of $\pm 0.5^\circ - \pm 2.5^\circ$, while G_{LUFHES} was measured when the shear angle is in the range of $0.5^\circ - 4.0^\circ$). To determine if the disagreement between G_{KESF} and G_{LUFHES} is due to the different shear angles in the KES-F and LUFHES shear tests, both G_{KESF} and G_{LUFHES} obtained under shear angle between 0.5° and 2.5° are shown in Table 5.8. The G_{KESF} obtained in forward and backward shear deformation are also given.

Table 5.8 Shear modulus of knitted fabrics G_{KESF} and G_{LUFHES} when shear angles are between 0.5° and 2.5°

Fabric		G_{KESF} (Pa)		G_{LUFHES} (Pa)	
		Forward	Backward	1 st cycle	2 nd -5 th cycle
K1	Wale	7.10E+04	5.88E+04	3.57E+04	4.11E+04
	Course	6.21E+04	6.42E+04	3.80E+04	4.39E+04
K2	Wale	3.37E+04	2.23E+04	1.46E+04	2.04E+04
	Course	3.37E+04	2.42E+04	1.42E+04	2.05E+04
K3	Wale	2.46E+04	1.48E+04	3.45E+04	5.34E+04
	Course	3.53E+04	2.23E+04	3.58E+04	5.71E+04
K4	Wale	7.68E+04	6.06E+04	3.86E+04	5.08E+04
	Course	7.59E+04	5.57E+04	3.59E+04	4.98E+04
K5	Wale	5.71E+04	4.15E+04	2.16E+04	2.79E+04
	Course	5.73E+04	4.61E+04	2.93E+04	3.76E+04
K6	Wale	5.14E+04	4.66E+04	2.25E+04	3.22E+04
	Course	5.84E+04	4.22E+04	2.80E+04	4.27E+04
K7	Wale	1.57E+04	1.19E+04	1.05E+04	1.38E+04
	Course	2.11E+04	1.77E+04	1.18E+04	1.56E+04

R^2 of the linear regression equations between the shear modulus G_{KESF} and G_{LUFHES} for 7 knitted fabrics shown in Table 5.8 are given in Table 5.9.

Table 5.9 Correlation between G_{KESF} and G_{LUFHES} for 7 knitted fabrics when fabrics have identical range of shear angles (0.5° - 2.5°)

R^2		G_{KESF}		G_{LUFHES}	
		Forward	Backward	1 st cycle	2 nd – 5 th cycle
G_{KESF}	Forward	1.0	/	/	/
	Backward	0.92	1.0	/	/
G_{LUFHES}	1 st cycle	0.47	0.43	1.0	/
	2 nd – 5 th cycles	0.28	0.21	0.90	1.0

It is found in Table 5.9 that G_{KESF} and G_{LUFHES} of those knitted fabrics measured in identical range of shear angles in the KES-F and LUFHES shear tests still have poor correlation. This concludes that the poor correlation between G_{KESF} and G_{LUFHES} is not due to their different shear angles in the two shear test methods.

Secondly, we suspect that the differences of shear modulus for the fabric K3 might be due to the different extension forces applied on fabric in the two shear

testing systems, fabric K3 would demonstrate different shear properties under different extension forces during the shear tests. The extension force applied on fabrics during shear test in the KES-F system is a constant force of 4.9N/m while the extension force exerted on fabric in shear test in LUFHES varies from fabric to fabric but at a constant elongation of 0.24%.

This can be seen in Table 5.10 that the elongations of the fabric K3 in wale direction are 0.15% and 0.32% under the extension forces of 2N/m and 4.9N/m, respectively; and that the elongations of the fabric K3 in course direction are 0.89% and 5.23% under the extension forces of 2N/m and 4.9N/m, respectively. The differences of the elongations in wale and course directions under the extension force of 4.9N/m are about 16 times (0.32% and 5.23%), it is the greatest difference among those knitted fabrics.

The extension forces and shear forces exerted onto the fabric shells during the LUFHES shear test are shown in Table 5.10. It is found that, for most of the fabrics, the shear forces in unidirectional shear testing (KES-F) and biaxial shear testing (LUFHES) under similar extension forces are significantly different. However, for fabric K3, the shear force in the wale direction is 3.9N/m under extension force of 2.7N/m (elongation of 0.24%) in biaxial shear testing and it is 3.0N/m under extension force of 4.9N/m (elongation of 5.23%) in unidirectional testing (KES-F). Similarly, the shear force in the course direction is 4.2N/m under extension force of 6.4N/m (elongation of 0.24%) in biaxial shear testing and it is 4.6N/m under extension force of 4.9N/m (elongation of 0.32%) in unidirectional testing (KES-F). This indicates that the fabric shear forces are similar (4.2N/m and 4.6N/m) when elongations in unidirectional and biaxial directions are similar (0.24% and 0.32%); however, when their elongations are different (0.24% and 5.23%), their shear forces are also similar (3.9N/m and 3.0N/m). Therefore, it is difficult to say that the difference of shear modulus obtained in the two systems is due to the two different extension forces applied.

In addition, the difference might also be due to the differences of unidirectional and biaxial fabric deformations, or the special structures of the fabric K3. This needs further investigation.

Table 5.10 Force applied to shear knitted fabrics to 4° in the KES-F and the LUFHES shear test

Sample		Shear force, F_{shear} (N/m), applied to shear fabric at the shear angle of 4°		$F_{\text{shear-KESF}} / F_{\text{shear-LUFHES}}$	Extension force (N/m) applied in perpendicular direction at the shear angle of 4° in LUFHES test (elongation of 0.24%)	Elongation (%) in unidirectional shear test (obtained in Titan tensile test)	
		KES-F test	LUFHES test			2N/m	4.9N/m
K1	wale	5.0	2.5	1.99	5.4	0.66	1.28
	course	4.4	2.9	1.52	6.7	1.39	2.83
K2	wale	3.0	1.2	2.51	3.8	1.34	3.00
	course	3.0	1.3	2.25	4.3	3.52	7.68
K3	wale	3.0	3.9	0.77	2.7	0.15	0.32
	course	4.6	4.2	1.08	6.4	0.89	5.23
K4	wale	6.6	3.1	2.12	5.1	0.53	1.55
	course	6.6	3.2	2.03	6.6	0.76	2.02
K5	wale	2.8	1.0	2.80	3.3	1.01	1.89
	course	2.7	1.6	1.72	4.8	3.51	7.22
K6	wale	2.2	1.0	2.34	3.7	0.79	2.53
	course	2.6	1.4	1.79	4.4	1.18	4.16
K7	wale	1.4	0.8	1.68	2.4	1.21	3.13
	course	2.0	1.1	1.86	3.3	7.64	19.73

5.3.1.3 G_{KESF} and G_{LUFHES} for nonwoven fabrics

R^2 of linear regression equations between G_{KESF} and G_{LUFHES} for 4 nonwoven fabrics are shown in Table 5.11. It is found that G_{KESF} and G_{LUFHES} of the 4 nonwoven fabrics show the worst linear relationship with R^2 less than 0.2, which means the KES-F and LUFHES systems have significant differences in measuring shear modulus of these four nonwoven fabrics.

Table 5.11 Correlation between G_{KESF} and G_{LUFHES} for 4 nonwoven fabrics (Constant shear angle of $\pm 0.5^\circ$ - $\pm 2.5^\circ$ in the KES-F shear test and Constant shear angle of 0.5° - 4.0° in the LUFHES shear test)

R^2		G_{KESF}	G_{LUFHES}	
			1 st cycle	2 nd – 5 th cycle
G_{KESF}		1.0	/	/
G_{LUFHES}	1 st cycle	0.11	1.0	/
	2 nd – 5 th cycle	0.17	0.97	1.0

More importantly it is noted that, as shown in Table 5.3, G_{KESF} in the MD is greater than that in the CD, but G_{LUFHES} in the MD is smaller than that in the CD. This is a significant difference between the two testing systems, as this will give totally different conclusions to identical fabrics. The analysis below aims to understand what causes this difference between shear modulus obtained in KES-F and LUFHES and which conclusion is correct.

Similar to knitted fabrics, we suspect that the different shear modulus of nonwoven fabrics obtained in the KES-F and LUFHES systems might be because of the different shear angles in these two testing systems. Therefore, shear modulus of nonwoven fabrics obtained in both the KES-F and LUFHES systems in identical shear angles (0.5° - 2.5°) are given in Table 5.12. The G_{KESF} obtained in forward and backward shear deformations are also given.

Table 5.12 G_{KESF} and G_{LUFHES} for 4 nonwoven fabrics obtained when shear angle is between 0.5° and 2.5°

Fabric		G_{KESF} (Pa)		G_{LUFHES} (Pa)	
		Forward	Backward	1 st cycle	2 nd -5 th cycle
N1	MD	1.07E+06	7.08E+05	2.44E+05	2.41E+05
	CD	6.62E+05	4.89E+05	3.74E+05	3.52E+05
N8	MD	8.63E+05	5.18E+05	1.18E+05	1.20E+05
	CD	3.92E+05	3.19E+05	2.22E+05	1.38E+05
N10	MD	1.99E+05	1.47E+05	5.90E+04	6.42E+04
	CD	1.73E+05	1.38E+05	1.27E+05	1.26E+05
N11	MD	8.06E+05	5.81E+05	1.34E+05	1.48E+05
	CD	3.91E+05	3.37E+05	3.03E+05	2.13E+05

It is found in Table 5.12 that, for all the nonwoven fabrics, the new G_{KESF} in the MD is still greater than that in the CD, and the new G_{LUFHES} in the MD is still smaller than that in the CD. This means that the differences between G_{KESF} and

G_{LUFHES} are not due to the different shear angles used in the KES-F and LUFHES shear tests.

The forces applied to shear these four nonwoven fabrics to 4° in the KES-F ($F_{\text{shear-KESF}}$) and LUFHES shear tests ($F_{\text{shear-LUFHES}}$) are given in Table 5.13.

Table 5.13 Force applied to shear nonwoven fabrics to 4° in the KES-F and the LUFHES shear tests

		Shear force, F_{shear} (N/m), applied to shear fabric at the shear angle of 4°		Extension force (N/m) applied in the perpendicular direction at the shear angle of 4° in LUFHES test (Or constant extension strain of 0.24%)	$F_{\text{shear-KESF}} /$ $F_{\text{shear-LUFHES}}$
		KES-F test	LUFHES test		
N1	MD	14.2	4.3	10.43	3.28
	CD	9.5	6.3	16.15	1.50
N8	MD	16.7	2.6	5.32	6.39
	CD	8.7	5.0	11.73	1.72
N10	MD	4.8	1.2	2.95	3.96
	CD	3.9	3.2	10.61	1.20
N11	MD	19.1	3.6	6.79	5.27
	CD	10.1	7.1	17.90	1.43

It is shown that the shear forces applied to shear nonwoven fabrics in the CD in the KES-F shear tests ($F_{\text{shear-KES-F}}$) are close to those in the LUFHES shear tests ($F_{\text{shear-LUFHES}}$) and ($F_{\text{shear-KESF}}/F_{\text{shear-LUFHES}} = 1.2 - 1.7$), while the forces applied to shear nonwoven fabrics in the MD in the KES-F shear tests ($F_{\text{shear-KESF}}$) are much greater than those in the LUFHES shear tests ($F_{\text{shear-LUFHES}}$) and ($F_{\text{shear-KESF}}/F_{\text{shear-LUFHES}} = 3.3 - 6.4$). Thus, it is indicated that the poor correlation between G_{KESF} and G_{LUFHES} of nonwovens is due to their difference of shear modulus in MD.

The possible cause for the noticeable difference of shear modulus of nonwoven in the MD might be the different elongations of the fabrics in the CD in the KES-F (4.9N/m) and LUFHES systems during the shear tests. The elongations of these nonwoven fabrics under the extension forces of 2N/m and 4.9N/m are shown in Table 5.14. It is apparent that the shear modulus of nonwoven fabrics are obtained in the KES-F system after the fabrics have a greater elongation of 0.86 – 7.2%, while the shear modulus of nonwoven fabrics are obtained in the LUFHES system after the fabrics have a smaller elongation of 0.66 – 3.41%.

Table 5.14 Elongation of nonwoven fabric with 2N/m and 4.9N/m

		Elongation (%)		Ratio of elongations under 4.9N/m over under 2N/m
		2N/m	4.9N/m	
N1	MD	1.01	1.26	1.25
	CD	1.16	1.75	1.50
N8	MD	0.66	0.86	1.30
	CD	1.76	2.98	1.69
N10	MD	0.83	1.04	1.26
	CD	3.41	7.20	2.11
N11	MD	0.79	0.92	1.17
	CD	1.61	2.77	1.73

Another possible reason is the different fabric deformations in the LUFHES and the KES-F shear tests. In the LUFHES shear test, fabric shell has biaxial deformation, and because the gauge length between top and bottom sample holder is fixed, the extension force applied onto the fabric in the longitudinal direction increases gradually with the increase of shear angle. Extension force varies from fabric to fabric at the shear angle of 4°; it is 2.95 - 10.43N/m in the MD, and 10.61-17.90N/m in the CD (see Table 5.13). In the KES-F shear test, fabric has unidirectional deformation, and the maximum extension force applied onto the fabric in the longitudinal direction is 4.9N/m due to its gauge length varies during the shear test.

It is thus concluded that shear modulus obtained in the KES-F and LUFHES shear tests are different for nonwoven fabrics, and the results obtained in the LUFHES system are more reasonable and in agreement with the nonwoven structural characteristics (i.e., shear forces are smaller in shear test in MD when most of fibres aligned in MD).

5.3.2 Shear modulus obtained in the KES-F, LUFHES and FAST systems

The shear modulus obtained in the FAST system, G_{FAST} , are obtained in the extension of fabric strips cut in bias directions (45° and 135°) and cannot differentiate the shear modulus in warp/weft, wale/course and MD/CD directions, while shear modulus obtained in the KES-F and LUFHES systems are in two orthogonal directions. The correlation between G_{FAST} and G_{LUFHES} as well as the correlation between G_{FAST} and G_{KESF} of the 22 fabrics are shown in Table 5.15.

Table 5.15 R^2 of linear regression equations between G_{FAST} and G_{KESF} as well as R^2 between G_{FAST} and G_{LUFHES}

R^2			G_{FAST} (Pa)
G_{KESF} (Pa)	Woven fabrics	Warp	0.83
		Weft	0.81
	Knitted fabrics	Wale	0.91
		Course	0.92
	Nonwoven fabrics	MD	0.88
		CD	0.79
G_{LUFHES} (Pa) 1 st cycle	Woven fabrics	Warp	0.77
		Weft	0.73
	Knitted fabrics	Wale	0.64
		Course	0.73
	Nonwoven fabrics	MD	0.69
		CD	0.89
G_{LUFHES} (Pa) 2 nd -5 th cycle	Woven fabrics	Warp	0.78
		Weft	0.67
	Knitted fabrics	Wale	0.39
		Course	0.47
	Nonwoven fabrics	MD	0.72
		CD	0.77

It is found that, for woven, knitted and nonwoven fabrics, G_{FAST} has very good linear relationships with G_{KESF} in both directions with R^2 greater than 0.79. However, it is found that the good linear relationship ($R^2=0.83$) between G_{KESF} and G_{FAST} for woven fabrics is due to fabric W3 has significantly greater shear modulus than other fabrics as shown in Figure 5.12. Excluding shear modulus of fabric W3, R^2 between G_{KESF} and G_{FAST} of woven fabrics is only around 0.41 which suggests a poor linear relationship between G_{KESF} and G_{FAST} .

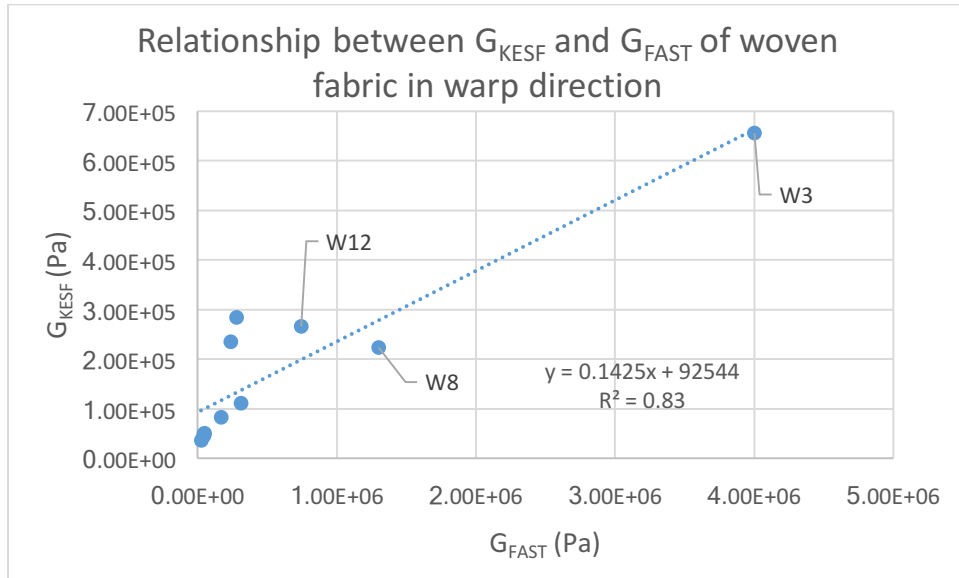


Figure 5.12 Relationship between G_{KESF} and G_{FAST} of woven fabrics in warp direction

It is shown that shear modulus of W12, W8 and W3 are much greater than those of other woven fabrics. Based on equation 5.11, the shear angles of fabrics in the FAST bias extension test are calculated and given in Table 5.16.

Table 5.16 Shear angle of fabric in the FAST bias extension test

Fabric	Shear angle in FAST (degree)	Fabric	Shear angle in FAST (degree)
W1	8.25	K1	1.52
W2	1.17	K2	5.82
W3	0.01	K3	4.94
W4	4.53	K4	1.74
W6	0.46	K5	5.35
W7	5.32	K6	4.53
W8	0.16	K7	8.23
W9	4.70	N1	0.43
W10	4.06	N8	0.87
W11	2.86	N10	2.14
W12	0.10	N11	0.43

It is shown that shear angles of fabrics W3, W8 and W12 in the FAST bias extension test are 0.01° , 0.16° and 0.09° , respectively. Such small shear angles suggest that the fabric shear deformations are still in the early stage ($<0.5^\circ$) of shear deformation in the FAST bias extension test. Shear angle of other woven

fabrics varies in a wide range from 0.46° to 8.25° . While the fabric shear angles in G_{KESF} measurements are in the range of 0.5° to 2.5° . Therefore the differences between G_{FAST} and G_{KESF} are due to they are obtained under different shear deformation angles, and several woven fabrics, such as fabric W3, have insufficient shear deformations in FAST test.

It is known from Table 5.15 that G_{FAST} has relatively poorer linear relationships with G_{LUFHES} obtained in the first cycle of the LUFHES test in both directions with R^2 between 0.64 and 0.89, while has much poorer linear relationships with G_{LUFHES} obtained in the 2nd-5th cycles of LUFHES test in both directions with R^2 between 0.39 and 0.77. The linear relationship between G_{FAST} and G_{LUFHES} for woven fabrics in the warp direction, knitted fabrics in the course direction and nonwoven fabrics in the CD are much better than those in another direction.

Since the FAST bias extension test shows the combined effect of shear deformations in both fabric directions (e.g., warp and weft for woven fabrics), the average values of G_{LUFHES} at the two orthogonal directions of fabrics, $G_{LUFHES-Average}$, are calculated and given in Table 5.17 (1) (2) to compare with G_{FAST} . Two average values of G_{LUFHES} , geometric mean (GM) and arithmetical mean (AM), are given and the correlation coefficients, R^2 , of the linear regression equations between G_{FAST} and the average of G_{LUFHES} are shown in Table 5.18.

Table 5.17 (1) Average of G_{LUFHES} in two directions obtained in LUFHES (woven fabrics)

Fabric	$G_{LUFHES-Average}$ (Pa)			
	First cycle		2 nd – 5 th cycle	
	GM	AM	GM	AM
W1	2.25E+05	2.26E+05	2.52E+05	2.53E+05
W2	1.58E+05	1.59E+05	1.64E+05	1.64E+05
W3	4.21E+05	4.23E+05	4.32E+05	4.34E+05
W4	4.68E+04	4.72E+04	5.50E+04	5.53E+04
W6	9.12E+04	9.19E+04	1.37E+05	1.38E+05
W7	7.35E+04	7.40E+04	7.46E+04	7.48E+04
W8	1.43E+05	1.44E+05	1.95E+05	1.97E+05
W9	4.36E+04	4.41E+04	5.12E+04	5.15E+04
W10	2.84E+04	2.85E+04	3.95E+04	3.96E+04
W11	4.02E+04	4.02E+04	4.66E+04	4.66E+04
W12	2.08E+05	2.09E+05	2.41E+05	2.42E+05

Table 5.17 (2) Average of G_{LUFHES} in two directions obtained in LUFHES (knitted fabrics and nonwoven fabrics)

Fabric	G_{LUFHES} -Average (Pa)			
	First cycle		2 nd – 5 th cycle	
	GM	AM	GM	AM
K1	3.64E+04	3.65E+04	4.32E+04	4.33E+04
K2	1.38E+04	1.38E+04	1.99E+04	1.99E+04
K3	2.99E+04	3.00E+04	4.82E+04	4.82E+04
K4	3.57E+04	3.57E+04	4.84E+04	4.85E+04
K5	2.40E+04	2.46E+04	3.19E+04	3.25E+04
K6	2.47E+04	2.50E+04	3.57E+04	3.62E+04
K7	9.89E+03	9.96E+03	1.34E+04	1.35E+04
N1	3.24E+05	3.31E+05	3.37E+05	3.43E+05
N8	1.60E+05	1.70E+05	1.54E+05	1.58E+05
N10	7.58E+04	8.43E+04	8.30E+04	9.04E+04
N11	1.96E+05	2.12E+05	1.98E+05	2.07E+05

Table 5.18 R^2 of the linear regression equations between G_{FAST} and G_{LUFHES} (average of two directions)

R^2		G_{LUFHES} -Average (Pa)			
		1 st cycle		2 nd -5 th cycle	
		GM	AM	GM	AM
G_{FAST} (Pa)	Woven fabrics	0.76	0.76	0.73	0.74
	Knitted fabrics	0.71	0.71	0.44	0.44
	Nonwoven fabrics	0.78	0.81	0.75	0.75

It is found in Table 5.18 that the average of G_{FAST} has good linear relationship with G_{LUFHES} obtained in the first cycle for all tested woven, knitted and nonwoven fabrics, with R^2 greater than 0.70, and it has relatively poorer linear relationship with G_{LUFHES} in the 2nd -5th cycles, and both arithmetical mean and geometric mean hardly make any difference to the correlation coefficients between G_{FAST} and G_{LUFHES} .

It is found in Figure 5.13 that the R^2 (greater than 0.70) between G_{FAST} and G_{LUFHES} for woven fabrics is also due to the significant higher shear modulus of fabric W3, W8 and W12 than those of other fabrics. R^2 between G_{FAST} and G_{LUFHES} decreases to 0.55 after excluding these three fabrics. As discussed, fabric shear angle varies from fabric to fabric under 4.9N/m applied in bias direction in the FAST bias extension test, and fabric W3, W8 and W12 have very small shear angle under 4.9N/m. While the fabric shear angles in G_{LUFHES} measurements are in the range of 0.5° to 4.0° . Therefore the differences between G_{FAST} and G_{LUFHES} are also because of the insufficient shear deformations of woven fabrics in FAST test.

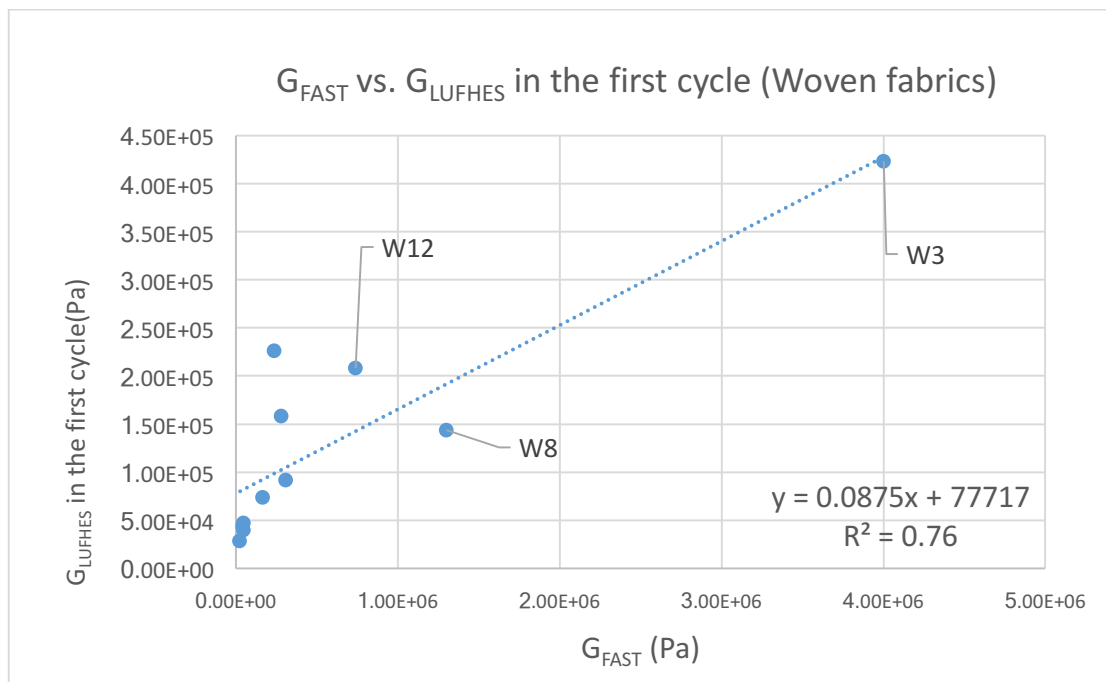


Figure 5.13 Relationship between arithmetical mean of $G_{LUFHES-Average}$ and G_{FAST} of woven fabrics

It is also found in Figure 5.14 that shear modulus of fabric K3 stray away from the linear regression trends between $G_{LUFHES-Average}$ and G_{FAST} for knitted fabrics, and the same phenomenon was also found in the correlation between G_{KESF} and G_{LUFHES} shown in section 5.3.1.2.

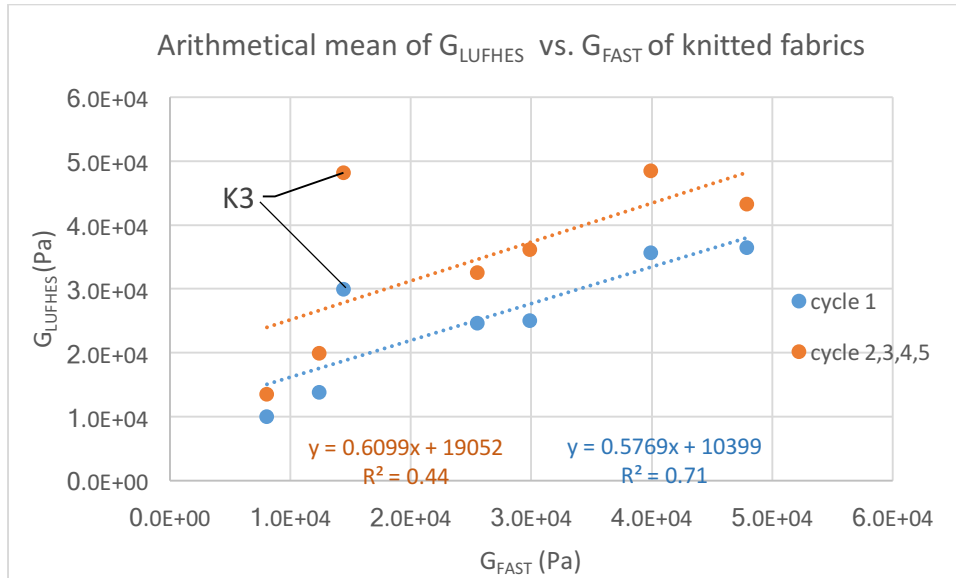


Figure 5.14 Relationship between arithmetical mean of $G_{LUFHES-Average}$ and G_{FAST} of knitted fabrics

As a summary of the shear modulus obtained in the FAST, KES-F and LUFHES systems, it is concluded that G_{KESF} , G_{FAST} , and G_{LUFHES} are measured under different shear angles and it seems that the different shear angles lead to the difference between G_{KESF} and G_{FAST} , as well as the difference between G_{LUFHES} and G_{FAST} , for woven fabrics. However, G_{KESF} and G_{FAST} have very good linear correlations for knitted and nonwoven fabrics. G_{LUFHES} are measured under different extension forces from those in the KES-F and FAST systems, and the differences of the extension forces applied lead to the disagreements between G_{LUFHES} and G_{KESF} as well as G_{FAST} for most of loose bonded fabrics such as nonwoven fabrics and some knitted fabrics.

G_{KESF} and G_{LUFHES} have good linear correlation for all of the woven fabrics and most of the knitted fabric (except some fabrics such as fabric K3). It indicates that the comparison of shear modulus of woven fabrics and knitted fabrics using the KES-F system is likely to be in identical trend to the comparison done in the LUFHES system but might disagree in some knitted fabrics. G_{KESF} and G_{LUFHES} have apparent differences for nonwoven fabrics.

5.4 Differences of shear rigidity (SR) obtained in the LUFHES, FAST and KES-F shear tests

Shear rigidity (SR) is defined as the shear load required to deform unit width of fabric to unit strain (De Boos and Tester, 1994). It shows the combined effect of both fabric material (shear modulus) and fabric thickness.

Similar to the shear modulus shown in the section 5.3, only one shear rigidity of each fabric is obtained by using the FAST system, SR_{KESF} and SR_{LUFHES} in two orthogonal fabric directions are obtained in the KES-F and LUFHES shear tests.

According to the equation 5.25 which is used to calculate the normalized shear modulus of the KES-F, the normalized shear rigidity is calculated by:

$$SR_{KESF-Norm} = (G_{KESF} - \frac{N}{t}) \times t = SR_{KESF} - N \dots \dots \dots (5.36)$$

Shear rigidity obtained in the FAST, KES-F and LUFHES systems are compared in Table 5.19. It is shown in Table 5.19(1) (2) that the difference between SR_{KESF} and $SR_{KESF-Norm}$ is a constant, 4.9N/m, for all fabrics. This constant difference won't affect the correlation between SR_{KESF} and SR_{LUFHES}/SR_{FAST} , so only the original shear rigidity obtained in the KES-F system is discussed below.

When fabrics are discriminated and ranked by using the shear rigidity obtained in the three measuring systems, the differences between these three systems in the discrimination of fabrics could be identified.

Table 5.19 (1) Shear rigidity (SR) obtained in the KES-F, LUFHES and FAST systems of knitted fabrics

Fabric		SR _{KESF} (N/m)		SR _{LUFHES} (N/m)		SR _{FAST} (N/m)
		Original	Normalized	1 st cycle	2 nd -5 th cycle	
K1	Wale	68.41	63.51	36.23	42.42	50.34
	Course	66.50	61.60	40.43	48.41	
K2	Wale	35.54	30.64	17.02	24.38	15.74
	Course	36.88	31.98	18.03	26.16	
K3	Wale	34.59	29.69	51.10	81.73	25.17
	Course	50.45	45.55	53.73	86.98	
K4	Wale	79.87	74.97	40.83	55.22	46.23
	Course	76.43	71.53	41.99	57.19	
K5	Wale	37.07	32.17	14.40	19.80	19.09
	Course	38.98	34.08	22.50	28.95	
K6	Wale	33.44	28.54	14.55	20.88	20.30
	Course	34.39	29.49	19.45	28.29	
K7	Wale	20.25	15.35	12.86	17.52	11.74
	Course	28.28	23.38	16.21	21.90	

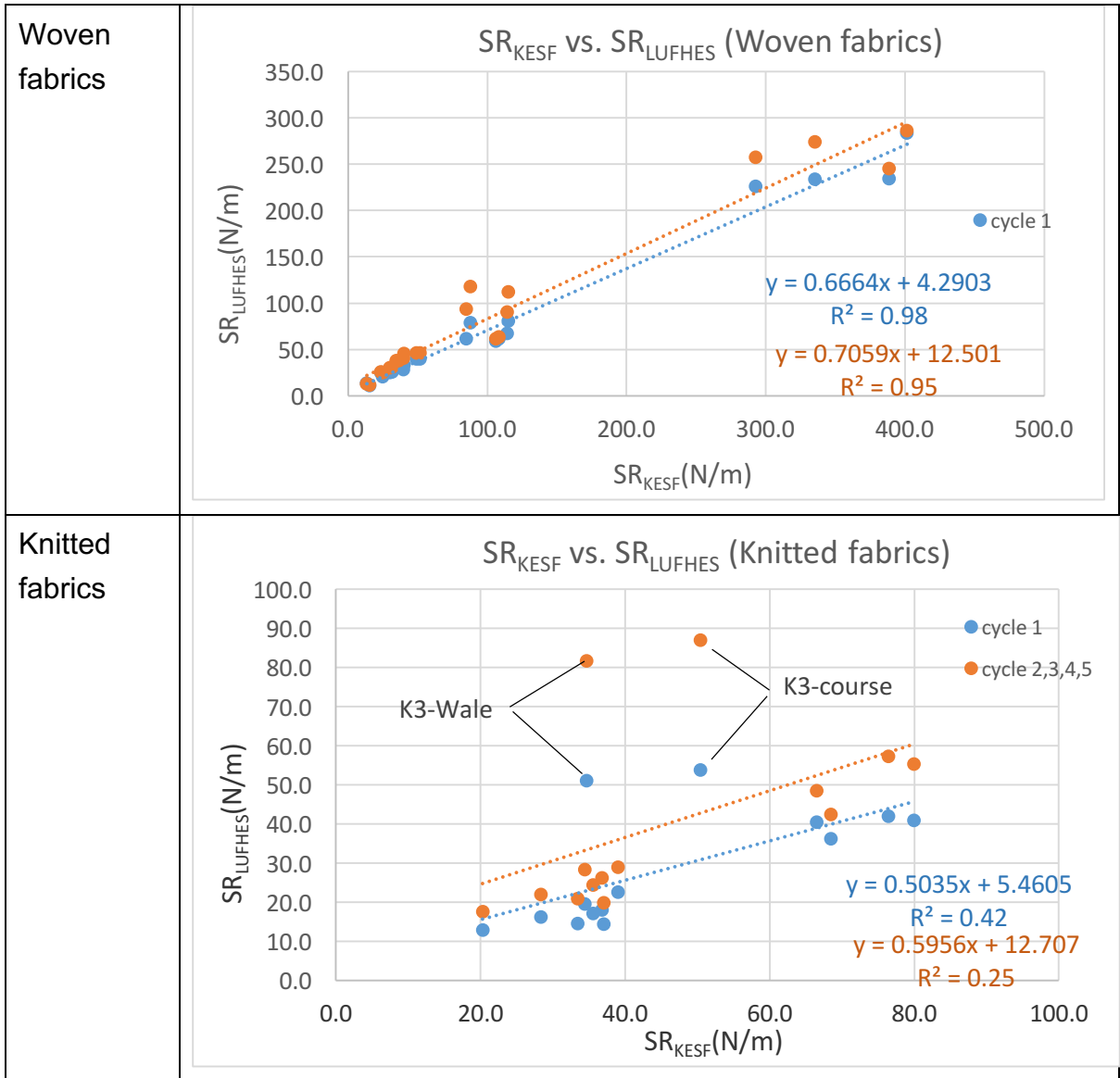
Table 5.19 (2) Shear rigidity (SR) obtained in the KES-F, LUFHES and FAST systems of woven fabrics and nonwoven fabrics

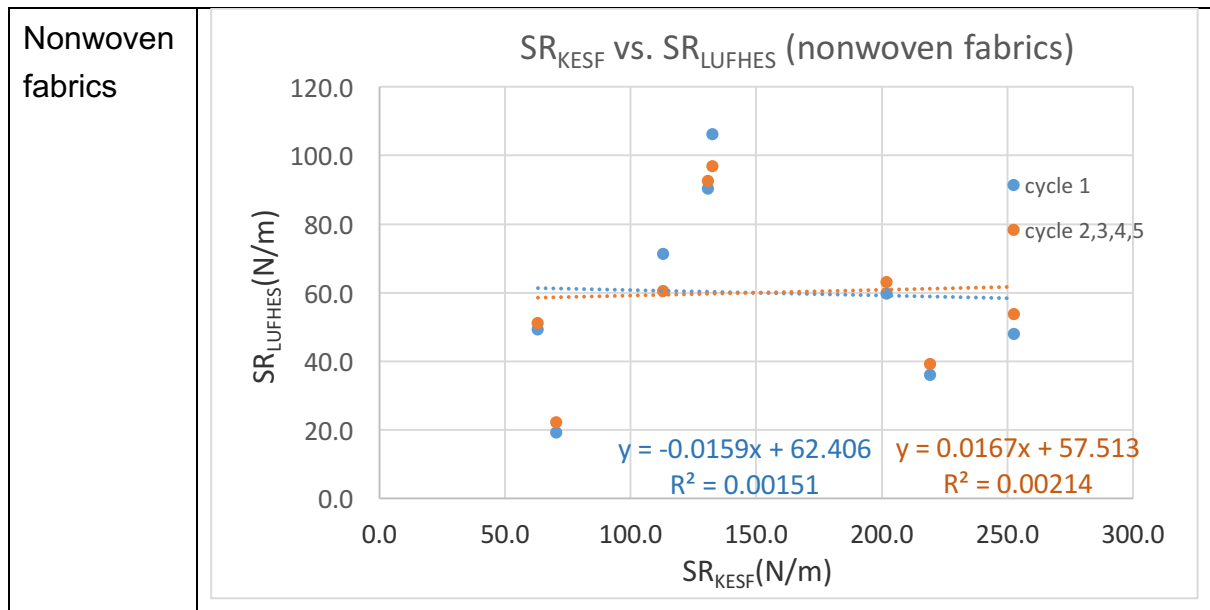
Fabric		SR _{KESF} (N/m)		SR _{LUFHES} (N/m)		SR _{FAST} (N/m)
		Original	Normalized	1 st cycle	2 nd -5 th cycle	
W1	Warp	23.50	18.60	24.60	25.50	23.71
	Weft	24.84	19.94	20.60	25.00	
W2	Warp	108.34	103.44	61.56	63.46	106.52
	Weft	106.05	101.15	58.90	61.18	
W3	Warp	401.66	396.76	283.36	285.80	2450.00
	Weft	388.66	383.76	234.40	244.80	
W4	Warp	31.53	26.63	25.58	30.26	30.75
	Weft	34.39	29.49	32.41	37.76	
W6	Warp	85.03	80.13	61.57	93.09	237.10
	Weft	87.90	83.00	78.59	117.50	
W7	Warp	13.38	8.48	13.26	12.82	26.82
	Weft	15.48	10.58	10.42	11.12	
W8	Warp	115.03	110.13	80.70	112.05	668.18
	Weft	113.89	108.99	66.82	89.95	
W9	Warp	30.00	25.10	24.72	30.02	28.60
	Weft	36.31	31.41	32.90	37.34	
W10	Warp	40.13	35.23	33.13	45.10	28.05
	Weft	39.55	34.65	28.27	40.25	
W11	Warp	49.11	44.21	39.44	46.24	45.94
	Weft	51.59	46.69	39.83	45.65	
W12	Warp	292.93	288.03	225.50	257.40	816.67
	Weft	335.92	331.02	233.20	273.90	
N1	MD	201.97	197.07	59.70	63.11	133.64
	CD	130.70	125.80	90.35	92.62	
N8	MD	219.27	214.37	36.14	39.31	120.49
	CD	112.93	108.03	71.33	60.55	
N10	MD	70.51	65.61	19.33	22.26	54.44
	CD	63.25	58.35	49.25	51.28	
N11	MD	252.52	247.62	48.05	53.87	204.17
	CD	132.42	127.52	106.29	96.82	

5.4.1 Differences of shear rigidity obtained in the LUFHES and the KES-F systems

The linear relationship between SR_{KESF} and SR_{LUFHES} obtained in both the first cycle and 2nd-5th cycle are shown in Table 5.20.

Table 5.20 Linear relationship between SR_{KESF} and SR_{LUFHES}





Shear rigidities obtained in the KES-F and LUFHES systems, SR_{KESF} and SR_{LUFHES} , have the same linear relationship as that of their corresponding shear modulus, G_{KESF} and G_{LUFHES} , shown in section 5.3.1. The differences between SR_{KESF} and SR_{LUFHES} are discussed for woven, knitted and nonwoven fabrics separately.

5.4.1.1 Differences between shear rigidity obtained in the KES-F and LUFHES of woven fabrics

For woven fabrics, SR_{KESF} has very good linear relationship with both SR_{LUFHES} obtained in the first cycle and the 2nd-5th cycle of the LUFHES test, their R^2 are greater than 0.95. Comparatively, SR_{KESF} and SR_{LUFHES} obtained in the first cycle of LUFHES test have slightly greater correlation coefficient. It suggests that the ranking order of woven fabrics in terms of shear rigidity should be very similar in both KES-F and LUFHES systems.

5.4.1.2 Differences between shear rigidity obtained in the KES-F and the LUFHES of knitted fabrics

For knitted fabrics, SR_{KESF} and SR_{LUFHES} do not have good linear relationship due to the fabric K3 which has a special 1x1 rib knitted structure. Based on the discussion about the difference between G_{KESF} and G_{LUFHES} in section 5.3.1.2, it is known that differences between fabric elongations before shear test starts in the LUFHES and the KES-F might lead to the difference between SR_{KESF} and SR_{LUFHES} for knitted fabric K3, but further investigation is required.

After excluding the influences of shear rigidity of fabric K3 in both wale and course directions, R^2 between SR_{KESF} and SR_{LUFHES} for knitted fabrics increase to around

0.9 as shown in Figure 5.15. This suggests that SR_{KESF} and SR_{LUFHES} are different for K3, but have very strong linear relationship for all of the knitted fabrics except fabric K3, the ranking of knitted fabrics (except fabric K3) in terms of shear rigidity obtained in the two systems will be the same.

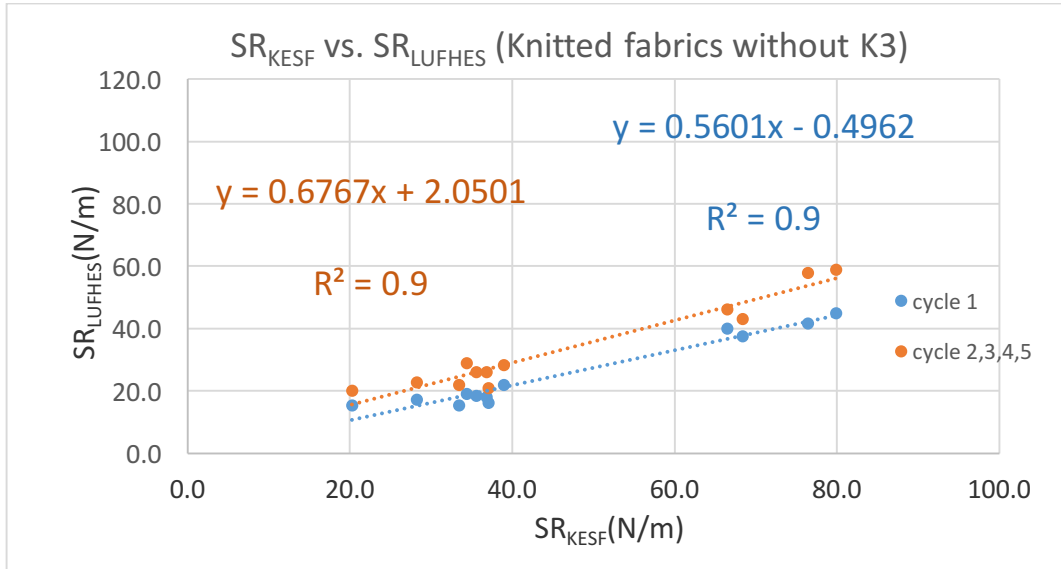


Figure 5.15 Relationship between SR_{KESF} and SR_{LUFHES} (knitted fabrics without K3)

5.4.1.3 Differences between shear rigidity obtained in the KES-F and the LUFHES of nonwoven fabrics

For nonwoven fabrics, it is shown in Table 5.20 that SR_{KESF} does not have linear relationship with SR_{LUFHES} obtained in both the first cycle and the 2nd-5th cycle of LUFHES shear test. In the KES-F shear test, SR_{KESF} in the MD are greater than those in the CD. However, in the LUFHES shear test, SR_{LUFHES} in the MD are smaller than those in the CD. This trend is also found in the comparison between G_{KESF} and G_{LUFHES} in section 5.3.1.3. As discussed, the different fabric elongations produced by different extension forces and the different fabric deformations in the KES-F and the LUFHES shear tests might cause the difference between SR_{KESF} and SR_{LUFHES} .

Bending deformation of yarns/fibre around contact area is reported to exist in the shear deformation of fabrics (Hu, 2000; Leaf and Sheta, 1984). When more fibres aligned in the MD in nonwoven fabrics, more fibres are bent when the fabric is sheared in the CD. It suggests that nonwoven fabric theoretically have greater shear rigidity in the CD, which agrees well with the shear modulus obtained in LUFHES.

5.4.2 Differences of shear rigidities obtained in the FAST, LUFHES and KES-F tests

The ranking of fabrics in terms of shear rigidity obtained in the FAST, LUFHES and KES-F systems are investigated by analysing their linear relationships. The correlation coefficients R^2 between them are shown in Table 5.21.

Table 5.21 R^2 of the linear regression equations between SR_{FAST} and SR_{KESF} as well as between SR_{FAST} and SR_{LUFHES}

R^2			SR_{FAST} (Pa)
SR_{KESF} (Pa)	Woven fabrics	Warp	0.87
		Weft	0.80
	Knitted fabrics	Wale	0.90
		Course	0.91
	Nonwoven fabrics	MD	0.83
		CD	0.78
SR_{LUFHES} (Pa) 1 st cycle	Woven fabrics	Warp	0.84
		Weft	0.72
	Knitted fabrics	Wale	0.44
		Course	0.45
	Nonwoven fabrics	MD	0.51
		CD	0.94
SR_{LUFHES} (Pa) 2 nd -5 th cycle	Woven fabrics	Warp	0.79
		Weft	0.64
	Knitted fabrics	Wale	0.24
		Course	0.24
	Nonwoven fabrics	MD	0.58
		CD	0.74

It is shown that SR_{FAST} and SR_{KESF} , as well as SR_{FAST} and SR_{LUFHES} have strong linear relationship for woven fabrics. However, similar to the linear relationship between G_{FAST} and G_{KESF} and the relationship between G_{FAST} and G_{LUFHES} for woven fabrics, it is found that the high R^2 between SR_{FAST} and SR_{KESF} as well as R^2 between SR_{FAST} and SR_{LUFHES} are due to shear rigidity of several fabrics (such as W3 and W8) are significantly greater than those of other fabrics as shown in Figure 5.16. After excluding the shear rigidity of five fabrics marked in Figure 5.16, R^2 between SR_{KESF} and SR_{FAST} of other six woven fabrics is only around 0.62,

which suggests the linear correlation between SR_{KESF} and SR_{FAST} is not good. Same trend is also found in the relationship between SR_{LUFHES} and SR_{FAST} .

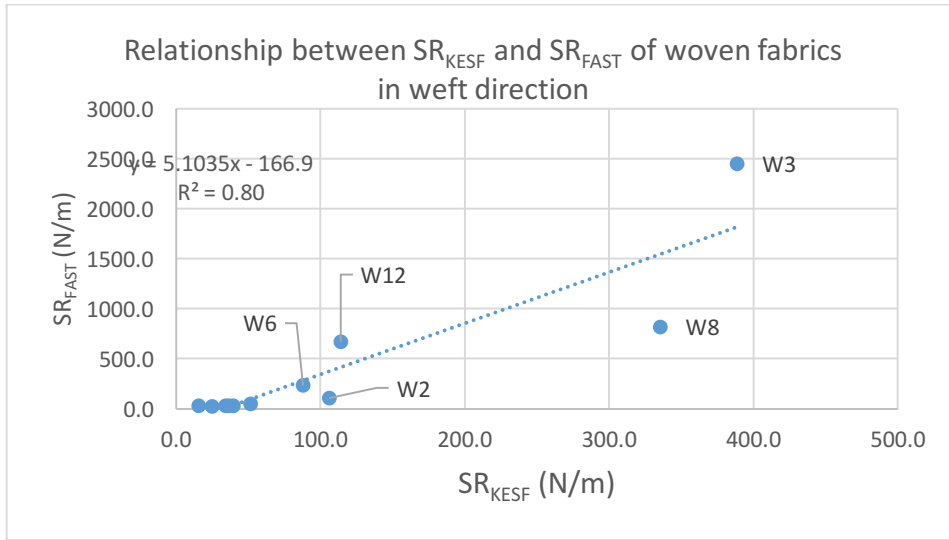


Figure 5.16 Relationship between SR_{KESF} and SR_{FAST} of woven fabrics

Based on the discussion in section 5.3.2, it is known that the difference between SR_{KESF} and SR_{FAST} and the difference between SR_{LUFHES} and SR_{FAST} for woven fabrics might be because of the insufficient shear deformations of woven fabrics, such as fabric W3 and W8, in FAST test.

SR_{FAST} and SR_{KESF} have good linear relationship for both knitted fabrics and nonwoven fabrics. However, SR_{FAST} and SR_{LUFHES} only have good linear relationship for nonwoven fabrics in the CD but do not have good linear relationship for knitted fabrics. While R^2 between SR_{FAST} and SR_{LUFHES} in the first cycle increases from around 0.45 to greater than 0.93 after excluding K3 as shown in Figure 5.17.

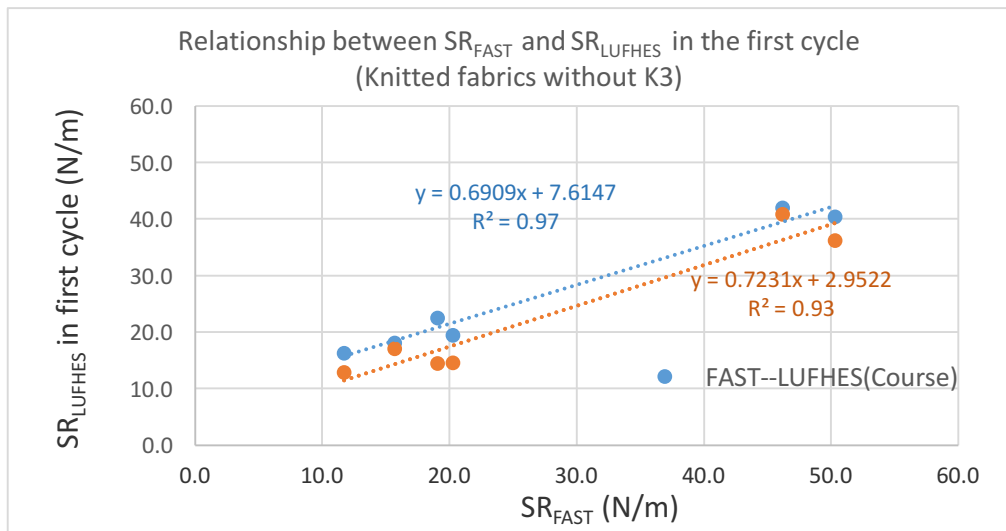


Figure 5.17 Relationship between SR_{FAST} and SR_{LUFHES} (1st cycle) for knitted fabrics without K3

Because fabric deformation in the FAST bias extension test is in bias direction which involves shear deformation of two orthogonal directions in fabric (i.e., warp and weft), averages of SR_{LUFHES} of two directions which have combined effect of two directions are calculated to compare with SR_{FAST} . Both geometric mean (GM) and arithmetical mean (AM) are calculated and shown in Table 5.22, and the R^2 of linear regression equations between SR_{FAST} and the averages of SR_{LUFHES} are given in Table 5.23.

Table 5.22 Average of shear rigidity at two directions obtained in LUFHES

Fabric	Average of SR_{LUFHES} (N/m)			
	First cycle		2 nd – 5 th cycle	
	GM	AM	GM	AM
W1	22.51	22.60	25.25	25.25
W2	60.22	60.23	62.31	62.32
W3	257.72	258.88	264.51	265.30
W4	28.80	29.00	33.80	34.01
W6	69.56	70.08	104.58	105.29
W7	11.75	11.84	11.94	11.97
W8	73.43	73.76	100.39	101.00
W9	28.52	28.81	33.48	33.68
W10	30.60	30.70	42.61	42.67
W11	39.64	39.64	45.95	45.95
W12	229.32	229.35	265.52	265.65
K1	38.27	38.33	45.31	45.41
K2	17.52	17.53	25.26	25.27
K3	52.40	52.41	84.31	84.35
K4	41.41	41.41	56.19	56.20
K5	18.00	18.45	23.94	24.38
K6	16.82	17.00	24.30	24.58
K7	14.44	14.53	19.59	19.71
N1	73.44	75.02	76.45	77.86
N8	50.77	53.73	48.79	49.93
N10	30.86	34.29	33.79	36.77
N11	71.46	77.17	72.22	75.35

Table 5.23 R^2 of the linear regression equations between SR_{FAST} and SR_{LUFHES} (average of two directions)

R^2		SR_{LUFHES} (N/m)			
		1 st cycle		2 nd -5 th cycle	
		GM	AM	GM	AM
SR_{FAST} (N/m)	Woven fabrics	0.79	0.79	0.72	0.72
	Knitted fabrics	0.45	0.45	0.24	0.24
	Knitted fabrics (exclude K3)	0.96	0.96	0.89	0.89
	Nonwoven fabrics	0.74	0.80	0.67	0.69

It is found that SR_{FAST} have good linear relationship with the averages of SR_{LUFHES} obtained in the first cycle for all tested woven, knitted (except K3) and nonwoven fabrics, with R^2 greater than 0.74, and that it has relatively poorer linear relationship with SR_{LUFHES} in 2nd -5th cycles.

However, it was found that the good linear relationship for woven fabrics ($R^2 > 0.72$) are still due to the significantly high shear rigidity of several fabrics (such as W3, W8, etc.), and after excluding the shear rigidity of these fabrics, linear relationship between other woven fabrics is not strong. In addition, arithmetical mean and geometric mean do not have significant differences to the linear correlation between SR_{FAST} and SR_{LUFHES} . This suggests that the ranking order of knitted fabrics (except K3) and nonwoven fabric sorted by using SR_{FAST} should be similar to their ranking order sorted by using the average SR_{LUFHES} .

In summary, fabric ranking in terms of their shear rigidities obtained in the FAST, KES-F and LUFHES systems were compared, it was found that the relationship between SR_{KESF} , SR_{FAST} , and SR_{LUFHES} are similar to the relationship between G_{KESF} , G_{FAST} , and G_{LUFHES} . It is concluded that ranking order of fabrics in terms of shear rigidity in the FAST might be different from those in the KES-F and the LUFHES, especially for woven fabrics. For most knitted fabrics (except K3) and nonwoven fabrics, their ranking order sorted by using SR_{FAST} might be similar to those sorted by using SR_{KESF} or average of SR_{LUFHES} .

It was also found that the comparison of shear rigidity of woven fabrics and most knitted fabrics using the KES-F system is likely to be in identical ranking order to the comparison done in the LUFHES system but might disagree in some knitted fabrics, such as K3. But SR_{KESF} and SR_{LUFHES} have apparent differences for nonwoven fabrics.

5.5 Summary

The main findings of this chapter are summarised as below:

1. Shear modulus obtained in LUFHES had similar magnitudes to those obtained in the KES-F and FAST systems;
2. Shear modulus and shear rigidity of woven fabrics obtained in the LUFHES and the KES-F shear tests were linearly correlated ($R^2 > 0.9$). It was indicated that the comparison of fabrics by using the LUFHES and the KES-F systems in terms of shear modulus and shear rigidity will be in good agreement. It was also indicated that the different extension forces applied on fabrics in the LUFHES (3.6N/m to 23.7N/m) and the KES-F (4.9N/m) shear tests hardly affect shear modulus and shear rigidity of woven fabrics obtained in the two systems;
3. For some woven fabrics, insufficient shear deformations in FAST test lead to the disagreements between their shear modulus obtained in the FAST and shear modulus obtained in the LUFHES as well as the KES-F tests. This was because, for those fabrics (such as woven fabric W3), the extension force of 4.9N/m (which is recommended in the FAST manual book) applied in bias direction in the FAST test was too small to produce apparent shear deformations for measuring fabric shear modulus;
4. For knitted and nonwoven fabrics, shear modulus and shear rigidity obtained in the FAST and the KES-F under the extension forces of 4.9N/m were linearly correlated. It was indicated that the comparison of fabrics by using the FAST and the KES-F systems in terms of shear modulus and shear rigidity were in good agreement;
5. For knitted fabrics except fabric K3, their shear modulus and shear rigidity obtained in the LUFHES agreed well with those obtained in the KES-F and the FAST;
6. For all of the nonwoven fabrics tested, there were significant differences between shear modulus/shear rigidity obtained in the LUFHES and the KES-F tests, especially for the shear modulus in the MD. More importantly, the relative magnitude of shear modulus in the two fabric directions (MD and CD) obtained in the LUFHES was a reverse to the relative magnitude of those obtained in the KES-F. A greater shear modulus in the MD than that in the CD was obtained in the KES-F tests, but a smaller shear modulus in the MD than that in the CD was obtained in the LUFHES. There were two possible causes for this difference. The first one was the greater elongation the fabric had before its shear testing in the KES-F, while there was a relatively smaller fabric elongation before its shear testing in the LUFHES system. Shear modulus obtained after nonwoven fabric having a greater elongation might be different from the one obtained when it has a smaller elongation. The second possible reason might be the different types of fabric deformations incurred in the LUFHES (biaxial fabric deformations when gauge length was fixed during testing) and the KES-F shear tests (unidirectional fabric deformation when gauge length varied during testing). Shear modulus obtained in LUFHES were reasonable and in agreement with the nonwoven

structural characteristics (i.e., shear forces were smaller in shear test in the MD when most of fibres aligned in the MD).

Chapter 6 Compression buckling force of fabric shells measured in the LUFHES and bending rigidities measured in the KES-F and the FAST systems

Fabric buckling and bending are two different but closely linked fabric deformations, they are involved in the evaluation of fabric stiffness and softness in the LUFHES as well as the KES-F and FAST, respectively.

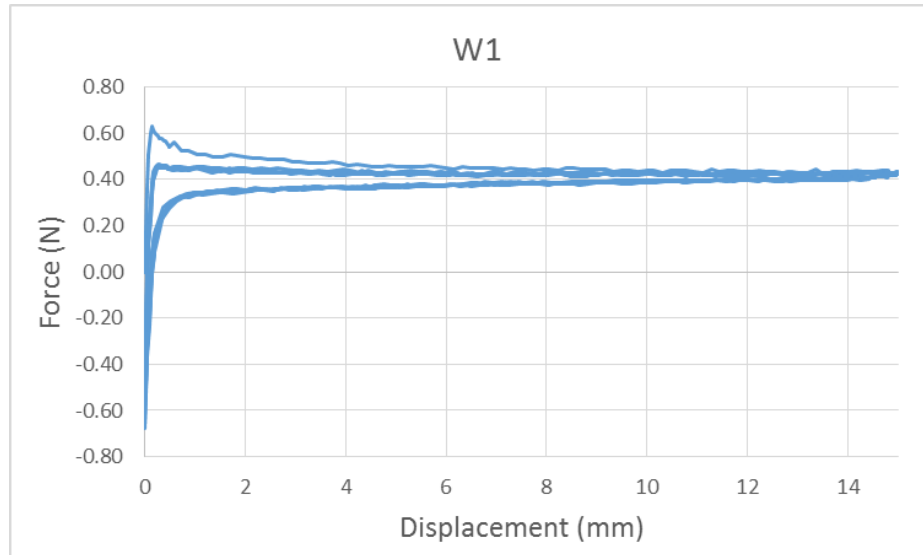
The compression buckling force of a thin two dimensional elastic plate during compression buckling process is known to be related to its bending rigidity (Grosberg and Swani, 1966a; Dahlberg, 1961; Lindberg et al., 1961). However, it is not clear whether and how the buckling of fabric cylindrical shells measured in LUFHES and the bending of fabric plates measured in both the KES-F and FAST systems are correlated. In this chapter, the correlation between the critical compression buckling force of fabric cylindrical shells measured in LUFHES and the fabric bending rigidity measured in both the KES-F and FAST systems are analysed as an example to reveal the correlation and differences between using bending and buckling to discriminate fabrics.

6.1 Measurements of fabric compression buckling force and bending rigidity

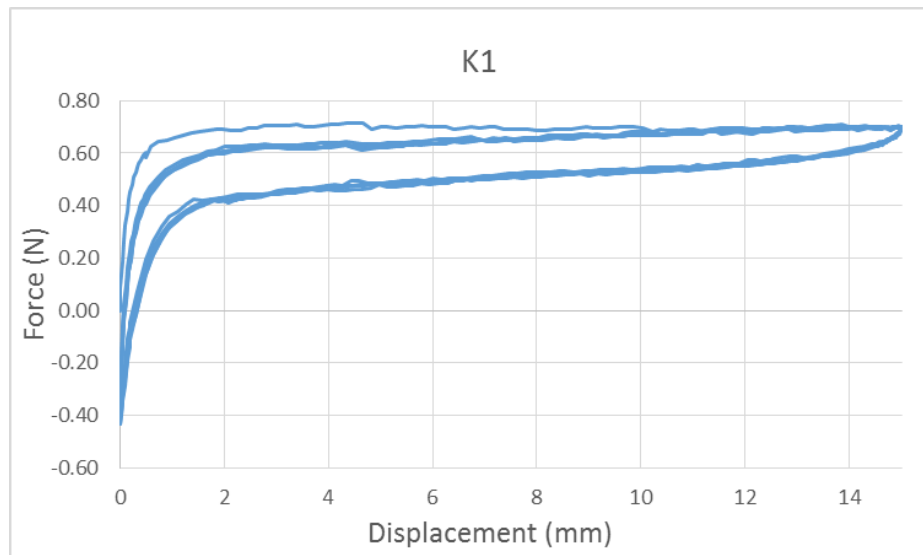
Compression buckling forces of the twenty-two fabrics described in chapter 5 are obtained in LUFHES and their bending rigidity are measured in both the KES-F and FAST systems, respectively.

6.1.1 Compression buckling force measured in the LUFHES

An example of compression force-displacement curve of a woven fabric cylindrical shell obtained in cyclic axial compression buckling-recovery process in the LUFHES is shown in Figure 6.1(a), in which a pronounced maximum force at a buckling yield point is shown. However, the compression buckling curve of some fabrics, especially knitted fabrics, does not show an apparent buckling yield point but has a transition period as shown in Figure 6.1(b). Therefore a unified method used to determine the buckling force in both of these two compression buckling curves in LUFHES software are illustrated in Figure 6.2 (LUFHES Software).



(a)



(b)

Figure 6.1 Compression buckling curves of woven fabric W1 and knitted fabric K1

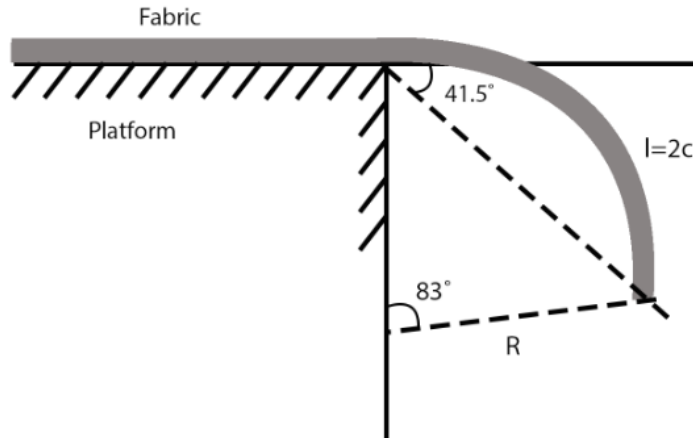


Figure 6.3 Fabric bending length obtained in the FAST cantilever bending test

It is noticed that the overhanging fabric bends is not a perfect arc and that the curvature of the arc varies from fabric to fabric due to their different bending length. In order to estimate the curvature of the bent fabric, it is assumed that the overhanging fabric bends like a perfect arc, then the corresponding central angle of this arc is 83° as shown in Figure 6.3. The relationship between arc length, central angle and radius is shown in equation 6.1 below:

$$2c = 83^\circ \times \frac{\pi R}{180^\circ} \dots\dots\dots (6.1)$$

Thus curvature (k) of this arc is determined by using equation 6.2 (Gere and Timoshenko, 1997),

$$k = \frac{1}{R} = \frac{0.724}{c} \dots\dots\dots (6.2)$$

Fabric bending length is used to evaluate fabric bending resistance. According to the manual of the FAST system, the fabric bending rigidity (BR_{FAST}) which is defined as the bending moment required to bend unit width of fabric to unit curvature is calculated by using equation 6.3 below (De Boos and Tester, 1994):

$$BR_{FAST} = m \cdot c^3 \cdot 9.8 \times 10^{-12} \dots\dots\dots (6.3)$$

Where BR_{FAST} is bending rigidity (Nm) obtained in the FAST bending test; m is fabric mass per unit area (g/m^2); c is bending length (mm).

It is noted that the fabric bending rigidity (BR_{FAST}) obtained is associated with the fabric curvature determined using the equation 6.3.

6.1.3 Bending rigidity obtained in the KES-F system

Fabric bending rigidity evaluated in the KES-F system is in pure bending deformation during the curvature of the fabric changes from 0.5 to 2.5 cm^{-1} . A typical fabric bending moment-curvature curve obtained in the KES-F system is shown in Figure 6.4.

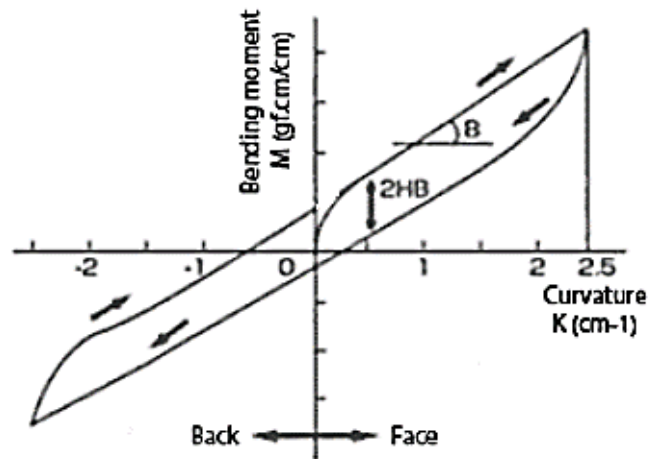


Figure 6.4 Fabric pure bending curve in the KES-F system

The bending rigidity in the KES-F system is obtained based on the relationship between bending moment and curvature below (Gürdal et al., 1999):

$$M = BR \cdot k \dots\dots\dots (6.4)$$

Where M is bending moment (gf.cm/cm), k is curvature (cm^{-1}), and BR is the bending rigidity ($\text{N}\cdot\text{m}$) which is defined as the bending moment required to bend unit width of fabric to unit curvature.

It is known from equation 6.4 that bending rigidity, BR , is the slope of bending moment-curvature curve. The average slope obtained in the range of curvature between $\pm 0.5\text{cm}^{-1}$ and $\pm 1.5\text{cm}^{-1}$ is denoted as bending rigidity (KES-F Manual) in SI unit, BR_{KESF} (Nm),

$$BR_{KESF} = BR \times 10^{-4} \dots\dots\dots (6.5)$$

6.2 Compression buckling force and bending rigidities

Bending rigidity measured in both the KES-F and FAST systems is defined as the bending moment required to bend unit width of fabric to unit curvature. Because the measurement mechanisms in the two systems are different, there are two bending rigidities obtained in both the KES-F and FAST systems, and it is still not clear what their differences are. It is thus necessary to know which fabric bending rigidity would be better correlated with compression buckling forces measured in the LUFHES. Fabric bending rigidities obtained in the KES-F and FAST systems (BR_{KES-F} and BR_{FAST}) are shown in Table 6.1, their differences are analysed in the section 6.2.1 before the correlation between compression buckling force of fabric shells, P_{cr} , (shown in Table 6.1) and bending rigidities are investigated in section 6.2.2.

Table 6.1 Fabric compression buckling force (P_{cr}) measured in the LUFHES and bending rigidity obtained in both the FAST and the KES-F systems (BR_{KES-F} and BR_{FAST})

Fabric		Critical buckling force P_{cr} (N)	Axial displacement (mm)	Bending rigidity (Nm)	
				FAST (BR_{FAST})	KES-F(BR_{KES-F})
W1	Warp	0.48	0.06	6.80E-07	6.67E-07
	Weft	0.50	0.05	2.99E-06	2.59E-06
W2	Warp	0.88	0.06	1.01E-05	7.37E-06
	Weft	0.88	0.08	8.16E-06	5.22E-06
W3	Warp	3.14	0.10	9.41E-05	3.75E-05
	Weft	4.47	0.11	9.79E-05	4.95E-05
W4	Warp	0.92	0.15	1.67E-05	1.57E-05
	Weft	0.97	0.13	1.72E-05	1.76E-05
W6	Warp	1.56	0.05	3.39E-05	1.82E-05
	Weft	1.18	0.12	1.12E-05	6.88E-06
W7	Warp	0.59	0.14	1.07E-05	1.29E-05
	Weft	0.65	0.13	1.31E-05	1.50E-05
W8	Warp	1.29	0.06	2.99E-05	1.65E-05
	Weft	1.19	0.05	8.78E-06	6.25E-06
W9	Warp	0.73	0.10	3.76E-06	6.27E-06
	Weft	0.71	0.14	4.82E-06	6.59E-06
W10	Warp	0.82	0.27	8.93E-06	1.19E-05
	Weft	0.77	0.25	6.01E-06	9.39E-06
W11	Warp	1.16	0.22	1.93E-05	2.38E-05
	Weft	1.08	0.19	1.80E-05	2.07E-05
W12	Warp	8.93	1.10	2.71E-04	1.29E-04
	Weft	5.21	0.28	5.57E-05	6.59E-05
K1	Wale	0.59	0.29	6.22E-06	2.57E-05
	Course	0.54	0.30	4.09E-06	6.66E-06
K2	Wale	0.50	0.23	3.67E-06	1.10E-05
	Course	0.52	0.30	2.59E-06	3.18E-06
K3	Wale	1.46	0.09	6.01E-05	3.68E-05
	Course	1.01	0.34	9.48E-06	7.17E-06
K4	Wale	0.75	0.38	1.05E-05	2.93E-05
	Course	0.69	0.38	6.19E-06	1.13E-05
K5	Wale	0.47	0.19	3.17E-06	4.65E-06
	Course	0.39	0.29	1.61E-06	8.57E-07
K6	Wale	0.47	0.16	2.21E-06	1.83E-06
	Course	0.45	0.23	1.62E-06	9.40E-07
K7	Wale	0.49	0.24	5.21E-06	1.06E-05
	Course	0.44	0.40	3.10E-06	1.80E-06
N1	MD	0.47	0.18	6.30E-07	1.41E-06
	CD	0.41	0.22	5.41E-07	5.53E-07
N8	MD	0.46	0.16	3.51E-06	2.95E-06
	CD	0.41	0.23	6.17E-07	6.25E-07
N10	MD	0.48	0.15	6.48E-06	2.40E-06
	CD	0.39	0.41	7.71E-07	8.83E-07
N11	MD	0.56	0.13	6.58E-06	5.18E-06
	CD	0.48	0.24	1.16E-06	1.53E-06

6.2.1 Differences of bending rigidities obtained in the KES-F and FAST systems

The correlation coefficients, R^2 , of linear regression equations between BR_{KESF} and BR_{FAST} of woven, knitted and nonwoven fabrics are shown in Table 6.2.

Table 6.2 Correlation coefficients, R^2 , of linear regression equations between bending rigidities obtained in the FAST and the KES-F systems

Types of fabrics	correlation coefficients, R^2 , between BR_{KESF} and BR_{FAST}
Woven fabrics	0.91
Knitted fabrics	0.55
Nonwoven fabrics	0.73

It is shown in Table 6.2 that, BR_{KESF} and BR_{FAST} for woven fabrics have strong linear relationship, their correlation coefficients, R^2 , is 0.91. This good correlation is in agreement with previous research conclusions (Ancutiene et al., 2010; Yick et al., 1996), in which strong correlation between bending rigidity of both heavy-weight and light-weight woven fabrics obtained in the KES-F and FAST systems were found.

However, the correlation coefficients, R^2 , between BR_{KESF} and BR_{FAST} for knitted and nonwoven fabrics are much smaller, only 0.55 and 0.73, respectively (see Figure 6.5 and Figure 6.6) and suggest that bending rigidity measured in the FAST and the KES-F systems for knitted and nonwoven fabrics do not have good linear relationship. It is shown in Figure 6.5 and Figure 6.6 that these poorer correlations are mainly due to the data points of K3-wale and K3-course in Figure 6.5 and N10-MD in Figure 6.6. They stray away from the trend of other fabrics in that group of fabrics. If the data of these three samples are excluded from the two Figures, R^2 between BR_{FAST} and BR_{KESF} of knitted and nonwoven fabrics are 0.85 and 0.97, respectively. This suggests that strong linear relationships exist between BR_{FAST} and BR_{KESF} for most of knitted and nonwoven fabrics.

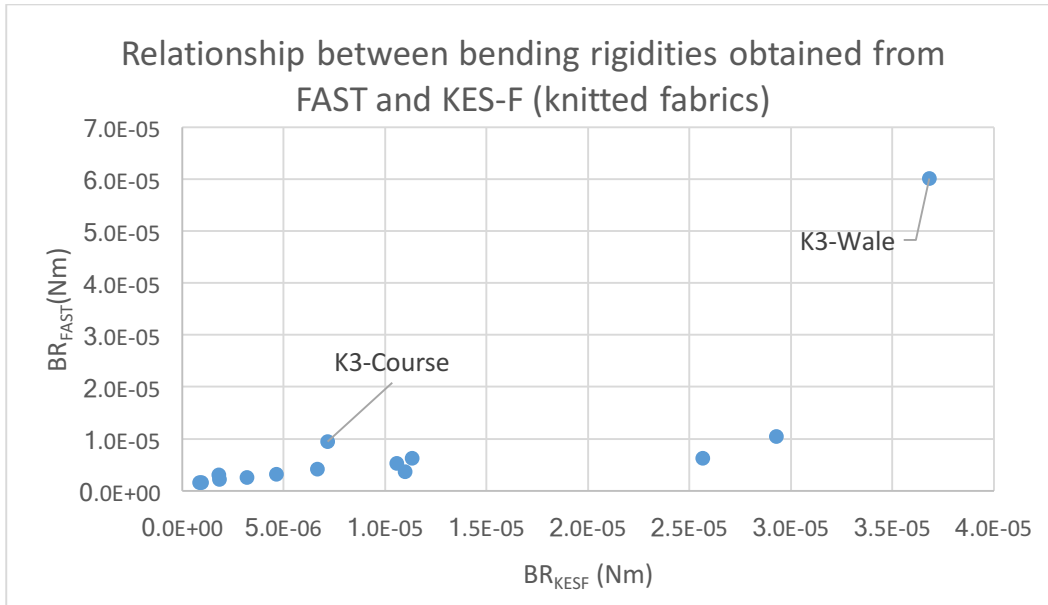


Figure 6.5 Correlation between bending rigidities obtained in both the FAST and the KES-F systems for seven knitted fabrics

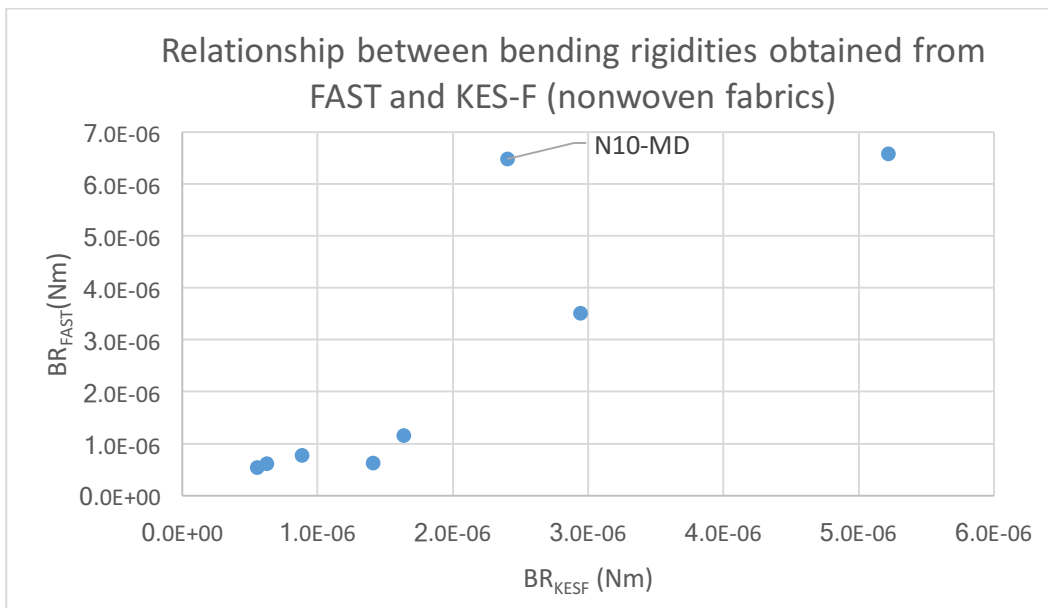


Figure 6.6 Correlation between bending rigidities obtained in the FAST and the KES-F systems for four nonwoven fabrics

It is crucial to find out the reasons why bending rigidities measured in both the KES-F and the FAST systems for some knitted and nonwoven fabrics are not correlated well, as we do not know if the results from any of the KES-F and FAST systems are wrong and it is not clear for us that the bending rigidity obtained in which system (KES-F or FAST) should be taken forward to compare with the fabric compression buckling forces.

It is noticed that fabric bending rigidity is obtained in the KES-F system when the fabric bending curvature is in the range between 0.5cm^{-1} and 1.5cm^{-1} , the bending

moment-curvature curves of K3 knitted fabric (both wale and course directions, K3-wale and K3-course) obtained in the KES-F bending length test are compared with a normal knitted fabric, K7 (see Figure 6.7 and Figure 6.8) and the nonwoven fabric N10 in the machine direction (N10-MD) are compared with a normal nonwoven fabric N1 (see Figure 6.9).

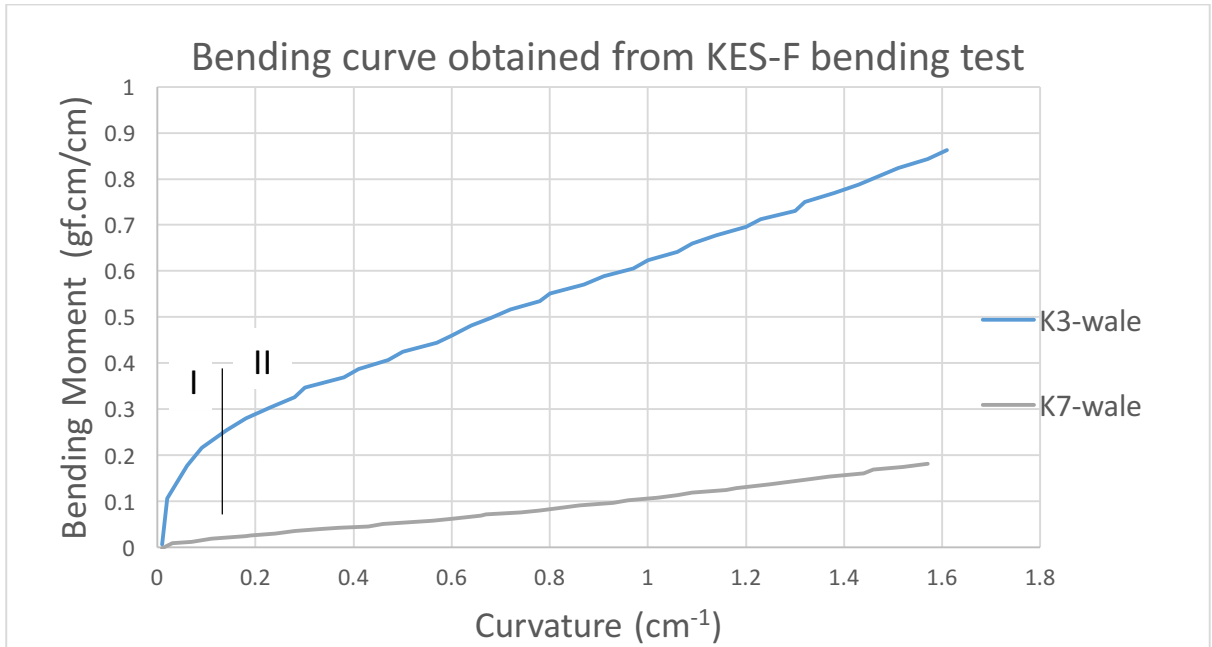


Figure 6.7 Bending curve of K3-wale and K7-wale obtained in the KES-F bending test

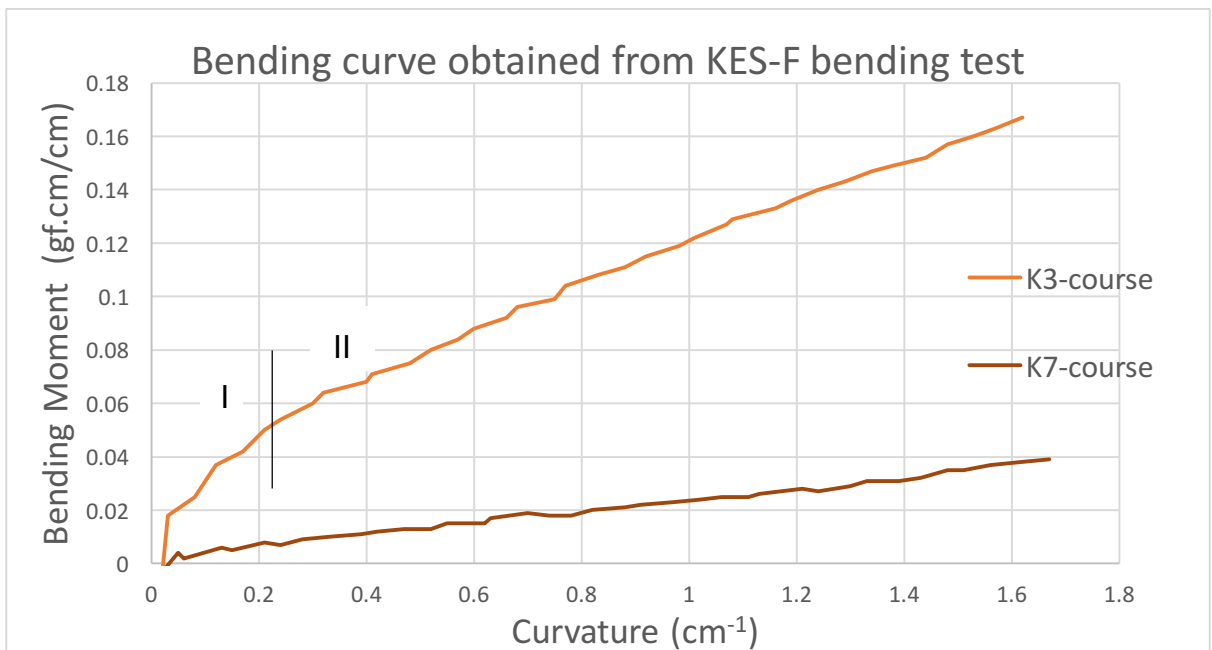


Figure 6.8 Bending curve of K3-course and K7-course obtained in the KES-F bending test

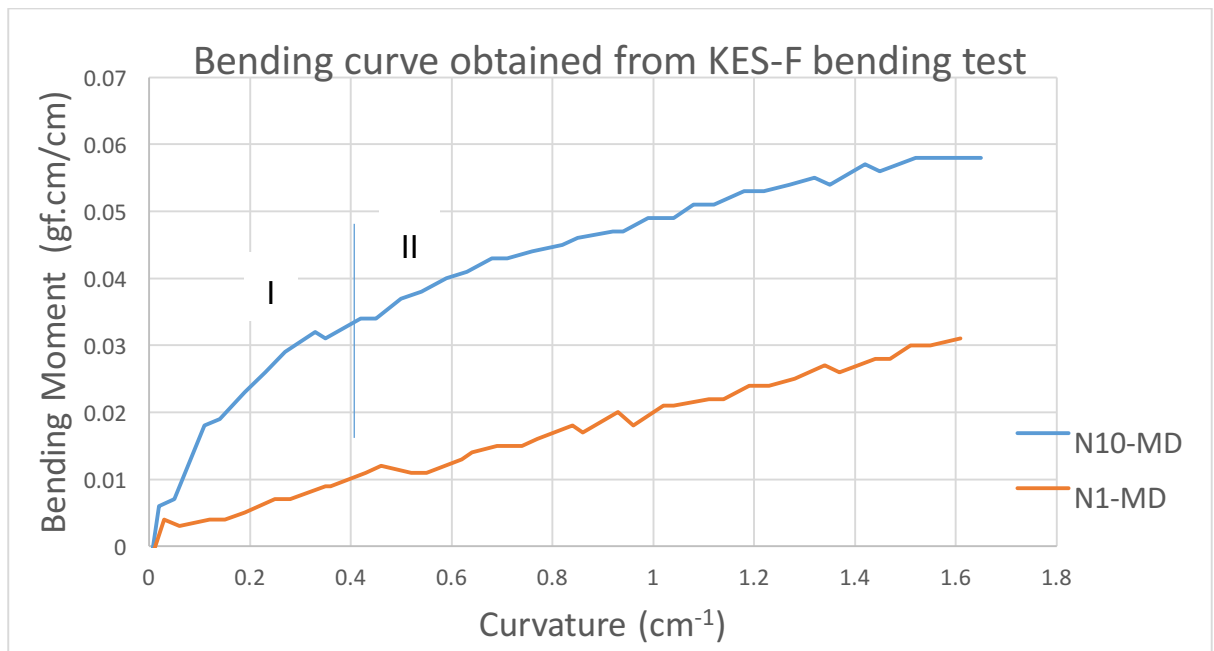


Figure 6.9 Bending curve of N10-MD and N1-MD obtained in the KES-F bending length test

In comparison with the KES-F bending curve of the normal knitted fabric (K7) and the normal nonwoven fabric (N1), a common characteristic for the bending moment-curvature curves of K3-wale, K3-course and N10-MD is that their KES-F bending curves are not linear but have two sections, the initial section having greater slope of bending moment-curvature (or greater stiffness) when the curvature is small (0.2cm^{-1} for K3 and 0.4cm^{-1} for N10-MD) and the second section having relatively smaller slope of bending moment-curvature when the curvature is greater (0.2cm^{-1} to 1.5cm^{-1} for K3 and 0.4cm^{-1} to 1.5cm^{-1} for N10-MD). In the section II, the slope is nearly constant, this corresponds to the findings that the fabric stiffness in a range of greater curvature is close to constant (Bueno, M. et al., 2008). In contrast, the bending moment against bending-curvature of normal fabrics K7-wale, K7-course and N1-MD have a linear relationship throughout the entire range of curvature from 0 to 1.5cm^{-1} .

In summary, for all of the woven fabrics, most of the knitted fabrics and nonwoven fabrics, their bending moment obtained in the KES-F vary linearly with their bending curvatures (e.g., 0 to 1.5cm^{-1}); however, the bending moment of some knitted and nonwoven fabrics vary nonlinear with their bending curvatures, they would have greater bending rigidity when their bending curvature is small (e.g., 0 to 0.2cm^{-1} for K3 and 0 to 0.4cm^{-1} for N10-MD) and have smaller bending rigidity when their bending curvature is greater (e.g., 0.2cm^{-1} to 1.5cm^{-1} for K3 and 0.4cm^{-1} to 1.5cm^{-1} for N10-MD).

The conclusions above obtained in the analysis of the bending rigidity from the KES-F is very important to understand the bending curvature obtained in the FAST. As shown in equation 6.2, the fabric bending curvature varies with its bending length obtained; thus, the fabric bending rigidity obtained in the FAST is at various fabric bending curvatures. The bending curvatures of the 22 fabrics in the FAST bending length test are shown in Table 6.3.

Table 6.3 Fabric bending curvature in the FAST bending length test

Fabric	Curvature (cm ⁻¹)		Fabric	Curvature (cm ⁻¹)	
	Warp/Wale/MD	Weft/Course/CD		Warp/Wale/MD	Weft/Course/CD
W1	0.68	0.42	K1	0.52	0.60
W2	0.37	0.39	K2	0.63	0.71
W3	0.23	0.23	K3	0.29	0.54
W4	0.36	0.36	K4	0.47	0.56
W6	0.30	0.44	K5	0.59	0.74
W7	0.34	0.32	K6	0.63	0.69
W8	0.30	0.45	K7	0.61	0.73
W9	0.60	0.56	N1	0.48	0.50
W10	0.48	0.55	N8	0.30	0.53
W11	0.41	0.42	N10	0.23	0.48
W12	0.18	0.31	N11	0.24	0.44

It is apparent that the minimum fabric curvature in the FAST bending test is around 0.23 cm⁻¹ (W3 and N10-MD) and maximum fabric curvature is around 0.74 cm⁻¹ (K5-Course). Bending rigidities obtained at such smaller bending curvature for all of the woven fabrics and most of the knitted and nonwoven fabrics might not be different from those obtained at greater bending curvatures (e.g., 0.5cm⁻¹-1.5cm⁻¹ in the KES-F system) as their bending moment-bending curvature relationship is linear. However, for a few fabrics (K3 and N10 fabrics), they do not have such linear bending moment-bending curvature relationship, the bending rigidity obtained in smaller and greater bending curvatures will have greater differences.

It is shown in Figure 6.7, Figure 6.8, and Figure 6.9 that the section I of fabric K3-wale, K3-course and N10-MD are within the bending curvature of 0.5cm⁻¹. As shown in Table 6.3, the bending rigidity measured for K3-wale, K3-course and N10-MD in the FAST are at the bending curvature of 0.29cm⁻¹, 0.54cm⁻¹ and 0.23cm⁻¹, which are around the range of 0-0.5cm⁻¹, this is in contrast the bending curvature of the three fabrics measured in the KES-F system which are within the

range of $0.5-1.5\text{cm}^{-1}$. Therefore we believe that it is the different fabric curvatures in the FAST and the KES-F bending tests that lead to their different bending rigidities in the FAST and the KES-F systems, and this is the reason why BR_{KESF} and BR_{FAST} have a poor linear relationship when K3-wale, K3-course and N10-MD are included, while have a good linear relationship when K3-wale, K3-course and N10-MD are excluded.

6.2.2 Correlation between compression buckling force and bending rigidity

It is known that the compression buckling force is obtained before any fabric buckling deformation is formed, the fabric bending curvature at this compression buckling point must be small, so it is anticipated that the compression buckling force measured in LUFHES might correspond to the bending rigidity measured at smaller bending curvatures if the fabric buckles in a smaller curvature. It is known in the section 6.2.1 that the bending rigidity measured in the KES-F system is from a range of relatively greater bending curvature (greater than 0.5cm^{-1}) than that in the FAST system.

The relationship between compression buckling force measured in the LUFHES and the bending rigidity obtained in the KES-F and the FAST are investigated. R^2 of linear regression equations between them for woven, knitted and nonwoven fabrics are shown in Table 6.4.

Table 6.4 R^2 of linear regression equations between critical compression buckling force (P_{cr}) and bending rigidity obtained in the FAST and the KES-F systems

		R^2	BR_{KESF} (Nm)	BR_{FAST} (Nm)
P _{cr} (N)	Woven fabrics		0.96	0.89
	Knitted fabrics		0.52	0.82
	Nonwoven fabrics		0.83	0.59

It is shown that, for woven fabrics, critical compression buckling force has strong linear relationship with both BR_{KESF} and BR_{FAST} , R^2 between them are 0.96 and 0.89, respectively. It indicates that woven fabric which has greater bending rigidity is likely to have greater critical buckling force in shell buckling.

For knitted fabrics, critical compression buckling force only has strong linear relationship with BR_{FAST} ($R^2= 0.82$), but does not have strong linear relationship with BR_{KESF} ($R^2= 0.52$). Conversely, critical compression buckling force of nonwoven fabrics only has strong linear relationship with BR_{KESF} ($R^2= 0.83$), but

does not have strong linear relationship with BR_{FAST} ($R^2 = 0.59$). Knitted fabrics and nonwoven fabrics are discussed separately in following sections.

The relationship between critical compression buckling force of knitted fabrics and BR_{KESF} are shown in Figure 6.10 and the relationship between critical buckling force of nonwoven fabrics and BR_{FAST} are shown in Figure 6.11.

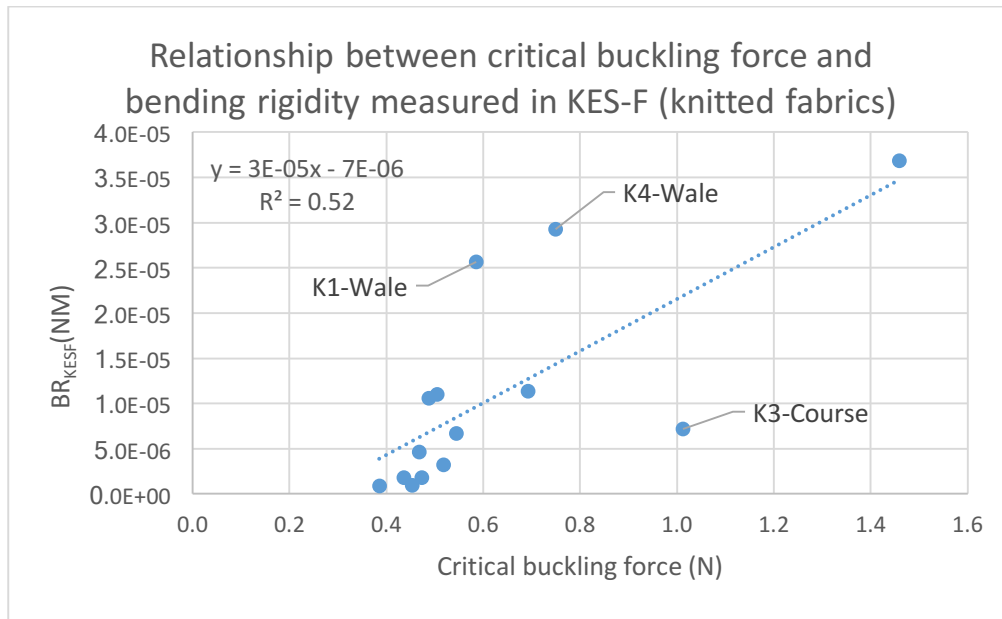


Figure 6.10 Relationship between critical compression buckling force and bending rigidity obtained in the KES-F systems (knitted fabrics)

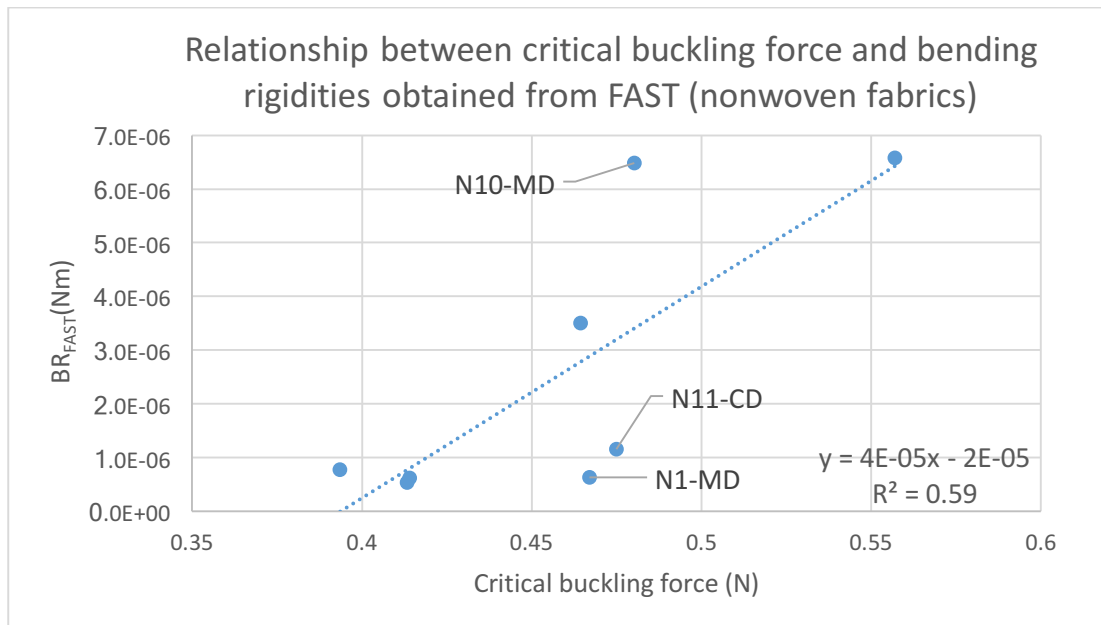


Figure 6.11 Relationship between critical buckling force and bending rigidity measured in the FAST system (nonwoven fabrics)

It is shown that data points of K1-wale, K3-course, and K4-wale are far away from the trend of other knitted fabrics in the relationship between critical compression buckling force and BR_{KESF} (Figure 6.10), and data point of N1-MD, N10-MD and N11-CD are far away from the main trend in the relationship between critical compression buckling force and BR_{FAST} (Figure 6.11). It is suggested that there is no statistic relation between P_{cr} obtained in the LUFHES buckling test and the bending rigidity obtained in the KES-F bending test of knitted fabrics, and there is no statistic relation between P_{cr} and bending rigidity obtained in FAST of nonwoven fabric. In addition, the poor linear relationship between P_{cr} of knitted fabrics and BR_{KESF} , and the poor linear relationship between P_{cr} of nonwoven fabrics and BR_{FAST} are not due to the data of a specific fabric, so it might be related to the fabric deformation in buckling and bending.

Different from bending test, fabric shell only has axial displacement before external force reaches the critical buckling force, fabric curvature is zero during this process. The axial displacement of fabrics when critical buckling force is reached is given in Table 6.1

It is shown that axial displacement of most woven fabrics is from 0.05mm-0.15mm (W1-W9), that of some fabric is around 0.2mm-0.3mm (W10, W11 and W12-weft). Only W12-wale has significantly huge axial displacement before buckling, 1.10mm. The axial displacement of most nonwoven fabrics is around 0.10-0.25mm. Only N10-CD has greater axial displacement of 0.41mm. Generally speaking, most of knitted fabrics have greater axial displacement before buckling than woven and nonwoven fabrics, around 0.25mm-0.4mm.

Critical compression buckling forces of both woven and nonwoven fabrics have better correlation with BR_{KESF} , but critical buckling forces of knitted fabrics have better correlation with BR_{FAST} . Due to the different axial deformations of fabrics before buckling, and different fabric curvatures in the FAST and the KES-F bending tests, it implies that P_{cr} of fabric which has smaller axial deformation (0-0.25mm) might have better correlation with BR_{KESF} , but P_{cr} of fabric which has greater axial deformation (0.25mm-0.4mm) might have better correlation with D_{FAST} .

Due to the good correlation between critical compression buckling force and bending rigidity obtained in either the FAST or the KES-F system, it is anticipated that the bending rigidity might be related to the buckling energy when the buckling deformation displacement is a constant.

6.3 Summary

The main findings in this chapter are as below:

1. Critical compression buckling forces of woven and nonwoven fabrics had good correlation with bending rigidities measured in the KES-F system. However, critical compression buckling forces of knitted fabrics had good correlation with bending rigidities measured in the FAST system. It was suggested that using bending rigidity might be similar to using buckling force in discriminating fabric;
2. Bending rigidity obtained in the FAST bending test agreed well with bending rigidity obtained in the KES-F bending test for all the woven fabrics, most knitted and nonwoven fabrics tested;
3. For fabric whose bending moment vary nonlinearly with its curvature (e.g., fabrics K3 and N10), bending rigidity measured in the FAST bending test was not in agreement with its bending rigidity measured in the KES-F bending test, because its bending rigidity were measured in different range of curvature in the KES-F and FAST tests.

Chapter 7 Fabric friction properties in relation to fabric structure and roughness

For fabrics directly contact with skin, fabric surface friction and roughness are related to fabric tactile comfort and fabric handle which affect consumer perceptions and preferences.

In this chapter, theoretical analysis of fabric-fabric friction and fabric-metal sensor friction are conducted to show the major wavelength spectrum in fabric-fabric friction process and fabric-sensor friction process. Friction coefficient obtained in LUFHES friction test is based on fabric-fabric frictions, while fabric roughness and fabric friction coefficient are measured between sensors and fabric in the KES-F system. The friction and roughness profiles of 5 fabrics measured in both systems are analysed using Fast Fourier Transform (FFT) and compared with theoretical analysis to determine how the wavelength spectrum is related to fabric geometrical structure. The wavelengths and its amplitudes are analysed to decide if they could be used to differentiate fabric surface structures and roughness.

7.1 Analysis of fabric-fabric friction profile in the LUFHES

In the LUFHES friction test, the extension force/dynamic friction force against its relative displacement of the ripstop fabric W1 is obtained as shown in Figure 7.1. The extension/friction-displacement curve has two sections, fabric extension section and fabric friction section (i.e., the dynamic fabric friction process after the fabric relative displacement occurs). In fabric extension section, the extension force gradually increases with the fabric extension and then reaches maximum (i.e., static friction force). In fabric friction section, the contact length between two fabric layers decreases with the relative displacement of the fabric, so does the friction force. Therefore the spectral analysis of the friction coefficient profile by using FFT spectrum analysis is conducted after a rectification calculation is applied as shown in Appendix D.

In this section, the spectral profile of the fabric coefficient obtained is then compared with the theoretical spectral profile to uncover the relationship between fabric friction profiles and fabric structure.

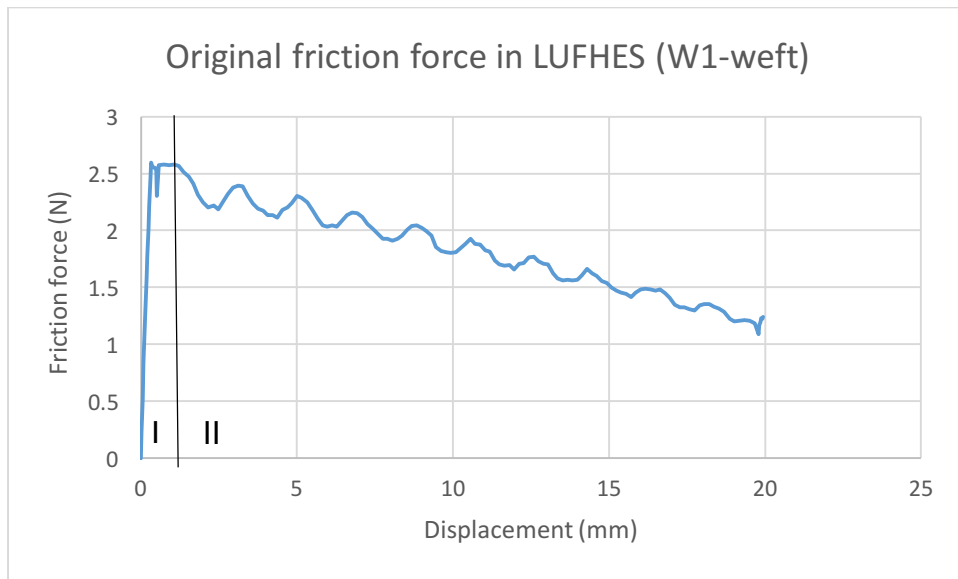


Figure 7.1 The extension forces and dynamic friction force profile against relative displacement of the ripstop fabric in weft direction in the LUFHES

7.1.1 Theoretical analysis of fabric-fabric friction of a ripstop fabric

In this section, the fabric-fabric friction profile of a ripstop fabric is taken as a case study to demonstrate how fabric structure and surface profile affect its surface friction properties. The theoretical analysis of fabric-fabric friction in a unit woven structure of the ripstop fabric in weft direction is analysed based on its structural parameters.

7.1.1.1 The fabric structure of a ripstop fabric

The surface structure of a ripstop woven fabric (W1) is shown in Figure 7.2. Both warp and weft yarns of this ripstop fabric are filaments having hardly any twist, so these filaments are oriented in either warp or weft directions.

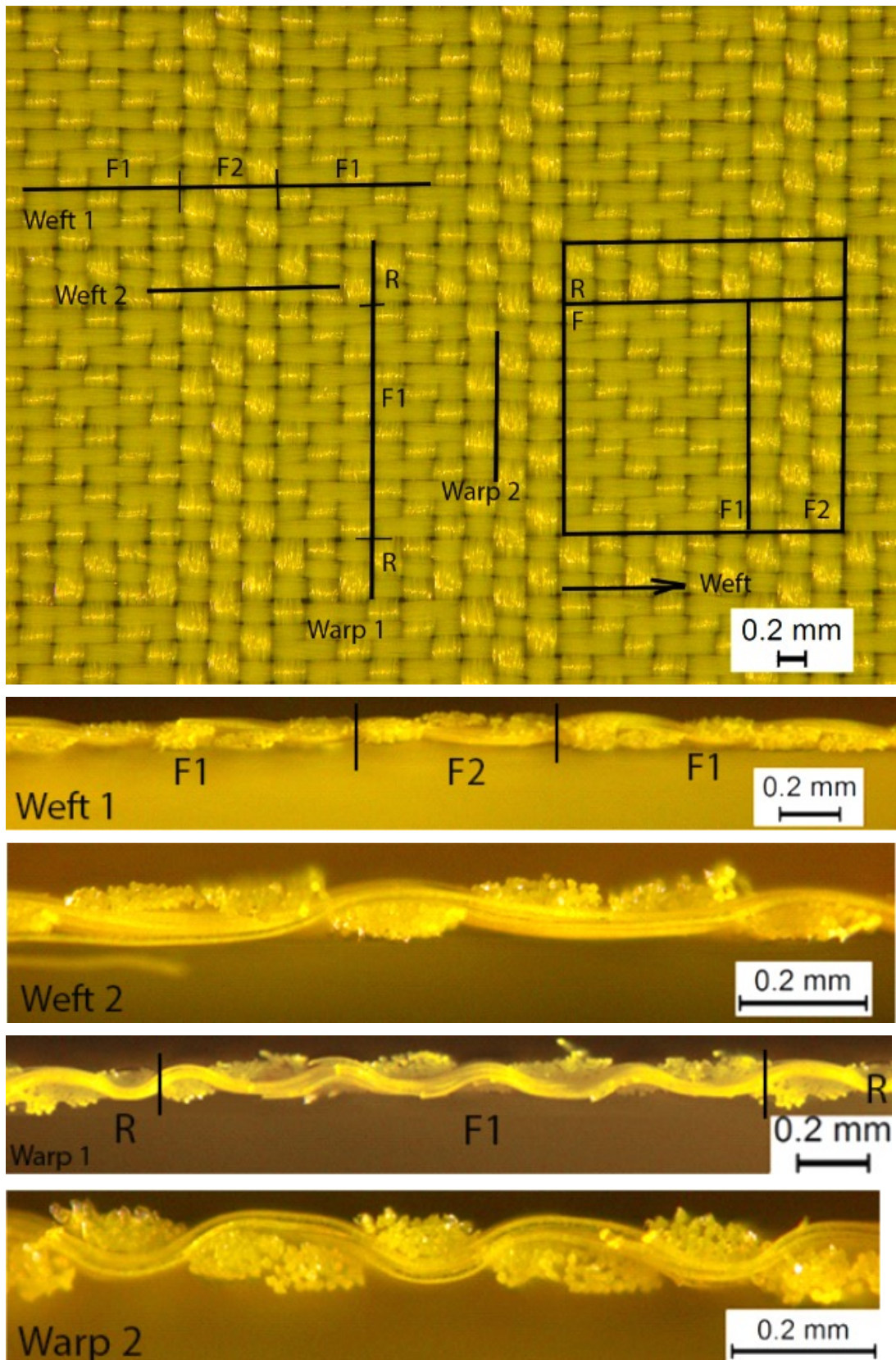


Figure 7.2 Ripstop fabric surface and cross-section structure

A unit structure of this ripstop fabric, which is repeated to form the whole ripstop structure, is highlighted in Figure 7.2. This unit structure is simplified as consisting of two smaller strips in weft direction, ripstop strip (R) and flat strip (F). Ripstop

strip (R) contains nine warp yarns and three weft yarns. Each weft yarn in R area contains 3 loops, the weft yarn in one loop has a 1/2 weave structure. Flat strip (F) contains two sub-structures in the weft direction, shown as F1 and F2 in Figure 7.2. F1 contains 6 warp yarns and F2 contains 3 warp yarns. F2 forms the ripstop strip in the warp direction. In the F2 area, weft yarn has a 1/2 weave structure, which is the same with the ripstop (R) strip. F1 area contains 2 loops in the weft direction, weft yarn in each loop has a 2/1 weave structure.

In summary, the unit ripstop fabric structure consists of two strips: ripstop strip and twill woven strip; when two fabric surfaces against each other in the friction movement, there are three types of friction interactions between the two fabric surfaces, they are,

- 1) Ripstop strip against ripstop strip
- 2) Twill woven strip against twill woven strip
- 3) Ripstop strip against twill woven strip

7.1.1.2 Models of the fabric surface of ripstop fabrics

In order to establish a theoretical surface friction profile of the ripstop fabric shown in Figure 7.2, the fabric surface structure is modelled as an assembly of cross points having different surface structures which have different friction properties. The two types of crossover points at the fabric surfaces in the weft direction: cross point of weft yarn surface and cross point of warp yarn surface, are represented by two symbols shown below,



Figure 7.3 Symbols used to represent warp and weft yarn surface

Therefore, the structure of a weft yarn in R area (1/2 twill structure) in Figure 7.2 could be represented as the symbol shown in Figure 7.4 below:



Figure 7.4 Symbol of a weft yarn in R area

Because the fabric surface in the F1 area contains more weft yarns than warp yarns, the F1 area structure is simplified as weft yarn cross points of while F2 area still has a 1/2 twill structure. A weft yarn in F area could be represented as the symbol shown in Figure 7.5 below:

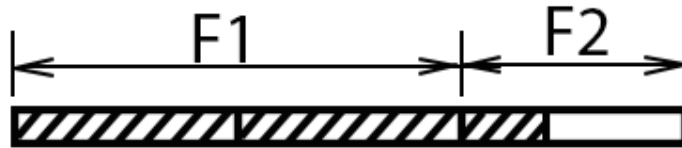


Figure 7.5 Symbol of a weft yarn in F area

The ripstop strip R shown in Figure 7.2 contains three weft yarns having identical 1/2 twill structure and they are marked as X, Y, and Z. Three weft yarns with their cross points are shown in Figure 7.6, and we define that *A* and *B* are the lengths of the weft yarn cross point and warp yarn cross point on the fabric surface in weft direction, respectively, each pair of adjacent weft yarns has a relative displacement, *C*, in the weft direction and they have the same width, *D*. The structure of F2 also contains three weft yarns having a 1/2 twill structure, and it is assumed that the twill structure of three weft yarns in F2 has the same relationship as those in ripstop strip R.

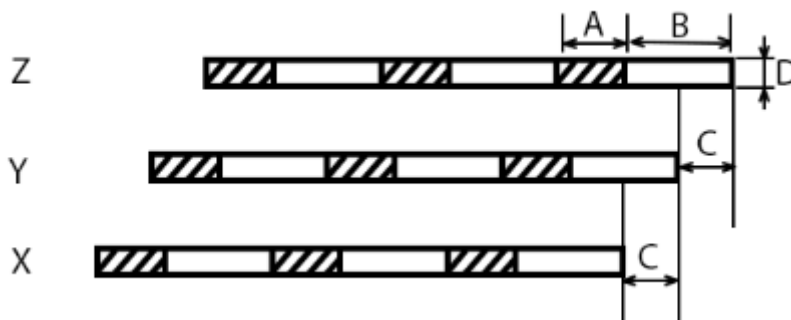


Figure 7.6 Three weft yarns in ripstop strip R

Based on the structure of ripstop fabric shown in Figure 7.2, it is assumed that lengths of *A*, *B* and *C* have following relationship:

$$A \leq 2C \leq B \leq A + C \quad \text{and} \quad A + B < 4C \dots\dots\dots (7.1)$$

When these yarns between top and bottom fabric contact each other (see Figure 7.7), A_x and B_x are the contact lengths of top weft yarn and bottom weft yarn and the contact length of top warp yarn and bottom weft yarn, respectively; they change with the movement of yarns.;



Figure 7.7 Contact length of weft-weft and warp-weft yarn cross points when top fabric contact bottom fabric.

Thus, there are three types of friction take place in the contact area between different warp/weft yarn cross points in both top and bottom fabric layers when they have relative movement, their friction coefficients are shown below,

μ_1 : friction coefficient between warp yarn and warp yarn cross points;

μ_2 : friction coefficient between warp yarn and weft yarn cross points;

μ_3 : friction coefficient between weft yarn and weft yarn cross points;

The cross-sections of both R and F areas in warp and weft directions are shown in Figure 7.2 to investigate the effect of the height of warp and weft yarn protrudes on fabric friction properties. According to the adhesion-shearing theory of friction, a higher fabric surface protrude would produce greater shear effect to generate greater friction force. It is learned from the cross-section structure (Figure 7.2) that the difference between the heights of the cross-over points of warp and weft yarns are not significant, it is therefore expected that warp and weft yarns have identical possibility to produce shear deformations and friction effects during friction process.

When the top fabric moves in the weft direction, the warp yarn cross points contain fibres perpendicular to the direction of fabric movement in the weft direction, and weft yarn cross points contain fibres parallel to the direction of fabric movement in weft direction, these fibres would have different frictional performance when they move against the fibres in top fabrics. Friction tests of carbon fibre tows indicate that friction coefficient between parallel-parallel tows is greater than the friction coefficient between parallel-perpendicular tows (Cornelissen et al., 2013). The yarns of this ripstop fabric are low-twisted filaments, so the frictional performance of its fibres might be similar to that of carbon fibre tows. Thus, it is assumed that friction coefficient between weft and weft yarn cross points (parallel to movement direction) is greater than the friction coefficient between weft and warp yarn cross points, $\mu_3 > \mu_2$. When warp yarn cross points move against warp yarn cross points (perpendicular to movement direction), digging in of the filament could take place. In addition, according to adhesion-shearing theory (Gupta, 2008), the shear force of asperities on fabric surface has to be overcome to initiate and keep the friction movement. Thus, it is assumed that friction coefficient between warp and warp yarn cross points

(perpendicular-perpendicular to movement direction) is greater than the friction coefficient between weft and weft yarn cross points (parallel-parallel to movement direction), $\mu_1 > \mu_3$. In summary, it is assumed $\mu_1 > \mu_3 > \mu_2$ in this theoretical analysis.

When the normal pressure, P , applied on the contact area between two fabric surfaces and produce a relative displacement of S during friction movement, the friction force is denoted as F .

7.1.1.3 Friction force between unit structures of ripstop fabric

Two types of frictions shown in Figure 7.8 are discussed. The first one (Figure 7.8 (a)) is when top ripstop strip (R) overlaps with bottom ripstop strip (R) and top flat strip (F) overlaps with bottom flat strip (F). The second one (Figure 7.8 (b)) is when the top ripstop strip (R) contacts the flat strip (F) of bottom fabric.

As shown in Figure 7.8, structure R contains 3 weft yarns, and structure F has four repeated structures which contain 3 weft yarns. Therefore, the top and bottom structures could be divided into five parts, and each part contains three weft yarns. During the first type of friction movement (Figure 7.8 (a)), four parts have flat strip-flat strip movements and one part has ripstop strip-ripstop strip movement. During the second type of friction movement (Figure 7.8 (b)), two parts have ripstop strip-flat strip friction movement, and three parts have flat strip-flat strip friction movement.

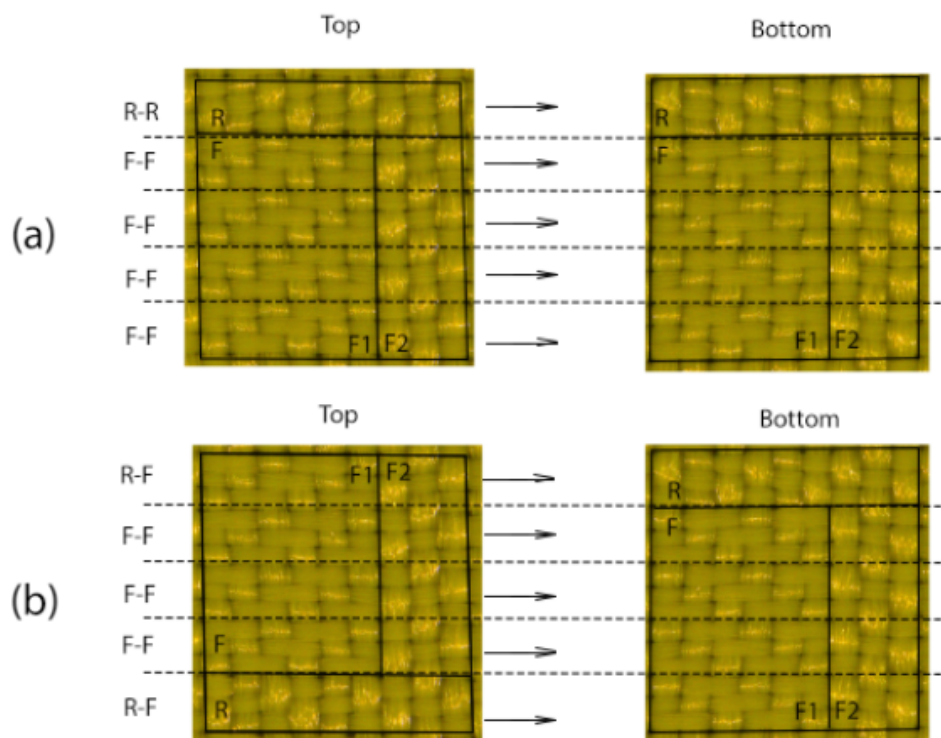


Figure 7.8 Two movements in fabric to fabric friction. (a) Top fabric moving against bottom fabric of identical structure. (b) Top fabric moving against bottom fabric of mirroring structure.

The total friction displacement of the unit structure is $3(A + B)$ in weft direction, and the analysis of the theoretical friction forces during these movements are shown in Appendix B. It is assumed that the pressure 'P' is a constant and homogeneously applied on the fabric surface.

The two situations are discussed in the sections 7.1.1.3.1 and 7.1.1.3.2, respectively.

7.1.1.3.1 Friction force when top fabric moves against bottom fabric of identical structure

As shown in Figure 7.8 (a), this friction movement contains four flat strip-flat strip friction movements and one ripstop strip-ripstop strip movement. The theoretical frictional force of this type of fabric-fabric friction when top fabric moves against bottom fabric of identical structure during the displacement of $3(A + B)$ is shown in equation 7.2 below (see Appendix B).

$$\begin{aligned}
 F &= \left\{ \begin{array}{ll}
 Pd(31A + 9B - 4S + 30C)\mu_3 + 2PD(14A + 15B - 30C + 4S)\mu_2 + PD(6B + 30C - 14A - 4S)\mu_1 & (0 \leq S < 4C - B - A) \\
 PD(38A + 24B + 7S - 14C)\mu_3 + 2PD(7A + 14C - 7S)\mu_2 + PD(21B + 7S - 7A - 14C)\mu_1 & (4C - B - A \leq S < A + 2C - B) \\
 PD(35A + 27B - 20C + 10S)\mu_3 + 2PD(10A - 3B + 20C - 10S)\mu_2 + PD(24B - 10A - 20C + 10S)\mu_1 & (A + 2C - B \leq S < A) \\
 PD(49A + 27B - 20C - 4S)\mu_3 + 2PD(20C - 3B - 4A + 4S)\mu_2 + PD(24B + 4A - 20C - 4S)\mu_1 & (A \leq S < 4C - B) \\
 PD(49A + 13B + 36C - 18S)\mu_3 + 2PD(11B - 4A - 36C + 18S)\mu_2 + PD(10B + 4A + 36C - 18S)\mu_1 & (4C - B \leq S < 2C) \\
 PD(45A + 17B + 14C - 7S)\mu_3 + 2PD(7B - 14C + 7S)\mu_2 + PD(14B + 14C - 7S)\mu_1 & (2C \leq S < 2A) \\
 PD(39A + 17B + 14C - 4S)\mu_3 + 2PD(7B + 6A - 14C + 4S)\mu_2 + PD(14B - 6A + 14C - 4S)\mu_1 & (2A \leq S < A + 4C - B) \\
 PD(36A + 20B + 2C - S)\mu_3 + 2PD(4B + 9A - 2C + S)\mu_2 + PD(17B - 9A + 2C - S)\mu_1 & (A + 4C - B \leq S < A + 2C) \\
 PD(50A + 20B + 30C - 15S)\mu_3 + 2PD(15S + 4B - 5A - 30C)\mu_2 + PD(17B + 5A + 30C - 15S)\mu_1 & (A + 2C \leq S < A + B) \\
 PD(39A + 9B + 6C)\mu_3 + 2PD(15B + 6A - 6C)\mu_2 + PD(6B - 6A + 6C)\mu_1 & (A + B \leq S < 4C) \\
 PD(39A + 9B - 6C + 3S)\mu_3 + 2PD(6C + 15B + 6A - 3S)\mu_2 + PD(6B - 6A - 6C + 3S)\mu_1 & (4C \leq S < 2A + 2C) \\
 PD(33A + 9B - 12C + 6S)\mu_3 + 2PD(12A + 15B + 12C - 6S)\mu_2 + PD(6B - 12A - 12C + 6S)\mu_1 & (2A + 2C \leq S < 2A + B) \\
 PD(45A + 15B - 12C)\mu_3 + 2PD(12C + 9B)\mu_2 + PD(12B - 12C)\mu_1 & (2A + B \leq S < A + 4C) \\
 PD(51A + 15B + 12C - 6S)\mu_3 + 2PD(9B + 6S - 12C - 6A)\mu_2 + PD(12B + 12C - 6S + 6A)\mu_1 & (A + 4C \leq S < A + B + 2C) \\
 PD(48A + 12B + 6C - 3S)\mu_3 + 2PD(12B + 3S - 6C - 3A)\mu_2 + PD(9B + 6C - 3S + 3A)\mu_1 & (A + B + 2C \leq S < 3A + B) \\
 PD(39A + 9B + 6C)\mu_3 + 2PD(6A + 15B - 6C)\mu_2 + PD(6B - 6A + 6C)\mu_1 & (3A + B \leq S < 2A + 4C) \\
 PD(33A + 9B - 6C + 3S)\mu_3 + 2PD(6C + 15B + 12A - 3S)\mu_2 + PD(6B - 12A - 6C + 3S)\mu_1 & (2A + 4C \leq S < 2A + B + 2C) \\
 PD(45A + 15B + 6C - 3S)\mu_3 + 2PD(9B + 3S - 6C)\mu_2 + PD(12B + 6C - 3S)\mu_1 & (2A + B + 2C \leq S < 2A + 2B) \\
 PD(31A + 9B + 4S - 10C)\mu_3 + 2PD(15B + 14A - 4S + 10C)\mu_2 + PD(6B - 14A + 4S - 10C)\mu_1 & (2A + 2B \leq S < A + B + 4C) \\
 PD(36A + 6B - 6C + 3S)\mu_3 + 2PD(6C + 18B + 9A - 3S)\mu_2 + PD(3B - 9A - 6C + 3S)\mu_1 & (A + B + 4C \leq S < 3A + B + 2C) \\
 PD(15A - B - 20C + 10S)\mu_3 + 2PD(30A + 25B + 20C - 10S)\mu_2 + PD(10S - 30A - 20C - 4B)\mu_1 & (3A + B + 2C \leq S < 3A + 2B) \\
 PD(33A + 11B + 4S - 20C)\mu_3 + 2PD(20C + 12A + 13B - 4S)\mu_2 + PD(8B - 12A + 4S - 20C)\mu_1 & (3A + 2B \leq S < 2A + B + 4C) \\
 PD(45A + 17B + 4C - 2S)\mu_3 + 2PD(2S + 7B - 4C)\mu_2 + PD(14B + 4C - 2S)\mu_1 & (2A + B + 4C \leq S < 2A + 2B + 2C) \\
 PD(51A + 15B + 6C - 3S)\mu_3 + 2PD(9B + 3S - 6C - 6A)\mu_2 + PD(12B + 6C + 6A - 3S)\mu_1 & (2A + 2B + 2C \leq S < 4A + 2B) \\
 PD(23A + B + 6C + 4S)\mu_3 + 2PD(22A + 23B - 4S - 6C)\mu_2 + PD(6C + 4S - 2B - 22A)\mu_1 & (4A + 2B \leq S < 3A + B + 4C) \\
 PD(2A - 6B - 22C + 11S)\mu_3 + 2PD(22C + 30B + 43A - 11S)\mu_2 + PD(11S - 9B - 43A - 22C)\mu_1 & (3A + B + 4C \leq S < 3A + 2B + 2C) \\
 PD(20A + 6B - 10C + 5S)\mu_3 + 2PD(10C - 5S + 18B + 25A)\mu_2 + PD(3B - 25A - 10C + 5S)\mu_1 & (3A + 2B + 2C \leq S \leq 3A + 3B)
 \end{array} \right.
 \end{aligned}$$

..... (7.2)

7.1.1.3.2 Friction force when top fabric moves against bottom fabric of mirroring structure

As shown in Figure 7.8 (b), this friction movement contains two ripstop strip-flat strip friction movements and three flat strip-flat strip friction movements. The theoretical frictional force of this type of fabric-fabric friction when top fabric moves

against bottom fabric of mirroring structure during the displacement of $3(A + B)$ is shown in equation 7.3 below (see Appendix B).

$$\begin{aligned}
 & \left. \begin{aligned}
 & PD(35A + 7B - 3S + 22C)\mu_3 + 2PD(10A + 17B - 22C + 3S)\mu_2 + PD(4B + 22C - 10A - 3S)\mu_1 & (0 \leq S < 4C - B - A) \\
 & PD(40A + 18B + 5S - 10C)\mu_3 + 2PD(5A + 6B + 10C - 5S)\mu_2 + PD(15B - 5A - 10C + 5S)\mu_1 & (4C - B - A \leq S < A + 2C - B) \\
 & PD(38A + 20B + 7S - 14C)\mu_3 + 2PD(7A + 4B + 14C - 7S)\mu_2 + PD(17B - 7A - 14C + 7S)\mu_1 & (A + 2C - B \leq S < A) \\
 & PD(48A + 20B - 3S - 14C)\mu_3 + 2PD(4B - 3A + 14C + 3S)\mu_2 + PD(17B + 3A - 14C - 3S)\mu_1 & (A \leq S < 4C - B) \\
 & PD(48A + 10B - 13S + 26C)\mu_3 + 2PD(14B - 3A - 26C + 13S)\mu_2 + PD(7B + 3A + 26C - 13S)\mu_1 & (4C - B \leq S < 2C) \\
 & PD(45A + 13B - 5S + 10C)\mu_3 + 2PD(11B - 10C + 5S)\mu_2 + PD(10B + 10C - 5S)\mu_1 & (2C \leq S < 2A) \\
 & PD(41A + 13B - 3S + 10C)\mu_3 + 2PD(11B + 4A - 10C + 3S)\mu_2 + PD(10B + 10C - 4A - 3S)\mu_1 & (2A \leq S < A + 4C - B) \\
 & PD(39A + 15B - S + 2C)\mu_3 + 2PD(9B + 6A - 2C + S)\mu_2 + PD(12B + 2C - 6A - S)\mu_1 & (A + 4C - B \leq S < A + 2C) \\
 & PD(49A + 15B - 11S + 22C)\mu_3 + 2PD(9B - 4A - 22C + 11S)\mu_2 + PD(12B + 22C + 4A - 11S)\mu_1 & (A + 2C \leq S < A + B) \\
 & PD(41A + 7B + 4C)\mu_3 + 2PD(17B + 4A - 4C)\mu_2 + PD(4B + 4C - 4A)\mu_1 & (A + B \leq S < 4C) \\
 & PD(41A - 4C + 7B + 2S)\mu_3 + 2PD(4A + 17B + 4C - 2S)\mu_2 + PD(4B + 2S - 4C - 4A)\mu_1 & (4C \leq S < 2A + 2C) \\
 & PD(37A - 8C + 7B + 4S)\mu_3 + 2PD(8A + 17B + 8C - 4S)\mu_2 + PD(4B + 4S - 8C - 8A)\mu_1 & (2A + 2C \leq S < 2A + B) \\
 & PD(45A - 8C + 11B)\mu_3 + 2PD(13B + 8C)\mu_2 + PD(8B - 8C)\mu_1 & (2A + B \leq S < A + 4C) \\
 & PD(49A + 8C + 11B - 4S)\mu_3 + 2PD(13B + 4S - 8C - 4A)\mu_2 + PD(8B + 8C - 4S + 4A)\mu_1 & (A + 4C \leq S < A + B + 2C) \\
 & PD(47A + 4C + 9B - 2S)\mu_3 + 2PD(15B + 2S - 4C - 2A)\mu_2 + PD(6B + 2A + 4C - 2S)\mu_1 & (A + B + 2C \leq S < 3A + B) \\
 & PD(41A + 4C + 7B)\mu_3 + 2PD(17B + 4A - 4C)\mu_2 + PD(4B + 4C - 4A)\mu_1 & (3A + B \leq S < 2A + 4C) \\
 & PD(37A - 4C + 7B + 2S)\mu_3 + 2PD(17B + 8A + 4C - 2S)\mu_2 + PD(4B + 2S - 4C - 8A)\mu_1 & (2A + 4C \leq S < 2A + B + 2C) \\
 & PD(45A + 4C + 11B - 2S)\mu_3 + 2PD(13B - 4C + 2S)\mu_2 + PD(8B - 2S + 4C)\mu_1 & (2A + B + 2C \leq S < 2A + 2B) \\
 & PD(35A + 7B + 3S - 8C)\mu_3 + 2PD(17B + 10A + 8C - 3S)\mu_2 + PD(4B - 8C - 10A + 3S)\mu_1 & (2A + 2B \leq S < A + B + 4C) \\
 & PD(39A - 4C + 5B + 2S)\mu_3 + 2PD(6A + 19B + 4C - 2S)\mu_2 + PD(2B + 2S - 4C - 6A)\mu_1 & (A + B + 4C \leq S < 3A + B + 2C) \\
 & PD(24A + 7S - 14C)\mu_3 + 2PD(24B + 21A + 14C - 7S)\mu_2 + PD(7S - 3B - 14C - 21A)\mu_1 & (3A + B + 2C \leq S < 3A + 2B) \\
 & PD(36A + 8B + 3S - 14C)\mu_3 + 2PD(16B + 9A + 14C - 3S)\mu_2 + PD(3S + 5B - 14C - 9A)\mu_1 & (3A + 2B \leq S < 2A + B + 4C) \\
 & PD(44A + 12B - S + 2C)\mu_3 + 2PD(12B + A - 2C + S)\mu_2 + PD(9B + 2C - A - S)\mu_1 & (2A + B + 4C \leq S < 2A + 2B + 2C) \\
 & PD(49A + 4C + 11B - 2S)\mu_3 + 2PD(13B + 2S - 4C - 4A)\mu_2 + PD(8B + 4C - 2S + 4A)\mu_1 & (2A + 2B + 2C \leq S < 4A + 2B) \\
 & PD(29A + B + 3S + 4C)\mu_3 + 2PD(23B + 16A - 4C - 3S)\mu_2 + PD(4C - 16A + 3S - 2B)\mu_1 & (4A + 2B \leq S < 3A + B + 4C) \\
 & PD(14A - 4B + 8S - 16C)\mu_3 + 2PD(28B + 31A + 16C - 8S)\mu_2 + PD(8S - 16C - 31A - 7B)\mu_1 & (3A + B + 4C \leq S < 3A + 2B + 2C) \\
 & PD(26A + 4B + 4S - 8C)\mu_3 + 2PD(20B + 19A + 8C - 4S)\mu_2 + PD(B + 4S - 8C - 19A)\mu_1 & (3A + 2B + 2C \leq S \leq 3A + 3B)
 \end{aligned} \right\} \dots\dots\dots (7.3)
 \end{aligned}$$

7.1.2 Theoretical spectrum profile of friction coefficient

The surface structural parameters A, B, C and D of the ripstop fabric shown in Figure 7.6 are measured by using image analysis method in Photoshop. Ten measurements are made for each length; their average lengths and standard deviations are shown in Table 7.1.

Table 7.1 Fabric structural lengths, A, B, C and D of the ripstop fabric shown in Figure 7.6

woven structural parameters	Average length (mm)	Standard deviation (mm)
A	0.25	0.01
B	0.47	0.01
C	0.23	0.01
D	0.14	0.01

μ_1 , μ_2 and μ_3 are unknown but they have relationship below (see section 7.1.1.2),

$$\mu_1 > \mu_3 > \mu_2$$

In order to obtain a spectrum profile, rather than a real amplitude of the friction coefficient of the ripstop fabric, the arbitrary values of μ_1 , μ_2 and μ_3 are assumed in Table 7.2.

Table 7.2 Arbitrary values of μ_1 , μ_2 and μ_3 for the ripstop fabric

	μ_1	μ_2	μ_3
Arbitrary values	0.5	0.3	0.4

The normal force applied on the unit structure of the fabric is thus $P \times (3A + 3B) \times 15D$, the theoretical friction coefficient of the fabric is obtained in the equation below,

$$\text{Friction coefficient} = \frac{\text{Friction force}}{\text{Normal force}} \dots\dots\dots (7.4)$$

7.1.2.1 Theoretical friction coefficient profiles when top fabric moves against bottom fabric of identical structure

When top fabric frictions against bottom fabric of identical structure, the ripstop strip moves against the ripstop strip together with flat area moves against flat area. In this case, the theoretical friction coefficient profiles of a piece of the ripstop fabric when have a displacement of 6.5mm (three units length) are obtained based on the equation 7.2 in section 7.1.1.3.1 and the parameters given in Table 7.1 and Table 7.2. The theoretical friction profile is shown in Figure 7.9.

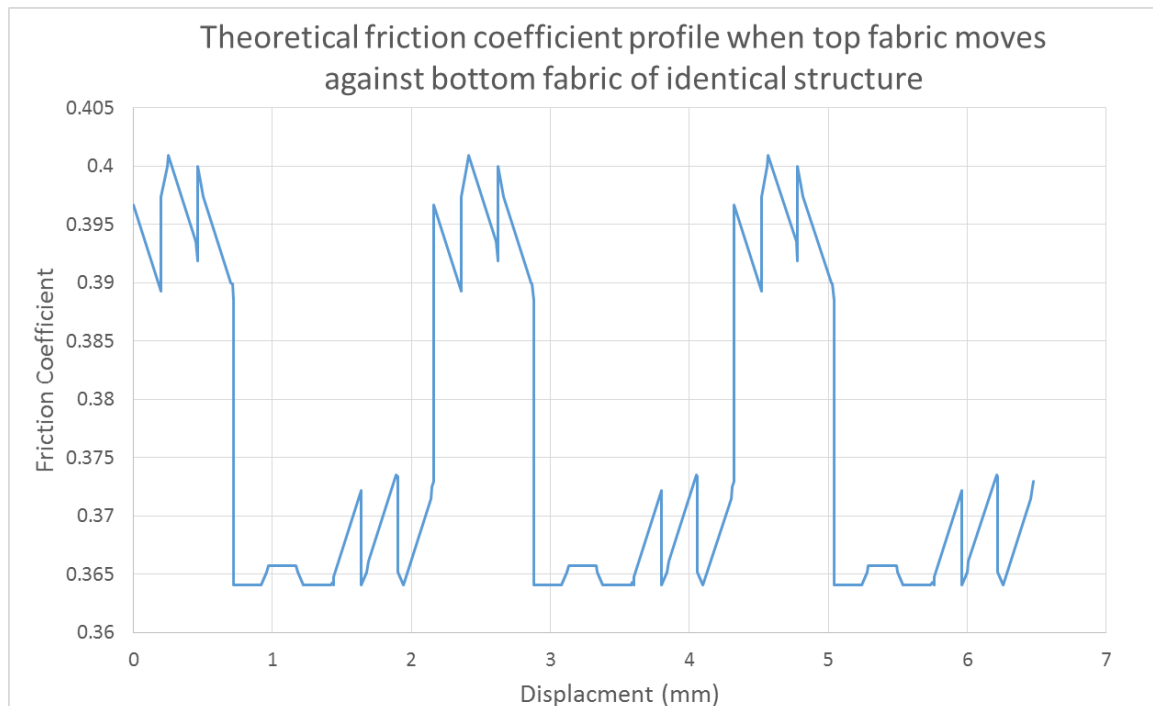


Figure 7.9 Theoretical friction coefficient profile when top fabric moves against identical fabric structures of bottom fabric

The FFT spectral analysis of theoretical friction coefficient profiles shown in Figure 7.9 is conducted by using OriginPro and presented in Figure 7.10. Due to the smallest structure length in weft direction is around 0.23mm (see Table 7.1), wavelengths less than 0.2mm obtained in FFT analysis are considered less related to the ripstop structure in weft direction, and only wavelengths greater than 0.2mm are shown in Figure 7.10.

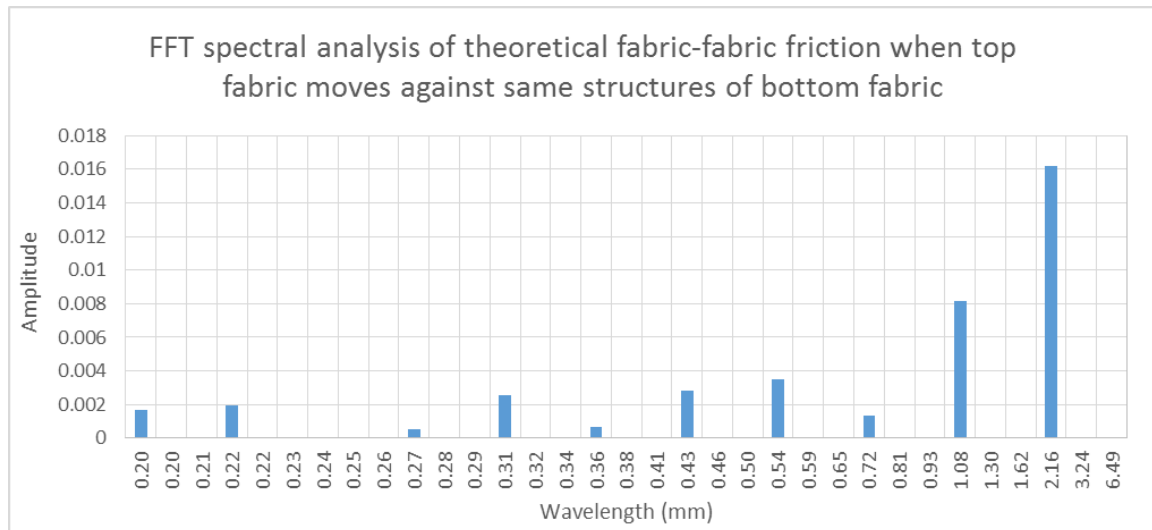


Figure 7.10 Spectrum of the theoretical fabric-fabric friction profile when top fabric moves against the same structures of bottom fabric

It is noticed that the greatest amplitude appears at the wavelength of 2.16mm, and this wavelength is the same as length of unit structure of ripstop fabric ($3A+3B$), so it is also the distance of two ripstop strips on the fabric surface in weft direction. There are other six peaks shown at wavelengths of 1.08mm, 0.54mm, 0.43mm, 0.31mm and 0.20mm, which are $1/2$, $1/4$, $1/5$, $1/7$, $1/10$ and $1/11$ of 2.16mm. Therefore the theoretical fabric friction profile obtained in the fabric-fabric friction process is related to the characteristic length between two ribs of this ripstop fabric, and its sub-lengths (half, quarter, $1/5$, $1/7$, $1/10$ and $1/11$).

7.1.2.2 Theoretical friction coefficient profiles when top fabric moves against bottom fabric of mirroring structure

Symbol values are substituted into equation 7.3 listed in 7.1.1.3.2. The friction coefficient profile is obtained and shown in Figure 7.11.

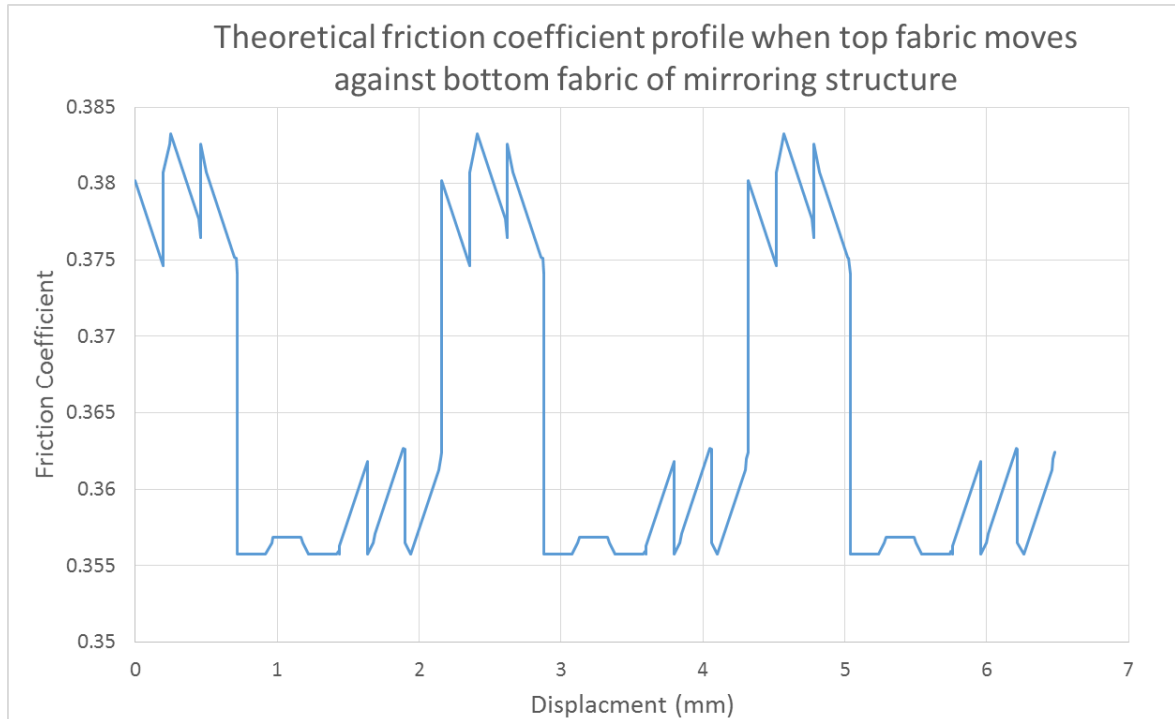


Figure 7.11 Theoretical friction coefficient profile when top fabric moves against bottom fabric of mirroring structure.

Compared with the curves shown in Figure 7.9, the amplitude of the curves in Figure 7.11 are relatively smaller. It is thus concluded that the amplitude of friction coefficient profile is much more significant when fabric moves against bottom fabrics of identical structures.

The spectrum of FTT analysis of the theoretical friction coefficient within the displacement of 6.5mm which is three units weave length is shown in Figure 7.12 below. Similarly, only wavelengths greater than 0.2mm are shown in Figure 7.12, because the minimum structure length in weft direction is 0.23mm, wavelengths smaller than 0.2mm are considered less related to ripstop surface structure.

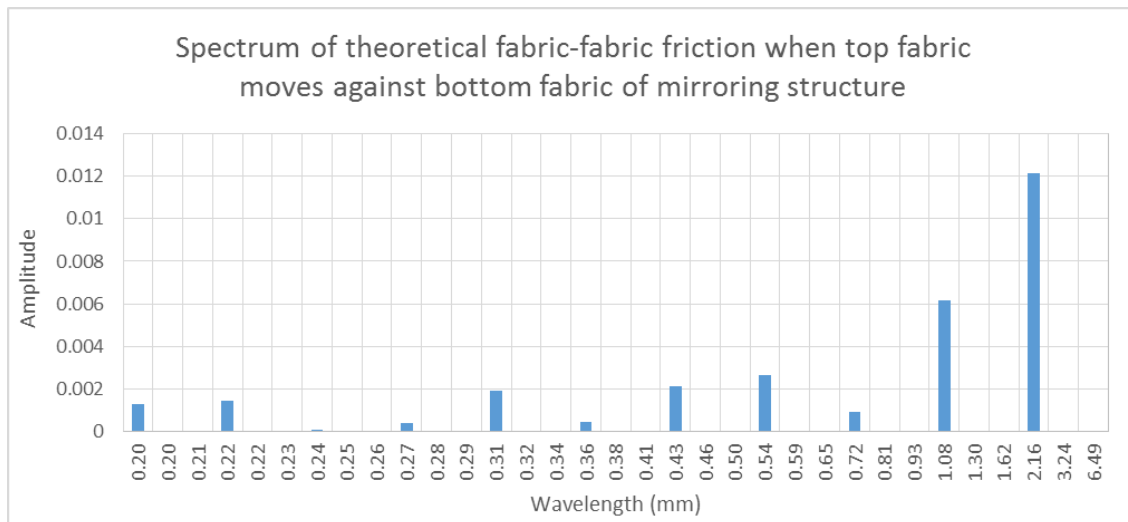


Figure 7.12 Spectrum of theoretical fabric-fabric friction coefficient when top fabric moves against bottom fabric of mirroring structure

It is shown that the wavelengths of peaks in Figure 7.12 are identical as those shown in Figure 7.10. The highest peak is shown at the wavelength of 2.16mm, which is in agreement with the characteristic length between two ripstop ribs of this ripstop fabric. Other peaks having high amplitudes are shown at wavelengths of 1.08mm, 0.54mm, 0.43mm, 0.31mm, 0.22mm and 0.20mm, and they correspond to half, quarter, 1/5, 1/7, 1/10 and 1/11 of the length between ripstop ribs (2.16mm). Therefore these wavelengths of peaks are all related to the length between two ripstop ribs of this ripstop fabric or its sub-lengths.

In summary of section 7.1.2, in the spectra of theoretical fabric-fabric friction profile, peaks having high amplitudes are all related to the length between two ripstop ribs, 2.16mm. It suggests that the ripstop ribs have the most significant effect on the fabric-fabric friction in the theoretical analysis.

7.1.3 Fabric friction profile of the ripstop fabric in the LUFHES test

The fabric-fabric friction profile of the ripstop fabric in weft direction shown in Figure 7.1 is obtained in the LUFHES system and the spectra of the friction coefficient profiles are obtained through FFT analysis.

Friction tests are conducted three times for each fabric in the same direction and each of them is analysed by using FFT analysis. The wavelength-amplitude profile of the three LUFHES friction tests are shown in Figure 7.13. Because the distance between two ripstop ribs is 2.16mm in weft direction and it is the greatest wavelength shown in our theoretical spectrum analysis, the spectrum for the wavelengths less than 5.5mm, which is almost double the length of largest structure, is shown in this analysis.

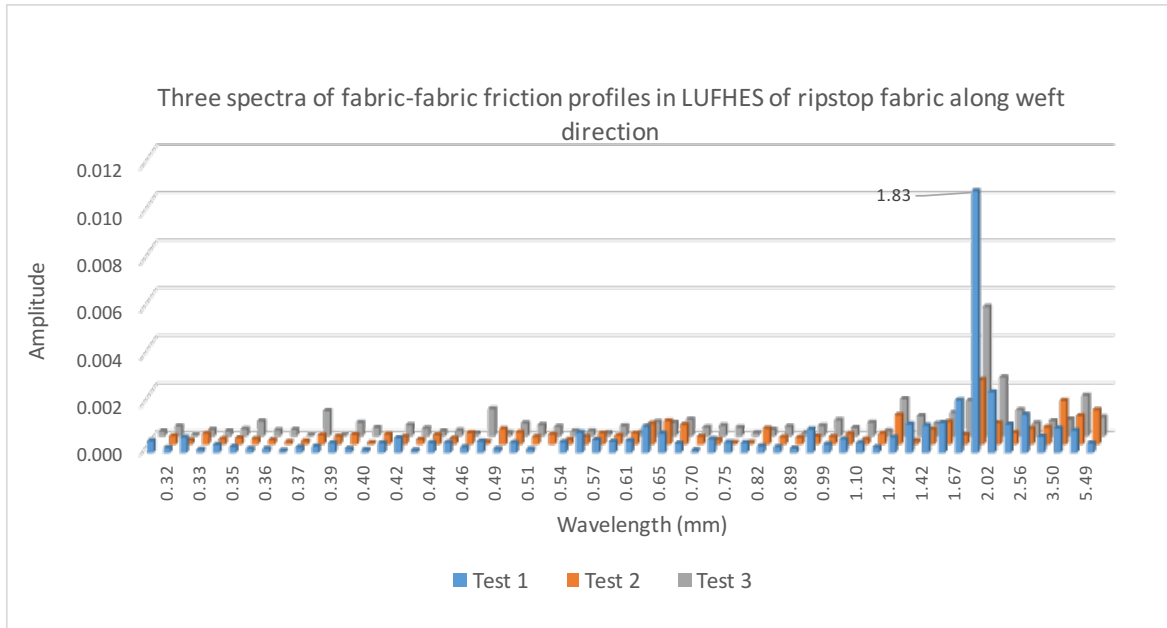


Figure 7.13 Three spectra of the fabric-fabric friction profiles in LUFHES repeat tests

The three tests are found to have good reproducibility. The peaks around 1.83mm appear in all of the profiles of the three tests. In order to eliminate random errors produced in one test, the average amplitudes of groups in the three tests are shown in Figure 7.14 for our analysis.

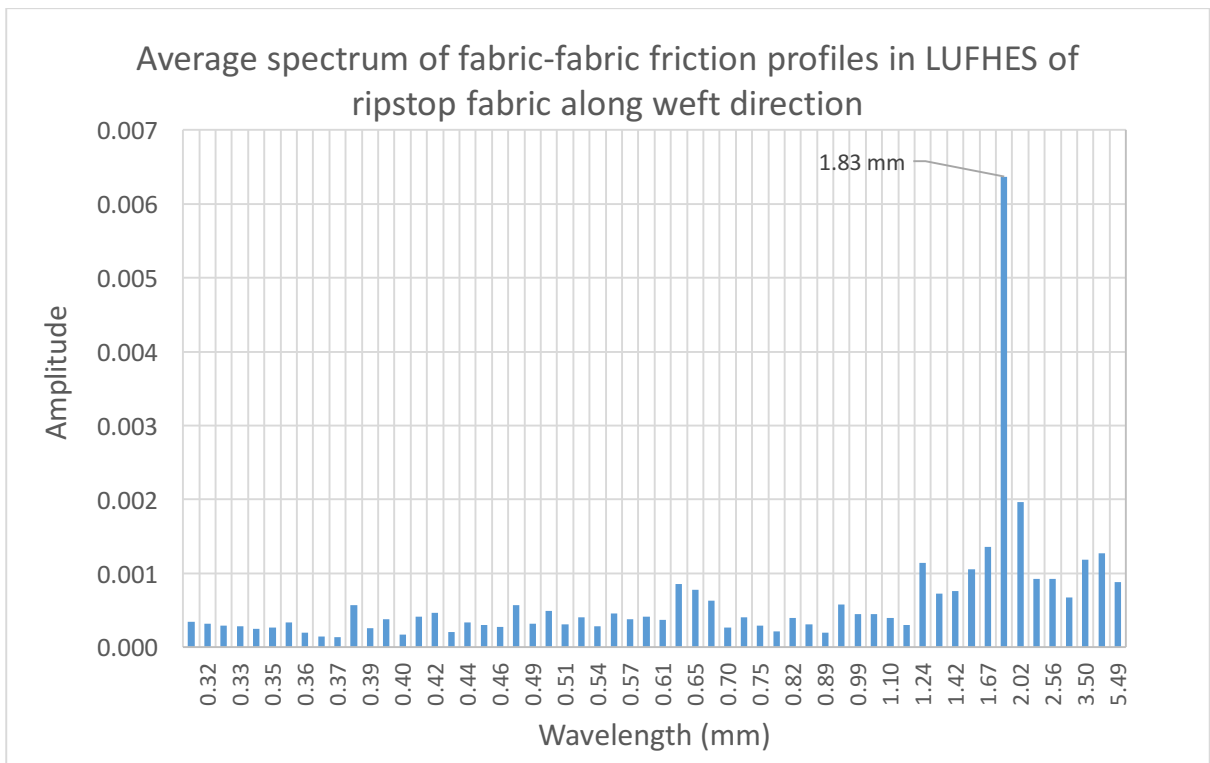


Figure 7.14 Spectrum of fabric-fabric friction profile of the ripstop fabric in the LUFHES system.

There is only one apparent peak which has the greatest amplitude shown at the wavelength of 1.83mm in Figure 7.14. 1.83mm is close to the wavelength of 2.16mm, which is the length between two ripstop ribs. Therefore, it is concluded that the LUFHES fabric-fabric friction test of this ripstop fabric is highly affected by the ripstop ribs on the fabric surface.

In comparison of the friction spectrum obtained in the LUFHES test with the spectrum obtained in theoretical friction analysis, it is found that the friction profiles obtained in the LUFHES friction tests do not detect short wavelengths less than 0.3mm, which might be the resolution limit of the LUFHES measurement system.

In summary, the wavelength of the highest peak in the spectrum of friction profile of the ripstop fabric obtained in the LUFHES friction test corresponds to the distance between two adjacent ripstop ribs of the ripstop fabric in its weft direction. This is in agreement with the conclusions from the spectrum obtained in theoretical analysis of the fabric-fabric friction profiles.

7.2 Analysis of fabric roughness profile in the KES-F system

In contrary to the fabric-fabric friction properties measured in the LUFHES system, metal sensors contacting the fabric surface are used in the KES-F system to detect the surface roughness profile and friction coefficient of a fabric (with 20N/m tension) during their movements on the fabric surface. The spectra are obtained through FFT analysis of the roughness and friction coefficient profiles. In this section, theoretical model of the metal sensor-fabric friction profile of the ripstop fabric shown in Figure 7.2 is established and its spectrum analysis is conducted and compared with the characteristic wavelengths obtained in the spectra of the KES-F roughness and friction profiles.

7.2.1 Theoretical analysis of metal sensor-fabric friction in the KES-F system

In the KES-F roughness test, the vertical movement of a sensor is detected. According to the adhesion-shearing theory, the friction coefficient between a sensor and its contact area is proportional to the vertical height of the contact area. Therefore, the relative height of the weft and warp yarn cross points on a fabric surface is represented by the relative friction coefficient of the warp and weft cross points.

7.2.1.1 Model of fabric friction when metal sensor moves against ripstop strip

Models of the ripstop fabric are described in the section 7.1.1, and the surface of ripstop fabric, the assumptions and analysis in the section 7.1.1.1 and 7.1.1.2 also stand for the KES-F metal sensor-fabric friction. In addition, the length of the KES-F metal sensor in the direction of friction movement and the contact length of the metal sensor and the weft yarn cross point in the fabric surface are denoted as U and U_x , respectively. U_x changes with the relative locations of the sensor on the fabric surface during the movement of fabric surface (see Figure 7.15).

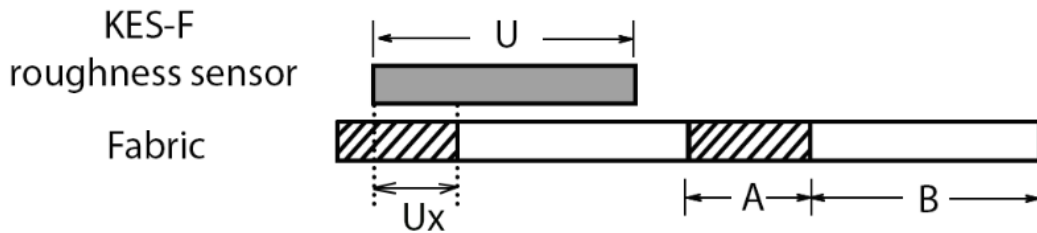


Figure 7.15 Model of the KES-F roughness sensor moves against ripstop fabric

μ_4 and μ_5 are the friction coefficients between metal sensor and fabric when the sensor moves against warp yarn cross point and weft yarn cross point, respectively. In the wear test between cast iron and aluminium composites mixed with carbon fibres with different orientations (Caliman, 2016), it was found that the wear speed measured of the composite with parallel orientation is smaller than that of the composite with perpendicular orientation. It was indicated that the friction coefficient between metal and fibre aligned parallel to movement direction (μ_5) is smaller than that between metal and fibre aligned perpendicularly (μ_4). Thus, in this analysis, when metal sensor moves in weft direction, we assume:

$$\mu_4 > \mu_5 \dots\dots\dots (7.5)$$

Fabric structural lengths, A , B and C , still have the same relationship shown in the equation 7.1. They also have the relationship with the length of sensor (U) as shown in the equation 7.6.

$$2A \leq U \leq 2A + B - 2C \dots\dots\dots (7.6)$$

7.2.1.2 Friction force produced by the KES-F roughness sensor and fabric surface

The friction force produced between the sensor and a unit structure of ripstop fabric in weft direction includes the sensor moves against one part of ripstop strip and four parts of flat strip. The five parts are added up to obtain the profile of the friction force between the KES-F roughness sensor and the fabric surface of the ripstop fabric. The details of the derivation of the equations are given in Appendix

C, and the equations for the profile of the friction force between the KES-F sensor and the fabric surface of the ripstop fabric are shown in equation 7.7 below, where the normal force on the studied area is $P \times E \times 15D$ when a constant pressure P is applied onto the fabric via the mental sensor.

$$F = \left\{ \begin{array}{ll}
 PD(13U + 2A - 2C)\mu_5 + PD(2C + 2U - 2A)\mu_4 & (0 \leq S < A + 2C - U) \\
 PD(12U + 3A - S)\mu_5 + PD(S + 3U - 3A)\mu_4 & (A + 2C - U \leq S < A + B - U) \\
 PD(13U + 2A - B)\mu_5 + PD(B + 2U - 2A)\mu_4 & (A + B - U \leq S < C) \\
 PD(13U + 2A + C - B - S)\mu_5 + PD(B + 2U - 2A + S - C)\mu_4 & (C \leq S < A) \\
 PD(13U + A + C - B)\mu_5 + PD(B + 2U - A - C)\mu_4 & (A \leq S < A + B + C - U) \\
 PD(14U + S - 2B)\mu_5 + PD(2B + U - S)\mu_4 & (A + B + C - U \leq S < 2C) \\
 PD(14U + 2C - 2B)\mu_5 + PD(2B + U - 2C)\mu_4 & (2C \leq S < 2A + B - U) \\
 PD(2A + 13U + 2C - B - S)\mu_5 + PD(B + 2U + S - 2C - 2A)\mu_4 & (2A + B - U \leq S < A + C) \\
 PD(A + 13U + C - B)\mu_5 + PD(B + 2U - C - A)\mu_4 & (A + C \leq S < A + B + 2C - U) \\
 PD(14U + S - C - 2B)\mu_5 + PD(2B + U - S + C)\mu_4 & (A + B + 2C - U \leq S < 2A + B + C - U) \\
 PD(13U + 2A - B)\mu_5 + PD(B + 2U - 2A)\mu_4 & (2A + B + C - U \leq S < A + 2C) \\
 PD(13U + A - B + S - 2C)\mu_5 + PD(B + 2U + 2C - A - S)\mu_4 & (A + 2C \leq S < A + B) \\
 PD(9U + 10A + 4B - 4S + 2C)\mu_5 + PD(6U - 2C - 10A + 4S - 4B)\mu_4 & (A + B \leq S < 2A + B + 2C - U) \\
 PD(4U + 20A + 9B - 9S + 12C)\mu_5 + PD(11U - 12C - 20A + 9S - 9B)\mu_4 & (2A + B + 2C - U \leq S < 2A + 2B - U) \\
 PD(5U + 18A + 7B - 8S + 12C)\mu_5 + PD(10U - 12C - 18A + 8S - 7B)\mu_4 & (2A + 2B - U \leq S < A + B + C) \\
 PD(9U + 11A + 4B - 5S + 9C)\mu_5 + PD(6U - 9C - 11A + 5S - 4B)\mu_4 & (A + B + C \leq S < 2A + B) \\
 PD(9U + 9A + 3B - 4S + 9C)\mu_5 + PD(6U - 9C - 9A + 4S - 3B)\mu_4 & (2A + B \leq S < 2A + 2B + C - U) \\
 PD(10U + 7A + B - 3S + 8C)\mu_5 + PD(5U - 8C - 7A + 3S - B)\mu_4 & (2A + 2B + C - U \leq S < A + B + 2C) \\
 PD(14U - 2B + 2C)\mu_5 + PD(U + 2B - 2C)\mu_4 & (A + B + 2C \leq S < 3A + 2B - U) \\
 PD(15A + 8B + 9U - 5S + 2C)\mu_5 + PD(6U + 5S - 8B - 15A - 2C)\mu_4 & (3A + 2B - U \leq S < 2A + B + C) \\
 PD(13A + 7B + 9U - 4S + C)\mu_5 + PD(6U + 4S - 7B - 13A - C)\mu_4 & (2A + B + C \leq S < 2A + 2B + C - U) \\
 PD(11A + 5B + 10U - 3S - C)\mu_5 + PD(5U + 3S - 5B - 11A + C)\mu_4 & (2A + 2B + 2C - U \leq S < 3A + 2B + C - U) \\
 PD(26A + 15B + 5U - 8S + 4C)\mu_5 + PD(10U + 8S - 15B - 26A - 4C)\mu_4 & (3A + 2B + C - U \leq S < 2A + B + 2C) \\
 PD(24A + 14B + 5U - 7S + 2C)\mu_5 + PD(10U + 7S - 14B - 24A - 2C)\mu_4 & (2A + B + 2C \leq S < 2A + 2B) \\
 PD(4S + 9U - 14C - 2A - 8B)\mu_5 + PD(6U + 14C + 2A + 8B - 4S)\mu_4 & (2A + 2B \leq S < 3A + 2B + 2C - U) \\
 PD(3S + 8U - 12C + A - 6B)\mu_5 + PD(7U + 12C - A + 6B - 3S)\mu_4 & (3A + 2B + 2C - U \leq S < 3A + 3B - U) \\
 PD(8S + 13U - 12C - 14A - 21B)\mu_5 + PD(2U + 12C + 14A + 21B - 8S)\mu_4 & (3A + 3B - U \leq S < 2A + 2B + C) \\
 PD(9U - 3C + 8A - 3B - S)\mu_5 + PD(6U + 3C + S + 3B - 8A)\mu_4 & (2A + 2B + C \leq S < 3A + 2B) \\
 PD(4S - 7A - 3C + 9U - 13B)\mu_5 + PD(6U + 3C - 4S + 13B + 7A)\mu_4 & (3A + 2B \leq S < 3A + 3B + C - U) \\
 PD(9S - 22A - 8C + 14U - 28B)\mu_5 + PD(U + 8C - 9S + 28B + 22A)\mu_4 & (3A + 3B + C - U \leq S < 2A + 2B + 2C) \\
 PD(10U - 10B + 10C)\mu_5 + PD(5U + 10B - 10C)\mu_4 & (2A + 2B + 2C \leq S < 4A + 3B - U) \\
 PD(9U - 7B + 10C + 4A - S)\mu_5 + PD(6U + 7B - 10C + S - 4A)\mu_4 & (4A + 3B - U \leq S < 3A + 2B + C) \\
 PD(9U - 17B - 11A + 5C + 4S)\mu_5 + PD(6U + 17B - 4S - 5C + 11A)\mu_4 & (3A + 2B + C \leq S < 3A + 3B + 2C - U) \\
 PD(14U - 32B - 26A - 5C + 9S)\mu_5 + PD(U + 32B - 9S + 5C + 26A)\mu_4 & (3A + 3B + 2C - U \leq S < 4A + 3B + C - U) \\
 PD(13U - 29B - 22A - 4C + 8S)\mu_5 + PD(2U + 29B - 8S + 4C + 22A)\mu_4 & (4A + 3B + C - U \leq S < 3A + 2B + 2C) \\
 PD(13U - 39B - 37A - 14C + 13S)\mu_5 + PD(2U + 39B - 13S + 14C + 37A)\mu_4 & (3A + 2B + 2C \leq S \leq 3A + 3B)
 \end{array} \right. \dots\dots\dots (7.7)$$

7.2.1.3 Friction coefficient profiles and spectrum of the ripstop fabric

The sensor used in the KES-F roughness test is shown in Figure 2.4. A load of 10g is applied onto the sensor to make sure that the sensor has a good contact with the fabric surface. The length of U for the KES-F roughness sensor is 0.5mm in the moving direction, and the structural lengths of A, B, C and D for the ripstop fabric are shown in Table 7.1. μ_4 and μ_5 are assumed to be 0.5 and 0.3, respectively.

Theoretical friction coefficient profile of three units length is shown in Figure 7.16 below, which is obtained by substituting the above values into the equations 7.7 listed in section 7.2.1.2.

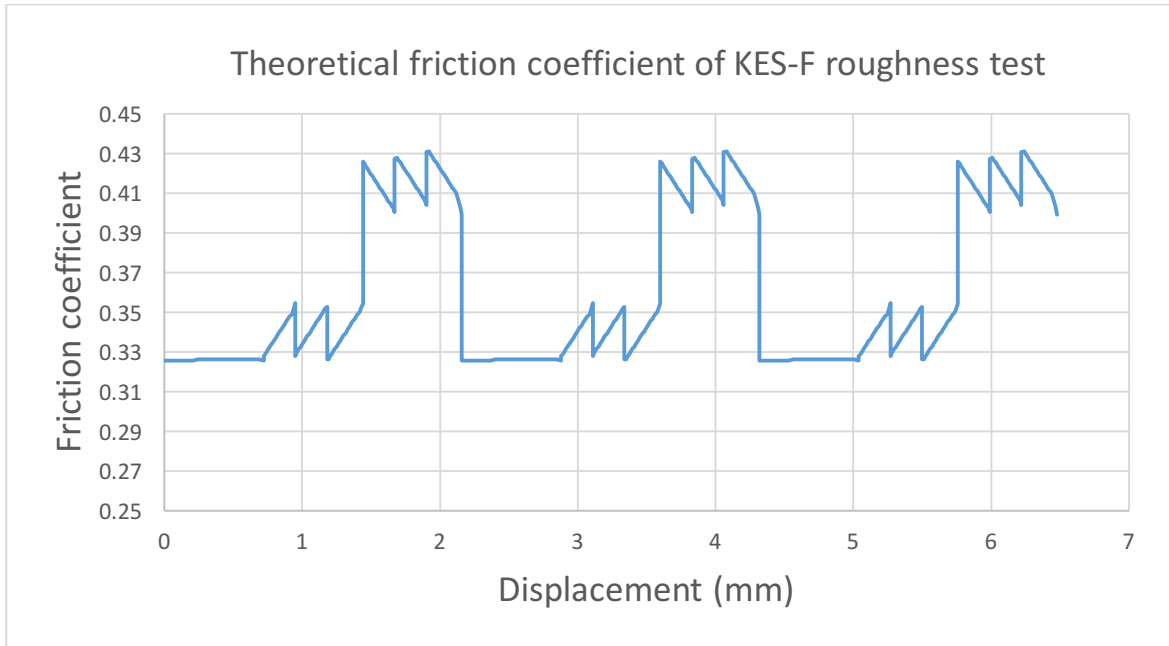


Figure 7.16 Theoretical friction coefficient profile of the ripstop fabric during the KES-F roughness test using a metal sensor

As a comparison, the amplitude of the metal sensor-fabric friction coefficient profile in the first half of each loop in Figure 7.16 varies little (from 0.3256 to 0.3264), while the amplitude of the friction coefficient varies even less in the fabric-fabric friction coefficient profiles in Figure 7.9 (e.g. from 0.3129 to 0.3135) and Figure 7.11. This might be related to the arbitrary friction coefficients used in these two theoretical analysis.

The FFT spectrum of the theoretical metal sensor-fabric friction profile of three units having a length of 6.5mm is shown in Figure 7.17.

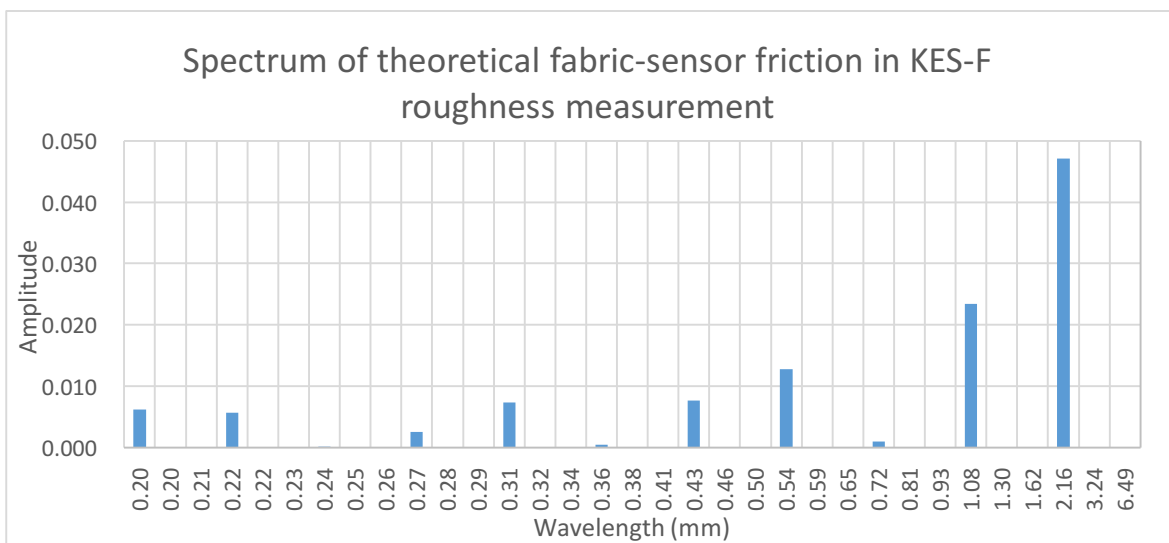


Figure 7.17 Theoretical spectrum of the metal sensor-fabric friction profile of the ripstop fabric during the KES-F roughness test

The characteristic wavelengths of the major peaks having relatively greater amplitudes in Figure 7.17 are 0.20, 0.22, 0.31, 0.54, 0.1.08, and 2.16 mm. All of them are same as those obtained in the spectrum of fabric-fabric theoretical friction profiles shown in Figure 7.10 and Figure 7.12.

The greatest peak appears at the wavelength of 2.16mm, which is the same as the distance between two ripstop ribs in weft direction; while the wavelengths of other peaks, 0.20mm, 0.22mm, 0.31mm, 0.43mm, 0.54mm, and 1.08mm are $1/11$, $1/10$, $1/7$, $1/5$, $1/4$, and $1/2$ of 2.16mm, respectively.

However, it is noticed that the amplitude differences between peak at 2.16mm and other peaks in Figure 7.17 are greater than those in theoretical fabric-fabric profile (see Figure 7.12 and Figure 7.14). One of the possible reasons is that the arbitrary friction coefficients of both warp cross points and weft cross points might not show the actual friction coefficient of the real ripstop fabric, this might lead to the amplitudes of the peaks at smaller wavelengths are smaller, and thus lead to the greater gap between these amplitudes and the amplitude at the wavelength of 2.16mm.

7.2.2 Spectrum of the sensor-fabric roughness profile in the KES-F test

According to the manual of the KES-F system, the KES-F roughness test contains two rounds, and the total fabric movement for each round is 30mm. Fabric is accelerated in the start 5mm and slowed down at the end 5mm. Its movement in 20mm in the middle is in a constant speed of 1mm/s, so the data of this 20mm is used for the FFT spectral analysis in this study. An example of the original vertical displacement of the sensor obtained in the KES-F roughness test of the ripstop fabric (see Figure 7.2) is shown in Figure 7.18.

The spectra of the two rounds of the KES-F roughness tests are show in Figure 7.19, the average amplitudes of the two spectra are shown in Figure 7.20. As the distance between two adjacent ripstop ribs is around 2.16mm, the wavelengths less than 4.4mm are shown in the spectrum and discussed.

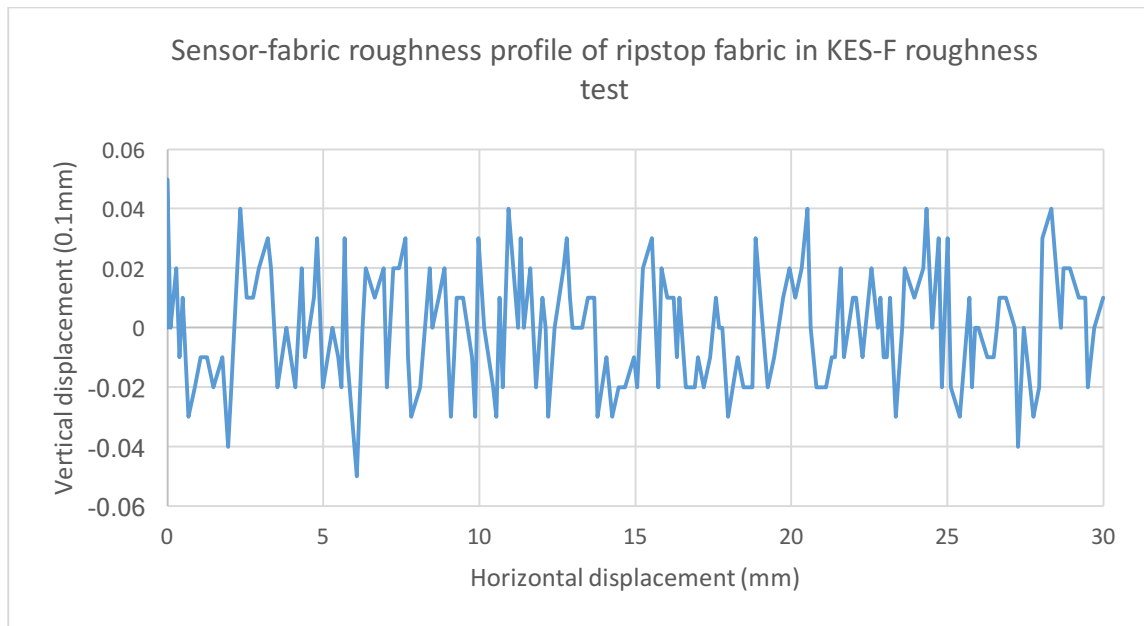


Figure 7.18 Vertical displacement profile of the sensor obtained in the KES-F roughness test of the ripstop fabric shown in Figure 7.2

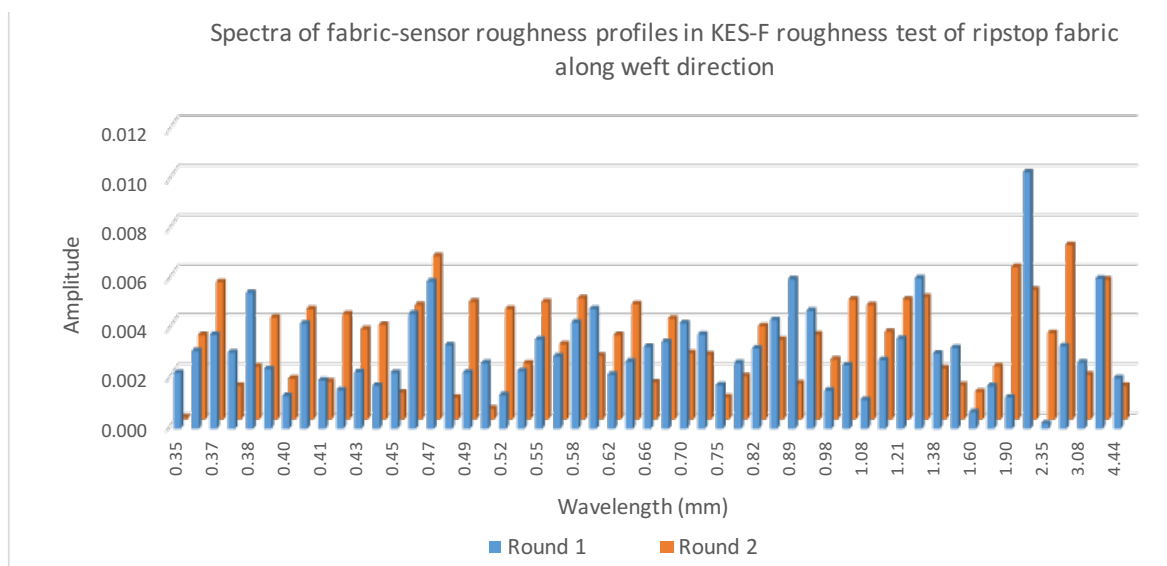


Figure 7.19 Spectra of roughness profiles of the ripstop fabric in the KES-F roughness test

It is shown in Figure 7.19 that the spectra of the KES-F roughness profiles do not have good reproducibility. The greatest amplitude peak in round 1 is at the wavelength of 2.11mm which corresponds to the distance between two ripstop ribs (2.16mm). But the greatest amplitude peak in round 2 is at the wavelength of 2.63 which is almost four times the length of 1/2 weave structure (0.72mm). This suggests that the reproducibility of the KES-F roughness test of the ripstop fabric in weft direction is a problem.

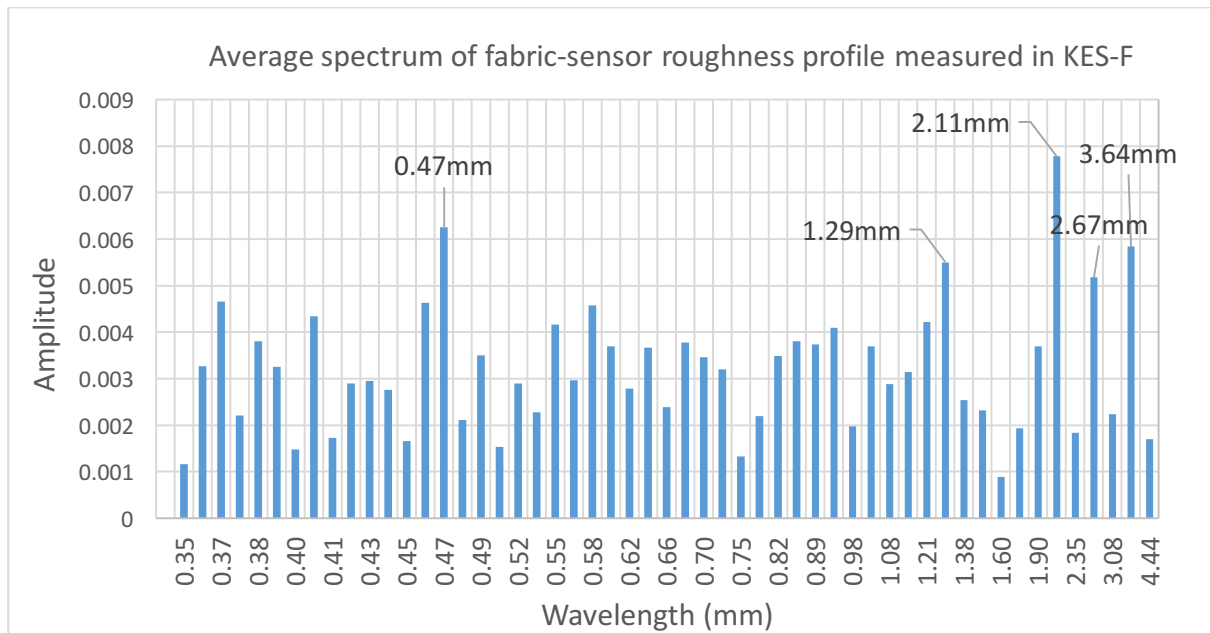


Figure 7.20 Average of the two spectra of the KES-F roughness tests shown in Figure 7.19

In Figure 7.20, the peaks having high amplitudes are shown at the wavelength around 0.47mm, 1.29mm, 0.55mm, 2.11mm, 2.66mm and 3.64mm. In comparison of the spectrum of roughness profile obtained in the KES-F roughness test with the spectrum of theoretical fabric friction profile for the KES-F test, it is found that the peak at wavelength of around 1/5 length between two ripstop ribs, appears in the spectrum of both theoretical (0.43mm) and experimental (0.47mm) profiles; so does the peak which is related to 1/2 length between two ripstop ribs at the wavelength of 1.08mm in theoretical analysis and 1.29mm in experimental test. In addition, peak at the wavelength of 2.11mm, which corresponds to the distance between two adjacent ripstop ribs appears in both the theoretical and experimental spectra. Therefore the peaks obtained in the spectrum of the experimental KES-F roughness profile correspond to those obtained in the spectrum of the theoretical metal sensor-fabric friction profile. The characteristic wavelengths of the spectrum are related to the fabric weave structural lengths, for example, the distance between two adjacent ripstop ribs (2.16mm) and its sub-lengths (e.g. 1/5 and 1/2).

7.2.3 Spectrum of the sensor-fabric friction profile in the KES-F test

During the KES-F friction test, the dynamic friction coefficient between a metal sensor assembly and a fabric is obtained when the sensor assembly moves against the fabric surface. The width of the sensor is about 5mm. An example of the friction profile of the ripstop fabric obtained in the KES-F friction test is shown in Figure 7.21.

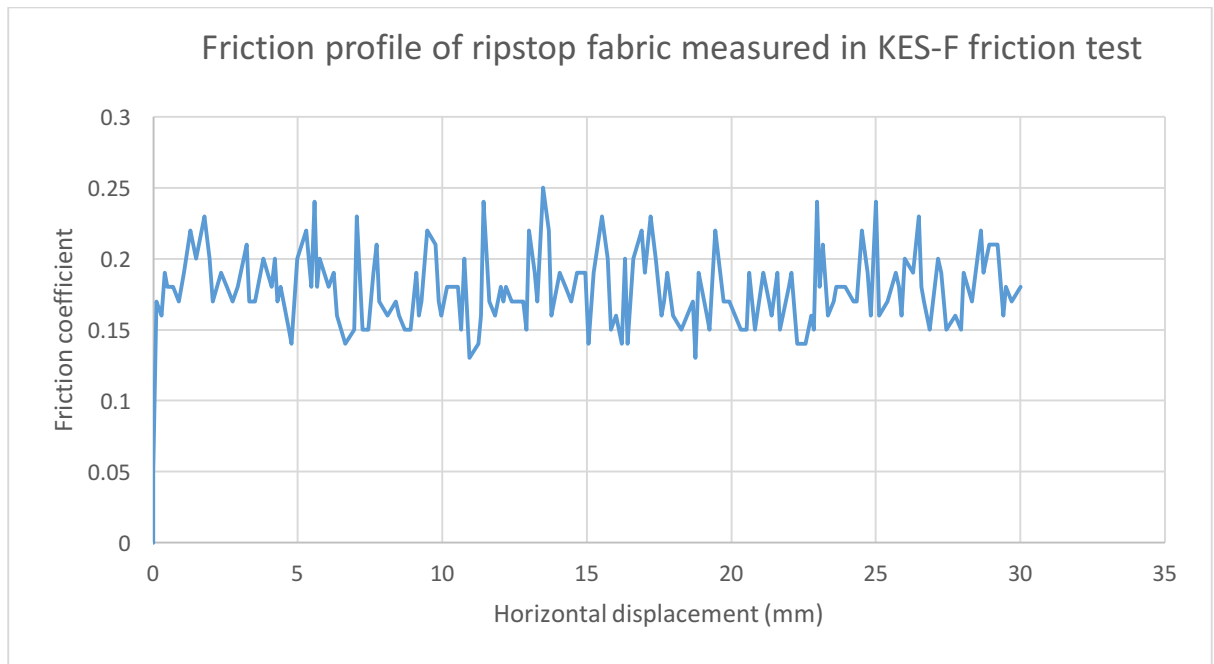


Figure 7.21 Friction profile of ripstop fabric in weft direction measured in the KES-F friction test

It is shown that the friction coefficient obtained in the KES-F friction test and the LUFHES friction test are different, the friction coefficient is around 0.33 in the LUFHES test, while it is around 0.17 in the KES-F friction test. It is proved that the friction coefficient between fabric and fabric is greater than that between sensor and fabric.

The KES-F friction test also contains two rounds. Total length of fabric movement in each round is 30mm, but according to the manual of the KES-F, the fabric movement from 5mm to 25mm is in a constant speed of 1mm/s, so the data of this 20mm is used for the FFT spectral analysis. The spectra of two rounds of the KES-F friction test are shown in Figure 7.22, and the average amplitudes of the two spectra are shown in Figure 7.23. Because the distance between two adjacent ripstop ribs is around 2.16mm, the wavelengths within 4.4mm are shown in the spectrum and discussed.

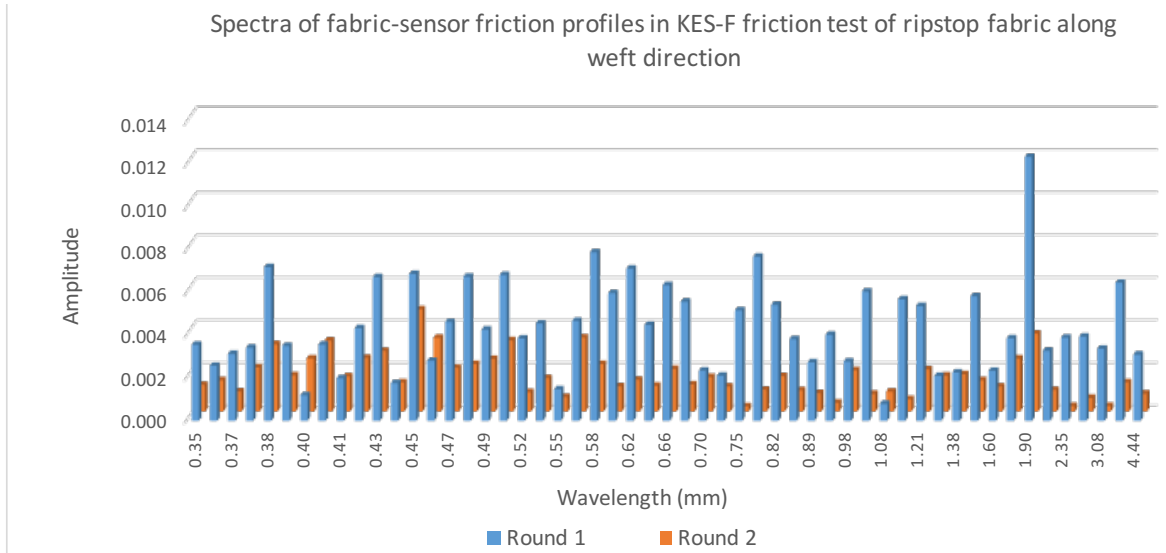


Figure 7.22 Spectra of friction profile of the ripstop fabric in the KES-F friction test

It is shown in Figure 7.22 that the spectra of the KES-F friction tests do not have good reproducibility. Amplitudes of round 1 are much greater than those of round 2. The highest peak in round 2 is shown at the wavelength of 0.45mm, which corresponds to 1/5 length of two adjacent ripstop ribs (0.43mm). But the highest peak in round 1 is shown at the wavelength of 1.90mm, which corresponds to the distance between two ripstop ribs (2.16mm). Therefore the reproducibility of friction test of the ripstop fabric in weft direction in the KES-F friction test is a problem.

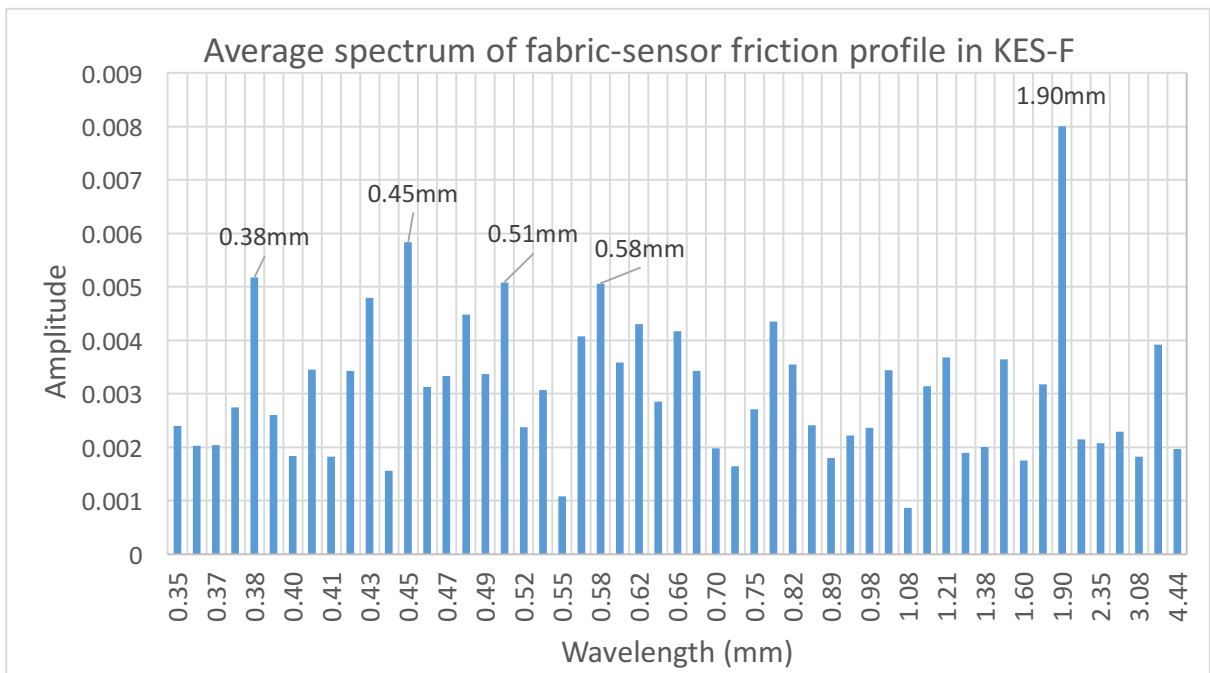


Figure 7.23 Average of two spectra of the KES-F friction tests shown in Figure 7.22

In Figure 7.23, the peaks having high amplitudes are shown at the wavelengths around 0.38mm, 0.45mm, 0.51mm, 0.58mm and 1.90mm. The highest peak is shown at 1.90mm, and it corresponds to the distance between adjacent ripstop ribs (2.16mm), and other peaks correspond to its sub-lengths: peak at 0.38mm and 0.45mm correspond to the 1/5 length of two ripstop ribs (0.43mm); the peak at 0.51mm and 0.58mm correspond to the 1/4 length of two ripstop ribs (0.54mm).

7.3 Comparison of the three spectra of the LUFHES fabric-fabric friction, the KES-F sensor- fabric friction and the KES-F sensor-fabric roughness profiles

The spectrum of the KES-F roughness profile describes the fabric surface roughness structure and the spectrum of its friction profile from a wider metal sensor describes the friction coefficient variations. They are compared with the spectrum of the LUFHES fabric-fabric friction profile to identify their characteristics.

The wavelengths of major peaks and their corresponding amplitudes are summarised in Table 7.3.

Table 7.3 Comparison of wavelengths of major peaks and their corresponding amplitude obtained in the spectra of LUFHES friction, the KES-F friction, and the KES-F roughness profiles

Wavelength (mm)	Amplitudes of peaks		
	LUFHES friction test	KES-F friction test	KES-F Roughness test
~ 0.40	/	0.0052	0.0047
~ 0.45	/	0.0058	0.0063
~ 0.50	/	0.0051	
~ 0.60	/	0.0051	0.0046
~ 1.30	/		0.0055
~ 1.90	0.0064	0.0080	
~ 2.10	/		0.0078
~ 2.70	/		0.0052
~ 3.60	/	0.0039	0.0058

All of the three methods do not show the wavelength less than 0.3mm in the spectrum. Strong peaks are shown around the wavelengths which correspond to the characteristic length of distance between the two adjacent ripstop ribs (2.16mm) in all the FFT spectrum of three tests.

The greatest amplitude of the peak is around 1.90mm in the spectra from both the LUFHES (0.0064) and the KES-F friction profiles (0.0080), and around 2.10mm in the spectrum from the KES-F roughness profile (0.0078). Comparatively, peaks have relatively high amplitudes are obtained around 0.4~0.6mm, 1.3mm, 2.7mm and 3.6mm in the KES-F friction spectrum and the KES-F roughness spectrum. In the LUFHES spectrum, the amplitudes of the peaks at these wavelengths are quite small. As these wavelengths might be related to the sub-lengths of the distance between two ripstop ribs, this might be an advantage for using the spectrum of the LUFHES fabric-fabric friction profile to pick up main wavelengths of the fabric surface roughness structure without producing many sub-wavelengths.

7.4 The characteristic wavelengths in relation to fabric surface structural parameters

It is known from sections 7.1 and 7.2 that both fabric-fabric friction and fabric-sensor friction are related to fabric surface structure (ripstop ribs) of ripstop fabric in weft direction. It is also known from the section 7.3 that the spectrum of fabric-fabric friction profile has advantages in picking up the main wavelength which corresponds to the fabric characteristic length. In this section, it is intended to find out if characteristic wavelengths of spectrum peaks obtained in these three measurements could be used to discriminate different fabric surface structures, and if the spectrum from fabric-fabric friction still has advantages over the spectrum from fabric-sensor friction/roughness test in picking up the main fabric surface structures.

The surface characteristics of five fabrics are studied in this section, they include four woven fabrics (W1, ripstop fabric; W4, plain fabric; W7, satin fabric; and W12, twill fabric), and a nonwoven fabric (N1, thermal point-bonded spunbond nonwoven).

The FFT spectra of the fabric surface profiles are obtained in the average of two rounds of the KES-F roughness and friction tests and three repeats of the LUFHES tests.

7.4.1 Ripstop fabric (W1)

The experimental results of fabric-fabric friction (LUFHES) and sensor-fabric friction (KES-F) characteristics of this ripstop fabric in weft direction were compared with their theoretical analysis in the previous sections 7.1 and 7.2. It was found that the wavelengths of peaks in the spectra of profiles obtained in the KES-F friction and the KES-F roughness test correspond to the length and sub-lengths between two ripstop ribs, which is the main characteristic structure on fabric surface. Comparatively, the spectrum of LUFHES fabric-fabric friction profile has an advantage in picking up the main wavelength which corresponds to characteristic length on fabric surface. In this section, the friction characteristic in its warp direction is discussed.

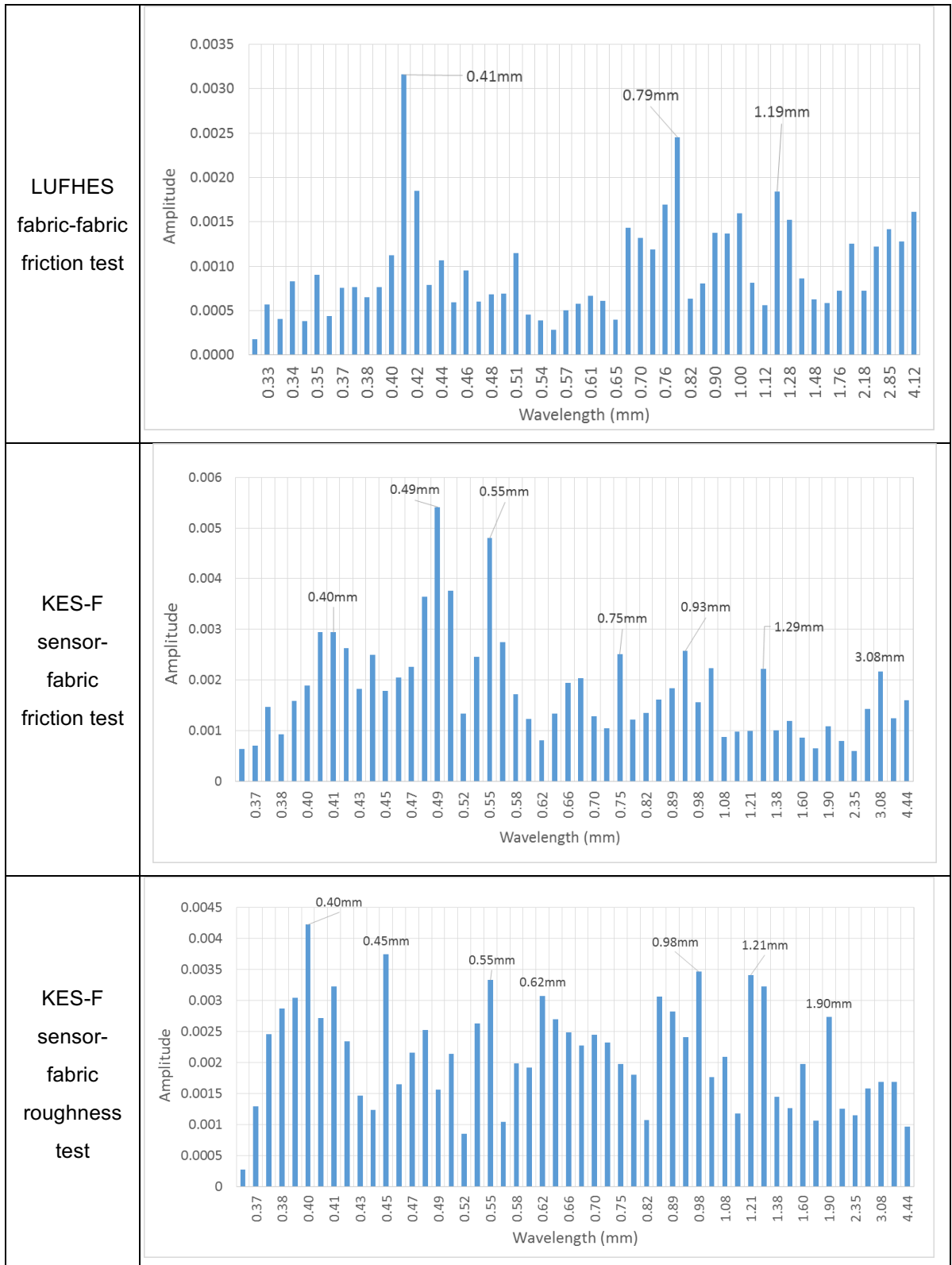
7.4.1.1 Fabric structure

The structure of ripstop fabric in warp direction is similar to that in weft direction (see Figure 7.2); this ripstop fabric has ripstop strips and flat strips in warp direction as well. The warp yarn in flat strip has a 1/2 weave structure, and has a 2/1 weave structure in ripstop strip. The length of 1/2 (or 2/1) twill weave structure in warp direction is around 0.42mm, and the distance between two ripstop ribs in warp direction is around 2.10mm.

7.4.1.2 Fabric surface spectrum of ripstop fabric in warp direction

The fabric surface spectra of the ripstop fabric in warp direction obtained in the three tests are shown in Table 7.4. The greatest structural length in warp direction is 2.1mm, which is the distance between two adjacent ripstop ribs, therefore the wavelengths less than 4.2mm are considered to include all of the possible wavelengths related to the fabric structural parameters in the spectral analysis as shown in Table 7.4.

Table 7.4 Fabric surface spectra of the ripstop fabric (W1) in warp direction



In the spectrum of LUFHES friction profile, the highest peak is at the wavelength of 0.41mm, and the second and the third top peak are around the wavelength of 0.79mm and 1.19mm, respectively. Apparently, these wavelengths are rounded

up to 0.4, 0.8 and 1.2mm, which are multiples of 0.40mm. Because the length of the 1/2 twill weave structure is around 0.42mm, these three wavelengths are all related to this fabric characteristic length.

In the spectrum of the KES-F roughness profile, the highest peak is also shown around 0.40mm having an amplitude of 0.0042. Its amplitude is greater than that of the spectrum of LUFHES friction profile (0.0032). This difference is because of their different meanings. The amplitude in the KES-F roughness test means the height of protrude over fabric surface while it is friction coefficient in LUFHES friction test. Peaks having relatively high amplitudes are also shown around 0.45mm, 0.55mm, 0.98mm and 1.21mm. The peak at wavelength of 1.21mm which is triple of 0.40mm corresponding to the length of 1/2 twill structure in warp direction (0.42mm). While the other wavelengths are related to the sub-lengths between the ripstop ribs, such as 1/5, 1/4 and 1/2 of 2.10mm.

In the spectrum of the KES-F friction profile, the top two peaks are obtained around wavelength of 0.49mm and 0.55mm. These two wavelengths correspond to 1/4 of 2.10mm which is the length between ripstop ribs.

In the comparison between spectra obtained in these three testing methods, it is shown the characteristic wavelength of 1/2 twill weave structure is easier to be identified in the spectrum of LUFHES friction profile.

Different from the friction test in the weft direction of this ripstop fabric, it seems that the ripstop strips hardly affect both fabric-fabric friction and fabric-sensor friction in the warp direction. Comparatively, the 1/2 twill structure has the most apparent influence on both LUFHES fabric-fabric friction test and the KES-F roughness test. This could be explained by the cross-section structures in warp direction of this ripstop fabric ('warp 1' as shown in Figure 7.2). It is shown that the flat strip (F) is slightly higher than the ripstop strip (R) over the fabric surface. Thus, the flat strip has greater effect on friction in warp direction than ripstop strip does. Warp yarn in flat strip has the 1/2 twill structure, so high peaks in the spectra are shown at wavelengths corresponding to the length of this structure (0.42mm). This also verifies that friction/roughness profiles are related to fabric surface structure, and comparatively the LUFHES fabric-fabric friction test is more sensitive.

7.4.2 Plain fabric (W4)

7.4.2.1 Fabric structure

The structure of plain woven fabric surface is shown in Figure 7.24.

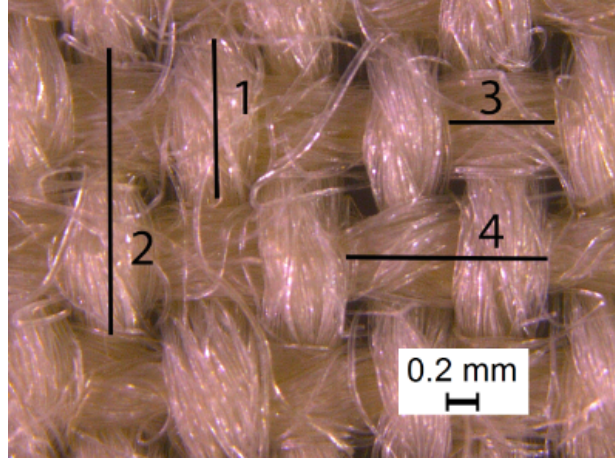


Figure 7.24 Surface structural parameters of plain woven fabric (W4) in both warp and weft directions

The plain woven fabric has similar structure in warp and weft directions: cross point of warp yarn and weft yarn alternately appear on fabric surface. A unit structure which is repeated to form the plain woven fabric contains one warp yarn cross point and one weft yarn cross point in both warp and weft directions.

Lengths of four structural parameters are marked in Figure 7.24. In warp direction, $L1$ is the length of warp/weft cross point and $L2$ is the length of the unit structure. In weft direction, $L3$ is the length of warp/weft cross point and $L4$ is the length of the unit structure of this plain woven fabric. Based on its fabric count: 175 warp yarns and 130 weft yarns within 10cm (see Table 3.1), $L1$ - $L4$ could be calculated and shown in Table 7.5.

Table 7.5 Length of structural parameters of plain woven fabric (W4)

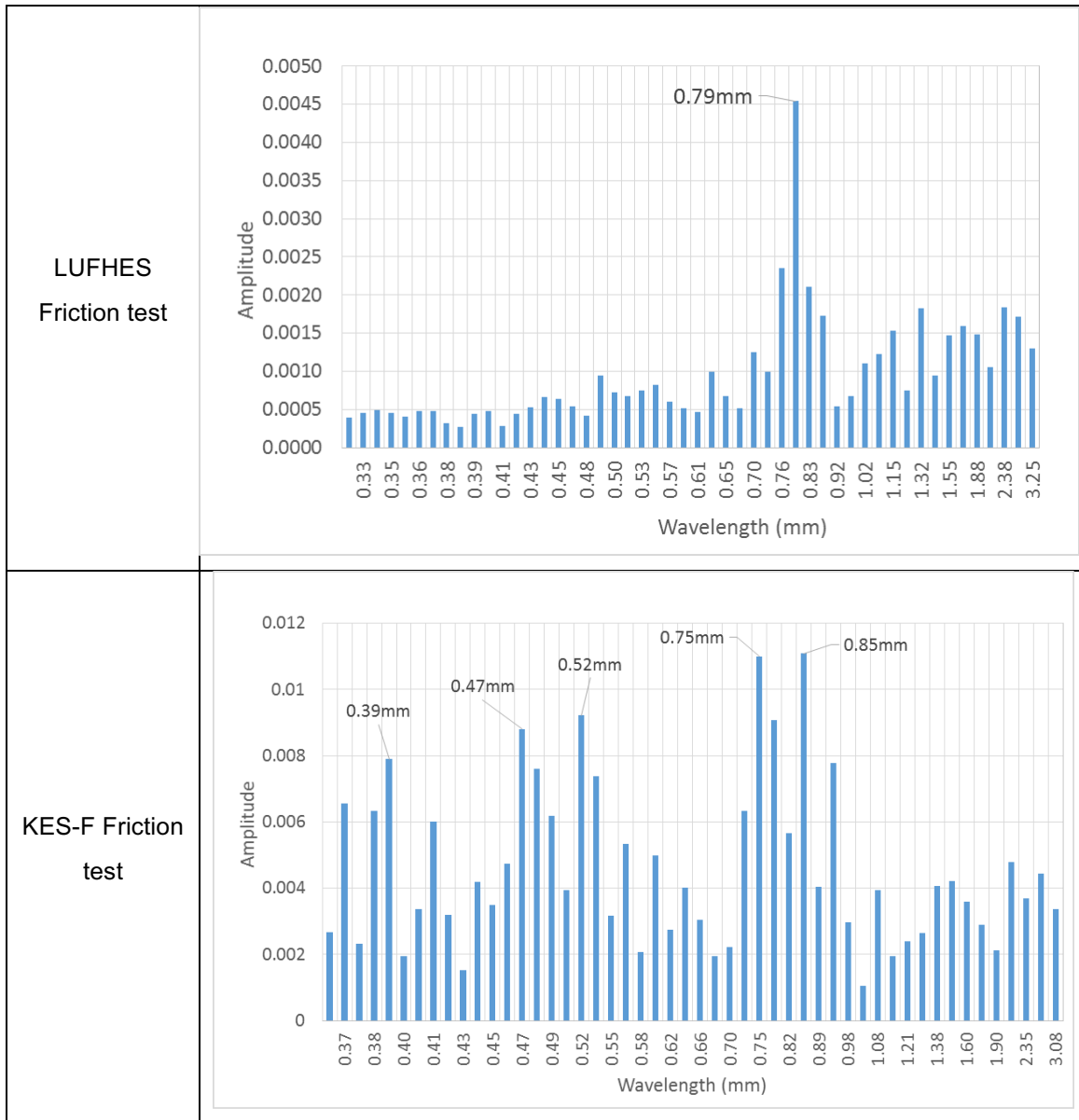
	Warp direction		Weft direction	
	L1	L2	L3	L4
Lengths (mm)	0.77	1.54	0.57	1.14

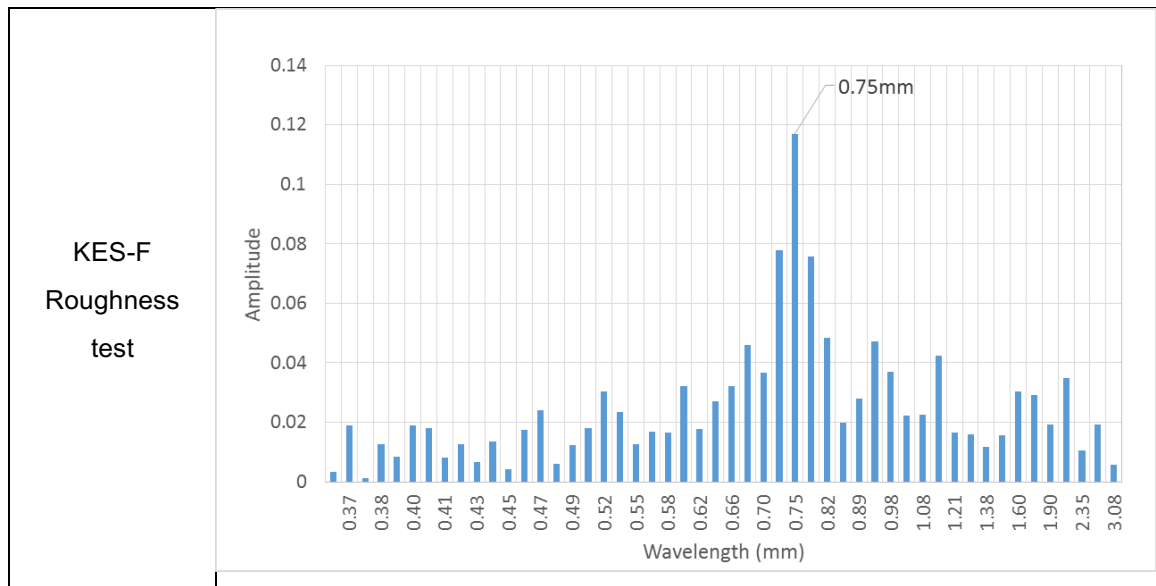
7.4.2.2 Fabric surface spectrum of the plain woven fabric (W4) in the warp direction

The fabric surface spectra of the plain woven fabric in the warp direction obtained in the three tests are shown in Table 7.6. The greatest structural length in warp direction is around 1.54mm, which is the length of the unit plain woven structure, therefore wavelengths less than 3.1mm in the spectra are considered to include

all of the possible wavelengths related to the fabric structural parameters as shown in Table 7.6.

Table 7.6 Fabric surface spectra of the plain woven fabric (W4) in warp direction





It is shown that both the spectra of LUFHES friction and KES-F roughness profiles have only one strong peak at wavelength around 0.79 and 0.75mm, respectively, which correspond to the length of warp/weft yarn cross point in the warp direction of this plain woven fabric (0.77mm in Table 7.5)

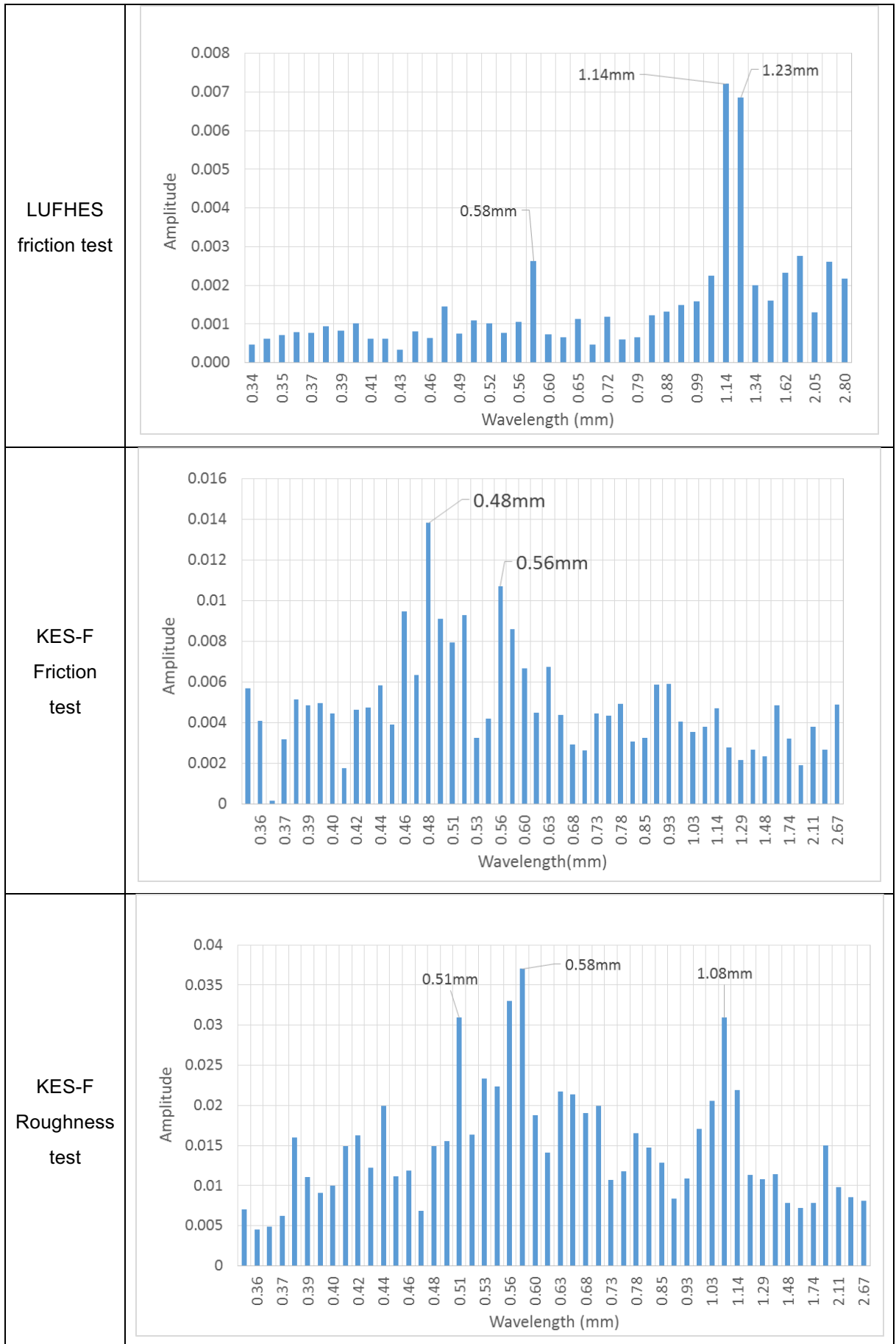
The top two peaks in the spectrum of KES-F friction profile are at the wavelength around 0.75mm and 0.85mm, which also correspond to the length of warp/weft cross point. But the spectrum of the KES-F friction profile also has peaks having high amplitudes at wavelength of 0.40mm, 0.45mm and 0.5mm, which are around $1/5$ and $1/4$ of the length of unit plain woven structure (1.54mm in Table 7.5)

Therefore the LUFHES friction test and the KES-F roughness test have close relationship to the warp/weft yarn cross point on fabric surface, and they have advantages over the KES-F friction test because their spectra do not contain peaks having high amplitudes at wavelengths which correspond to the sub-lengths of main characteristic structure.

7.4.2.3 Fabric surface spectrum of the plain woven fabric (W4) in weft direction

The fabric surface spectra of the plain woven fabric in weft direction obtained in the three tests are shown in Table 7.6. The greatest structural length in weft direction is around 1.14mm, which is the length of the unit plain woven structure, therefore the wavelengths less than 2.3mm are discussed and shown in Table 7.7.

Table 7.7 Fabric surface spectra of the plain woven fabric (W4) in weft direction



In the spectrum of the LUFHES friction profile, the highest two peaks are shown at wavelength of 1.14mm and 1.23mm, which correspond to the length of unit plain woven structure in weft direction (1.14mm in Table 7.5). The third highest peak is at the wavelength of 0.58mm, which corresponds to the length of warp/weft yarn cross point on fabric surface in weft direction (0.57mm in Table 7.5). Therefore all peaks having high amplitudes in the spectrum of the LUFHES friction profile are related to the two characteristic structures on fabric surface.

In both the spectra of the KES-F friction and the KES-F roughness profiles, the highest two peaks are shown around 0.50mm and 0.60mm. Wavelengths of these two peaks correspond to the length of warp/weft yarn cross point (0.57mm). It is also found that only the spectrum of the KES-F roughness test has a peak at wavelength of 1.08mm, which corresponds to the length of unit plain woven structure (1.14mm).

Therefore both the spectra of the LUFHES friction and the KES-F roughness profiles have peaks having high amplitudes shown at wavelengths correspond to both length of warp/weft yarn cross point and the length of unit structure of this plain woven fabric in weft direction. Peaks in the spectrum of the KES-F friction profile could not correspond to the length of unit plain weave structure.

In summary, for this plain woven fabric in both warp and weft directions, using the spectra of both the LUFHES friction profile and the KES-F roughness profile has advantages over using that of the KES-F friction profile because they could provide more information of the fabric surface structure, such as the yarn float length and unit weave structure length of the fabric.

7.4.3 Satin fabric (W7)

7.4.3.1 Fabric structure

The structure of the satin fabric structure is shown in Figure 7.25.

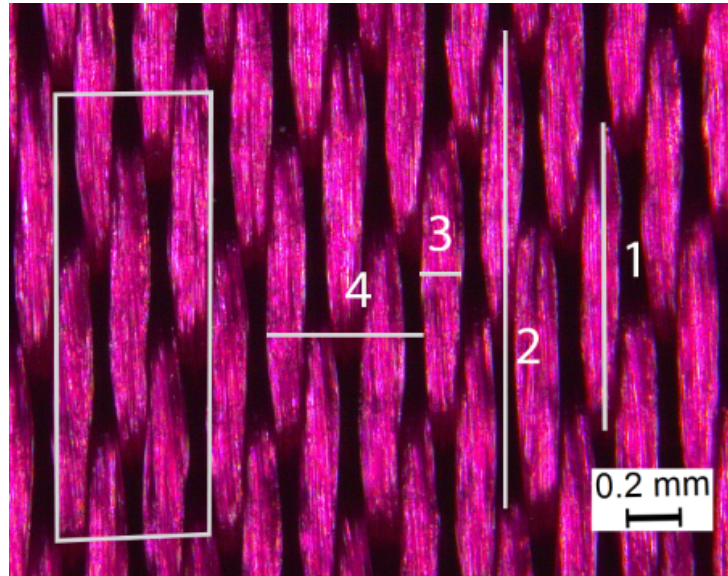


Figure 7.25 Structural parameters of Satin fabric (W7) in both warp and weft directions

The satin fabric shown in Figure 7.25 has a 5/3 satin structure, the surface having long floating warp yarns is studied. A unit structure is marked in Figure 7.25; it contains 5 warp yarns and 5 weft yarns. Lengths of four structural parameters are marked in Figure 7.25 as well. In warp direction, $L1$ is the length of floating warp yarn on fabric surface, and $L2$ is the length of the unit satin structure. In weft direction, $L3$ is the length of a single warp yarn, and $L4$ is the length of the unit satin structure. These four lengths are calculated based on the fabric count: 785 warp yarns and 285 weft yarns within 10 cm (see Table 3.1), and given in Table 7.8.

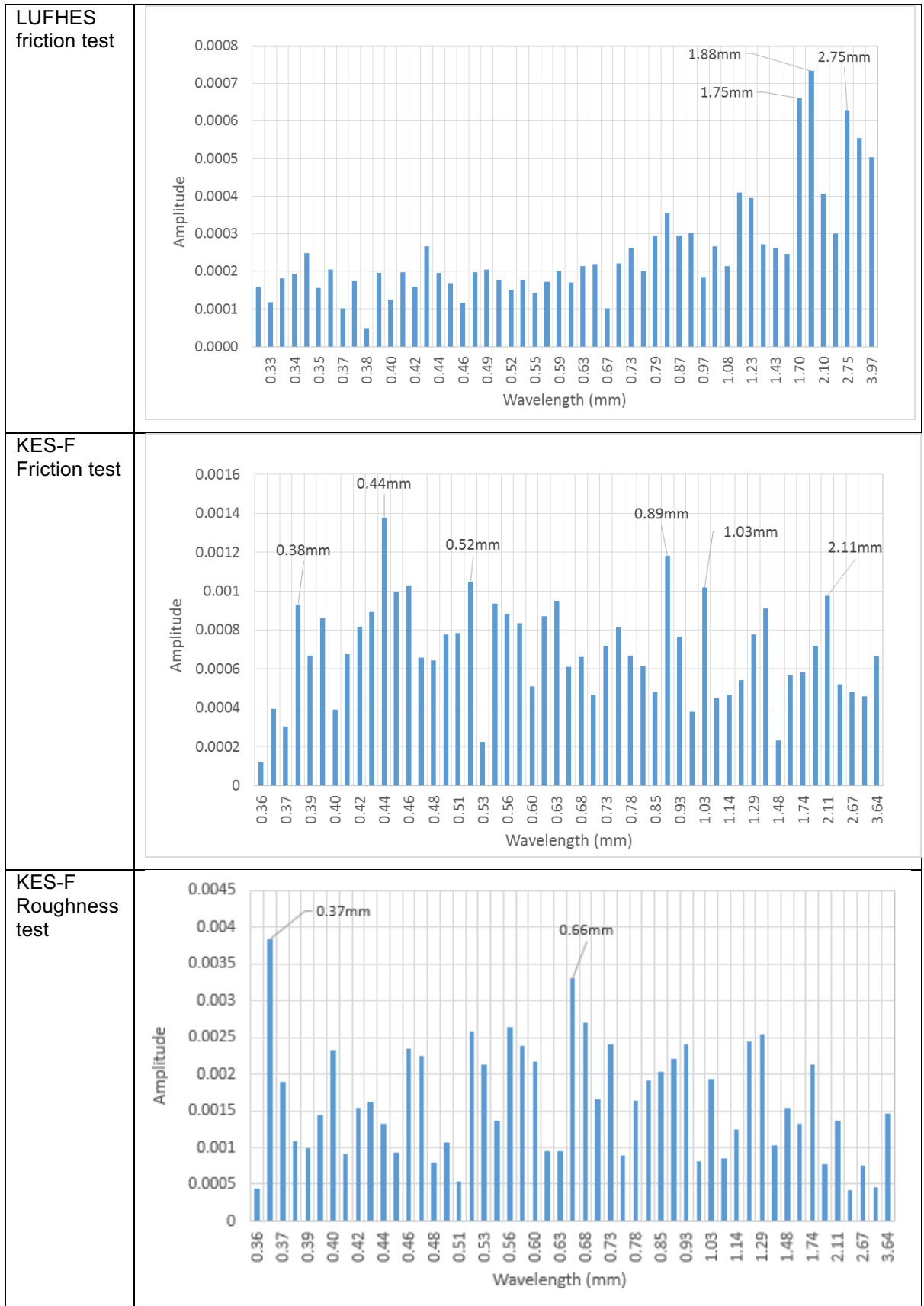
Table 7.8 Lengths of structural parameters of satin fabric (W7)

	Warp direction		Weft direction	
	L1	L2	L3	L4
Length (mm)	1.4	1.75	0.13	0.64

7.4.3.2 Fabric surface spectrum of the satin fabric (W7) in warp direction

The spectra of the satin fabric in warp direction obtained in three tests are shown in Table 7.9. The greatest structural length in warp direction is around 1.75mm, which is the length of the unit satin structure (see Figure 7.25 and Table 7.8), therefore the wavelength less than 3.5mm are shown in Table 7.9.

Table 7.9 Fabric surface spectra of the satin fabric (W7) in warp direction



It is shown that spectrum of the LUFHES friction profile has noticeable differences with the spectra of both the KES-F friction profile and the KES-F roughness profile. In the spectrum of the LUFHES friction profile, amplitude of peaks at wavelengths less than 1.0mm is small. However, many peaks having high amplitudes are shown at wavelength less than 1.0mm in the spectrum of both the KES-F friction profile and the KES-F roughness profile.

The top two peaks in the spectrum of the LUFHES friction profile are at the wavelengths of 1.75mm and 1.90mm, which correspond to the length of unit structure of satin fabric surface (1.75mm). The other strong peak is shown at wavelength of 2.75mm, which is around $5/3$ of the length of the unit satin structure and could not directly correspond to fabric surface structure.

The top two peaks in the spectrum of the KES-F friction profile are at the wavelength of 0.44mm and 0.89mm. They are multiples of 0.44mm, which is around $1/4$ of 1.75mm, the length of unit satin structure. There are three peaks shown at 0.52mm, 1.03mm and 2.10mm, their wavelengths are around multiples of 0.50mm, which corresponds to the sub-length ($1/3$) of the floating warp yarn (1.4mm). Wavelengths of these peaks are all related the sub-lengths of the floating warp yarn or unit satin structure.

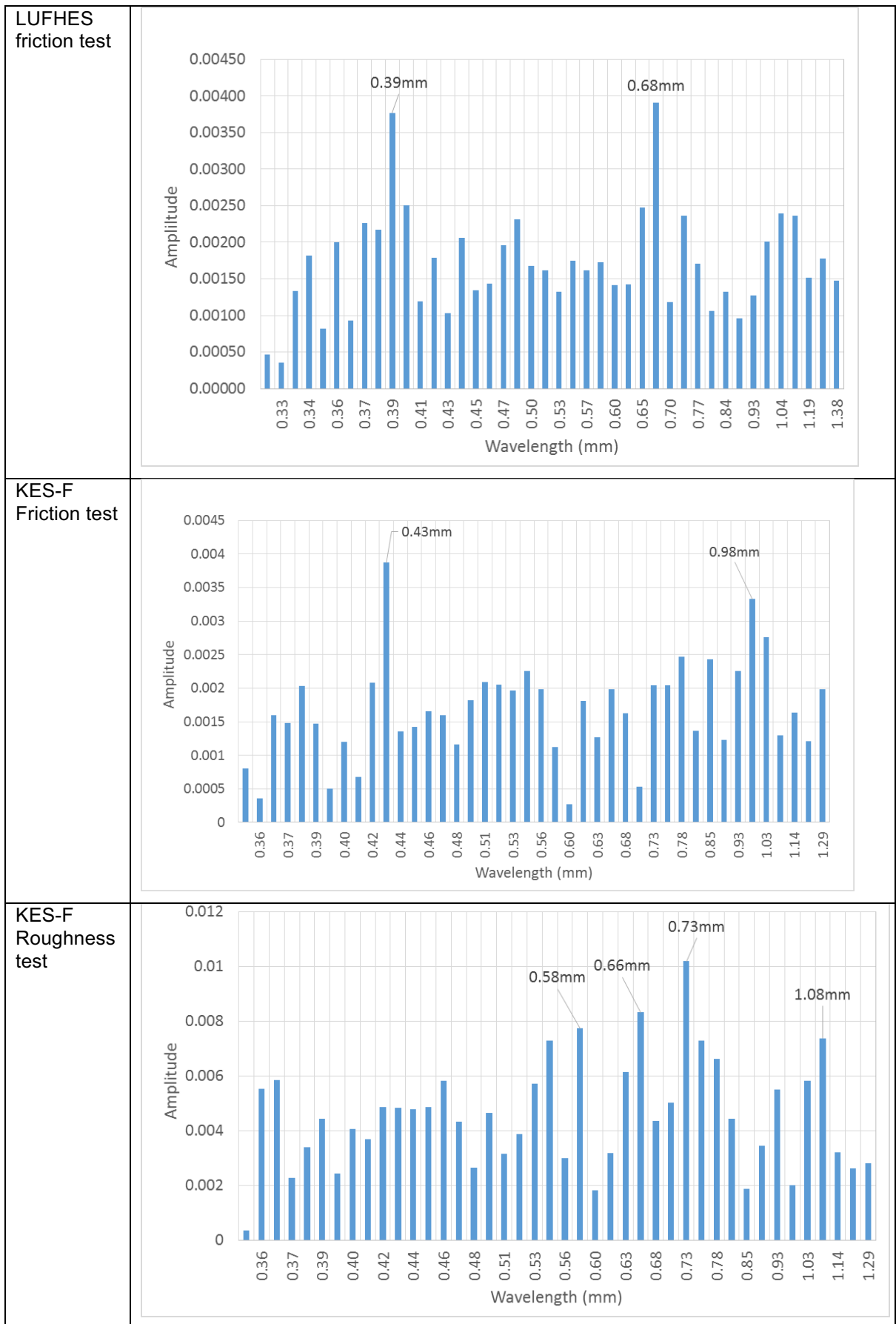
The highest peak in the spectrum of the KES-F roughness profile is shown at 0.37mm. A peak having relatively small amplitude is shown at wavelength of 0.38mm is also shown in the spectrum of the KES-F friction profile. Based on Table 7.9, 0.37mm corresponds to the length of unit satin structure (1.75mm) minus the length of floating warp yarn (1.4mm), so it represents the length of the warp yarn part which is not shown/float on fabric surface. Another peak having high amplitude is shown at wavelength of 0.66mm, which seems also related to this structure, because 0.66mm is almost the double of 0.37mm.

In summary, peaks having high amplitudes in the spectrum of the LUFHES friction profile and the KES-F roughness profile could correspond to characteristic lengths on fabric surface. However, wavelengths of peaks in the spectrum of the KES-F friction profile could only correspond to sub-lengths of fabric surface structure. Thus, using the spectra of the LUFHES friction profile and the KES-F friction roughness profile has advantages in studying this satin fabric structure in warp direction.

7.4.3.3 Fabric surface spectrum of the satin fabric (W7) in weft direction

The fabric surface spectra of the satin fabric in weft direction obtained in the three tests are shown in Table 7.10. The greatest structural length in weft direction is around 0.64mm, therefore the wavelengths less than 1.30mm are discussed.

Table 7.10 Fabric surface spectra of the satin fabric (W7) in weft direction



The top two peaks in the spectrum of the LUFHES friction profile are shown at the wavelength of 0.39mm and 0.68mm. According to the Table 7.8, it is known that 0.39mm is triple length of single yarn in weft direction (0.13mm), and 0.68mm corresponds to the length of unit satin structure (0.64mm)

The top two peaks in the spectrum of the KES-F friction profile are shown at wavelength of 0.43mm and 0.98mm which are around three times and eight times length of single yarn in weft direction (0.13mm), so these two peaks might be related to this structure.

In the spectrum of the KES-F roughness profile, the highest peak is shown at wavelength of 0.73mm, and other peaks which also have high amplitudes are shown at wavelengths of 0.58mm, 0.66mm, and 1.08mm. Among these wavelengths, 0.58mm and 0.66mm are close to the length of unit satin structure (0.64mm), 0.73mm and 1.08mm are around six times and eight times length of single yarn in the weft direction (0.13mm), respectively.

In summary, for both warp and weft directions of this satin fabric, peaks having high amplitudes are shown in both the spectra of the LUFHES friction profile and the KES-F roughness profile at wavelengths which correspond to characteristic structure lengths. However, the spectrum of the KES-F friction profile only has peaks at wavelengths which are related to sub-lengths or multiple lengths of the characteristic structures.

7.4.4 Twill fabric (W12)

7.4.4.1 Fabric structure

The surface structure of twill fabric (W12) is shown in Figure 7.26.

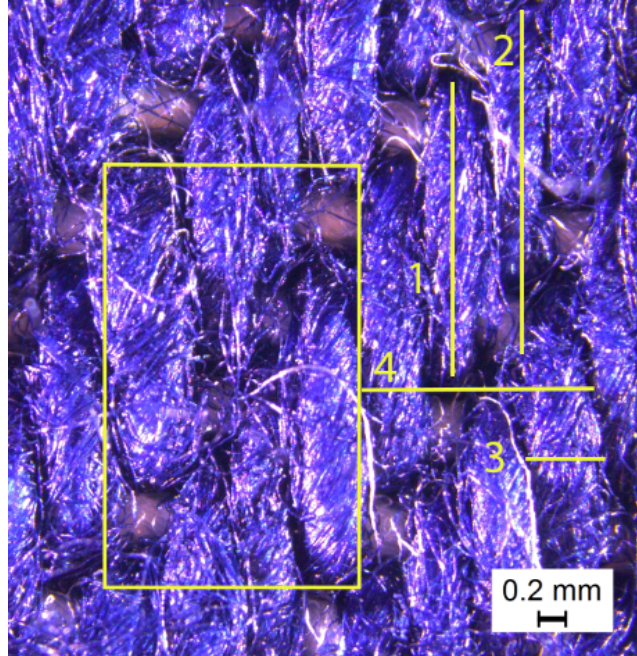


Figure 7.26 Structural parameters of twill woven fabric (W12) in both warp and weft directions

The twill woven fabric has a 3/1 weave structure, the surface having floating warp yarns is investigated in this study. A unit twill structure which contains four warp yarns and four weft yarns are marked in Figure 7.26, and four structural parameters are marked as well. In the warp direction, $L1$ is the length of the floating warp yarn, and $L2$ is the length of unit twill structure. In the weft direction, $L3$ is the length of a single warp yarn and $L4$ is the length of the unit twill structure. It is known that this twill fabric has 260 warp yarns and 160 weft yarns within 10cm (see Table 3.1), the above four lengths are calculated and given in Table 7.11.

Table 7.11 Lengths of structural parameters of twill fabric (W12)

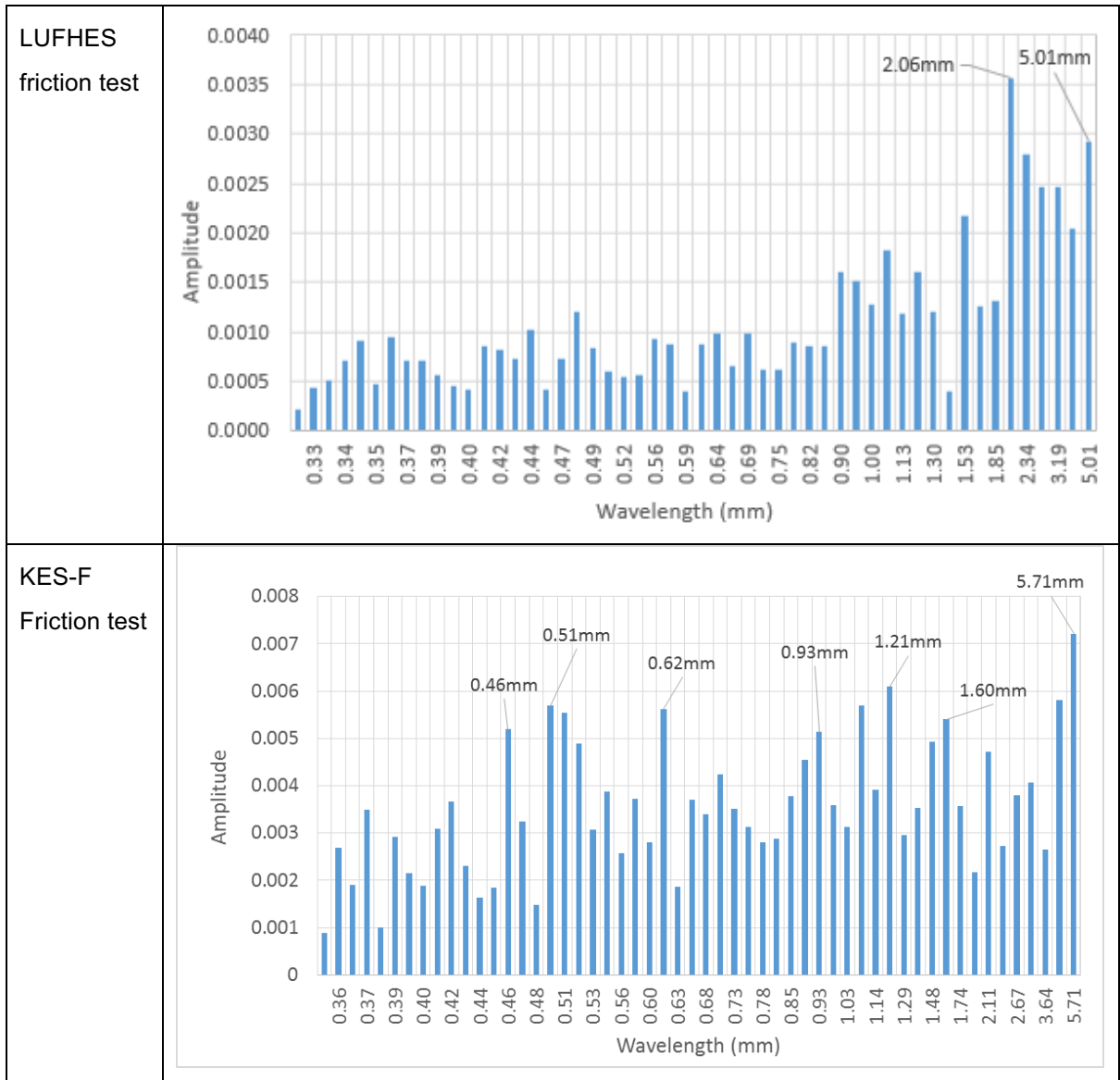
Structures	Warp direction		Weft direction	
	L1	L2	L3	L4
Lengths (mm)	1.9	2.5	0.38	1.54

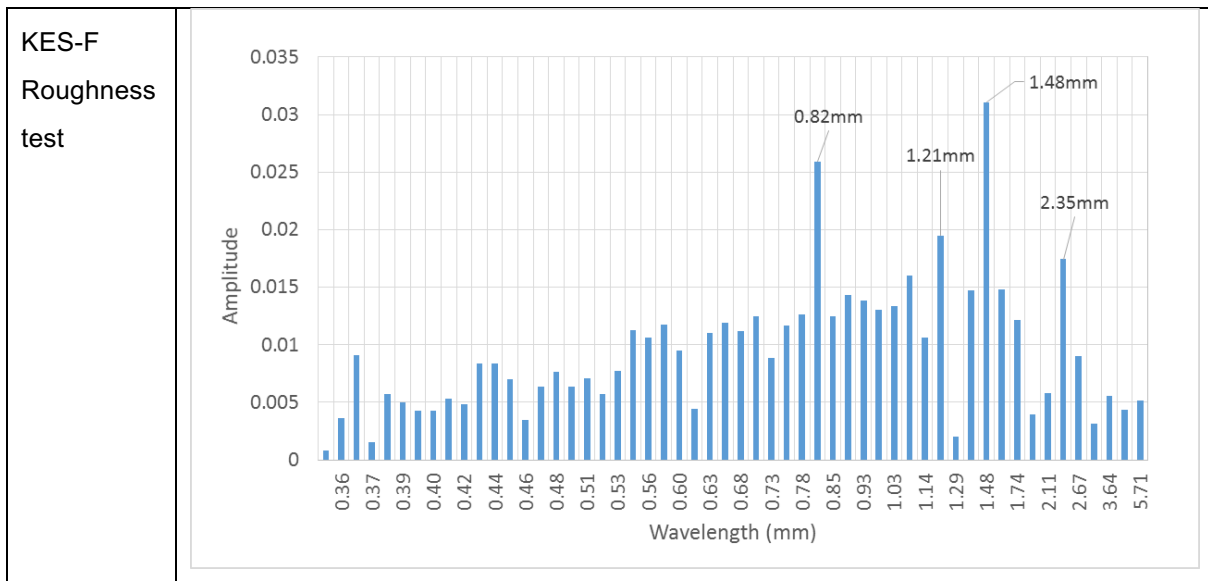
7.4.4.2 Fabric surface spectrum of the twill fabric (W12) in warp direction

The fabric surface spectra of the twill woven fabric in the warp direction obtained in the three tests are shown in Table 7.12. The greatest structural length in warp

direction is around 2.5mm, therefore the wavelengths less than 5.0mm are discussed and shown in the spectra in Table 7.12.

Table 7.12 Fabric surface spectra of the twill woven fabric (W12) in warp direction





In the spectrum of the LUFHES friction profile, the highest peak is shown at the wavelength of 2.06mm which corresponds to the length of floating warp yarn on fabric surface (1.9mm). Another peak having high amplitude is shown at 5.01mm, which is the double length of unit twill structure.

In the spectrum of the KES-F friction profile, the highest peak is shown at wavelength of 5.71mm, which also corresponds to the double length of unit twill structure. Peaks having high amplitudes are also shown at wavelengths of 0.46mm, 0.51mm, 0.62mm, 0.93mm, 1.21mm and 1.60mm. These wavelengths do not correspond to the fabric characteristic structural lengths directly, so they are related to their sub-lengths. For example, 0.62mm and 0.93mm are around $1/3$ and $1/2$ of 1.9mm, which is the length of floating warp yarn.

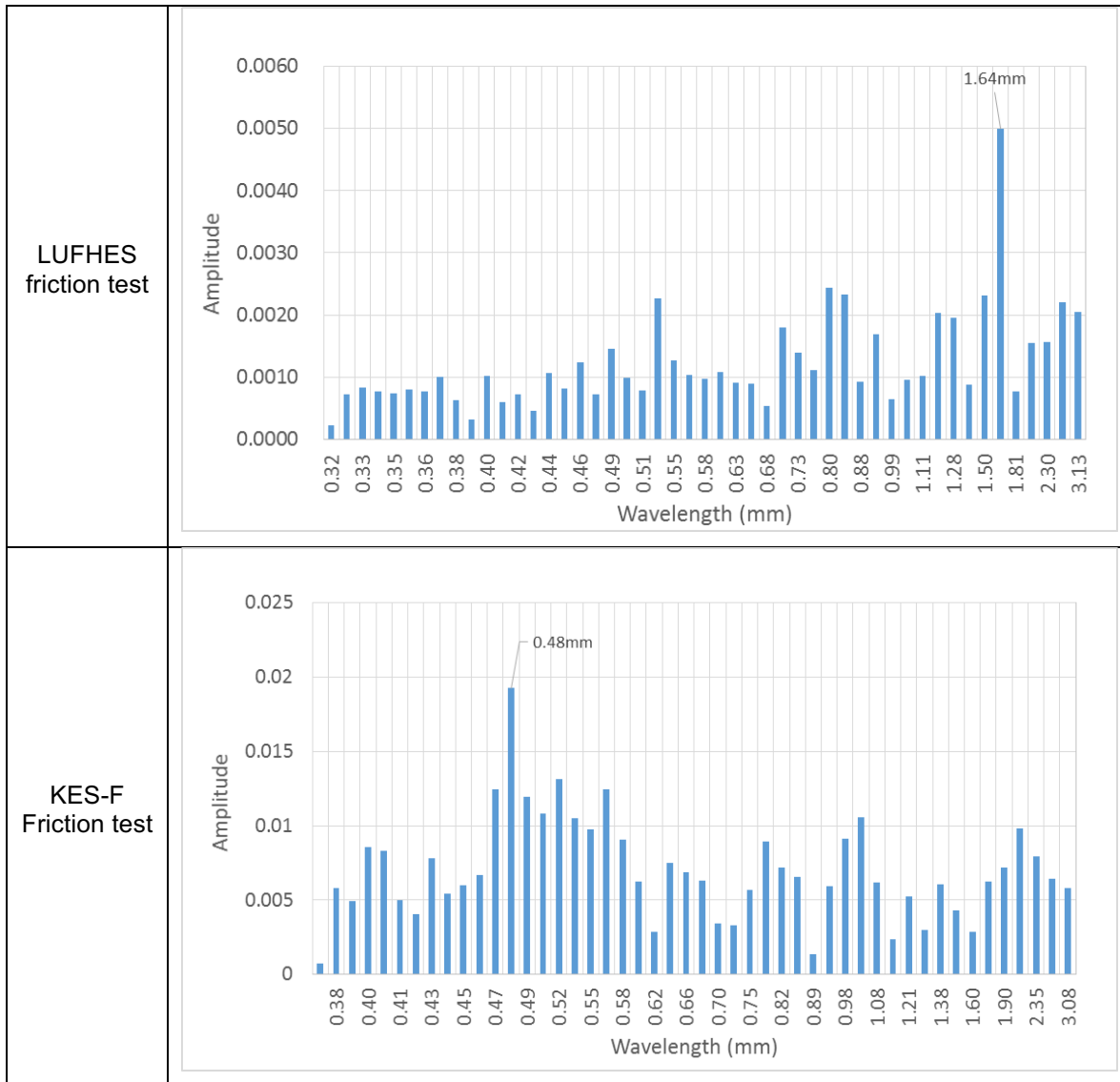
In the spectrum of the KES-F roughness profile, the highest three peaks are shown at 1.48mm, 0.82mm and 1.21mm. These three wavelengths could not directly correspond to fabric structural length, but correspond to $3/5$, $1/3$ and $1/2$ of the length of unit twill structure (2.5mm). There is a peak shown at wavelength of 2.35mm which corresponds to the length of unit twill structure, but the amplitude of this peak is relatively small.

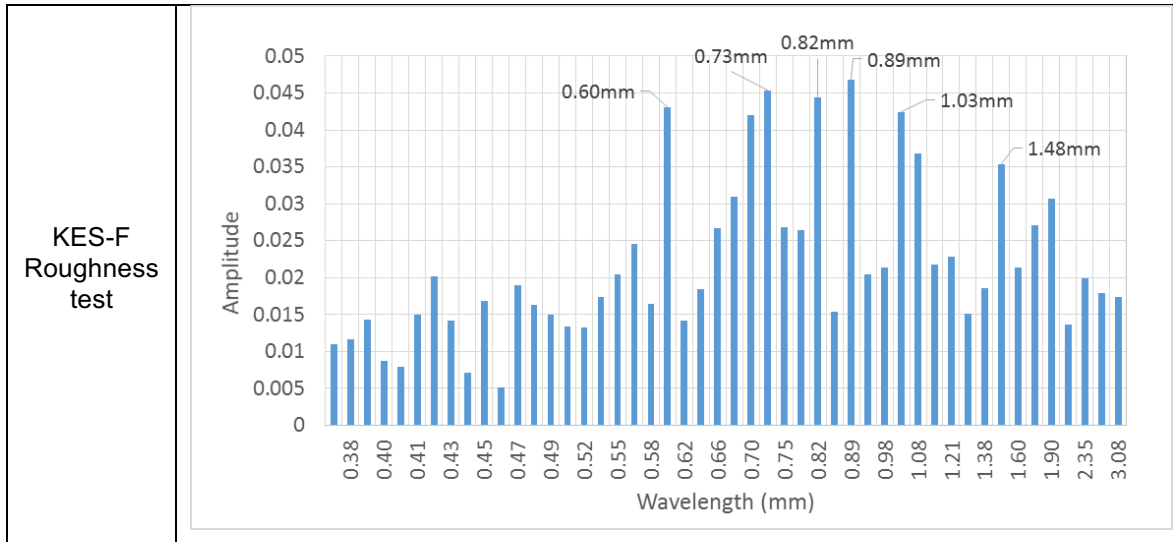
In the comparison of the spectra of these three tests, only the spectrum of the LUFHES friction profile has strong peaks at wavelengths corresponding to characteristic structural length. The wavelengths of peaks shown in the spectrum of the KES-F friction and the KES-F roughness profile could not correspond to the fabric characteristic structure lengths directly.

7.4.4.3 Fabric surface spectrum of the twill fabric (W12) in weft direction

The fabric surface spectra of the twill fabric in weft direction obtained in the three tests are shown in Table 7.13. The greatest structural length in weft direction is around 1.54mm, therefore the wavelength less than 3.1mm are shown and discussed.

Table 7.13 Fabric surface spectra of the twill woven fabric (W12) in weft direction





In both the spectra of the LUFHES friction profile and the KES-F friction profile, only one peak having high amplitude is shown at wavelengths of 1.64mm and 0.48mm, respectively. 1.64mm could correspond to the length of unit twill structure (1.54mm) and the 0.48mm could correspond to the length of single warp yarn in weft direction (0.38mm).

In the spectrum of the KES-F roughness profile, several peaks having high and similar amplitudes are shown at wavelengths between 0.60mm and 1.00mm. The wavelengths of these peaks could only correspond to the sub-lengths of unit structure or the multiple lengths of the single yarn. For example, 0.60mm and 1.03mm are around 1/3 and 2/3 of the length of unit twill structure (1.54mm), and 0.73mm almost double the length of single yarn in weft direction (0.38mm). There is a peak shown at wavelength of 1.48mm which corresponds to the length of unit twill structure, but its amplitude is relatively small.

In the comparison between the spectra of these three test, both top peaks in the spectra of the LUFHES friction profile and the KES-F friction profile could correspond to the characteristic structure length, but top peaks in the spectrum of the KES-F roughness profile could only correspond to the sub-lengths or multiple lengths of characteristic structures.

In summary, for both directions of twill woven fabric, only the spectra of the LUFHES friction profile have strong peaks shown at wavelengths corresponding to the characteristic structures. Many peaks at wavelengths corresponding to sub-length or multiple length of characteristic structures are shown in the spectra of the KES-F friction profile or the KES-F roughness profile in either warp or weft direction.

7.4.5 Nonwoven (N1)

7.4.5.1 Fabric structure

The structure of thermal point bonded nonwoven is shown in Figure 7.27.

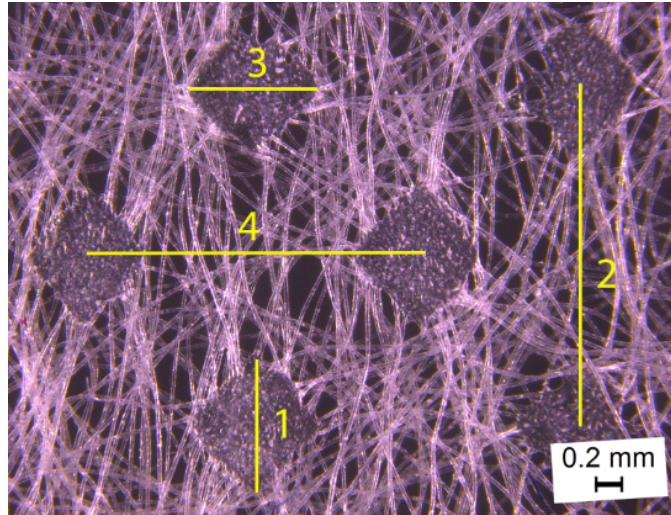


Figure 7.27 Structural parameters of nonwoven fabric (N1) in both CD and MD

Fibres in nonwoven are randomly aligned, the effect of bonding points on its fabric roughness is investigated. Four lengths of structures are marked on fabric surface. $L1$ and $L3$ are the lengths of bonding points in MD and CD, respectively, and $L2$ and $L4$ are the distance between two bonding points in MD and CD, respectively. These four structural lengths are measured at different places; their average lengths and standard deviations are given in Table 7.14.

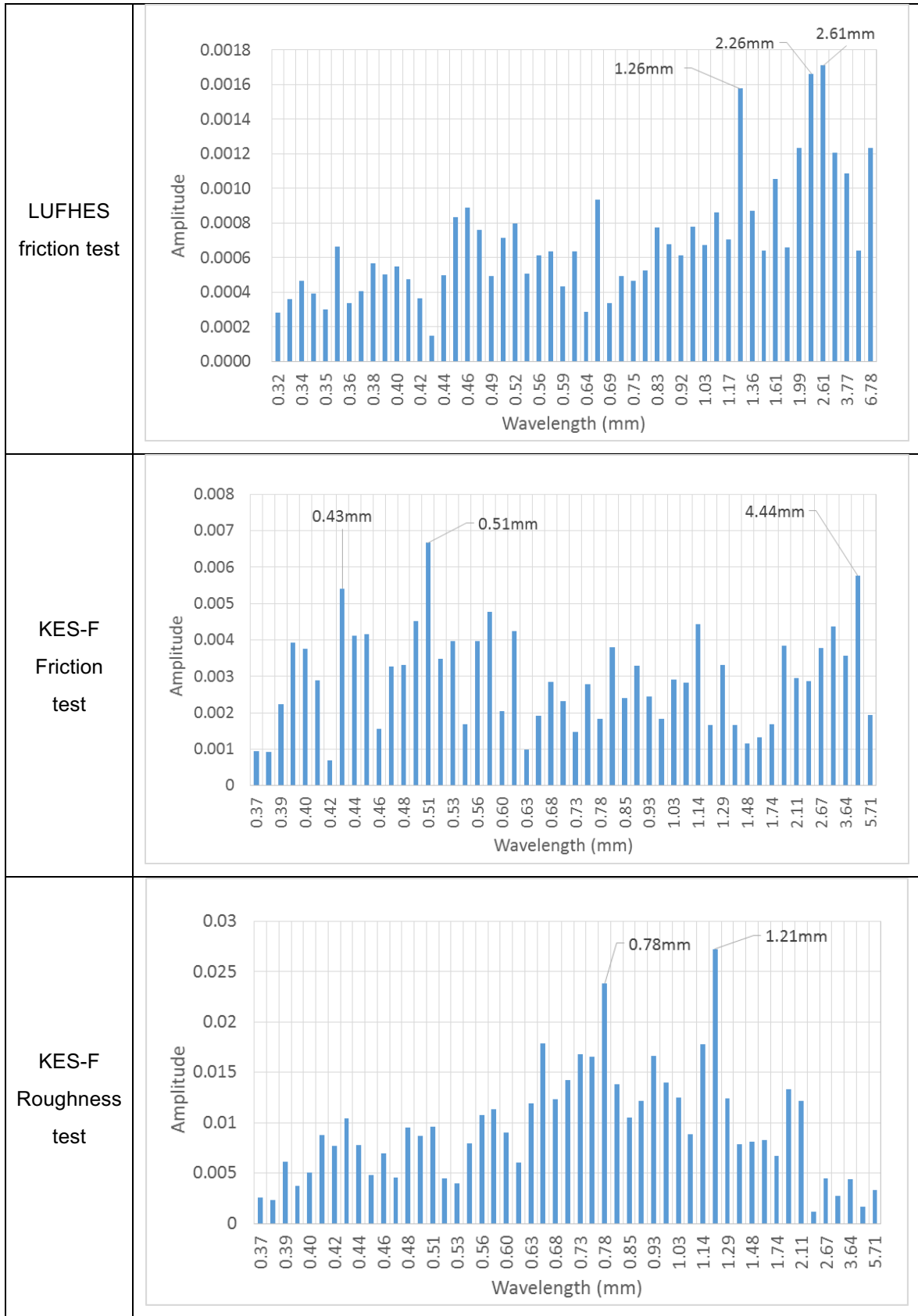
Table 7.14 Lengths and SD of structural parameters of nonwoven fabric (N1)

Structure	Machine direction		Cross direction	
	L1	L2	L3	L4
Average Length (mm)	1.13	2.70	1.03	2.61
Standard Deviation (mm)	0.050	0.069	0.025	0.027

7.4.5.2 Fabric surface spectrum of the nonwoven fabric (N1) in machine direction

The fabric surface spectra of the nonwoven fabric in MD obtained in the three tests are shown in Table 7.15. The greatest structural length, distance between two bonding points in MD is around 2.70mm, therefore the wavelengths less than 5.40mm are shown in the spectra and studied.

Table 7.15 Fabric surface spectra of the nonwoven fabric (N1) in machine direction



In the spectrum of the LUFHES friction profile, top two peaks are shown at wavelengths of 2.26mm and 2.61mm, which correspond to the distance between two bonding points in MD (2.70mm). The other peak having high amplitude is shown at wavelength of 1.26mm, which corresponds to the size of bonding point (1.13mm).

In the spectrum of the KES-F friction profile, the highest peak is shown at wavelength of 0.51mm, which is almost half of the size of bonding point (1.13mm). Other two peaks having high amplitude are obtained at wavelengths of 0.43mm and 4.44mm, which are around 1/3 of bonding point size (1.13mm) and 5/3 of the distance between bonding points (2.7mm), respectively, and could not correspond to characteristic structural lengths directly.

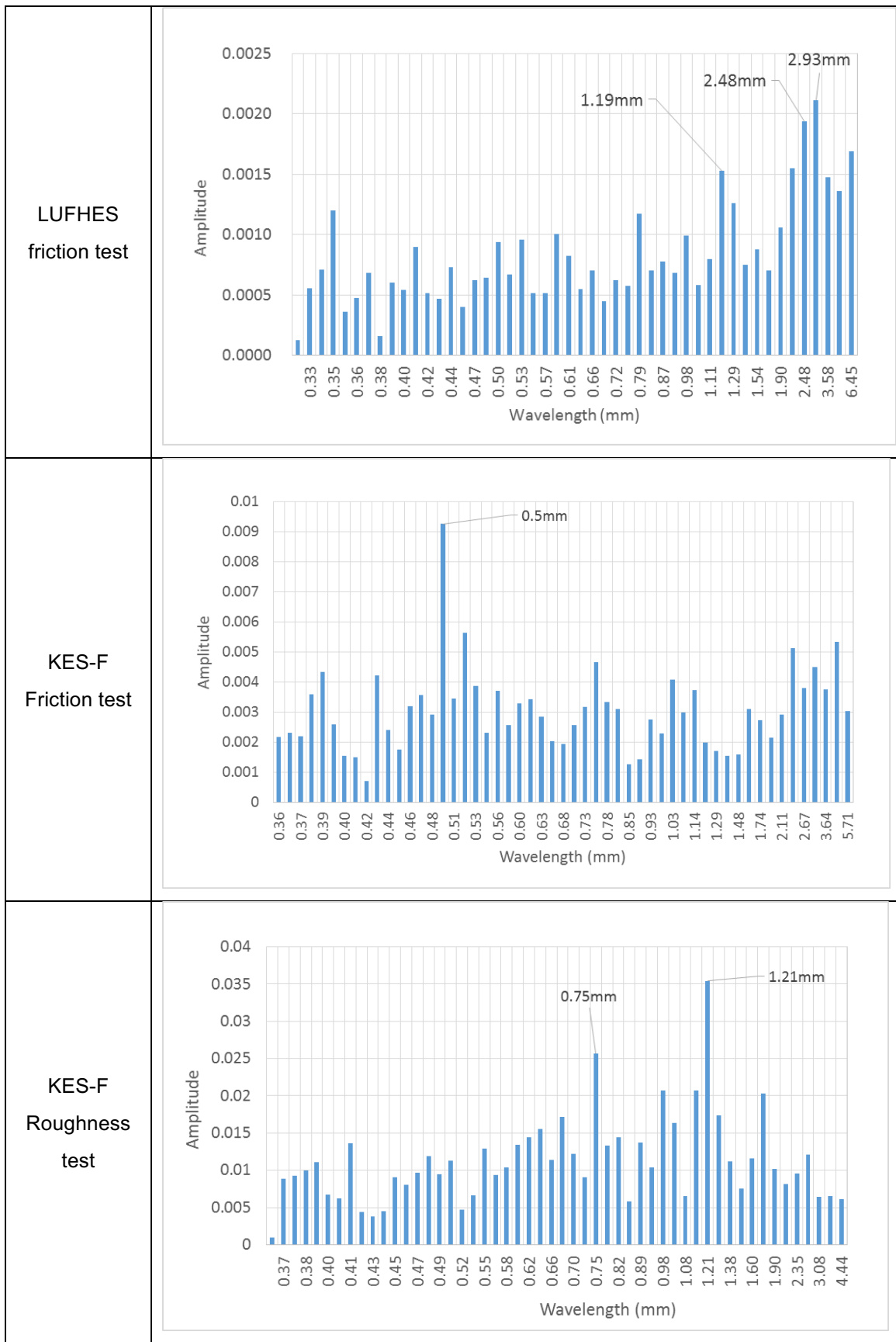
In the spectrum of the KES-F roughness profile, the highest peak is shown at wavelength of 1.21mm, which corresponds to the bonding point size (1.13mm). Another peak which has high amplitude is shown at wavelength of 0.78mm, which is around 1/3 of the distance between two bonding points.

In the comparison between the spectra of the three tests profiles, it is found that wavelength of peaks in the spectra of the LUFHES friction profiles correspond to both bonding point size and distance between two bonding points, and no strong peak is shown at wavelengths relating to sub-lengths of fabric structure. But many strong peaks having high amplitudes are shown in the spectrum of the KES-F friction and the KES-F roughness profile but could not correspond to fabric structure directly.

7.4.5.3 Fabric surface spectrum of the nonwoven fabric (N1) in cross direction

The fabric surface spectra of the nonwoven fabric in the CD obtained in the three tests are shown in Table 7.16. The greatest structural length in CD is around 2.61mm, therefore the wavelength less than 5.2mm are shown in the spectra and discussed.

Table 7.16 Fabric surface spectra of the nonwoven fabric (N1) in CD



In the spectrum of the LUFHES friction profile, the top two peaks are shown at wavelengths of 2.50mm and 2.95mm, which correspond to the distance between two bonding points (2.61mm). The other peak having high amplitude is shown at wavelength of 1.19mm, which could also correspond to the size of bonding point (1.03mm).

In the spectrum of the KES-F friction profile, a pronounced peak is shown at wavelength of 0.50mm, which is half of the bonding point length 1.03mm. The top peak in the spectrum of the KES-F roughness profile is shown at wavelength of 1.21mm, which corresponds to the bonding point length as well. Thus, the KES-F friction and roughness tests are significantly affected by the bonding point size. Another peak shown in the spectrum of the KES-F roughness profile is at the wavelength of 0.75mm, which is around 1/3 of the length between two bonding points (2.61mm).

For both MD and CD of this thermal pointed bonded nonwoven fabric, it is found that the spectra of the LUFHES friction profiles have strong peaks at wavelengths correspond to both bonding points and distances between two bonding points without many peaks shown at sub-lengths of these two structures. Comparatively speaking, the spectrum of the KES-F roughness profile has advantage over the spectrum of the KES-F friction profile in detecting the bonding point size, since many peaks at sub-wavelengths are obtained in the spectrum of the KES-F friction profile.

7.4.6 Fabric friction coefficients measured in the KES-F system and the LUFHES

The fabric friction coefficients of these five fabrics (W1, W4, W7, W12 and N1) obtained in both the LUFHES and the KES-F friction tests are shown in Table 7.17.

Table 7.17 Friction coefficients of fabrics obtained in the LUFHES and the KES-F friction tests

Fabric		Friction coefficient			
		LUFHES friction test		KES-F friction test	
		Mean	SD	Mean	SD
W1	Warp	0.40	0.037	0.17	0.009
	Weft	0.33	0.031	0.12	0.032
W4	Warp	0.76	0.013	0.15	0.010
	Weft	0.95	0.037	0.20	0.009
W7	Warp	0.33	0.036	0.10	0.012
	Weft	1.83	0.353	0.18	0.049
W12	Warp	0.58	0.030	0.16	0.008
	Weft	0.64	0.056	0.19	0.017
N1	MD	0.45	0.013	0.17	0.016
	CD	0.50	0.076	0.18	0.015

It is shown that friction coefficients obtained in the LUFHES fabric-fabric friction test are much greater than those obtained in the KES-F sensor-fabric friction test. The friction coefficients of these five fabrics obtained in the LUFHES fabric-fabric friction test vary in a wider range from 0.33 to 1.83, and those obtained in the KES-F friction test vary little in a small range from 0.10 to 0.20, 70% of them are between 0.16 and 0.20. The two smallest friction coefficients (W1 in weft and W7 in warp) appear in the results from both the KES-F and the LUFHES friction tests, but the greatest friction coefficient in the LUFHES is not in agreement with that in the KES-F test.

A possible reason for greater fabric-fabric friction coefficient is that the fabric diameter is smaller in comparison with the metal sensor used in the KES-F friction test, so when two fabrics are in contact, their surfaces might embed into each other structurally (Ajayi, 1992b). More external force is required to shear the asperities on fabric surface and leads to a greater friction coefficient. The greater fabric-fabric friction coefficient suggests that the difference between fabric surface structures could amplify the difference between fabric-fabric friction coefficients. In the research of Ajayi (1992b), friction between fabric-fabric, fabric-Perspex and fabric-rubber were compared. It was found that friction between fabric and fabric provides the most sensitive surface and gives the best discrimination of fabrics. Thus, the fabric-fabric friction coefficient obtained in the LUFHES is more

sensitive to the fabric surface structure and has an advantage in differentiating fabrics.

The correlation between the friction coefficients of these five fabrics obtained in the LUFHES and the KES-F friction tests are investigated. R^2 of linear regression equation between them is only 0.28 as shown in Figure 7.28. The poor linear relationship between these two friction coefficients suggests that the friction coefficient obtained in fabric-fabric friction test are different from those obtained in fabric-sensor friction test.

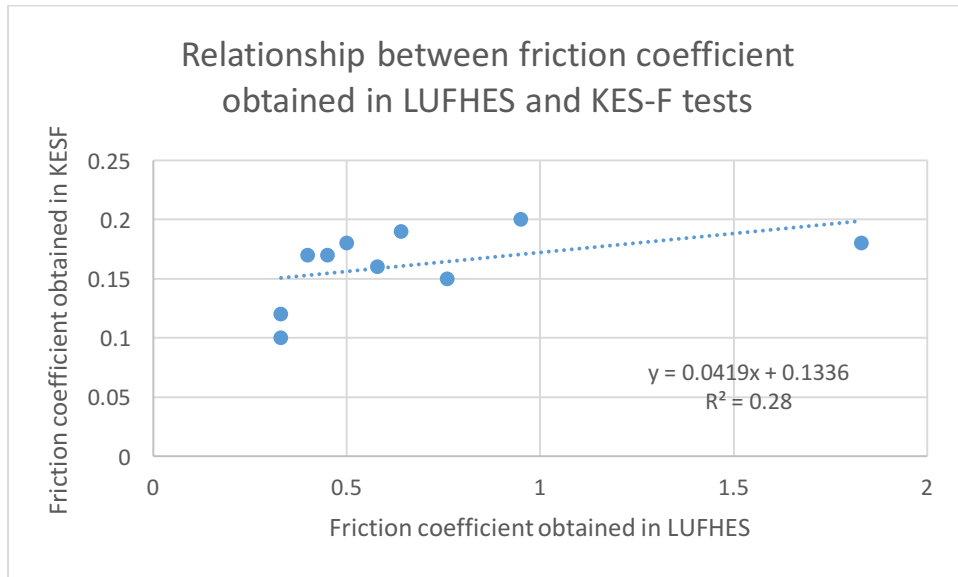


Figure 7.28 Relationship between friction coefficient obtained in the LUFHES and the KES-F friction tests

7.4.7 Summary

The relationships between fabric surface structures and the spectra of the LUFHES friction profiles, the KES-F friction profiles and the KES-F roughness profiles were verified by using five fabrics (4 woven fabrics and 1 nonwoven fabric) which have different surface characteristics in two directions. The relationships between wavelengths of strong peaks shown in the spectra and fabric characteristic structural lengths were investigated, it was found that wavelengths of strong peaks shown in the spectra of the LUFHES friction tests agree well with the characteristic structural lengths on fabric surface, especially for plain woven and ripstop woven fabrics and nonwoven fabric tested. In addition, compared with the spectra of the KES-F friction profiles and the KES-F roughness profiles, less peaks were shown in the spectra of the LUFHES friction profiles at wavelengths which correspond to the sub-lengths or multiple of the structural lengths.

It is indicated that fabric characteristic lengths are easier to be identified in fabric-fabric friction profile than in fabric-sensor friction profile and the fabric-fabric friction test could produce a wider range of fabric friction coefficients which might be helpful in differentiating fabric surface smoothness. The LUFHES fabric-fabric friction test is thus a potential better method to evaluate fabric geometrical roughness characteristics and differentiate fabric surface friction properties.

7.5 Summary

The main findings of this chapter are summarized as below:

1. Simplified models to produce the theoretical friction profiles for both fabric-fabric friction and fabric-metal sensor friction for a ripstop fabric were established. The wavelengths of 7 peaks shown in the FFT spectra of these two theoretical friction profiles were identical. It was found that the wavelength of the highest peak corresponded to the characteristic length of this ripstop fabric, the length between two ripstop ribs, and wavelengths of other six strong peaks corresponded to the sub-lengths of the length between two ripstop ribs, e.g. $1/2$, $1/4$, $1/5$, $1/7$, $1/10$ and $1/11$. Thus, both theoretical fabric-fabric and fabric-sensor friction profiles were highly related to the fabric surface structure;
2. For the ripstop fabric, the FFT spectra of the fabric-fabric friction profile obtained in the LUFHES and fabric-sensor friction profile and fabric-sensor roughness profiles obtained in the KES-F were analysed. It was shown that the LUFHES fabric-fabric friction test had better reproducibility than both the KES-F fabric-metal roughness test and friction test. All wavelengths of the highest peaks in these three spectra corresponded to the length between two ripstop ribs of the ripstop fabric. That is, the fabric-fabric friction and fabric-sensor friction profiles corresponded to the fabric structure and in agreement with the theoretical analysis;
3. For all the woven and nonwoven fabrics tested, the wavelengths of strong peaks shown in the spectra of the LUFHES fabric-fabric friction profiles agreed well with the characteristic lengths of the fabrics. Comparatively, fabric characteristic lengths were easier to be identified in fabric-fabric friction profiles than in fabric-sensor roughness/friction profiles. The spectra of the LUFHES friction profiles contained less peaks at wavelengths which were related to the sub-lengths of fabric characteristic lengths;
4. The LUFHES fabric-fabric friction tests could produce a wider range of fabric friction coefficients which might be helpful in differentiating fabric surface smoothness. The LUFHES fabric-fabric friction test is thus a potential better method to evaluate fabric geometrical roughness characteristics and differentiate fabric surface friction properties.

Chapter 8 Conclusions and future work

8.1 Conclusions

This is the first systematic study of fabric measurement in Leeds University Fabric Handle Evaluation System (LUFHES), it was found that the unique fabric low-stress mechanical properties obtained in the LUFHES such as shear and buckling properties of fabric shells as well as fabric-fabric self-friction property, have revealed insightful information of fabric deformation processes which have hardly been disclosed before. This information could be used to objectively discriminate fabric handle without involving subjective judgement and using standard fabrics. In comparison with the KES-F and FAST systems, fabric measurement in LUFHES is simpler, the shear, compression buckling and fabric-fabric friction results are obtained from identical specimen, fewer fabric specimen preparation is needed, and has potential to be used to evaluate fabric handle in lower cost.

The other specific conclusions on the fabric measurement in LUFHES obtained in this study are summarised below.

The effect of pre-tension on fabric shell during cyclic biaxial compression was investigated. It was found that pre-tensions applied on fabric shells stiffened fabric structure, which was quantified by using the fabric compression buckling Young's modulus. For most of woven, knitted and nonwoven fabrics, the compression buckling Young's modulus (E_1 , E_2 , E_4 and E_5) during fabric shell buckling and recovery processes increased linearly with the increase of pre-tension forces.

The energies consumed to buckle and recover fabric shells changed with the increases of pre-tension applied on fabric shells. Greater pre-tensions lead to greater energy consumptions to deform fabric shells in fabric compression buckling process (A_{1cp1} and A_1) and greater strain energy released from deformed fabric (A_2) to self-recover the elastic compression buckling deformations. Greater pre-tensions applied on fabric shells also lead to smaller energy consumptions to form recoverable (A_4) and permanent (A_3) fabric deformations during fabric shell buckling-recovery process.

The pre-tensions on fabric shells lead to fabric structural changes, which was quantified by using fabric Young's modulus, also caused the changes of energy consumptions in the fabric shell deformation process. For all of the woven fabrics, most of knitted fabrics and nonwoven fabrics tested, energies consumed to deform fabric shells in fabric compression buckling (A_{1cp1} and A_1) increased

linearly with the increase of compression buckling Young's modulus E1 and E2. While energy consumed to form permanent deformation (A3) and energy consumed to recover recoverable deformation (A4) decreased initially with the increase of the compression buckling Young's modulus E4 and E5, respectively. But when modulus E4 and E5 reached a specific value, energy A3 and A4 decreased hardly or slowly with the increases of modulus.

Suitable pre-tensions for the LUFHES fabric shell compression buckling tests for a wide range of woven, knitted and nonwoven fabrics were found in the range of 1.2N/m to 2.0N/m. When pre-tension in this range was applied on fabric shells, their energy consumption and Young's modulus did not have abrupt changes.

Fabric shear properties in the LUFHES shear test were evaluated by biaxial deformation of fabric cylindrical shells, which had same magnitude level as those obtained in both KES-F and FAST systems but had different meaning, provided a new insight into shear properties of fabric shell during biaxial deformations.

The shear modulus obtained in the LUFHES were compared with those obtained in the KES-F and FAST systems to learn about the differences between these three systems. For woven fabrics, the fabric shear modulus and shear rigidity obtained in the LUFHES and KES-F shear tests were linearly correlated ($R^2 > 0.9$). It was indicated that the comparison of fabrics by using LUFHES and KES-F tests in terms of shear modulus and shear rigidity were in good agreement. However, the shear modulus and shear rigidity obtained in the LUFHES tests were not linearly correlated with those obtained in the FAST tests. A possible reason was the insufficient shear deformations of woven fabrics in FAST test. For some fabrics (such as woven fabric W3 in this study), the extension force of 4.9N/m (which is recommended in the FAST manual) applied in bias direction in the FAST test was too small to produce apparent shear deformations required for measuring fabric shear modulus.

For knitted fabrics (except fabric K3), their shear modulus and shear rigidity obtained in the LUFHES test agreed well with those obtained in the KES-F and the FAST tests.

For nonwoven fabrics, their shear modulus and shear rigidity obtained in the LUFHES agreed well with those obtained in the FAST tests. However, for all of the nonwoven fabrics tested, there were significant differences between shear modulus/shear rigidity obtained in the LUFHES and KES-F tests, especially for the shear modulus in the MD. More importantly, the relative magnitude of shear modulus in the two fabric directions (MD and CD) obtained in the LUFHES test was a reverse to the relative magnitude of those obtained in the KES-F test.

There were two possible causes identified for this difference. The first one was the greater elongation the fabric had in the CD before its shear testing in the KES-F system, while there was a relatively smaller fabric elongation before its shear testing in the LUFHES system. Shear modulus obtained for nonwoven fabric having a greater elongation would be different from the one obtained for fabric having a smaller elongation. The second possible reason might be the different types of fabric deformations in the LUFHES shear test (biaxial fabric deformations when gauge length was fixed during testing) and KES-F shear test (unidirectional fabric deformation when gauge length varied during testing). Comparatively speaking, shear modulus obtained in the LUFHES tests were more reasonable and in agreement with the nonwoven structural characteristics (i.e. shear forces were smaller in shear test in the MD when most of fibres aligned in the MD).

Fabric buckling properties were measured in LUFHES in relation to the evaluation of fabric handle. Fabric buckling properties were different from fabric bending properties measured in the KES-F and FAST systems for evaluating fabric hand purposes. In theory, critical buckling force of a pure elastic cylindrical shell was correlated with the bending rigidity of material. However, based on the experiments of this project, such correlation between buckling and bending was found to depend on fabric types and measurement methods. It was found that critical compression buckling forces of the woven and nonwoven fabrics had good correlation with their pure bending rigidities measured in the KES-F system, and critical compression buckling forces of the knitted fabrics had good correlation with their cantilever bending rigidities measured in the FAST system. The differences between bending rigidities measured in the KES-F and FAST systems were caused by different fabric curvatures in the bending tests of these two systems.

Fabric to fabric self-friction measured in the LUFHES friction test is an important fabric property in the daily use of fabrics. Different from the LUFHES friction test, fabric surface properties were evaluated by moving metal sensors on fabric surface in KES-F surface tests. Simple models of the theoretical friction profiles for these two tests of a ripstop fabric were established. It was found that wavelengths of 7 peaks shown in FFT spectra of these two theoretical friction profiles were identical. The wavelength of the highest peak corresponded to the characteristic length of this ripstop fabric: the length between two ripstop ribs. Wavelengths of other six strong peaks corresponded to the sub-lengths of the length between two ripstop ribs, e.g. $1/2$, $1/4$, $1/5$, $1/7$, $1/10$ and $1/11$. Thus, both fabric-fabric and fabric-sensor roughness profiles were highly related to the fabric surface structure.

The experimental profiles of the ripstop fabric obtained in the LUFHES fabric-fabric friction test, KES-F fabric-sensor roughness/friction tests were analysed and compared. It was found that the LUFHES fabric-fabric friction test had better reproducibility than both KES-F fabric-metal roughness and friction tests. All wavelengths of the highest peaks in these three spectra corresponded to the characteristic length between two ripstop ribs of the ripstop fabric. That is, the fabric-fabric friction and fabric-sensor roughness/friction profiles were related to the fabric structure and in agreement with the theoretical analysis.

For other tested woven and nonwoven fabrics with different surface structures, the wavelengths of strong peaks shown in the spectra of the LUFHES fabric-fabric friction profiles agreed well with their characteristic surface structures.

Comparatively, the main fabric characteristic lengths were easier to be identified in fabric-fabric friction profiles than in fabric-sensor roughness/friction profiles. The spectra of the LUFHES friction profiles had advantages in discriminating the main fabric characteristic structures and contained less peaks at wavelengths which are related to the sub-lengths of fabric characteristic lengths.

In addition, it was found that the LUFHES fabric-fabric friction test produced a greater range of fabric friction coefficients than the KES-F fabric-sensor friction test did, this greater range of fabric friction coefficients might be helpful in differentiating fabric surface friction properties and fabric smoothness. LUFHES fabric-fabric friction test is thus a potential better method to evaluate fabric geometrical roughness characteristics and differentiate fabric surface friction properties.

8.2 Future work

The following future works are recommended to further improve the understanding of mechanical properties obtained in the LUFHES and its application in the discrimination of various fabrics:

1. Shear properties of some loosely bonded nonwoven fabric in machine direction obtained in the KES-F and the LUFHES shear tests have significant differences. It might be related to the different extension forces applied on fabrics in the KES-F and the LUFHES tests, this might produce different fabric elongations in these two testing systems. Moreover, due to gauge length in the KES-F system is not fixed but it is fixed in the LUFHES shear test, fabric might have different deformations in these two testing processes. Therefore further investigation is required to clarify the fabric deformations and property changes in this situation;
2. It is recommended to systematically investigate the influences of extension force on fabric shear property and corresponding fabric extension/shear

deformations in both the KES-F and the LUFHES tests, especially for loosely bonded knitted fabrics and nonwoven fabrics;

3. Fabric cylindrical shell is extended biaxially in the LUFHES shell twist test and the LUFHES extension test. Fabric plate is extended unidirectionally in the FAST and the KES-F tests. It is recommended to investigate the difference between these tensile testing systems and identify their difference in discriminating fabrics;
4. It was found that fabric-fabric self-friction test in the LUFHES friction test is highly related to fabric surface structure (the wavelengths in spectrum of fabric-fabric friction profile) of woven and nonwoven fabric. But knitted fabric has special loop structures on its surface, so it is recommended to investigate the relationship between fabric-fabric friction profile of knitted fabric and its loop structure;
5. Fabric-fabric friction test it is a potential method to evaluate fabric roughness. Therefore the relationship between parameters obtained in the fabric-fabric self-friction (e.g. the amplitudes in spectrum of fabric-fabric friction profile) and fabric roughness needs to be established;
6. It is recommended to conduct subjective assessments of various fabrics, and find out the relationship between subjective assessment results and fabric mechanical properties and energy consumption obtained in the LUFHES to see how the system could be used in fabric discriminations.

List of References

- Abbott, G.M., Grosberg, P. and Leaf, G.A.V. 1973. The Elastic Resistance to Bending of Plain-Woven Fabrics. *Journal of The Textile Institute*. **64**(6), pp.346-362.
- Afroz, F. and Siddika, A. 2014. Effect of warp yarn tension on crimp% in woven fabric. *European Scientific Journal*. **10**, pp.202-207.
- Ajayi, J.O. 1992a. Effects of Fabric Structure on Frictional Properties. *Textile Research Journal*. **62**(2), pp.87-93.
- Ajayi, J.O. 1992b. Fabric Smoothness, Friction, and Handle. *Textile Research Journal*. **62**(1), pp.52-59.
- Akgun, M. 2014. Assessment of the surface roughness of cotton fabrics through different yarn and fabric structural properties. *Fibers and Polymers*. **15**(2), pp.405-413.
- Alley, J. 1978. *Nozzle extraction process and handlemeter for measuring handle*. US Patent 4103550.
- Ancutiene, K., Strazdiene, E. and Nesterova, A. 2010. The relationship between fabrics bending rigidity parameters defined by KES-F and FAST equipment. *Materials Science*. **16**(4), pp.346-352.
- Arens, E. and Zhang, H. 2006. *Thermal and Moisture Transport in Fibrous Materials*. Cambridge: Woodhead Publishing.
- AWTA, L. *Wool comfort and handle*. [Online]. [Accessed 14/06]. Available from: <http://www.woolcomfortandhandle.com/index.php>
- Behera, B.K. and Hari, P.K. 1994. Fabric quality evaluation by objective measurement. *Indian Journal of Fibre & Textile Research*. **19**, pp.168-171.
- Behera, B.K. and Hari, P.K. 2010. *Woven textile structure: theory and applications*. Cambridge: Woodhead Publishing.
- Behera, B.K., Militky, J., Mishra, R. and Kremenakova, D. 2012. *Woven fabrics*. Croatia: InTech.
- Behery, H.M. 1986. Comparison of Fabric Hand Assessment in the United States and Japan. *Textile Research Journal*. **56**(4), pp.227-240.
- Behery, H.M. 2005. *Effect of Mechanical and Physical Properties on Fabric Hand*. North America by CRC Press LLC: Woodhead Publishing Limited in Association with the Textile Institute.
- Bensaid, S., Osselin, J.F., Schacher, L. and Adolphe, D. 2006. The effect of pattern construction on the tactile feeling evaluated through sensory analysis. *Journal of the Textile Institute*. **97**(2), pp.137-145.

- Bertaux, E., Lewandowski, M. and Derler, S. 2007. Relationship between Friction and Tactile Properties for Woven and Knitted Fabrics. *Textile Research Journal*. **77**(6), pp.387-396.
- Bishop, D.P. 1996. Fabrics: Sensory and Mechanical Properties. *Textile Progress*. **26**(3), pp.1-62.
- Bowden, F.P. and Tabor, D. 1954. *Friction and Lubrication of Solids*. Oxford: Clarendon Press.
- Bowden, F.P. and Tabor, D. 1973. *Friction: An Introduction to Tribology*. New York: Anchor Press.
- Brand, R.H. 1964. Measurement of Fabric Aesthetics: Analysis of Aesthetic Components. *Textile Research Journal*. **34**(9), pp.791-804.
- Brenner, F.C. and Chen, C.S. 1964. Mechanical behavior of fabrics part iii: effect of density of construction on recovery from deformation. *Textile Research Journal*. **35**(7), pp.587-591.
- Bueno, M., Pourdeyhimi, B. and Maze, B. 2008. *Structure and mechanics of textile fibre assemblies*. USA: CRC Press LLC.
- Bueno, M.A., Durand, B. and Renner, M. 1999. Non-contact Measurements of Sanding and Raising Effects. *Textile Research Journal*. **69**(8), pp.570-575.
- Bueno, M.A., Durand, B. and Renner, M. 2000. A Non-contact Measurement of The Roughness of Textile Fabrics. *Experimental Techniques*. **24**(2), pp.23-27.
- Bueno, M.A., Durand, B. and Renner, M. 2000. Optical characterization of the state of fabric surfaces. *Optical Engineering*. **39**(6), pp.1697-1703.
- Caliman, R. 2016. Friction behaviour of aluminium composites mixed with carbon fibers with different orientations. *IOP Conference Series: Materials Science and Engineering*. **145**, p022035.
- Carr, W.W., Posey, J.E. and Tincher, W.C. 1988. Frictional characteristics of apparel fabrics. *Textile Research Journal*. **58**, pp.129-136.
- Chandramouli, P.N. 2012. *Fundamentals of Strength of Materials*. India: Prentice-Hall of India Pvt.Ltd.
- Chattopadhyay, R. 2008. Design of Apparel Fabrics: Role of fibre, yarn and fabric parameters on its functional attributes. *Journal of Textile Engineering*. **54**(6), pp.179-190.
- Cornelissen, B., Rietman, B. and Akkerman, R. 2013. Frictional behaviour of high performance fibrous tows: Friction experiments. *Composites Part A: Applied Science and Manufacturing*. **44**, pp.95-104.
- Costanzo, L.S. 2009. *Physiology*. Philadelphia: Elsevier Health Sciences.

- Craig, K. 2016. *Time Domain & Frequency Domain*. [Online]. [Accessed 22/01]. Available from: <https://www.scribd.com/document/78630439/Time-Domain-Frequency-Domain>
- Dahlberg, B. 1961. Part II: Buckling. *Textile Research Journal*. **31**(2), pp.94-99.
- David, H.G., Stearn, A.E. and Denby, E.F. 1985. The subjective assessment of handle. In: *Third Japan-Australis Symposium on Objective Measurement: Applications to Product design and Process Control, Kyoto*. Textile machinery Society of Japan, pp.527-536.
- De Boos, A. and Tester, D. 1994. *Siro FAST-A system for fabric objective measurement and its applicatio in fabric and garment manufacture*. CSIRO.
- Derler, S., Gerhardt, L.C., Lenz, A., Bertaux, E. and Hadad, M. 2009. Friction of human skin against smooth and rough glass as a function of the contact pressure. *Tribology International*. **42**(11-12), pp.1565-1574.
- Ellis, B.C. and Garnsworthy, R.K. 1980. A Review of Techniques for the Assessment of Hand. *Textile Research Journal*. **50**(4), pp.231-238.
- Gere, J.M. and Timoshenko, S.P. 1997. *Mechanics of Materials*. PWS Publishing Company.
- Gibson, V.L. and Postle, R. 1978. An Analysis of the Bending and Shear Properties of woven, double-knitted, and warp-knitted outerwear fabrics. *Textile Research Journal*. **48**, pp.14-27.
- Glaser, R. and Caccese, V. 2014. Experimental determination of shear properties, buckling resistance and diagonal tension field of polyurethane coated nylon fabric. *The Journal of The Textile Institute*. **105**(9), pp.980-997.
- Grosberg, P. 1966. The Mechanical Properties of Woven Fabrics Part II: The Bending of Woven Fabrics. *Textile Research Journal*. **36**(3), pp.205-211.
- Grosberg, P. and Park, B.J. 1966. The Mechanical Properties of Woven Fabrics: Part V: The Initial Modulus and the Frictional Restraint in shearing of Plain Weave Fabrics. *Textile Research Journal*. **36**(5), pp.420-431.
- Grosberg, P. and Swani, N.M. 1966a. The Mechanical Properties of Woven Fabrics: Part III: The Buckling of Woven Fabrics. *Textile Research Journal*. **36**(4), pp.332-338.
- Grosberg, P. and Swani, N.M. 1966b. The mechanical properties of woven fabrics. Part IV: the determination of the bending rigidity and frictional restraint in woven fabrics. *Textile Research Journal*. **36**(4), pp.338-345.
- Grover, G., Sultan, M.A. and Spivak, S.M. 1993. A Screening Technique for Fabric Handle. *Journal of the Textile Institute*. **84**(3), pp.486-494.

Gruener, G. 2011. *Method and device for determining the softness of sanitary papers and textiles*. US Patent 8082791.

Gupta, B.S. 2008. *Friction in Textile Materials*. North America: CRC Press LLC.

Gürdal, Z., Haftka, T.R. and Hajela, P. 1999. *Design and optimization of laminated composite materials* New York: Wiley.

Guyton, A.C. and Hall, J.E. 2000. *Textbook of Medical Physiology* Philadelphia: Elsevier/Saunders.

Hearle, J.W.S. and Shanahan, W.J. 1978. An Energy Method for Calculations in Fabric Mechanics Part I: Principles of the Method. *The Journal of The Textile Institute*. **69**(4), pp.81-91.

Hendriks, C.P. and Franklin, S.E. 2009. Influence of Surface Roughness, Material and Climate Conditions on the Friction of Human Skin. *Tribology Letters*. **37**(2), pp.361-373.

Hosseini Ravandi, S.A., Toriumi, K. and Matsumoto, Y. 1994. Spectral Analysis of the Stick-Slip Motion of Dynamic Friction in the Fabric Surface. *Textile Research Journal*. **64**(4), pp.224-229.

Howell, H.G. 1953. The general case of friction of a string round a cylinder. *Journal of The Textile Institute*. **44**, pp.359-362.

Howell, H.G., Mieszkis, K.W. and Tabor, D. 1959. *Friction in Textiles*. London: Butterworths Scientific Publications.

Howorth, W.S. 1964. The Handle of Suiting, Lingerie, and Dress Fabrics. *Journal of the Textile Institute Transactions*. **55**(4), pp.T251-T260.

Howorth, W.S. and Oliver, P.H. 1958. The Application of Multiple Factor Analysis to the Assessment of Fabric Handle. *Journal of the Textile Institute Transactions*. **49**(11), pp.T540-T553.

Hu, J.L. 2000. *Structure and mechanics of woven fabrics*. Cambridge: Woodhead Publishing.

Hu, J.L., Xin, B.J. and Yan, H.J. 2002. Classifying Fleece Fabric Appearance by Extended Morphological Fractal Analysis. *Textile Research Journal*. **72**(10), pp.879-884.

Hu, J.Y., Hes, L., Li, Y., Yeung, K.W. and Yao, B.G. 2006. Fabric Touch Tester: Integrated evaluation of thermal–mechanical sensory properties of polymeric materials. *Polymer Testing*. **25**(8), pp.1081-1090.

Ishizawa, H., Nishimatsu, T., Kamijyo, M. and Toba, E. 2002. Measurement of surface properties of woven fabrics using optical fiber bundle. *Journal of Textile Engineering*. **48**(1), pp.5-10.

- KatoTech. 2016. *KES-F7 Thermo Labo*. [Online]. [Accessed 2016/12/01]. Available from: <http://www.english.keskato.co.jp/products/kes-f7.html>
- Kawabata, S. 1980. *The Standardization and Analysis of Hand Evaluation*. Textile Machinery Society of Japan.
- Kawabata, S. 1982. *The development of the objective measurement of fabric handle*. Kyoto: Textile Machinery Society of Japan.
- KES-F Manual.
- Kilby, W.F. 1963. Planar Stress–Strain Relationships in Woven Fabrics. *Journal of the Textile Institute Transactions*. **54**(1), pp.T9-T27.
- Kilinc-Balci, F.S. 2011. *Improving comfort in clothing*. Cambridge, UK: Woodhead Publishing Limited in association with The Textile Institute.
- Kim, J.O. and Slaten, B.L. 1999. Objective Evaluation of Fabric Hand: Part I: Relationships of Fabric Hand by the Extraction Method and Related Physical and Surface Properties. *Textile Research Journal*. **69**(1), pp.59-67.
- Leaf, G.A.V. and Sheta, A. 1984. The Initial Shear Modulus of Plain-Woven Fabrics. *Journal of the Textile Institute*. **75**(3), pp.157-163.
- Leckie, F.A. and Dal Bello, D.J. 2009. *Strength and stiffness of engineering systems* New York ; London Springer.
- Lee, S.M. 1995. *Dictionary of Composite Materials Technology*. Lancaster, United States: Technomic Publishing Co ,U.S. .
- Lee, Y.J. 2005. *Prediction of the clothing pressure based on the 3D shape deformation and mechanical properties of fabrics*. PhD thesis, Chungnam National University.
- Li, Y. 2001. The Science of Clothing Comfort. *Textile Progress*. **31**, pp.1-135.
- Li, Y., Jun, Y., Hu and Hes, L. 2003. *Textile fabric testing*. US Patent 6601457.
- Lincoln, B. 1952. Frictional and elastic properties of high polymeric materials. *British Journal of Applied Physics*. **3**, pp.260-263.
- Lindberg, J., Behre, B. and Dahlberg, B. 1961. Part III: Shearing and Buckling of Various Commercial Fabrics. *Textile Research Journal*. **31**(2), pp.99-122.
- Lloyd, D.W. and Leaf, G.A.V. 1990. Fabric objective assessment, handle, appearance, and quality control: some fundamental aspects. In: *The 8th International Wool Textile Research Conference, Christchurch, New Zealand*.
- Lord, P.R., Radhakrishnaiah, P. and Grove, G. 1988. Assessment of the Tactile Properties of Woven Fabrics Made from Various Types of Staple-fibre Yarn. *Journal of the Textile Institute*. **79**(1), pp.32-52.

LUFHES Software.

Ly, N.G., Tester, D.H., Buckenham, P., Roczniok, A.F., Adriaansen, A.L., Scaysbrook, F. and De Jong, S. 1991. Simple Instruments for Quality Control by Finishers and Tailors. *Textile Research Journal*. **61**(7), pp.402-406.

Mao, N. 2014. Towards objective discrimination & evaluation of fabric tactile properties: Quantification of biaxial fabric deformations by using energy methods. In: *Proceedings of 14th AUTEX World Textile Conference, Bursa, Turkey*.

Mao, N. and Taylor, M. 2012. *Evaluation apparatus and method*. WO Patent 2012/104627.

Mao, N., Wang, Y. and Qu, J. 2016. Smoothness and roughness: characteristics of fabrics-to-fabric self-friction properties. In: *The 90th textile institute world conference, Poznan, Poland*.

Minazio, G.P. 1995. FAST-fabric assurance by simple testing. *International Journal of Clothing Science and Technology*. **7**, pp.43-48.

Mooneghi, S.A., Saharkhiz, S. and Varkiani, S.M.H. 2014. Surface Roughness Evaluation of Textile Fabrics: A Literature Review. *Journal of Engineered Fibers and Fabrics*. **9**(2), pp.1-18.

Olympus. 2016. *Roughness (2D) parameter*. [Online]. [Accessed 22/02]. Available from: http://www.olympus-ims.com/en/knowledge/metrology/roughness/2d_parameter/

Pan, N. 2006. *System and method for fabric hand evaluation*. US patent 2006/0036410

Pan, N. and Yen, C.K. 1992. Physical Interpretations of Curves Obtained through the Fabric Extraction Process for Handle measurement. *Textile Research Journal*. **62**, pp.279-290.

Pan, N., Zeronian, H.S. and Ryu, H.S. 1993. An Alternative Approach to the Objective Measurement of Fabrics. *Textile Research Journal*. **63**(1), pp.33-43.

Pan, N., C.K., Y., T.S., Z. and S., Y.R. 1988. A new approach to the objective evaluation of fabric handle from mechanical properties I: Objective measure for total handle. *Textile Research Journal*. **58**, pp.438-444.

Peirce, F.T. 1930. The "Handle" of Cloth as a Measurable Quantity. *Journal of the Textile Institute Transactions*. **21**(9), pp.T377-T416.

Phabrometer. [Online]. [Accessed 02/07]. Available from: <http://www.phabrometer.com/>

Pimenidis, M.Z. 2009. *The Neurobiology of Orthodontics*. Springer-Verlag Berlin Heidelberg.

Pritchard, T.C. and Alloway, K.D. 1999. *Medical Neuroscience*. Hayes Barton Press.

Purves, D., Augustine, G. and Fitzpatrick, D. 2001. *Neuroscience*. Sunderland: Sinauer Associates.

Ramgulam, R.B., Amirbayat, J. and Porat, I. 1993. Measurement of Fabric Roughness by a Non- contact Method. *Journal of the Textile Institute*. **84**(1), pp.99-106.

Schacher, L., Bensaid, S., Jeguirim, S.E.-G. and Adolphe, D. 2011. *Advances in Modern Woven Fabrics Technology*. Croatia: InTech.

Shanahan, W.J. and Hearle, J.W.S. 1978. An Energy Method for Calculations in Fabric Mechanics Part II: Examples of Application of the Method to Woven Fabrics. *The Journal of The Textile Institute*. **69**(4), pp.92-100.

Siddiqi, Z.A. 2014. *Mechanics of materials*. Lahore, Pakistan: Help Civil Engineering Publisher.

Stockbridge, H.C.W., Kenchington, K.W.L., Corkindale, K.G. and Greenland, J. 1957. The Subjective Assessment of the Roughness of Fabrics. *Journal of the Textile Institute Transactions*. **48**(1), pp.T26-T34.

Sul, I.H., Hong, K.H., Shim, H. and Kang, T.J. 2006. Surface Roughness Measurement of Nonwovens Using Three-dimensional Profile Data. *Textile Research Journal*. **76**(11), pp.828-834.

Sular, V. and Okur, A. 2008. Handle evaluation of men's suitings produced in Turkey. *Fibres and Textiles in Eastern Europe*. **16**(2), pp.61-67.

Tokmak, O., Berkalp, B., Omer and Gersak, J. 2010. Investigation of the Mechanics and Performance of Woven Fabrics Using Objective Evaluation Techniques. Part I: The relationship between FAST, KES-F and Cusick's Drape-Meter Parameters. *Fibres and Textiles in Eastern Europe*. **18**, pp.55-59.

Tomlinson, S.E., Lewis, R. and Carré, M.J. 2009. The effect of normal force and roughness on friction in human finger contact. *Wear*. **267**(5-8), pp.1311-1318.

The TSA and its triumph in the tissue industry. 2012. [Online]. [Accessed 24/02]. Available from: <https://www.emtec-papertest.de/en/the-tsa-and-its-triumph-in-the-tissue-industry.html>

Vassiliadis, S.G. and Provatidis, C.G. 2004. Structural characterization of textile fabrics using surface roughness data. *Internation Journal of Clothing Science and Technology*. **16**(6), pp.445-457.

Vinson, R.J. 1989. *The Behavior of Thin Walled Structures: Beams, Plates, and Shells*. Dordrecht ; London Kluwer Academic.

Wang, X., Liu, X. and Hurren, C. 2008. *Fabric testing*. Cambridge: Woodhead Publishing.

Warwick, D., Dunn, R., Melikyan, E. and Vadher, J. 2009. *Hand Surgery*. Oxford: Oxford University Press.

Wauer, R.M. 1965. Consumers' and home economists' fabric descriptions. *Journal of Home Economics*. **57**(1), pp.33-35.

Wright, D. 2005. *Note on Design and Analysis of Machine Elements*.

Yick, k.L., Cheng, K.P.S., Dhingra, R.C. and How, Y.L. 1996. Comparison of Mechanical Properties of Shirting Materials measured on the KES-F and FAST instruments. *Textile Research Journal*. **66**(10), pp.622-633.

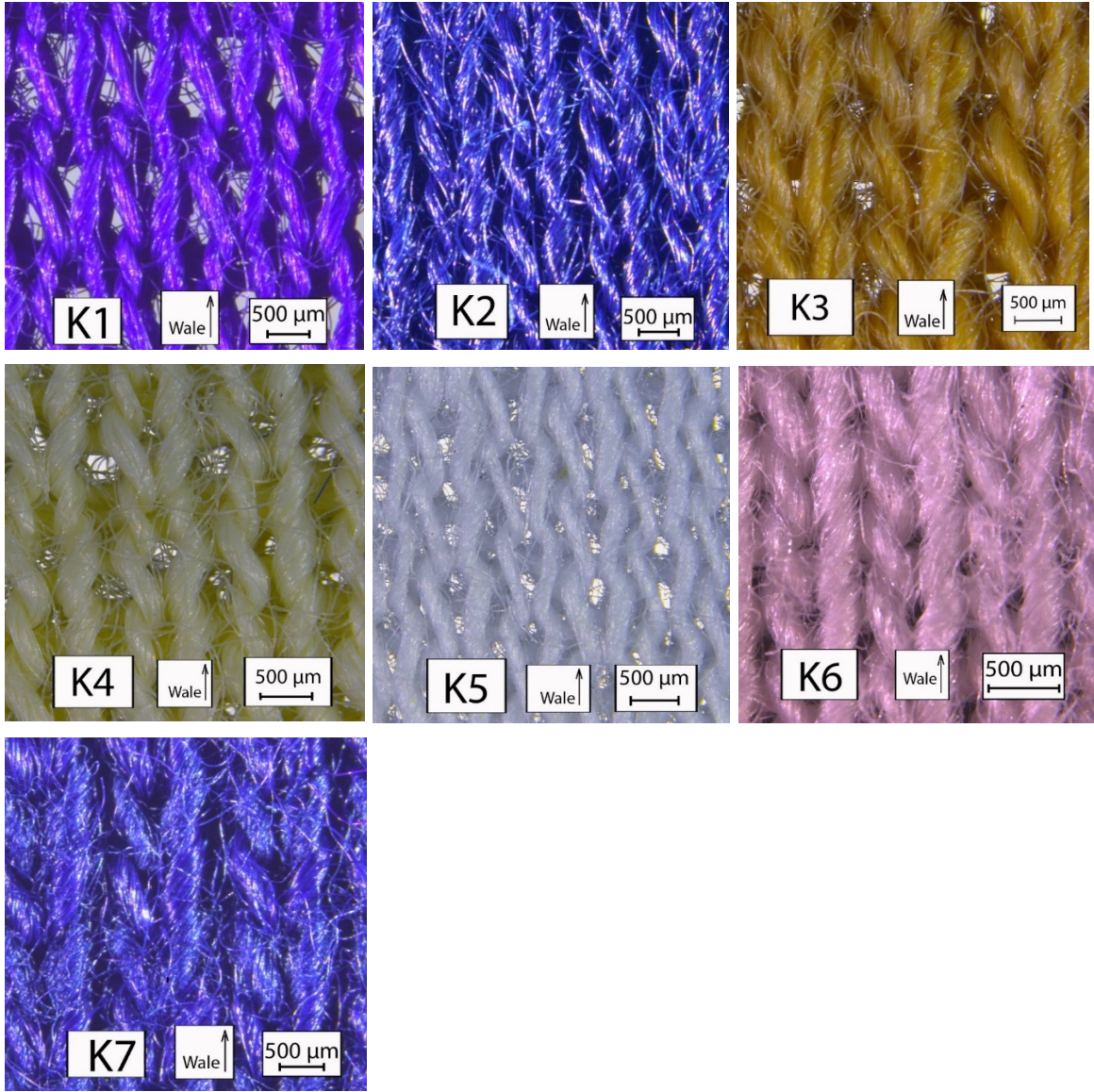
Young, C.W. and Budynas, G.R. 2002. *Roark's formulas for stress and strain*. United States of America: McGraw Hill.

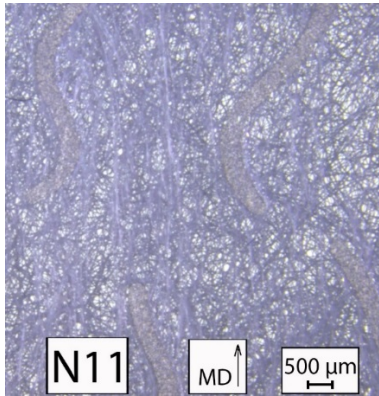
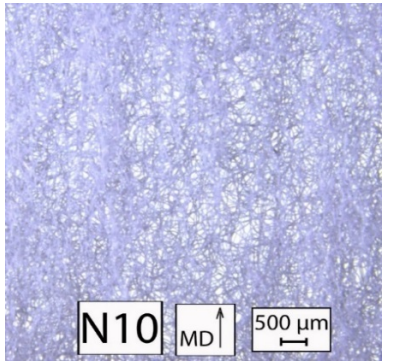
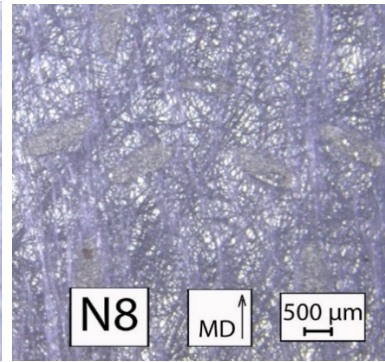
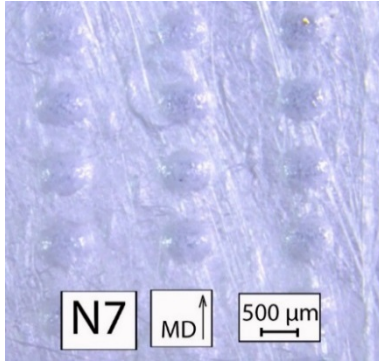
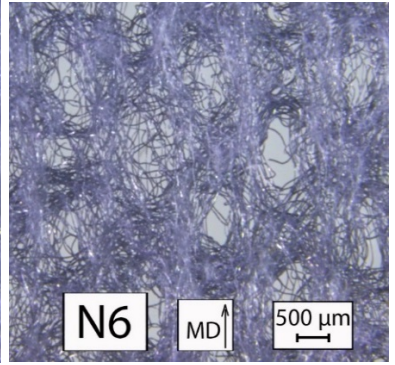
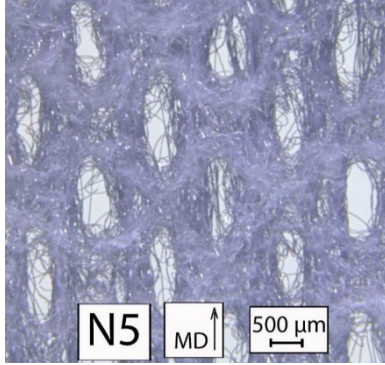
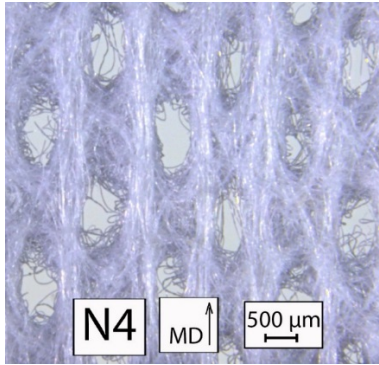
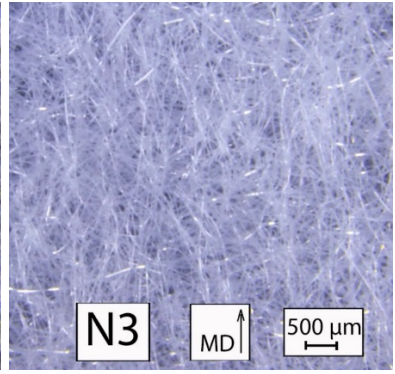
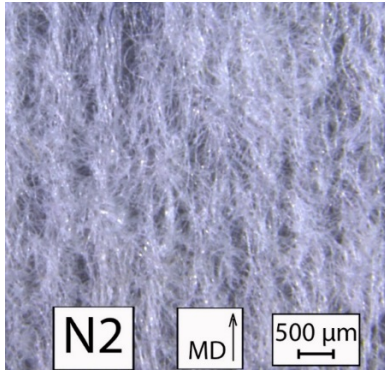
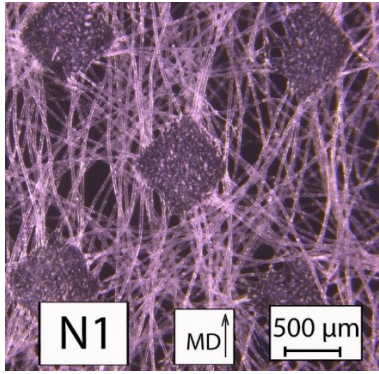
Zahidul. 2011. Textile. [Online]. [Accessed 2015/07/21]. Available from: <http://zahidul-hoque.blogspot.co.uk/2011/05/v-behaviorurldefaultvml.html>

Zhou, J., Li, Y., Lam, J. and Cao, X. 2010. The Poisson Ratio and Modulus of Elastic Knitted Fabrics. *Textile Research Journal*. **80**, pp.1965-1969.

Appendix A Fabric material







Appendix B Theoretical analysis of fabric friction profile between fabric and fabric surfaces of a ripstop fabric

B.1 Model of fabric friction when ripstop strip against ripstop strip

According to the structure of ripstop fabric, it is known that the ripstop strip (R) contains three weft yarns, and one loop of flat strip (F) also contains three weft yarns. During friction between fabric and fabric, these three weft yarns of bottom fabric are marked as X, Y and Z, and the three weft yarns of top fabric are marked as X', Y' and Z'. The positions of three yarns are shown in Figure B. 1 as an example.

In a unit cell of a ripstop strip (R) containing three weft yarns, X, Y and Z (Figure B. 1), the friction force produced by each of the three yarns are established, respectively, then they are added up to obtain the total friction force produced by the ripstop strip (R).

During the fabric-fabric friction test for two ripstop strips against each other, one ripstop strip moves on top of the bottom layer ripstop strip which is a flip over of the top layer ripstop strip. Because of the flip over of the bottom layer ripstop strip, the structure of yarn X of bottom layer fabric is the same as the structure of yarn Z' of the top layer fabric (see Figure B. 1).



Structure of bottom layer ripstop strip

Structure of top layer ripstop strip

Figure B. 1 Yarn structure of bottom layer fabric and top layer fabric

The relationship between three weft yarns of top layer ripstop strip and bottom layer ripstop strip can be illustrated in Figure B. 2

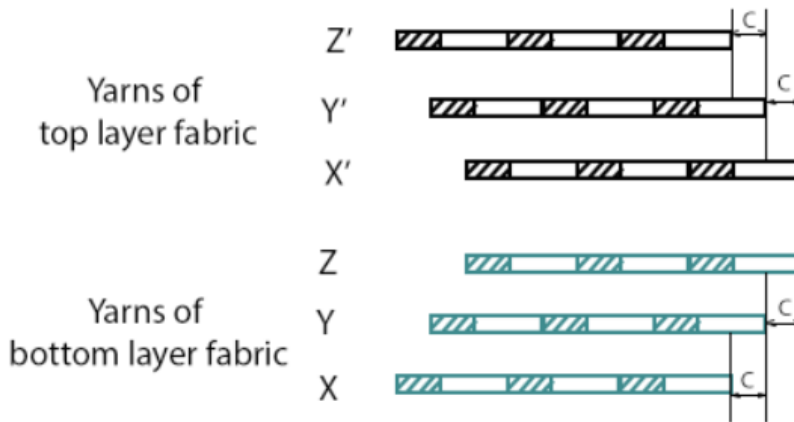


Figure B. 2 Yarns of top layer fabric and bottom layer fabric

When top and bottom ripstop strips (R in Figure 7.2) fully contact, and the yarn X of bottom layer and yarn X' of top layer contact at the start position (Figure B. 3), The positions of yarns Y-Y' and yarns Z-Z' at the starting point are shown below:

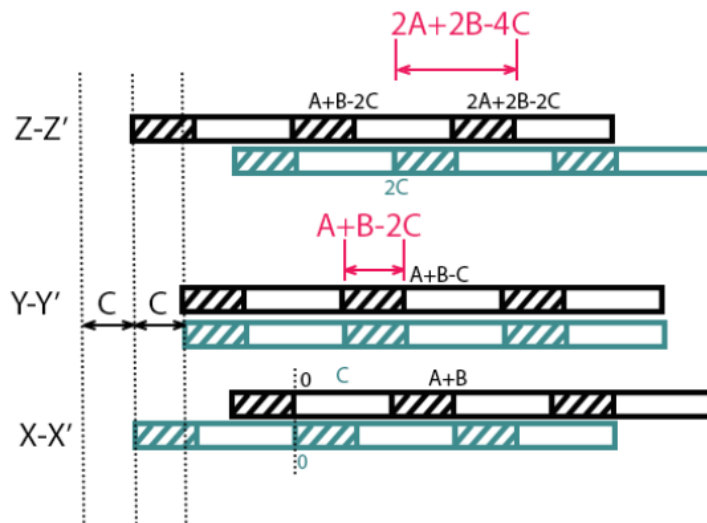


Figure B. 3 Location relationship between yarns X-X', Y-Y' and Z-Z' at the starting point in LUFHES friction test.

B.1.1 Friction force produced by the yarn X of bottom layer and yarn X' of top layer fabric

As shown in Figure 7.2, a weft yarn in ripstop strip (R) contains three loops of 1/2 twill structure. The friction model of yarn X of bottom layer and yarn X' of top layer is shown in Figure B. 4. Each weft yarn unit cell has three loops of 1/2 weave structure, these loops move together and simultaneously, so the total friction force of this pair of yarns is three times of the friction force produced by any one unit. A

complete process (3A+3B) contains 3 same repeats, displacement for each repeat is A+B, and only friction of one loop is discussed below.



Figure B. 4 Friction model of yarn X-X' at starting point

The model of one loop of the top fabric moves against the bottom fabric in the starting position is simplified in Figure B. 5 below:



Figure B. 5 Model of one loop of the top yarn moves against the bottom yarn in the starting position.

The friction force produced by the warp yarn part and weft yarn part of one loop of yarn X' of top layer fabric is analysed, respectively.

Weft yarn part

The friction force generated by the movement of the weft part of X', F₁, is the sum of the friction forces generated in both the contact area between the top weft yarn part and bottom warp/weft yarn parts, the contact area A_x changes with the relative displacement of S,

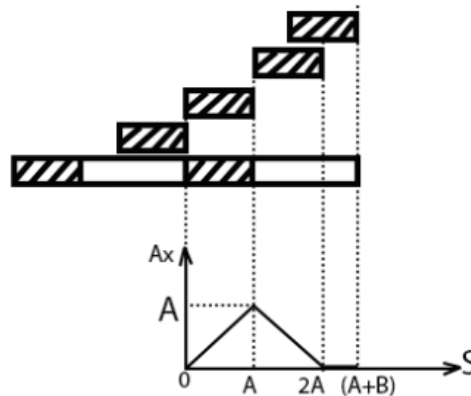


Figure B. 6 Changes of Ax with the relative displacement

We thus have

$$F_1 = PAD \frac{A_x}{A} \mu_3 + PAD \frac{A-A_x}{A} \mu_2 = PDA_x \mu_3 + PD(A-A_x) \mu_2 \dots \dots \dots (B. 1)$$

Where

$$A_x = \begin{cases} S & (0 \leq S < A) \\ -S + 2A & (A \leq S < 2A) \\ 0 & (2A \leq S \leq A + B) \end{cases} \dots \dots \dots (B. 2)$$

Substitute A_x into the equation of F_1 , we have:

$$F_1 = \begin{cases} PDS\mu_3 + PD(A - S)\mu_2 & (0 \leq S < A) \\ PD(2A - S)\mu_3 + PD(S - A)\mu_2 & (A \leq S < 2A) \dots\dots\dots (B. 3) \\ PDA\mu_2 & (2A \leq S \leq A + B) \end{cases}$$

Warp yarn part:

Similar to the analysis of the friction produced by the weft yarn part, the friction force generated by the movement of warp yarn part of top yarn is shown in Figure B. 7, and can be obtained in equations below,

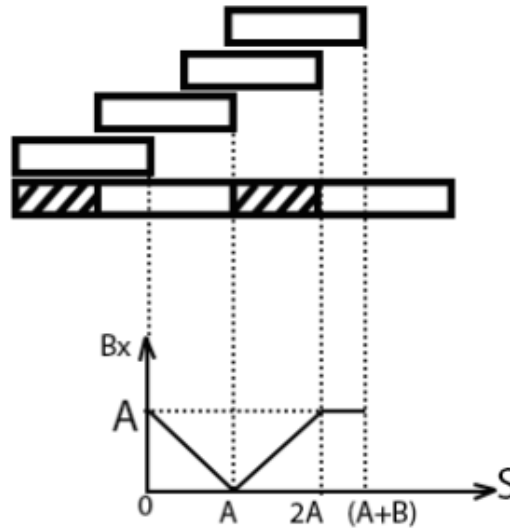


Figure B. 7 Changes of B_x as the relative displacement

$$F_2 = PBD \frac{B_x}{B} \mu_2 + PBD \frac{B - B_x}{B} \mu_1 = PDB_x \mu_2 + PD(B - B_x) \mu_1 \dots\dots\dots (B. 4)$$

Where

$$B_x = \begin{cases} -S + A & (0 \leq S < A) \\ S - A & (A \leq S < 2A) \dots\dots\dots (B. 5) \\ A & (2A \leq S \leq A + B) \end{cases}$$

Substitute B_x into the equation of F_2 :

$$F_2 = \begin{cases} PD(A - S)\mu_2 + PD(B + S - A)\mu_1 & (0 \leq S < A) \\ PD(S - A)\mu_2 + PD(B + A - S)\mu_1 & (A \leq S < 2A) \dots\dots\dots (B. 6) \\ PDA\mu_2 + PD(B - A)\mu_1 & (2A \leq S \leq A + B) \end{cases}$$

Therefore, the friction force produced by one loop structure of yarn X' of top layer moves against yarn X of bottom layer is a sum of F_1 and F_2 ,

$$F_x = F_1 + F_2 = \begin{cases} PDS\mu_3 + 2PD(A - S)\mu_2 + PD(B + S - A)\mu_1 & (0 \leq S < A) \\ PD(2A - S)\mu_3 + 2PD(S - A)\mu_2 + PD(B + A - S)\mu_1 & (A \leq S < 2A) \dots\dots (B. 7) \\ 2PDA\mu_2 + PD(B - A)\mu_1 & (2A \leq S \leq A + B) \end{cases}$$

B.1.2 Friction force produced by the yarn Y and Z of bottom layer fabric and yarn Y' and Z' of top layer fabric

It is learned from Figure B. 3 that the pair of yarns Y-Y' is away from the start position for A+B-2C, and the pair of yarns Z-Z' is away from the start position for 2A+2B-4C when the pair of yarn X-X' is at the start position.

The equation for the friction force generated by the movement of yarns Y-Y' at the same time as movement of yarns X-X' could be obtained by left shifting the S for a distance of (A+B-2C) in the equation B.7. Similarly, the equation for the friction force generated by movement of yarns Z-Z' at the same time as movement of yarns X-X' could be obtained by left shifting the S for a distance of (2A+2B-4C) in the equation B.7. The friction force generated by movement of yarns Y-Y' and movement of yarns Z-Z', F_y and F_z, are shown in equations B.8 and B.9 below.

$$F_y = \begin{cases} PD(A + 2C - B - S)\mu_3 + 2PD(B - 2C + S)\mu_2 + PD(2C - S)\mu_1 & (0 \leq S < A + 2C - B) \\ 2PDA\mu_2 + PD(B - A)\mu_1 & (A + 2C - B \leq S < 2C) \\ PD(S - 2C)\mu_3 + 2PD(A + 2C - S)\mu_2 + PD(B + S - A - 2C)\mu_1 & (2C \leq S \leq A + 2C) \\ PD(2A - S + 2C)\mu_3 + 2PD(S - 2C - A)\mu_2 + PD(B + A + 2C - S)\mu_1 & (A + 2C \leq S \leq A + B) \end{cases} \dots\dots\dots (B. 8)$$

$$F_z = \begin{cases} 2PDA\mu_2 + PD(B - A)\mu_1 & (0 \leq S < 4C - A - B) \\ PD(A + B + S - 4C)\mu_3 + 2PD(4C - B - S)\mu_2 + PD(2B + S - 4C)\mu_1 & (4C - A - B \leq S < 4C - B) \\ PD(A + 4C - B - S)\mu_3 + 2PD(B + S - 4C)\mu_2 + PD(4C - S)\mu_1 & (4C - B \leq S < A + 4C - B) \\ 2PDA\mu_2 + PD(B - A)\mu_1 & (A + 4C - B \leq S \leq A + B) \end{cases} \dots\dots\dots (B. 9)$$

Therefore, the friction force produced by one loop of top yarn moves against one loop of bottom yarn, F, a sum of the friction forces generated by the movement between yarns X-X', Y-Y' Z-Z', F_x, F_y and F_z, is shown below.

$$F_x + F_y + F_z = \begin{cases} PD(A + 2C - B)\mu_3 + 2PD(2A + B - 2C)\mu_2 + PD(2B + 2C - 2A)\mu_1 & (0 \leq S < 4C - A - B) \\ PD(2A + S - 2C)\mu_3 + 2PD(A + 2C - S)\mu_2 + PD(3B + S - A - 2C)\mu_1 & (4C - A - B \leq S < A + 2C - B) \\ PD(A + B + 2S - 4C)\mu_3 + 2PD(2A - B + 4C - 2S)\mu_2 + PD(4B + 2S - 4C - 2A)\mu_1 & (A + 2C - B \leq S < A) \\ PD(3A + B - 4C)\mu_3 + 2PD(4C - B)\mu_2 + PD(4B - 4C)\mu_1 & (A \leq S < 4C - B) \\ PD(3A + 4C - B - 2S)\mu_3 + 2PD(B + 2S - 4C)\mu_2 + PD(2B + 4C - 2S)\mu_1 & (4C - B \leq S < 2C) \\ PD(3A + 2C - B - S)\mu_3 + 2PD(B + S - 2C)\mu_2 + PD(2B + 2C - S)\mu_1 & (2C \leq S < 2A) \\ PD(A + 2C - B)\mu_3 + 2PD(B + 2A - 2C)\mu_2 + PD(2B + 2C - 2A)\mu_1 & (2A \leq S < A + 4C - B) \\ PD(S - 2C)\mu_3 + 2PD(3A + 2C - S)\mu_2 + PD(3B + S - 3A - 2C)\mu_1 & (A + 4C - B \leq S < A + 2C) \\ PD(2A + 2C - S)\mu_3 + 2PD(A + S - 2C)\mu_2 + PD(3B + 2C - A - S)\mu_1 & (A + 2C \leq S \leq A + B) \end{cases} \dots\dots\dots (B. 10)$$

Because each top yarn contains identical 3 pairs of warp-weft cross points, the friction force produced by three yarns in one loop ($0 \leq S < A + B$) of the ripstop strip, $F_{\text{ripstop-strip}}$, is shown in equation B.11 below,

$$\begin{aligned}
 F &= 3 \times (F_X + F_Y + F_Z) \\
 &= \begin{cases} 3PD(A + 2C - B)\mu_3 + 6PD(2A + B - 2C)\mu_2 + 3PD(2B + 2C - 2A)\mu_1 & (0 \leq S < 4C - A - B) \\ 3PD(2A + S - 2C)\mu_3 + 6PD(A + 2C - S)\mu_2 + 3PD(3B + S - A - 2C)\mu_1 & (4C - A - B \leq S < A + 2C - B) \\ 3PD(A + B + 2S - 4C)\mu_3 + 6PD(2A - B + 4C - 2S)\mu_2 + 3PD(4B + 2S - 4C - 2A)\mu_1 & (A + 2C - B \leq S < A) \\ 3PD(3A + B - 4C)\mu_3 + 6PD(4C - B)\mu_2 + 3PD(4B - 4C)\mu_1 & (A \leq S < 4C - B) \\ 3PD(3A + 4C - B - 2S)\mu_3 + 6PD(B + 2S - 4C)\mu_2 + 3PD(2B + 4C - 2S)\mu_1 & (4C - B \leq S < 2C) \\ 3PD(3A + 2C - B - S)\mu_3 + 6PD(B + S - 2C)\mu_2 + 3PD(2B + 2C - S)\mu_1 & (2C \leq S < 2A) \\ 3PD(A + 2C - B)\mu_3 + 6PD(B + 2A - 2C)\mu_2 + 3PD(2B + 2C - 2A)\mu_1 & (2A \leq S < A + 4C - B) \\ 3PD(S - 2C)\mu_3 + 6PD(3A + 2C - S)\mu_2 + 3PD(3B + S - 3A - 2C)\mu_1 & (A + 4C - B \leq S < A + 2C) \\ 3PD(2A + 2C - S)\mu_3 + 6PD(A + S - 2C)\mu_2 + 3PD(3B + 2C - A - S)\mu_1 & (A + 2C \leq S \leq A + B) \end{cases}
 \end{aligned}
 \tag{B. 11}$$

The displacement for a complete movement of ripstop strip is $(3A+3B)$. The friction force produced by three yarns when $0 \leq S \leq A + B$ is shown above, the friction force in the next $A + B \leq S \leq 3A + 3B$ is two repeats of the friction in $0 \leq S \leq A + B$.

B.2 Friction between flat strip and flat strip

From the analysis of flat strip in section 7.1.1.1, it is known that the 12 weft yarns in flat strip has four loops, each loop contains 3 weft yarns. These three yarns will be discussed separately in following parts.

B.2.1 Friction force produced by the yarn X of bottom layer and yarn X' of top layer

As introduced before, the structure of F1 area is simplified as weft yarns. Therefore the yarn X in F2 area and the yarn X' on top of it when the F2 area is flipped could be represented by:

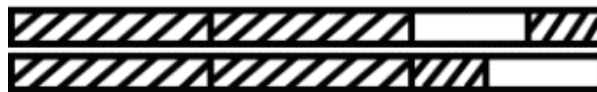


Figure B. 8 model when yarn X' of top layer flat strip moves on yarn X of bottom layer flat strip

Three structures are included in the above figure; they are defined as below:



Figure B. 9 Three structures involved in flat strip-flat strip friction (X-X')

During the friction movement, the top yarn X' moves against the fixed bottom yarn X. A complete movement could be separated into three steps shown in Figure B. 10. Displacement for each step is $A+B$.

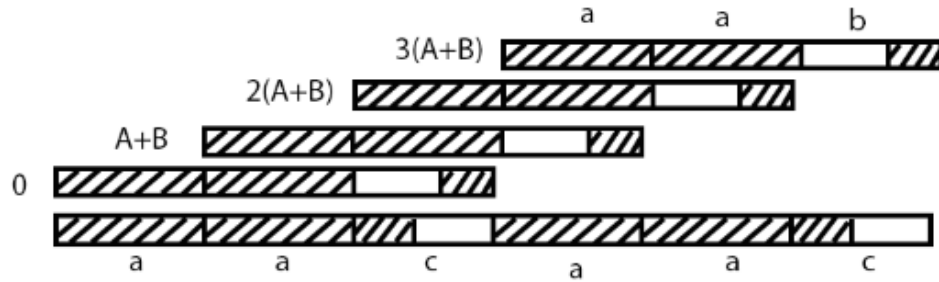


Figure B. 10 three steps when top layer flat strip moves against bottom layer of flat strip (X-X')

Top yarn has two 'a' structures and one 'b' structure, bottom yarn has two 'a' structure and one 'c' structure. During the movement, top yarn structures move against different bottom yarn structures, so they have different movements in these three steps:

Step 1 ($0 \leq S < A + B$): one 'a'(top) structure moves from 'a'(bottom) to 'a'(bottom) structure, one 'a'(top) moves from 'a'(bottom) to 'c'(bottom) structure, and one 'b'(top) structure moves from 'c'(bottom) to 'a'(bottom) structure.

Step 2 ($A + B \leq S < 2A + 2B$): one 'a'(top) moves from 'a'(bottom) to 'c'(bottom) structure, one 'a'(top) moves from 'c'(bottom) to 'a'(bottom) structure, and one 'b'(top) structure moves from 'a'(bottom) to 'a'(bottom) structure.

Step 3 ($2A + 2B \leq S \leq 3A + 3B$): 'a'(top) structure moves from 'a'(bottom) to 'a'(bottom) structure, one 'a'(top) moves from 'c'(bottom) to 'a'(bottom) structure, and one 'b'(top) structure moves from 'a'(bottom) to 'c'(bottom) structure.

According to the above analysis, six kinds of movements are involved in a complete movement. They are discussed in the following sections.

B.2.1.1 'b'(top) structure moves from 'a'(bottom) to 'c'(bottom)

Assume the moment when 'b' structure completely overlaps with 'a' structure is the start point:

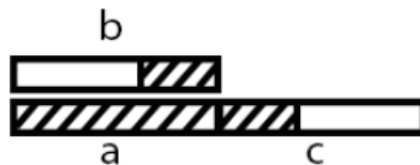


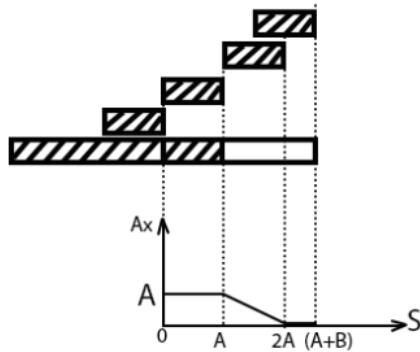
Figure B. 11 model of 'b' structure moves from 'a' structure to 'c' structure

The 'b' structure is separated into weft yarn part and warp yarn part.

Weft yarn part: the friction force produced by weft yarn in 'b' structure is:

$$F_1 = PDA_x\mu_3 + PD(A - A_x)\mu_2 \dots\dots\dots (B. 12)$$

A_x changes with the movement:



$$A_x = \begin{cases} A & (0 \leq S < A) \\ -S + 2A & (A \leq S < 2A) \\ 0 & (2A \leq S \leq A + B) \end{cases} \dots\dots\dots (B. 13)$$

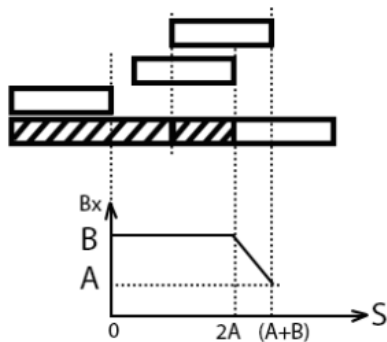
Therefore,

$$F_1 = \begin{cases} PDA\mu_3 & (0 \leq S < A) \\ PD(-S + 2A)\mu_3 + PD(S - A)\mu_2 & (A \leq S < 2A) \dots\dots\dots (B. 14) \\ PDA\mu_2 & (2A \leq S \leq A + B) \end{cases}$$

Warp yarn part: the friction force produced by warp yarn in 'b' structure is:

$$F_2 = PDB_x\mu_2 + PD(B - B_x)\mu_1 \dots\dots\dots (B. 15)$$

B_x changes with the movement:



$$B_x = \begin{cases} B & (0 \leq S < 2A) \\ -S + B + 2A & (2A \leq S \leq A + B) \\ A & (A + B \leq S) \end{cases} \dots\dots\dots (B. 16)$$

Therefore,

$$F_2 = \begin{cases} PDB\mu_2 & (0 \leq S < 2A) \\ PD(-S + B + 2A)\mu_2 + PD(S - 2A)\mu_1 & (2A \leq S \leq A + B) \dots\dots\dots (B. 17) \end{cases}$$

The friction produced by 'b' structure moves from 'a' structure to 'c' structure is:

$$F_1 + F_2 = \begin{cases} PDA\mu_3 + PDB\mu_2 & (0 \leq S < A) \\ PD(-S + 2A)\mu_3 + PD(B + S - A)\mu_2 & (A \leq S < 2A) \dots\dots\dots (B. 18) \\ PD(-S + B + 3A)\mu_2 + PD(S - 2A)\mu_1 & (2A \leq S \leq A + B) \end{cases}$$

B.2.1.2 'b'(top) structure moves from 'c'(bottom) to 'a'(bottom)

Assume the moment when 'b' structure completely overlaps with 'c' structure is the start point:

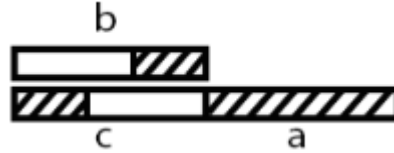


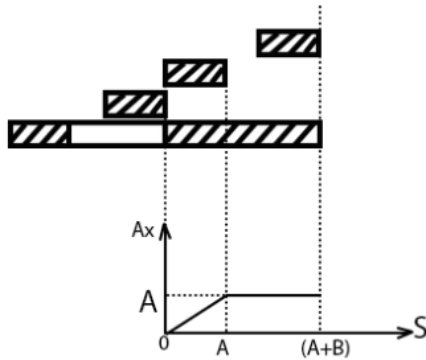
Figure B. 12 model of 'b' structure moves from 'c' structure to 'a' structure

The 'b' structure is separated into weft yarn part and warp yarn part:

Weft yarn part: the friction force produced by weft yarn in 'b' structure is:

$$F_1 = PDA_x\mu_3 + PD(A - A_x)\mu_2 \dots \dots \dots (B. 19)$$

A_x changes with the movement:



$$A_x = \begin{cases} S & (0 \leq S < A) \\ A & (A \leq S \leq A + B) \end{cases} \dots \dots \dots (B. 20)$$

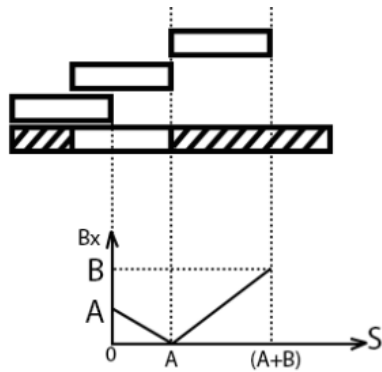
Therefore,

$$F_1 = \begin{cases} PDS\mu_3 + PD(A - S)\mu_2 & (0 \leq S < A) \\ PDA\mu_3 & (A \leq S \leq A + B) \end{cases} \dots \dots \dots (B. 21)$$

Warp yarn part: the friction force produced by warp yarn in 'b' structure is:

$$F_2 = PDB_x\mu_2 + PD(B - B_x)\mu_1 \dots \dots \dots (B. 22)$$

B_x changes with the movement:



$$B_x = \begin{cases} -S + A & (0 \leq S < A) \\ S - A & (A \leq S \leq A + B) \end{cases} \dots (B. 23)$$

Therefore,

$$F_2 = \begin{cases} PD(-S + A)\mu_2 + PD(B + S - A)\mu_1 & (0 \leq S < A) \\ PD(S - A)\mu_2 + PD(B + A - S)\mu_1 & (A \leq S \leq A + B) \end{cases} \dots (B. 24)$$

The friction produced by 'b' structure moves from 'c' structure to 'a' structure is:

$$F_1 + F_2 = \begin{cases} PDS\mu_3 + 2PD(A - S)\mu_2 + PD(B + S - A)\mu_1 & (0 \leq S < A) \\ PDA\mu_3 + PD(S - A)\mu_2 + PD(B + A - S)\mu_1 & (A \leq S \leq A + B) \end{cases} \dots (B. 25)$$

B.2.1.3 'b'(top) structure moves from 'a'(bottom) to 'a'(bottom)

Assume the moment when 'b' structure completely overlaps with 'a' structure is the start point:

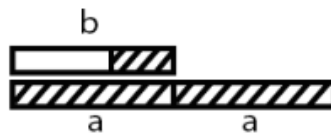


Figure B. 13 model of 'b' structure moves from 'a' structure to 'a' structure

Because the structure of bottom yarn does not change during this movement, the friction force produced by 'b' structure moves from 'a' structure to 'a' structure is:

$$F_1 + F_2 = PDB\mu_2 + PDA\mu_3 \dots (B. 26)$$

B.2.1.4 'a'(top) structure moves from 'a'(bottom) to 'c'(bottom)

Assume the moment when 'a' structure completely overlaps with 'a' structure is the start point:

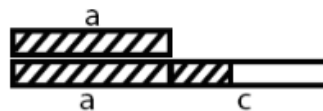
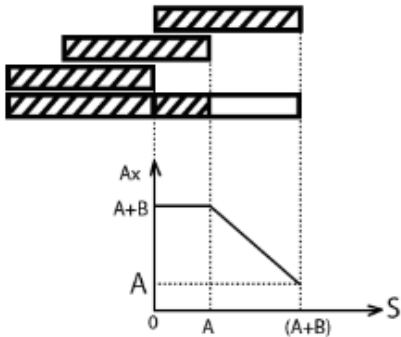


Figure B. 14 model of 'a' structure moves from 'a' structure to 'c' structure

The friction force produced by 'a' structure:

$$F = PDA_x\mu_3 + PD(A + B - A_x)\mu_2 \dots\dots\dots (B. 27)$$

A_x changes with the movement:



$$A_x = \begin{cases} A + B & (0 \leq S < A) \\ -S + 2A + B & (A \leq S \leq A + B) \end{cases} \dots\dots\dots (B. 28)$$

Therefore,

$$F = \begin{cases} PD(A + B)\mu_3 & (0 \leq S < A) \\ PD(-S + 2A + B)\mu_3 + PD(S - A)\mu_2 & (A \leq S \leq A + B) \end{cases} \dots\dots\dots (B. 29)$$

B.2.1.5 'a'(top) structure moves from 'c'(bottom) to 'a'(bottom)

Assume the moment when 'a' structure completely overlaps with 'c' structure is the start point:

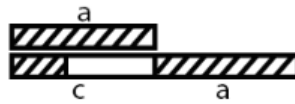
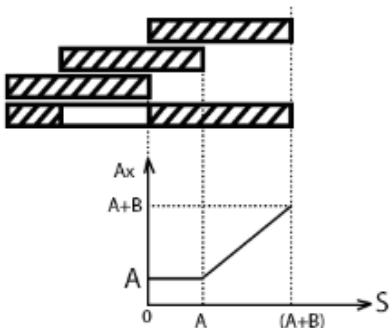


Figure B. 15 model of 'a' structure moves from 'c' structure to 'a' structure

The friction force produced by 'a' structure:

$$F = PDA_x\mu_3 + PD(A + B - A_x)\mu_2 \dots\dots\dots (B. 30)$$

A_x changes with the movement:



$$A_x = \begin{cases} A & (0 \leq S < A) \\ S & (A \leq S \leq A + B) \end{cases} \dots\dots\dots (B. 31)$$

Therefore,

$$F = \begin{cases} PDA\mu_3 + PDB\mu_2 & (0 \leq S < A) \\ PDS\mu_3 + PD(A + B - S)\mu_2 & (A \leq S \leq A + B) \end{cases} \dots\dots\dots (B. 32)$$

B.2.1.6 'a'(top) structure moves from 'a'(bottom) to 'a'(bottom)

Assume the moment when 'a' structure completely overlaps with 'a' structure is the start point:

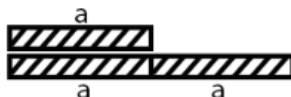


Figure B. 16 model of 'a' structure moves from 'a' structure to 'a' structure

Because the structure of bottom yarn does not change, the friction force produced by 'a' structure moves from 'a' structure to 'a' structure is a constant:

$$F = PD(A + B)\mu_3 \dots\dots\dots (B. 33)$$

B.2.1.7 The friction force produced by yarn X' of top flat strip moves again yarn X of bottom flat strip

As discussed, the movement of top yarn X' could be separated into 3 steps, and these 3 steps contain different movements which are related with the top and bottom yarn structure. Total displacement for the friction test is 3A+3B. Based on the analysis from B.2.1.1 to B.2.1.6, the friction force produced by top yarn X' moves on bottom yarn X is obtained by adding up the friction force produced by different movements.

0 ≤ S ≤ A + B:

$$F_x = \begin{cases} PD(2A + 2B + S)\mu_3 + 2PD(A - S)\mu_2 + PD(B + S - A)\mu_1 & (0 \leq S < A) \\ PD(4A + 2B - S)\mu_3 + 2PD(S - A)\mu_2 + PD(B + A - S)\mu_1 & (A \leq S \leq A + B) \end{cases}$$

A + B ≤ S ≤ 2A + 2B:

$$F_x = PD(3A + B)\mu_3 + 2PDB\mu_2 \quad (A + B < S \leq 2A + 2B)$$

2A + 2B ≤ S ≤ 3A + 3B:

$$F_x = \begin{cases} PD(3A + B)\mu_3 + 2PDB\mu_2 & (2A + 2B \leq S < 4A + 2B) \\ PD(S - A - B)\mu_3 + 2PD(3B + 4A - S)\mu_2 + PD(S - 4A - 2B)\mu_1 & (4A + 2B \leq S \leq 3A + 3B) \end{cases}$$

..... (B. 34)

B.2.2 Friction force produced by yarn Y' of top flat strip moves again yarn Y of bottom flat strip

In the study of the location relationship between three weft yarns in ripstop strip, it is learned that when the yarns X-X' are at the start position, yarns Y-Y' is away from the start position for (A+B-2C). Because the F2 structure in Figure 7.2 is the

same with the ripstop strip structure, and F1 structure is simplified as the weft structure, it is assumed that three weft yarns in flat area (F) also have the same location relationship as ripstop strip area analysed in Figure B. 3. The friction force produced by X-X' is obtained in section B.2.1.7, so the friction force produced by Y-Y' could be obtained based on their location relationships with X-X'.

To obtain the friction force of Y-Y', the equation B.34 has to move left for (A+B-2C):

0 ≤ S ≤ A + B:

$$F_Y = \begin{cases} PD(3A + B + 2C - S)\mu_3 + 2PD(B + S - 2C)\mu_2 + PD(2C - S)\mu_1 & (0 \leq S < 2C) \\ PD(2A + 2B + S - 2C)\mu_3 + 2PD(A - S + 2C)\mu_2 + PD(B + S - 2C - A)\mu_1 & (2C \leq S < A + 2C) \\ PD(4A + 2B + 2C - S)\mu_3 + 2PD(S - 2C - A)\mu_2 + PD(B + A + 2C - S)\mu_1 & (A + 2C \leq S \leq A + B) \end{cases}$$

A + B ≤ S ≤ 2A + 2B:

$$F_Y = PD(3A + B)\mu_3 + 2PDB\mu_2 \quad (A + B \leq S \leq 2A + 2B)$$

2A + 2B ≤ S ≤ 3A + 3B:

$$F_Y = \begin{cases} PD(3A + B)\mu_3 + 2PDB\mu_2 & (2A + 2B \leq S < 3A + 2C + B) \\ PD(S - 2C)\mu_3 + 2PD(3A + 2B + 2C - S)\mu_2 + PD(S - 3A - B - 2C)\mu_1 & (3A + 2C + B \leq S < 2A + 2B + 2C) \\ PD(3A + B)\mu_3 + 2PDB\mu_2 & (2A + 2B + 2C \leq S \leq 3A + 3B) \end{cases}$$

..... (B. 35)

B.2.3 Friction force produced by yarn Z' of top flat strip moves again yarn Z of bottom flat strip

As discussed in section B.2.2, friction force produced by Z-Z' could be obtained by moving the equation B.34 left for (2A+2B-4C). The results are shown below:

0 ≤ S ≤ A + B:

$$F_Z = \begin{cases} PD(2A + 4C - S)\mu_3 + 2PD(S + A + 2B - 4C)\mu_2 + PD(4C - S - A - B)\mu_1 & (0 \leq S < 4C - A - B) \\ PD(3A + 3B + S - 4C)\mu_3 + 2PD(4C - B - S)\mu_2 + PD(2B + S - 4C)\mu_1 & (4C - A - B \leq S < 4C - B) \\ PD(3A + B + 4C - S)\mu_3 + 2PD(B + S - 4C)\mu_2 + PD(4C - S)\mu_1 & (4C - B \leq S \leq A + B) \end{cases}$$

A + B ≤ S ≤ 2A + 2B:

$$F_Z = PD(3A + B)\mu_3 + 2PDB\mu_2 \quad (A + B \leq S \leq 2A + 2B)$$

2A + 2B ≤ S ≤ 3A + 3B:

$$F_Z = \begin{cases} PD(A + B + S - 4C)\mu_3 + 2PD(2A + 4C + B - S)\mu_2 + PD(S - 2A - 4C)\mu_1 & (2A + 2B \leq S < A + B + 4C) \\ PD(3A + B)\mu_3 + 2PDB\mu_2 & (A + B + 4C \leq S < 3A + 4C + B) \\ PD(S - 4C)\mu_3 + 2PD(2B + 3A + 4C - S)\mu_2 + PD(S - 3A - B - 4C)\mu_1 & (3A + 4C + B \leq S \leq 3A + 3B) \end{cases}$$

..... (B. 36)

B.2.4 Friction force between flat strip and flat strip

The friction force produced by flat strip moves against flat strip in a complete displacement (3A+3B) could be obtained by adding friction force produced by X-X', Y-Y' and Z-Z'.

$$\begin{aligned}
 & F_x + F_y + F_z \\
 = & \begin{cases}
 PD(7A + 3B - S + 6C)\mu_3 + 2PD(2A + 3B - 6C + S)\mu_2 + PD(6C - 2A - S)\mu_1 & (0 \leq S < 4C - B - A) \\
 PD(8A + 6B - 2C + S)\mu_3 + 2PD(A + 2C - S)\mu_2 + PD(3B - A - 2C + S)\mu_1 & (4C - B - A \leq S < A) \\
 PD(10A + 6B - 2C - S)\mu_3 + 2PD(2C - A + S)\mu_2 + PD(3B + A - 2C - S)\mu_1 & (A \leq S < 4C - B) \\
 PD(10A + 4B + 6C - 3S)\mu_3 + 2PD(2B - A - 6C + 3S)\mu_2 + PD(B + A + 6C - 3S)\mu_1 & (4C - B \leq S < 2C) \\
 PD(9A + 5B + 2C - S)\mu_3 + 2PD(B - 2C + S)\mu_2 + PD(2B + 2C - S)\mu_1 & (2C \leq S < A + 2C) \\
 PD(11A + 5B + 6C - 3S)\mu_3 + 2PD(3S + B - 2A - 6C)\mu_2 + PD(2B + 2A + 6C - 3S)\mu_1 & (A + 2C \leq S \leq A + B) \\
 3PD(3A + B)\mu_3 + 6PDB\mu_2 & (A + B < S \leq 2A + 2B) \\
 PD(7A + 3B + S - 4C)\mu_3 + 2PD(3B + 2A + 4C - S)\mu_2 + PD(S - 2A - 4C)\mu_1 & (2A + 2B \leq S < A + B + 4C) \\
 3PD(3A + B)\mu_3 + 6PDB\mu_2 & (A + B + 4C \leq S < 3A + 2C + B) \\
 PD(6A + 2B + S - 2C)\mu_3 + 2PD(4B + 3A + 2C - S)\mu_2 + PD(S - 3A - B - 2C)\mu_1 & (3A + 2C + B \leq S < 2A + 2B + 2C) \\
 3PD(3A + B)\mu_3 + 6PDB\mu_2 & (2A + 2B + 2C \leq S < 4A + 2B) \\
 PD(5A + B + S)\mu_3 + 2PD(5B + 4A - S)\mu_2 + PD(S - 4A - 2B)\mu_1 & (4A + 2B \leq S < 3A + 4C + B) \\
 PD(2A + 2S - 4C)\mu_3 + 2PD(7A + 6B + 4C - 2S)\mu_2 + PD(2S - 4C - 7A - 3B)\mu_1 & (3A + 4C + B \leq S \leq 3A + 3B)
 \end{cases}
 \end{aligned}
 \dots\dots\dots (B. 37)$$

B.3 Friction between ripstop strip and flat strip

In this section, the friction between ripstop strip (three weft yarns) and the flat strip (three weft yarns) will be discussed. It is assumed that the ripstop strip moves on top of the flat strip.

B.3.1 Friction force produced by yarn X of bottom flat strip and yarn X' of top ripstop strip

The yarn X in flat area is at the bottom, the yarn X' in ripstop strip is on top of it. When the ripstop strip is flipped, X-X' could be represented by:

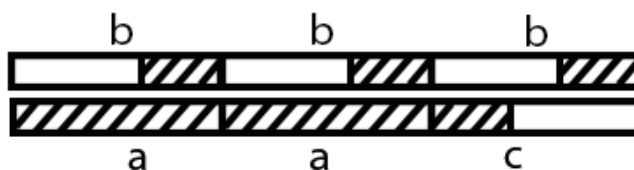


Figure B. 17 Model of a yarn of ripstop strip (X') moves on a yarn of flat strip (X)

During the friction movement, the top yarn X' moves against the fixed bottom yarn X. A complete movement could be separated into three steps:

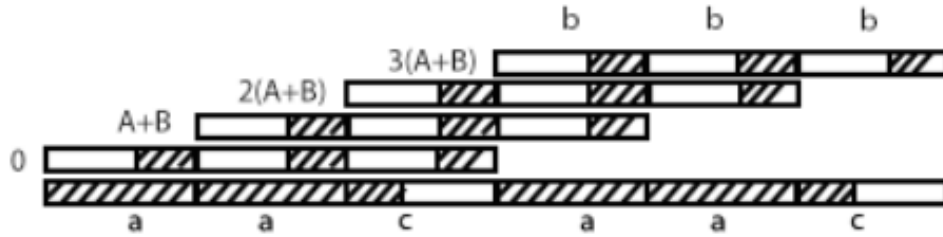


Figure B. 18 Three steps when top yarn X' of ripstop strip moves against the yarn X of flat strip

The whole displacement (3A+3B) is also divided into three steps, and it is found that the movement is the same for these three steps: one 'b'(top) structure moves from 'a'(bottom) to 'a'(bottom) structure, one 'b'(top) structure moves from 'a'(bottom) to 'c'(bottom) structure, and one 'b'(top) structure moves from 'c'(bottom) to 'a'(bottom) structure. Therefore, a complete process (3A+3B) contains 3 same repeats, displacement for each repeat is A+B, and only one loop is discussed below.

The friction force produced by the above three movements have been discussed in section B.2.1.1, B.2.1.2, and B.2.1.3. They are:

When 'b' structure moves from 'a' structure to 'c' structure:

$$F = \begin{cases} PDA\mu_3 + PDB\mu_2 & (0 \leq S < A) \\ PD(-S + 2A)\mu_3 + PD(B + S - A)\mu_2 & (A \leq S < 2A) \\ PD(-S + B + 3A)\mu_2 + PD(S - 2A)\mu_1 & (2A \leq S \leq A + B) \end{cases}$$

When 'b' structure moves from 'c' structure to 'a' structure:

$$F = \begin{cases} PDS\mu_3 + 2PD(A - S)\mu_2 + PD(B + S - A)\mu_1 & (0 \leq S < A) \\ PDA\mu_3 + PD(S - A)\mu_2 + PD(B + A - S)\mu_1 & (A \leq S \leq A + B) \end{cases}$$

When 'b' structure moves from 'a' structure to 'a' structure:

$$F = PDA\mu_3 + PDB\mu_2$$

Therefore, the friction force produced by X'-X in one repeat is:

$$F_X = \begin{cases} PD(2A + S)\mu_3 + 2PD(A + B - S)\mu_2 + PD(B + S - A)\mu_1 & (0 \leq S < A) \\ PD(4A - S)\mu_3 + 2PD(B + S - A)\mu_2 + PD(B + A - S)\mu_1 & (A \leq S < 2A) \dots\dots\dots (B. 38) \\ 2PDA\mu_3 + 2PD(A + B)\mu_2 + PD(B - A)\mu_1 & (2A \leq S \leq A + B) \end{cases}$$

B.3.2 Friction force produced by yarn Y of bottom flat strip and yarn Y' of top ripstop strip

As discussed in section B.2.2, it is also assumed that three weft yarns in this discussion have the same location relationship as shown in Figure B. 3.

Therefore, the friction force of Y-Y' is obtained by shifting F_X (equation B.38) to left for (A+B-2C):

$$F_Y = \begin{cases} PD(3A + 2C - B - S)\mu_3 + 2PD(2B - 2C + S)\mu_2 + PD(2C - S)\mu_1 & (0 \leq S < A + 2C - B) \\ 2PDA\mu_3 + 2PD(A + B)\mu_2 + PD(B - A)\mu_1 & (A + 2C - B \leq S < 2C) \\ PD(2A + S - 2C)\mu_3 + 2PD(A + B + 2C - S)\mu_2 + PD(B + S - A - 2C)\mu_1 & (2C \leq S \leq A + 2C) \\ PD(4A - S + 2C)\mu_3 + 2PD(B + S - 2C - A)\mu_2 + PD(B + A + 2C - S)\mu_1 & (A + 2C \leq S \leq A + B) \end{cases}$$

..... (B. 39)

B.3.3 Friction force produced by yarn Z of bottom flat strip and yarn Z' of top ripstop strip

The friction force produced by X-X' has to move left for (2A+2B-4C) to obtain the friction force produced by Z-Z'.

$$F_Z = \begin{cases} 2PDA\mu_3 + 2PD(A + B)\mu_2 + PD(B - A)\mu_1 & (0 \leq S < 4C - A - B) \\ PD(3A + B + S - 4C)\mu_3 + 2PD(4C - S)\mu_2 + PD(2B + S - 4C)\mu_1 & (4C - A - B \leq S < 4C - B) \\ PD(3A + 4C - B - S)\mu_3 + 2PD(2B + S - 4C)\mu_2 + PD(4C - S)\mu_1 & (4C - B \leq S < A + 4C - B) \\ 2PDA\mu_3 + 2PD(A + B)\mu_2 + PD(B - A)\mu_1 & (A + 4C - B \leq S \leq A + B) \end{cases}$$

..... (B. 40)

B.3.4 Friction force between ripstop strip and flat strip

The friction force produced when ripstop strip moves against flat strip in one loop is obtained by adding up the friction force produced by X-X', Y-Y' and Z-Z'.

$$F = F_X + F_Y + F_Z = \begin{cases} PD(7A + 2C - B)\mu_3 + 2PD(2A + 4B - 2C)\mu_2 + PD(2B + 2C - 2A)\mu_1 & (0 \leq S < 4C - A - B) \\ PD(8A + S - 2C)\mu_3 + 2PD(A + 3B + 2C - S)\mu_2 + PD(3B + S - A - 2C)\mu_1 & (4C - A - B \leq S < A + 2C - B) \\ PD(7A + B + 2S - 4C)\mu_3 + 2PD(2A + 2B + 4C - 2S)\mu_2 + PD(4B + 2S - 4C - 2A)\mu_1 & (A + 2C - B \leq S < A) \\ PD(9A + B - 4C)\mu_3 + 2PD(2B + 4C)\mu_2 + PD(4B - 4C)\mu_1 & (A \leq S < 4C - B) \\ PD(9A + 4C - B - 2S)\mu_3 + 2PD(4B + 2S - 4C)\mu_2 + PD(2B + 4C - 2S)\mu_1 & (4C - B \leq S < 2C) \\ PD(9A + 2C - B - S)\mu_3 + 2PD(4B + S - 2C)\mu_2 + PD(2B + 2C - S)\mu_1 & (2C \leq S < 2A) \\ PD(7A + 2C - B)\mu_3 + 2PD(4B + 2A - 2C)\mu_2 + PD(2B + 2C - 2A)\mu_1 & (2A \leq S < A + 4C - B) \\ PD(6A + S - 2C)\mu_3 + 2PD(3A + 3B + 2C - S)\mu_2 + PD(3B + S - 3A - 2C)\mu_1 & (A + 4C - B \leq S < A + 2C) \\ PD(8A + 2C - S)\mu_3 + 2PD(3B + A + S - 2C)\mu_2 + PD(3B + 2C - A - S)\mu_1 & (A + 2C \leq S \leq A + B) \end{cases}$$

..... (B. 41)

The displacement for a complete movement of ripstop strip is (3A+3B). The friction force produced by three yarns when $0 \leq S \leq A + B$ is shown above, the friction force in the next $A + B \leq S \leq 3A + 3B$ is two repeats of the friction in $0 \leq S \leq A + B$.

B.4 Friction between unit structure of ripstop fabric

Two kinds of friction movements shown in Figure B. 19 are discussed. The first one (Figure B. 19 (a)) is when top ripstop strip (R) overlaps with bottom ripstop strip (R) and top flat strip (F) overlaps with bottom flat strip (F). The second one (Figure B. 19 (b)) is when the top ripstop strip (R) contacts the flat strip (F) of bottom fabric. As shown in Figure B. 19, structure R contains 3 weft yarns, and

structure F has four repeated structures which contain 3 weft yarns. Therefore, the top and bottom structures could be divided into five parts, and each part contains three weft yarns. During the first kind of movement (Figure B. 19 (a)), four parts have flat-flat movements and one part has ripstop-ripstop movement. During the second kind of movement (Figure B. 19 (b)), two parts have ripstop-flat movement, and three parts have flat-flat movement. Equations of these two kinds of movements are derived below.

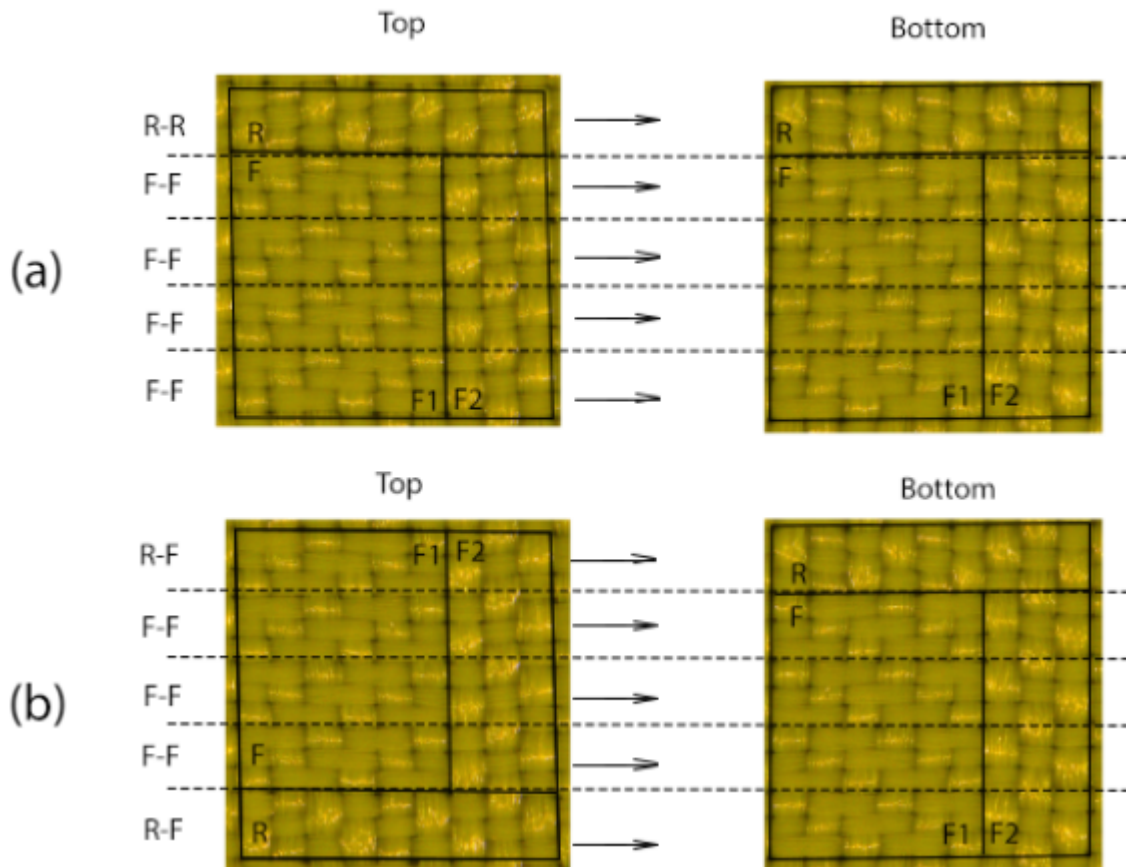


Figure B. 19 Two movements in fabric to fabric friction. (a) Top fabric moving against bottom fabric of identical structure. (b) Top fabric moving against bottom fabric of mirroring structure

B.4.1 Friction force when ripstop strip and flat area of top fabric move against the ripstop strip and flat area of bottom fabric respectively

As shown in Figure B. 19 (a), this movement contains four flat-flat movements and one ripstop-ripstop movement. The total displacement of friction test is $3(A + B)$, and the friction force for $3(A + B)$ is:

$$\begin{aligned}
 F = & \left\{ \begin{array}{ll}
 PD(31A + 9B - 4S + 30C)\mu_3 + 2PD(14A + 15B - 30C + 4S)\mu_2 + PD(6B + 30C - 14A - 4S)\mu_1 & (0 \leq S < 4C - B - A) \\
 PD(38A + 24B + 7S - 14C)\mu_3 + 2PD(7A + 14C - 7S)\mu_2 + PD(21B + 7S - 7A - 14C)\mu_1 & (4C - B - A \leq S < A + 2C - B) \\
 PD(35A + 27B - 20C + 10S)\mu_3 + 2PD(10A - 3B + 20C - 10S)\mu_2 + PD(24B - 10A - 20C + 10S)\mu_1 & (A + 2C - B \leq S < A) \\
 PD(49A + 27B - 20C - 4S)\mu_3 + 2PD(20C - 3B - 4A + 4S)\mu_2 + PD(24B + 4A - 20C - 4S)\mu_1 & (A \leq S < 4C - B) \\
 PD(49A + 13B + 36C - 18S)\mu_3 + 2PD(11B - 4A - 36C + 18S)\mu_2 + PD(10B + 4A + 36C - 18S)\mu_1 & (4C - B \leq S < 2C) \\
 PD(45A + 17B + 14C - 7S)\mu_3 + 2PD(7B - 14C + 7S)\mu_2 + PD(14B + 14C - 7S)\mu_1 & (2C \leq S < 2A) \\
 PD(39A + 17B + 14C - 4S)\mu_3 + 2PD(7B + 6A - 14C + 4S)\mu_2 + PD(14B - 6A + 14C - 4S)\mu_1 & (2A \leq S < A + 4C - B) \\
 PD(36A + 20B + 2C - S)\mu_3 + 2PD(4B + 9A - 2C + S)\mu_2 + PD(17B - 9A + 2C - S)\mu_1 & (A + 4C - B \leq S < A + 2C) \\
 PD(50A + 20B + 30C - 15S)\mu_3 + 2PD(15S + 4B - 5A - 30C)\mu_2 + PD(17B + 5A + 30C - 15S)\mu_1 & (A + 2C \leq S < A + B) \\
 PD(39A + 9B + 6C)\mu_3 + 2PD(15B + 6A - 6C)\mu_2 + PD(6B - 6A + 6C)\mu_1 & (A + B \leq S < 4C) \\
 PD(39A + 9B - 6C + 3S)\mu_3 + 2PD(6C + 15B + 6A - 3S)\mu_2 + PD(6B - 6A - 6C + 3S)\mu_1 & (4C \leq S < 2A + 2C) \\
 PD(33A + 9B - 12C + 6S)\mu_3 + 2PD(12A + 15B + 12C - 6S)\mu_2 + PD(6B - 12A - 12C + 6S)\mu_1 & (2A + 2C \leq S < 2A + B) \\
 PD(45A + 15B - 12C)\mu_3 + 2PD(12C + 9B)\mu_2 + PD(12B - 12C)\mu_1 & (2A + B \leq S < A + 4C) \\
 PD(51A + 15B + 12C - 6S)\mu_3 + 2PD(9B + 6S - 12C - 6A)\mu_2 + PD(12B + 12C - 6S + 6A)\mu_1 & (A + 4C \leq S < A + B + 2C) \\
 PD(48A + 12B + 6C - 3S)\mu_3 + 2PD(12B + 3S - 6C - 3A)\mu_2 + PD(9B + 6C - 3S + 3A)\mu_1 & (A + B + 2C \leq S < 3A + B) \\
 PD(39A + 9B + 6C)\mu_3 + 2PD(6A + 15B - 6C)\mu_2 + PD(6B - 6A + 6C)\mu_1 & (3A + B \leq S < 2A + 4C) \\
 PD(33A + 9B - 6C + 3S)\mu_3 + 2PD(6C + 15B + 12A - 3S)\mu_2 + PD(6B - 12A - 6C + 3S)\mu_1 & (2A + 4C \leq S < 2A + B + 2C) \\
 PD(45A + 15B + 6C - 3S)\mu_3 + 2PD(9B + 3S - 6C)\mu_2 + PD(12B + 6C - 3S)\mu_1 & (2A + B + 2C \leq S < 2A + 2B) \\
 PD(31A + 9B + 4S - 10C)\mu_3 + 2PD(15B + 14A - 4S + 10C)\mu_2 + PD(6B - 14A + 4S - 10C)\mu_1 & (2A + 2B \leq S < A + B + 4C) \\
 PD(36A + 6B - 6C + 3S)\mu_3 + 2PD(6C + 18B + 9A - 3S)\mu_2 + PD(3B - 9A - 6C + 3S)\mu_1 & (A + B + 4C \leq S < 3A + B + 2C) \\
 PD(15A - B - 20C + 10S)\mu_3 + 2PD(30A + 25B + 20C - 10S)\mu_2 + PD(10S - 30A - 20C - 4B)\mu_1 & (3A + B + 2C \leq S < 3A + 2B) \\
 PD(33A + 11B + 4S - 20C)\mu_3 + 2PD(20C + 12A + 13B - 4S)\mu_2 + PD(8B - 12A + 4S - 20C)\mu_1 & (3A + 2B \leq S < 2A + B + 4C) \\
 PD(45A + 17B + 4C - 2S)\mu_3 + 2PD(2S + 7B - 4C)\mu_2 + PD(14B + 4C - 2S)\mu_1 & (2A + B + 4C \leq S < 2A + 2B + 2C) \\
 PD(51A + 15B + 6C - 3S)\mu_3 + 2PD(9B + 3S - 6C - 6A)\mu_2 + PD(12B + 6C + 6A - 3S)\mu_1 & (2A + 2B + 2C \leq S < 4A + 2B) \\
 PD(23A + B + 6C + 4S)\mu_3 + 2PD(22A + 23B - 4S - 6C)\mu_2 + PD(6C + 4S - 2B - 22A)\mu_1 & (4A + 2B \leq S < 3A + B + 4C) \\
 PD(2A - 6B - 22C + 11S)\mu_3 + 2PD(22C + 30B + 43A - 11S)\mu_2 + PD(11S - 9B - 43A - 22C)\mu_1 & (3A + B + 4C \leq S < 3A + 2B + 2C) \\
 PD(20A + 6B - 10C + 5S)\mu_3 + 2PD(10C - 5S + 18B + 25A)\mu_2 + PD(3B - 25A - 10C + 5S)\mu_1 & (3A + 2B + 2C \leq S \leq 3A + 3B)
 \end{array} \right.
 \end{aligned}$$

..... (B. 42)

B.4.2 Friction force when ripstop strip and flat area of top fabric move against the flat strip and ripstop area of bottom fabric respectively

As shown in Figure B. 19 (b), this movement contains two rip-flat movements and three flat-flat movements. The friction force for $3(A + B)$ displacement is:

$$\begin{aligned}
 & \left. \begin{aligned}
 & PD(35A + 7B - 3S + 22C)\mu_3 + 2PD(10A + 17B - 22C + 3S)\mu_2 + PD(4B + 22C - 10A - 3S)\mu_1 & (0 \leq S < 4C - B - A) \\
 & PD(40A + 18B + 5S - 10C)\mu_3 + 2PD(5A + 6B + 10C - 5S)\mu_2 + PD(15B - 5A - 10C + 5S)\mu_1 & (4C - B - A \leq S < A + 2C - B) \\
 & PD(38A + 20B + 7S - 14C)\mu_3 + 2PD(7A + 4B + 14C - 7S)\mu_2 + PD(17B - 7A - 14C + 7S)\mu_1 & (A + 2C - B \leq S < A) \\
 & PD(48A + 20B - 3S - 14C)\mu_3 + 2PD(4B - 3A + 14C + 3S)\mu_2 + PD(17B + 3A - 14C - 3S)\mu_1 & (A \leq S < 4C - B) \\
 & PD(48A + 10B - 13S + 26C)\mu_3 + 2PD(14B - 3A - 26C + 13S)\mu_2 + PD(7B + 3A + 26C - 13S)\mu_1 & (4C - B \leq S < 2C) \\
 & PD(45A + 13B - 5S + 10C)\mu_3 + 2PD(11B - 10C + 5S)\mu_2 + PD(10B + 10C - 5S)\mu_1 & (2C \leq S < 2A) \\
 & PD(41A + 13B - 3S + 10C)\mu_3 + 2PD(11B + 4A - 10C + 3S)\mu_2 + PD(10B + 10C - 4A - 3S)\mu_1 & (2A \leq S < A + 4C - B) \\
 & PD(39A + 15B - S + 2C)\mu_3 + 2PD(9B + 6A - 2C + S)\mu_2 + PD(12B + 2C - 6A - S)\mu_1 & (A + 4C - B \leq S < A + 2C) \\
 & PD(49A + 15B - 11S + 22C)\mu_3 + 2PD(9B - 4A - 22C + 11S)\mu_2 + PD(12B + 22C + 4A - 11S)\mu_1 & (A + 2C \leq S < A + B) \\
 & PD(41A + 7B + 4C)\mu_3 + 2PD(17B + 4A - 4C)\mu_2 + PD(4B + 4C - 4A)\mu_1 & (A + B \leq S < 4C) \\
 & PD(41A - 4C + 7B + 2S)\mu_3 + 2PD(4A + 17B + 4C - 2S)\mu_2 + PD(4B + 2S - 4C - 4A)\mu_1 & (4C \leq S < 2A + 2C) \\
 & PD(37A - 8C + 7B + 4S)\mu_3 + 2PD(8A + 17B + 8C - 4S)\mu_2 + PD(4B + 4S - 8C - 8A)\mu_1 & (2A + 2C \leq S < 2A + B) \\
 & PD(45A - 8C + 11B)\mu_3 + 2PD(13B + 8C)\mu_2 + PD(8B - 8C)\mu_1 & (2A + B \leq S < A + 4C) \\
 & PD(49A + 8C + 11B - 4S)\mu_3 + 2PD(13B + 4S - 8C - 4A)\mu_2 + PD(8B + 8C - 4S + 4A)\mu_1 & (A + 4C \leq S < A + B + 2C) \\
 & PD(47A + 4C + 9B - 2S)\mu_3 + 2PD(15B + 2S - 4C - 2A)\mu_2 + PD(6B + 2A + 4C - 2S)\mu_1 & (A + B + 2C \leq S < 3A + B) \\
 & PD(41A + 4C + 7B)\mu_3 + 2PD(17B + 4A - 4C)\mu_2 + PD(4B + 4C - 4A)\mu_1 & (3A + B \leq S < 2A + 4C) \\
 & PD(37A - 4C + 7B + 2S)\mu_3 + 2PD(17B + 8A + 4C - 2S)\mu_2 + PD(4B + 2S - 4C - 8A)\mu_1 & (2A + 4C \leq S < 2A + B + 2C) \\
 & PD(45A + 4C + 11B - 2S)\mu_3 + 2PD(13B - 4C + 2S)\mu_2 + PD(8B - 2S + 4C)\mu_1 & (2A + B + 2C \leq S < 2A + 2B) \\
 & PD(35A + 7B + 3S - 8C)\mu_3 + 2PD(17B + 10A + 8C - 3S)\mu_2 + PD(4B - 8C - 10A + 3S)\mu_1 & (2A + 2B \leq S < A + B + 4C) \\
 & PD(39A - 4C + 5B + 2S)\mu_3 + 2PD(6A + 19B + 4C - 2S)\mu_2 + PD(2B + 2S - 4C - 6A)\mu_1 & (A + B + 4C \leq S < 3A + B + 2C) \\
 & PD(24A + 7S - 14C)\mu_3 + 2PD(24B + 21A + 14C - 7S)\mu_2 + PD(7S - 3B - 14C - 21A)\mu_1 & (3A + B + 2C \leq S < 3A + 2B) \\
 & PD(36A + 8B + 3S - 14C)\mu_3 + 2PD(16B + 9A + 14C - 3S)\mu_2 + PD(3S + 5B - 14C - 9A)\mu_1 & (3A + 2B \leq S < 2A + B + 4C) \\
 & PD(44A + 12B - S + 2C)\mu_3 + 2PD(12B + A - 2C + S)\mu_2 + PD(9B + 2C - A - S)\mu_1 & (2A + B + 4C \leq S < 2A + 2B + 2C) \\
 & PD(49A + 4C + 11B - 2S)\mu_3 + 2PD(13B + 2S - 4C - 4A)\mu_2 + PD(8B + 4C - 2S + 4A)\mu_1 & (2A + 2B + 2C \leq S < 4A + 2B) \\
 & PD(29A + B + 3S + 4C)\mu_3 + 2PD(23B + 16A - 4C - 3S)\mu_2 + PD(4C - 16A + 3S - 2B)\mu_1 & (4A + 2B \leq S < 3A + B + 4C) \\
 & PD(14A - 4B + 8S - 16C)\mu_3 + 2PD(28B + 31A + 16C - 8S)\mu_2 + PD(8S - 16C - 31A - 7B)\mu_1 & (3A + B + 4C \leq S < 3A + 2B + 2C) \\
 & PD(26A + 4B + 4S - 8C)\mu_3 + 2PD(20B + 19A + 8C - 4S)\mu_2 + PD(B + 4S - 8C - 19A)\mu_1 & (3A + 2B + 2C \leq S \leq 3A + 3B)
 \end{aligned}
 \right.
 \end{aligned}$$

..... (B. 43)

Appendix C Theoretical analysis of sensor-fabric friction profile of ripstop fabric in KES-F roughness test

C.1 Friction between KES-F metal sensor and ripstop strip

Ripstop strip contains three weft yarns, friction force produced by each of these three yarns with the metal sensor are discussed to give the friction force produced by the whole ripstop strip.

Provided that the starting position of the sensor moves against the fabric surface is from the left end of weft part of fabric as shown in Figure C. 1 below,

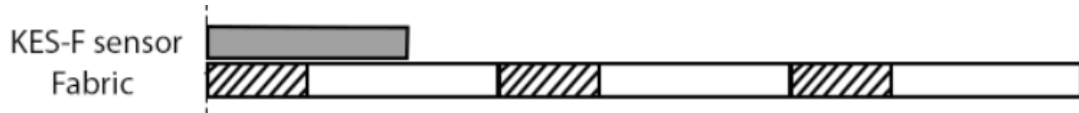


Figure C. 1 Starting position when sensor moves against ripstop strip of fabric surface

When the sensor contact yarn X at this starting position, the relative distance between the left end of the metal sensor and the left end of the weft part of the yarn Y is $(A+B-C)$, and the distance for yarn Z is $(A+B-2C)$. (See Figure C. 2).

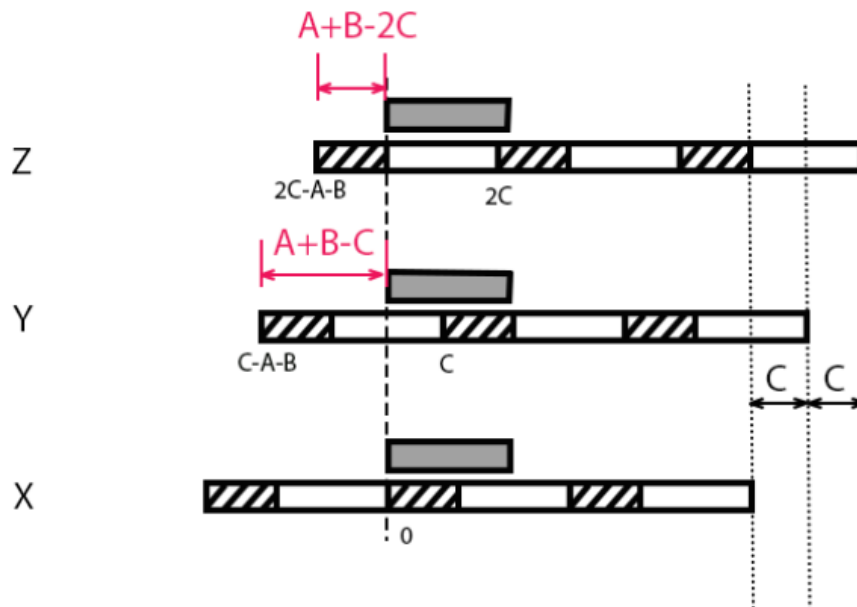
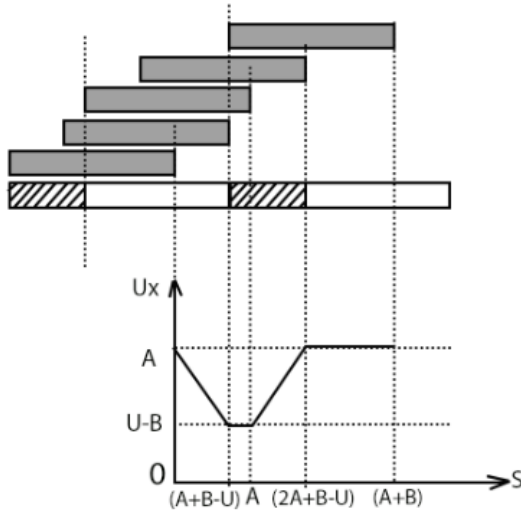


Figure C. 2 Location relationship between top, middle and bottom yarns in KES roughness test

The length of metal sensor in moving direction is labelled as U. Friction forces produced during the movement of the metal sensor on the ripstop fabric is shown in equation C.1 below,

$$F = PDU_x\mu_5 + PD(U-U_x)\mu_4 \dots\dots\dots (C. 1)$$

U_x changes as the movement of sensor, where



$$U_x = \begin{cases} -S + A & (0 \leq S < A + B - U) \\ U - B & (A + B - U \leq S < A) \\ S + U - B - A & (A \leq S < 2A + B - U) \\ A & (2A + B - U \leq S \leq A + B) \end{cases} \dots\dots\dots (C. 2)$$

The friction force in one loop length of the weave structure of yarn X is obtained by substituting U_x into equation C.1, thus shown in equation C.3 as follows,

$$F_x = \begin{cases} PD(A - S)\mu_5 + PD(U + S - A)\mu_4 & (0 \leq S < A + B - U) \\ PD(U - B)\mu_5 + PDB\mu_4 & (A + B - U \leq S < A) \\ PD(S + U - B - A)\mu_5 + PD(B + A - S)\mu_4 & (A \leq S < 2A + B - U) \\ PDA\mu_5 + PD(U - A)\mu_4 & (2A + B - U \leq S \leq A + B) \end{cases} \dots\dots\dots (C. 3)$$

The friction force of F_Y for the yarn Y is obtained by shifting F_X to left for (A+B-C), as shown in equations C.4.

$$F_y = \begin{cases} PDA\mu_5 + PD(U - A)\mu_4 & (0 \leq S < C) \\ PD(A + C - S)\mu_5 + PD(U + S - C - A)\mu_4 & (C \leq S < A + B + C - U) \\ PD(U - B)\mu_5 + PDB\mu_4 & (A + B + C - U \leq S < A + C) \\ PD(S + U - A - B - C)\mu_5 + PD(A + B + C - S)\mu_4 & (A + C \leq S < 2A + B + C - U) \\ PDA\mu_5 + PD(U - A)\mu_4 & (2A + B + C - U \leq S \leq A + B) \end{cases} \dots\dots\dots (C. 4)$$

Similarly, the friction force of F_Z for the yarn Z is obtained by shifting F_X to left for (A+B-2C), as shown in equations C.5.

$$F_Z = \begin{cases} PD(S + U - 2C)\mu_5 + PD(2C - S)\mu_4 & (0 \leq S < A + 2C - U) \\ PDA\mu_5 + PD(U - A)\mu_4 & (A + 2C - U \leq S < 2C) \\ PD(A + 2C - S)\mu_5 + PD(U + S - 2C - A)\mu_4 & (2C \leq S < A + B + 2C - U) \\ PD(U - B)\mu_5 + PDB\mu_4 & (A + B + 2C - U \leq S < A + 2C) \\ PD(S - 2C + U - B - A)\mu_5 + PD(A + B + 2C - S)\mu_4 & (A + 2C \leq S \leq A + B) \end{cases} \dots\dots\dots (C. 5)$$

Therefore, the friction force produced by the three yarns in the ripstop strip is the sum of the friction forces of the three yarns when $0 \leq S \leq A + B$, as shown in equation C.6 below,

$$F_x + F_y + F_z = \begin{cases} PD(U + 2A - 2C)\mu_5 + PD(2U + 2C - 2A)\mu_4 & (0 \leq S < A + 2C - U) \\ PD(3A - S)\mu_5 + PD(3U - 3A + S)\mu_4 & (A + 2C - U \leq S < A + B - U) \\ PD(2A + U - B)\mu_5 + PD(2U + B - 2A)\mu_4 & (A + B - U \leq S < C) \\ PD(2A + U + C - B - S)\mu_5 + PD(2U + B + S - C - 2A)\mu_4 & (C \leq S < A) \\ PD(A + U + C - B)\mu_5 + PD(2U + B - A - C)\mu_4 & (A \leq S < A + B + C - U) \\ PD(S + 2U - 2B)\mu_5 + PD(U + 2B - S)\mu_4 & (A + B + C - U \leq S < 2C) \\ PD(2U - 2B + 2C)\mu_5 + PD(U + 2B - 2C)\mu_4 & (2C \leq S < 2A + B - U) \\ PD(2A + 2C + U - B - S)\mu_5 + PD(2U + S + B - 2C - 2A)\mu_4 & (2A + B - U \leq S < A + C) \\ PD(U + A - B + C)\mu_5 + PD(2U + B - A - C)\mu_4 & (A + C \leq S < A + B + 2C - U) \\ PD(2U - 2B + S - C)\mu_5 + PD(U + 2B - S + C)\mu_4 & (A + B + 2C - U \leq S < 2A + B + C - U) \\ PD(U + 2A - B)\mu_5 + PD(B + 2U - 2A)\mu_4 & (2A + B + C - U \leq S < A + 2C) \\ PD(S + A + U - 2C - B)\mu_5 + PD(B + 2U + 2C - A - S)\mu_4 & (A + 2C \leq S \leq A + B) \end{cases} \dots\dots\dots (C. 6)$$

The friction force in the next $A + B \leq S \leq 3A + 3B$ is two repeats of the friction in $0 \leq S \leq A + B$.

C.2 Friction between KES-F metal sensor and flat strip

As the 12 weft yarns in flat strip have four loops, each loop contains 3 weft yarns. The three yarns in flat strip still have the relative location differences in Figure C. 2, and each yarn in the flat strip is simplified as having two ‘a’ structures of weft cross points and one ‘c’ structure of 1/2 twill woven structure. The friction forces between the metal sensor and the three yarns are discussed below.

The model of friction force between a metal sensor and bottom yarn is shown in Figure C. 3 below; the sensor-bottom yarn starts from the left edge of sensor contacts the left edge of the weft yarn ‘a’.

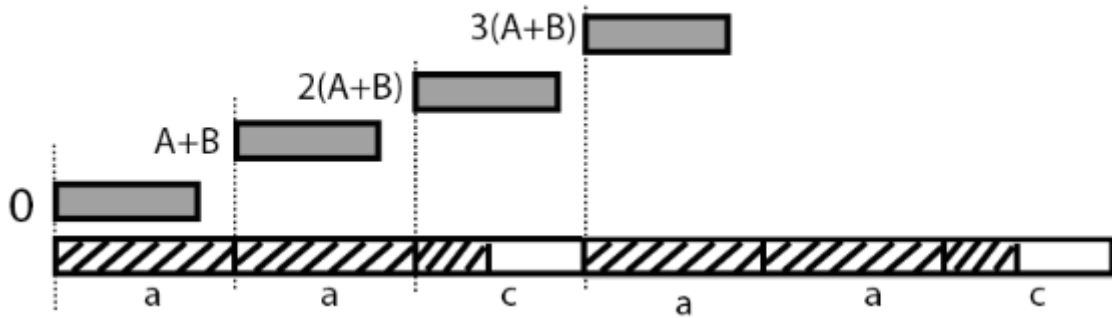


Figure C. 3 Model of friction between KES-F sensor and flat strip of ripstop fabric

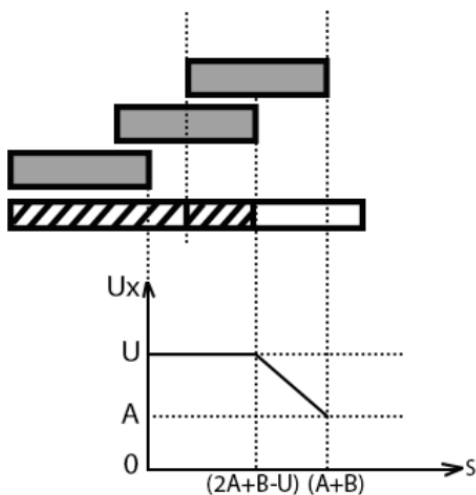
A complete displacement ($3A+3B$) contains three different movements:

1. 'U' moves from 'a' structure to 'a' structure when $0 \leq S \leq A + B$;
2. 'U' moves from 'a' structure to 'c' structure when $A + B \leq S \leq 2A + 2B$;
3. 'U' moves from 'c' structure to 'a' structure when $2A + 2B \leq S \leq 3A + 3B$.

When $0 \leq S \leq A + B$, sensor contacts with a weft yarn cross point, the friction produced is:

$$F_x = PDU\mu_5 \dots \dots \dots (C. 7)$$

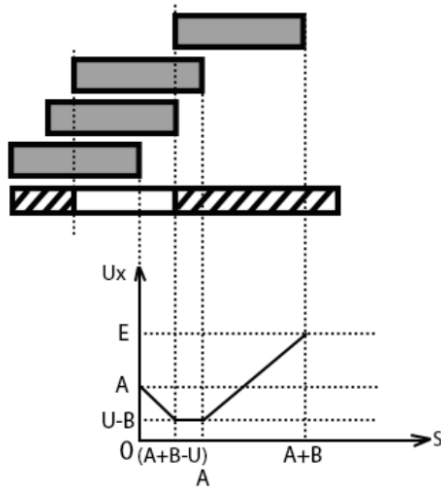
Friction force between sensor and the yarn X when the sensor moves from 'a' structure to 'c' structure is shown in Figure C. 4 and equation C.9. The friction force when sensor moves from 'c' structure to 'a' structure is shown in Figure C. 5 and equation C.11 below.



$$U_x = \begin{cases} U & (0 \leq S < 2A + B - U) \\ B + 2A - S & (2A + B - U \leq S \leq A + B) \end{cases} \dots \dots \dots (C. 8)$$

Figure C. 4 model of sensor moves from 'a' to 'c' structure

$$F_x = \begin{cases} PDU\mu_5 & (0 \leq S < 2A + B - U) \\ PD(B + 2A - S)\mu_5 + PD(U + S - B - 2A)\mu_4 & (2A + B - U \leq S < A + B) \end{cases} \dots \dots \dots (C. 9)$$



$$U_x = \begin{cases} -S + A & (0 \leq S < A + B - U) \\ U - B & (A + B - U \leq S < A) \\ S + U - A - B & (A \leq S \leq A + B) \end{cases} \dots\dots\dots (C. 10)$$

Figure C. 5 model of sensor moves from 'c' to 'a' structure

$$F_X = \begin{cases} PD(-S + A)\mu_5 + PD(U + S - A)\mu_4 & (0 \leq S < A + B - U) \\ PD(U - B)\mu_5 + PDB\mu_4 & (A + B - U \leq S < A) \dots\dots\dots (C. 11) \\ PD(S + U - A - B)\mu_5 + PD(A + B - S)\mu_4 & (A \leq S \leq A + B) \end{cases}$$

Therefore the friction force produced by the bottom yarn in the flat strip area in a complete friction loop (i.e., $0 \leq S \leq 3A + 3B$) is:

When $0 \leq S \leq A + B$:

$$F_X = PDU\mu_5$$

When $A + B \leq S \leq 2A + 2B$

$$F_X = \begin{cases} PDU\mu_5 & (A + B \leq S < 3A + 2B - U) \\ PD(2B + 3A - S)\mu_5 + PD(U + S - 2B - 3A)\mu_4 & (3A + 2B - U \leq S \leq 2A + 2B) \end{cases}$$

When $2A + 2B \leq S \leq 3A + 3B$

$$F_X = \begin{cases} PD(2B - S + 3A)\mu_5 + PD(U + S - 2B - 3A)\mu_4 & (2A + 2B \leq S < 3A + 3B - U) \\ PD(U - B)\mu_5 + PDB\mu_4 & (3A + 3B - U \leq S < 3A + 2B) \\ PD(S + U - 3A - 3B)\mu_5 + PD(3A + 3B - S)\mu_4 & (3A + 2B \leq S \leq 3A + 3B) \end{cases}$$

..... (C. 12)

The friction force produced by the yarn Y in flat strip is obtained by left shifting F_X for $(A+B-C)$:

$0 \leq S \leq A + B$:

$$F_Y = PDU\mu_5$$

$A + B \leq S < 2A + 2B$

$$F_Y = \begin{cases} PD(2A + B + C - S)\mu_5 + PD(U + S - B - C - 2A)\mu_4 & (A + B \leq S < A + B + C) \\ PDU\mu_5 & (A + B + C \leq S < 3A + 2B + C - U) \\ PD(3A + 2B + C - S)\mu_5 + PD(U + S - C - 2B - 3A)\mu_4 & (3A + 2B + C - U \leq S \leq 2A + 2B) \end{cases}$$

$$\underline{2A + 2B \leq S \leq 3A + 3B}$$

$$F_Y = \begin{cases} PD(S - 2A - 2B + U - C)\mu_5 + PD(C - S + 2A + 2B)\mu_4 & (2A + 2B \leq S < 2A + 2B + C) \\ PD(3A + 2B + C - S)\mu_5 + PD(U + S - C - 3A - 2B)\mu_4 & (2A + 2B + C \leq S < 3A + 3B + C - U) \\ PD(U - B)\mu_5 + PDB\mu_4 & (3A + 3B + C - U \leq S < 3A + 2B + C) \\ PD(S + U - 3A - 3B - C)\mu_5 + PD(3A + 3B + C - S)\mu_4 & (3A + 2B + C \leq S \leq 3A + 3B) \end{cases}$$

..... (C. 13)

The friction force produced by yarn Z could be obtained by shifting F_X left for $(A+B-2C)$:

$$\underline{0 \leq S \leq A + B}$$

$$F_Z = PDU\mu_5$$

$$\underline{A + B \leq S \leq 2A + 2B}$$

$$F_Z = \begin{cases} PDU\mu_5 & (A + B \leq S < 2A + B + 2C - U) \\ PD(2A + 2C - S + B)\mu_5 + PD(U + S - 2A - B - 2C)\mu_4 & (2A + B + 2C - U \leq S < A + B + 2C) \\ PDU\mu_5 & (A + B + 2C \leq S \leq 2A + 2B) \end{cases}$$

$$\underline{2A + 2B \leq S \leq 3A + 3B}$$

$$F_Z = \begin{cases} PD(S + U - 2C - 2A - 2B)\mu_5 + PD(2A + 2B + 2C - S)\mu_4 & (2A + 2B \leq S < 2A + 2B + 2C) \\ PD(2C + 3A + 2B - S)\mu_5 + PD(U + S - 3A - 2B - 2C)\mu_4 & (2A + 2B + 2C \leq S < 3A + 3B + 2C - U) \\ PD(U - B)\mu_5 + PDB\mu_4 & (3A + 3B + 2C - U \leq S < 3A + 2B + 2C) \\ PD(S + U - 3A - 3B - 2C)\mu_5 + PD(3A + 3B + 2C - S)\mu_4 & (3A + 2B + 2C \leq S \leq 3A + 3B) \end{cases}$$

..... (C. 14)

The friction force produced by three yarns in flat strip when $0 \leq S \leq 3A + 3B$ is obtained by adding up friction forces produced by X, Y and Z yarns:

$$F = \begin{cases} 3PDU\mu_5 & (0 \leq S < A + B) \\ PD(2U + 2A + B - S + C)\mu_5 + PD(U + S - B - C - 2A)\mu_4 & (A + B \leq S < 2A + B + 2C - U) \\ PD(U + 4A + 2B - 2S + 3C)\mu_5 + PD(2U + 2S - 2B - 3C - 4A)\mu_4 & (2A + B + 2C - U \leq S < A + B + C) \\ PD(2U + 2A + B - S + 2C)\mu_5 + PD(U + S - B - 2C - 2A)\mu_4 & (A + B + C \leq S < A + B + 2C) \\ 3PDU\mu_5 & (A + B + 2C \leq S < 3A + 2B - U) \\ PD(2B + 3A + 2U - S)\mu_5 + PD(U + S - 2B - 3A)\mu_4 & (3A + 2B - U \leq S < 3A + 2B + C - U) \\ PD(4B + 6A + U + C - 2S)\mu_5 + PD(2U + 2S - 4B - 6A - C)\mu_4 & (3A + 2B + C - U \leq S < 2A + 2B) \\ PD(2U - 3C + S - A - 2B)\mu_5 + PD(U + 3C + A + 2B - S)\mu_4 & (2A + 2B \leq S < 3A + 3B - U) \\ PD(3U + 2S - 4A - 5B - 3C)\mu_5 + PD(3C + 4A + 5B - 2S)\mu_4 & (3A + 3B - U \leq S < 2A + 2B + C) \\ PD(2U + A - B - C)\mu_5 + PD(C + U - A + B)\mu_4 & (2A + 2B + C \leq S < 3A + 2B) \\ PD(2U - 2A + S - 3B - C)\mu_5 + PD(C + U - S + 2A + 3B)\mu_4 & (3A + 2B \leq S < 3A + 3B + C - U) \\ PD(3U - 5A + 2S - 6B - 2C)\mu_5 + PD(2C - 2S + 5A + 6B)\mu_4 & (3A + 3B + C - U \leq S < 2A + 2B + 2C) \\ PD(2U - 2B + 2C)\mu_5 + PD(U - 2C + 2B)\mu_4 & (2A + 2B + 2C \leq S < 3A + 2B + C) \\ PD(S + 2U - 3A - 4B + C)\mu_5 + PD(U - C - S + 4B + 3A)\mu_4 & (3A + 2B + C \leq S < 3A + 3B + 2C - U) \\ PD(2S + 3U - 6A - 7B - C)\mu_5 + PD(C - 2S + 7B + 6A)\mu_4 & (3A + 3B + 2C - U \leq S < 3A + 2B + 2C) \\ PD(3S + 3U - 9A - 9B - 3C)\mu_5 + PD(3C - 3S + 9B + 9A)\mu_4 & (3A + 2B + 2C \leq S \leq 3A + 3B) \end{cases}$$

..... (C. 15)

C.3 Friction produced by KES-F sensor and fabric

The friction force produced between sensor and fabric include one part of sensor moves against ripstop strip and four parts of sensor moves against flat strip. Five parts are added up to obtain the friction force between KES-F sensor and fabric. Equations are listed below:

$$\begin{aligned}
 F &= \left\{ \begin{array}{l}
 PD(13U + 2A-2C)\mu_5 + PD(2C + 2U-2A)\mu_4 \quad (0 \leq S < A + 2C-U) \\
 PD(12U + 3A-S)\mu_5 + PD(S + 3U-3A)\mu_4 \quad (A + 2C-U \leq S < A + B-U) \\
 PD(13U + 2A-B)\mu_5 + PD(B + 2U-2A)\mu_4 \quad (A + B-U \leq S < C) \\
 PD(13U + 2A + C-B-S)\mu_5 + PD(B + 2U-2A + S-C)\mu_4 \quad (C \leq S < A) \\
 PD(13U + A + C-B)\mu_5 + PD(B + 2U-A-C)\mu_4 \quad (A \leq S < A + B + C-U) \\
 PD(14U + S-2B)\mu_5 + PD(2B + U-S)\mu_4 \quad (A + B + C-U \leq S < 2C) \\
 PD(14U + 2C-2B)\mu_5 + PD(2B + U-2C)\mu_4 \quad (2C \leq S < 2A + B-U) \\
 PD(2A + 13U + 2C-B-S)\mu_5 + PD(B + 2U + S-2C-2A)\mu_4 \quad (2A + B-U \leq S < A + C) \\
 PD(A + 13U + C-B)\mu_5 + PD(B + 2U-C-A)\mu_4 \quad (A + C \leq S < A + B + 2C-U) \\
 PD(14U + S-C-2B)\mu_5 + PD(2B + U-S + C)\mu_4 \quad (A + B + 2C-U \leq S < 2A + B + C-U) \\
 PD(13U + 2A-B)\mu_5 + PD(B + 2U-2A)\mu_4 \quad (2A + B + C-U \leq S < A + 2C) \\
 PD(13U + A-B + S-2C)\mu_5 + PD(B + 2U + 2C-A-S)\mu_4 \quad (A + 2C \leq S < A + B) \\
 PD(9U + 10A + 4B-4S + 2C)\mu_5 + PD(6U-2C-10A + 4S-4B)\mu_4 \quad (A + B \leq S < 2A + B + 2C-U) \\
 PD(4U + 20A + 9B-9S + 12C)\mu_5 + PD(11U-12C-20A + 9S-9B)\mu_4 \quad (2A + B + 2C-U \leq S < 2A + 2B-U) \\
 PD(5U + 18A + 7B-8S + 12C)\mu_5 + PD(10U-12C-18A + 8S-7B)\mu_4 \quad (2A + 2B-U \leq S < A + B + C) \\
 PD(9U + 11A + 4B-5S + 9C)\mu_5 + PD(6U-9C-11A + 5S-4B)\mu_4 \quad (A + B + C \leq S < 2A + B) \\
 PD(9U + 9A + 3B-4S + 9C)\mu_5 + PD(6U-9C-9A + 4S-3B)\mu_4 \quad (2A + B \leq S < 2A + 2B + C-U) \\
 PD(10U + 7A + B-3S + 8C)\mu_5 + PD(5U-8C-7A + 3S-B)\mu_4 \quad (2A + 2B + C-U \leq S < A + B + 2C) \\
 PD(14U-2B + 2C)\mu_5 + PD(U + 2B-2C)\mu_4 \quad (A + B + 2C \leq S < 3A + 2B-U) \\
 PD(15A + 8B + 9U-5S + 2C)\mu_5 + PD(6U + 5S-8B-15A-2C)\mu_4 \quad (3A + 2B-U \leq S < 2A + B + C) \\
 PD(13A + 7B + 9U-4S + C)\mu_5 + PD(6U + 4S-7B-13A-C)\mu_4 \quad (2A + B + C \leq S < 2A + 2B + 2C-U) \\
 PD(11A + 5B + 10U-3S-C)\mu_5 + PD(5U + 3S-5B-11A + C)\mu_4 \quad (2A + 2B + 2C-U \leq S < 3A + 2B + C-U) \\
 PD(26A + 15B + 5U-8S + 4C)\mu_5 + PD(10U + 8S-15B-26A-4C)\mu_4 \quad (3A + 2B + C-U \leq S < 2A + B + 2C) \\
 PD(24A + 14B + 5U-7S + 2C)\mu_5 + PD(10U + 7S-14B-24A-2C)\mu_4 \quad (2A + B + 2C \leq S < 2A + 2B) \\
 PD(4S + 9U-14C-2A-8B)\mu_5 + PD(6U + 14C + 2A + 8B-4S)\mu_4 \quad (2A + 2B \leq S < 3A + 2B + 2C-U) \\
 PD(3S + 8U-12C + A-6B)\mu_5 + PD(7U + 12C-A + 6B-3S)\mu_4 \quad (3A + 2B + 2C-U \leq S < 3A + 3B-U) \\
 PD(8S + 13U-12C-14A-21B)\mu_5 + PD(2U + 12C + 14A + 21B-8S)\mu_4 \quad (3A + 3B-U \leq S < 2A + 2B + C) \\
 PD(9U-3C + 8A-3B-S)\mu_5 + PD(6U + 3C + S + 3B-8A)\mu_4 \quad (2A + 2B + C \leq S < 3A + 2B) \\
 PD(4S-7A-3C + 9U-13B)\mu_5 + PD(6U + 3C-4S + 13B + 7A)\mu_4 \quad (3A + 2B \leq S < 3A + 3B + C-U) \\
 PD(9S-22A-8C + 14U-28B)\mu_5 + PD(U + 8C-9S + 28B + 22A)\mu_4 \quad (3A + 3B + C-U \leq S < 2A + 2B + 2C) \\
 PD(10U-10B + 10C)\mu_5 + PD(5U + 10B-10C)\mu_4 \quad (2A + 2B + 2C \leq S < 4A + 3B-U) \\
 PD(9U-7B + 10C + 4A-S)\mu_5 + PD(6U + 7B-10C + S-4A)\mu_4 \quad (4A + 3B-U \leq S < 3A + 2B + C) \\
 PD(9U-17B-11A + 5C + 4S)\mu_5 + PD(6U + 17B-4S-5C + 11A)\mu_4 \quad (3A + 2B + C \leq S < 3A + 3B + 2C-U) \\
 PD(14U-32B-26A-5C + 9S)\mu_5 + PD(U + 32B-9S + 5C + 26A)\mu_4 \quad (3A + 3B + 2C-U \leq S < 4A + 3B + C-U) \\
 PD(13U-29B-22A-4C + 8S)\mu_5 + PD(2U + 29B-8S + 4C + 22A)\mu_4 \quad (4A + 3B + C-U \leq S < 3A + 2B + 2C) \\
 PD(13U-39B-37A-14C + 13S)\mu_5 + PD(2U + 39B-13S + 14C + 37A)\mu_4 \quad (3A + 2B + 2C \leq S \leq 3A + 3B)
 \end{array} \right.
 \end{aligned}$$

..... (C. 16)

Appendix D Rectification of the fabric dynamic friction coefficient curves in LUFHES test

D.1 Rectification of the fabric friction coefficient curve due to fabric extension deformations

A model of the force applied on the fabric during LUFHES friction test is shown below to help analyse the fabric deformation in this test:

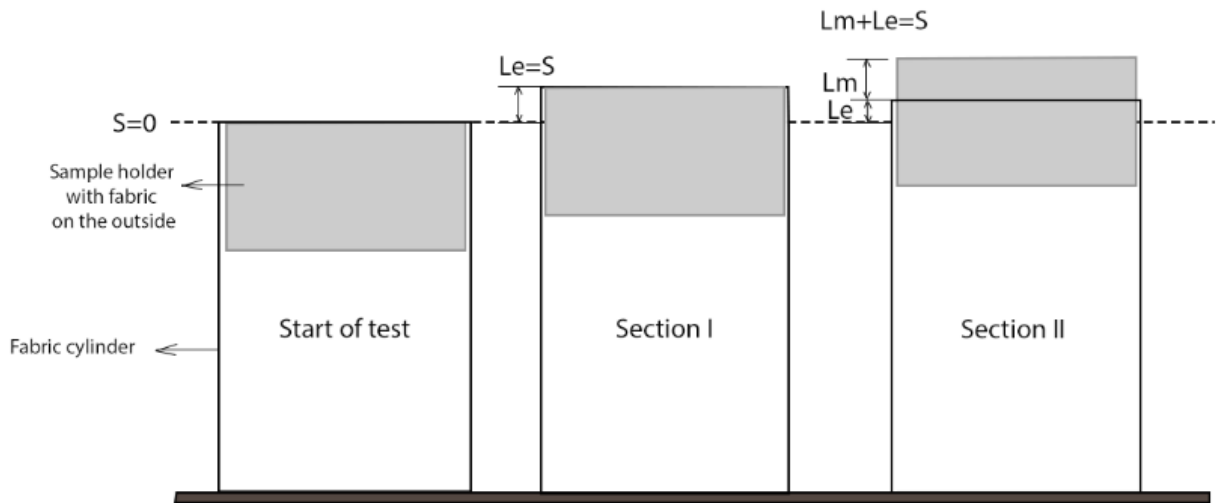


Figure D. 1 A model of the fabric extension deformation in LUFHES friction process

In Figure D. 1, S represents the displacement of sample holder, which is the x-axis of the extension/friction-displacement curve. Lm is the length of relative movement between two fabrics, and Le is the length of extension of fabric shell during LUFHES friction test.

In section I, fabric is extended and the external force exerted on the fabric equals to the elastic force produced due to its elastic extension, which increases almost linearly to the fabric extensions based on Hooke's law. Before reaching the maximum static friction force, two fabrics do not have relative movement. Therefore, $Le=S$.

In section II, the elastic force produced by extended fabric overcomes the fabric static friction force, so relative movement takes place between fabrics which is the Lm in Figure D. 1. Generally speaking, static friction force is larger than kinetic friction force, so less force is applied on fabric shell to keep its extension. Extended fabric will recover to some extent and have less Le than the final stage of section I. In section II, $Le + Lm = S$.

During the LUFHES friction test, fabric elastic force (F_e) equals to the friction force (F_f). Because the contact area decreases with the increase of L_m , the friction force is:

$$F_f = \mu d \cdot P \cdot C \cdot (40 - L_m) = U d \cdot P \cdot C \cdot (40 - S + L_e) \dots \dots \dots (D. 1)$$

Where μd is dynamic friction coefficient; P is the pressure applied on fabric, and it is assumed that pressure is a constant during friction test; C is the circumference of fabric cylinder; 40mm is the width of sample holder which is the contact width of two fabrics at the beginning of friction test.

According to Hooke's Law,

$$F = K \cdot \Delta L \dots \dots \dots (D. 2)$$

Where F is the applied force, K is constant factor characteristic of deformed object, ΔL is the deformation.

Therefore, the relationship between elastic force F_e and extension length L_e is:

$$F_e = K \cdot L_e \dots \dots \dots (D. 3)$$

K is a constant which is a characteristic of fabric cylinder. Based on the equation of Young's modulus:

$$E = \frac{\sigma}{\varepsilon} = \frac{\frac{F}{A}}{\frac{\Delta L}{L}} = \frac{F \cdot L}{A \cdot \Delta L} \dots \dots \dots (D. 4)$$

Where E is the Young's modulus of a material; F is the external force applied to deform an object; L is the original length of the deformed object; A is the area of cross-section; ΔL is the length of deformation with external force. Substitute the equation of Hook's law ($F = K \cdot \Delta L$) into the Young's modulus equation. It is obtained that:

$$E = \frac{F \cdot L}{A \cdot \Delta L} = \frac{K \cdot L}{A} \dots \dots \dots (D. 5)$$

Therefore,

$$K = \frac{E \cdot A}{L} \dots \dots \dots (D. 6)$$

It is learned that K is inversely proportional to fabric cylinder's original length. In LUFHES friction test, the original length of fabric cylinder increases with the increase of L_m . Therefore, the original length of fabric cylindrical shell without extension is equal to $(L_0 + L_m)$, where L_0 is the original length of fabric cylinder.

The equation of elastic force is:

$$F_e = \frac{E \cdot A}{L_0 + L_m} \cdot L_e = \frac{E \cdot C \cdot t}{L_0 + S - L_e} \cdot L_e \dots \dots \dots (D. 7)$$

Where t is the thickness of fabric. It is assumed that the displacement of sample holder is $S1$ in section II, and the external force applied to keep sliding is $F1$ at this moment. $F1$ is measured and recorded during LUFHES friction test.

It is known that:

$$F1 = Ff = Fe \dots\dots\dots (D. 8)$$

Therefore,

$$F1 = \mu d \cdot P \cdot C \cdot (40 - S1 + Le) = \frac{E \cdot C \cdot t}{L_0 + S1 - Le} \cdot Le \dots\dots\dots (D. 9)$$

Equations of Le and μd are obtained:

$$Le = \frac{F1 \cdot (L_0 + S1)}{E \cdot C \cdot t + F1} \dots\dots\dots (D. 10)$$

$$\mu d = \frac{F1}{PC \cdot (40 - S1 + \frac{F1 \cdot (L_0 + S1)}{E \cdot C \cdot t + F1})} \dots\dots\dots (D. 11)$$

In friction test, pressure is applied by an extended elastic band. In LUFHES friction test, the extension of band (L_{ext}) is depended on fabric thickness. The original band lengths of all LUFHES friction test are the same, thicker fabric could produce a larger band extension. Because elastic band is formed into a round shape, the calculation of its extension length L_{ext} is based on the length of its central line.

$$L_{ext} = \pi \cdot (2R_0 + 4t + t') - L_{ori} \dots\dots\dots (D. 12)$$

R_0 is the radius of sample holder; t is the thickness of fabric; two layers of fabric are used in friction test; t' is the thickness of band; L_{ori} is original band length.

The elastic force Fb of elastic band was tested in Instron, the relationship between force (F_b) and extension (L_{ext}) is represented by a regression equation:

$$F_b = 0.00003 \cdot L_{ext}^3 - 0.0035 \cdot L_{ext}^2 + 0.2062 \cdot L_{ext} + 0.3716 \dots\dots (D. 13)$$

Elastic force of band could be obtained by substituting L_{ext} into the regression equation of force Fb . Then, the Young's modulus of elastic band is calculated by:

$$E' = \frac{\sigma}{\varepsilon} = \frac{\frac{F}{A}}{\frac{\Delta L}{L}} = \frac{F \cdot L}{A \cdot \Delta L} = \frac{Fb \cdot L_{ori}}{W \cdot t' \cdot L_{ext}} \dots\dots\dots (D. 14)$$

In the above equation, Fb is the force applied to extend elastic band; L_{ori} is the original length of elastic band; L_{ext} is the length of extension; W is the width of elastic band, and t' is the thickness of band.

Then, the pressure produced by extended elastic band is calculated by (Lee, Y.J., 2005):

$$P = E' \cdot t' \cdot \left(\frac{1}{r_0} - \frac{1}{r} \right) \dots\dots\dots (D. 15)$$

in which E' is the Young's modulus of elastic band, t' is the thickness of elastic band, r_0 is the original radius and r is the extended radius.

Original radius (r_0) and the radius after extending (r) are calculated by:

$$r_0 = \frac{L_{ori}}{2\pi} \dots \dots \dots (D. 16)$$

$$r = \frac{L_{ori} + L_{ext}}{2\pi} \dots \dots \dots (D. 17)$$

Then, the equation to calculate pressure P in LUFHES friction test is obtained as below:

$$P = 2\pi \cdot \frac{Fb \cdot L_{ori}}{W \cdot L_{ext}} \cdot \left(\frac{1}{L_{ori}} - \frac{1}{L_{ori} + L_{ext}} \right) \dots \dots \dots (D. 18)$$

According to above equations, the values of Le and μd could be obtained. Le and μd of ripstop fabric and a wool plain woven fabric are shown below to compare.

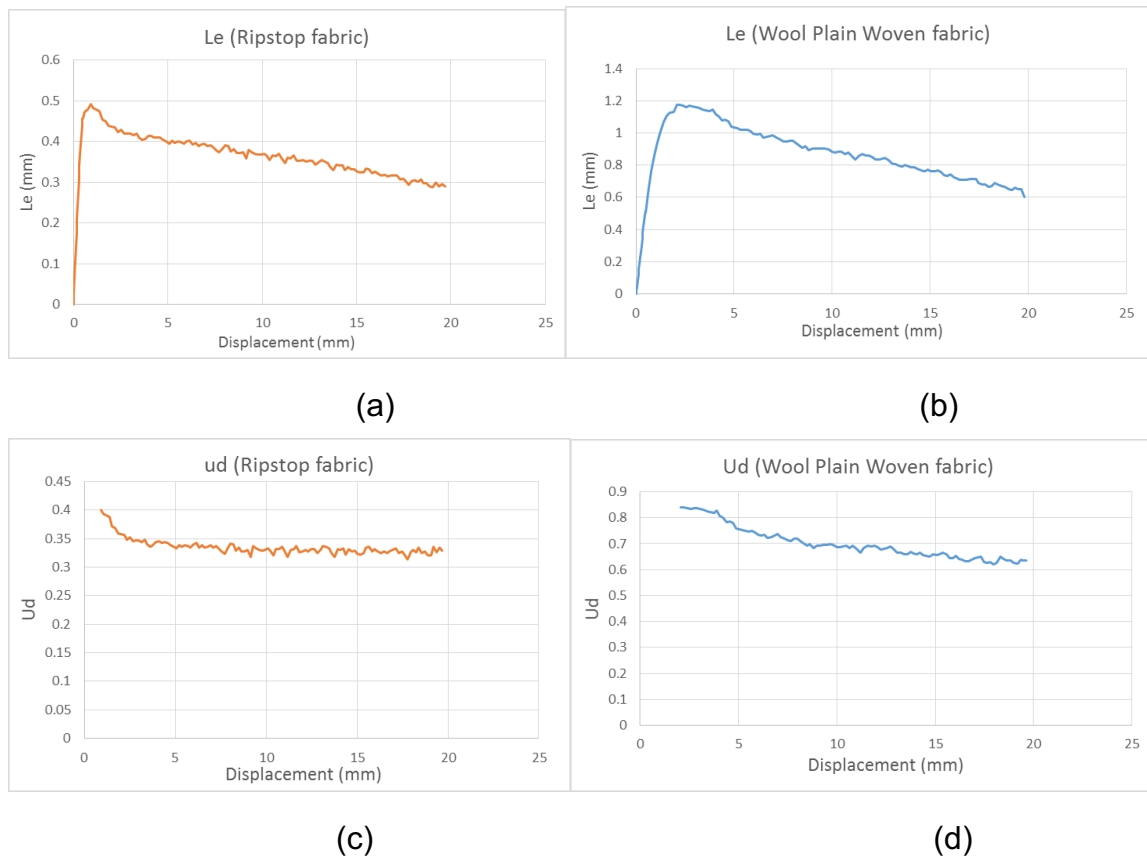


Figure D. 2 Le and μd of a ripstop fabric and a wool plain woven fabric. (a) Le of ripstop fabric. (b) Le of wool plain woven fabric. (c) μd of ripstop fabric. (d) μd of wool plain woven fabric.

According to the curves of Le , it is learned that the extension of fabric increases in section I but decreases with the increase of displacement in section II. It is because in section II relative movement has started, contact area between two fabrics decreases with the increase of displacement, less friction force is applied on fabric cylindrical shell and leads to decreasing extension of fabric. Ripstop

fabric has less Le than the plain fabric. From μd results of these two fabrics, it is known that plain fabric has greater static friction coefficient (around 0.85) than ripstop fabric (around 0.4). Therefore, more force is required to start movement between two plain fabrics, and more elongation of plain fabric is produced. Another difference between these two fabrics exists at the beginning of section II which is regarded as the transition from static friction to dynamic friction when relative movement is just start between fabric and fabric. Le of ripstop fabric has a sharp decrease for around 2mm and then the decreasing slope becomes stable. Comparatively, the transition of plain fabric is not as noticeable as that of ripstop fabric.

Differences are also shown in the μd curves of these two fabrics. As mentioned plain fabric has greater friction coefficient than ripstop fabric. It means ripstop fabric has smoother surface than plain fabric. In the transition part from static friction to dynamic friction, the friction coefficient of ripstop fabric has a sharper decrease in a shorter distance than that of plain fabric. This trend is similar to that shown in the Le curve. In addition, the friction coefficient of ripstop fabric is relatively stable, almost horizontal, after the transition step. However, the friction coefficient of plain fabric decreases with the increase of displacement, from 0.75 to 0.65.

In order to study the mechanism of the decrease of μd , a friction test between the wool plain fabric and paper is conducted to compare with the friction between fabric and fabric.

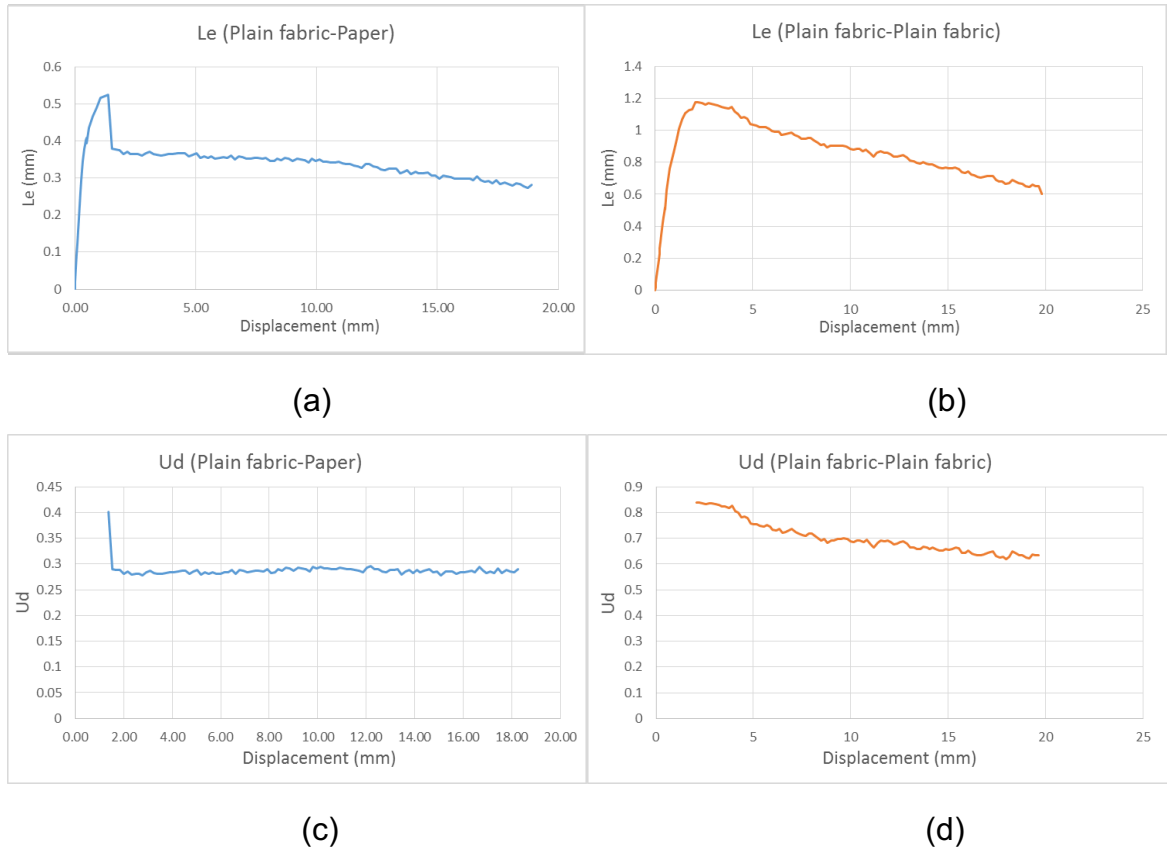


Figure D. 3 Comparison between friction of fabric-paper and fabric-fabric. (a) L_e of fabric-paper friction test. (b) L_e of fabric-fabric friction test. (c) μ_d of fabric-paper friction test. (d) μ_d of fabric-fabric test.

Huge differences are shown in Figure D. 3 between these two friction tests.

Firstly, the friction coefficient between fabric and paper is less than that between fabric and fabric. A possible reason is that when two fabrics are in contact, their surface might embed into each other structurally. More external force is required to shear the asperities on fabric surface and leads to a greater friction coefficient.

It is also noticed that μ_d of fabric-paper test is stable, but that of fabric-fabric test decreases with the increase of displacement. A possible reason of this difference is shown in Figure D. 4. In the friction test between fabric and paper, the asperities of fabric are compressed because of applied pressure. The change of fabric surface barely increases with the increase of relative movement, so μ_d is stable in fabric-paper test. Comparatively, in the friction between fabric and fabric, fabrics interact structurally. According to the adhesion-shearing theory of friction, the asperities on fabric surface shear with each other repeatedly to produce relative movement. During the friction test, there is no time for the deformed asperities to recover, so the repeated shearing changes fabric surface temporarily. The asperities on fabric surface might be flattened little by little with the increase of relative movement, so less and less external force is required to keep sliding. Another possible reason which could flatten the asperities is the

decreasing of yarn crimp because of the extension of fabric. The large friction between fabric and fabric might cause fabric extension in the contact area between two fabrics. Fabric extension could reduce yarn crimp in the loaded direction. Normally, crimp-exchange will happen, which is known as Poisson effect, the yarn crimp of yarns in another direction will increase. However, because of the support effect of sample holder, the increase of crimp in another direction might be very small. As a result, the decrease of yarn crimp could also lead to the reduction of both friction force and friction coefficient.

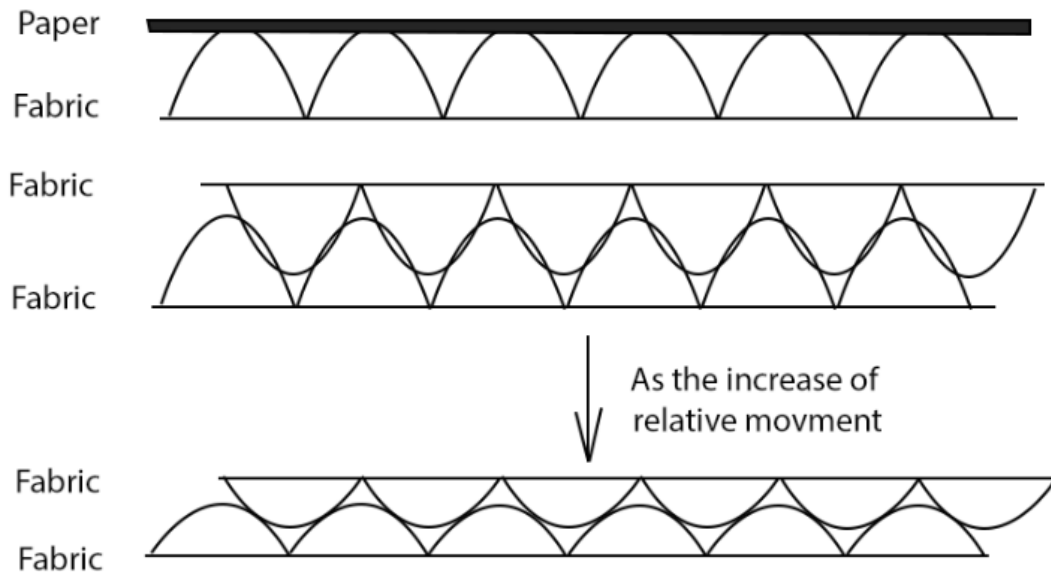


Figure D. 4 Model of friction test between fabric and paper, and fabric and fabric.

Two curves also show difference at the beginning of movement. In the test of fabric-paper, friction coefficient and Le have a sudden drop, which is not shown in the test of fabric-fabric. The drop in Le suggests that the extended fabric has a quick recovery, which might be the recovery of fabric elastic extension. This kind of quick recovery is not shown in fabric-fabric friction. A possibility is because of greater friction coefficient between fabric and fabric, almost double that between fabric and paper, greater force is required to start relative movement. This large force produces not only elastic extension but also plastic extension of fabric. To recover the extension, fabric shell needs to move downwards. However, a large fabric-fabric friction force prevents the recovery, so the recovery of extension needs longer time which is shown as longer displacement in the curves. Another possibility is because the relative movement between fabric and paper happens almost at the same time in the contact area due to the small friction coefficient and simple contact situation between fabric and paper. Therefore the transition from static friction to dynamic friction is very quick and shown as a sudden drop in the curve. However, for the friction between fabric and fabric, the relative movement might take place gradually due to greater friction force and complex

contact situation. In some area, the contact area between asperities might be small, so the relative movement happens early. However, in some other area the asperities might deeply embed into each other, so more force is required and the movement of this area is later. Generally, static friction force is greater than dynamic friction force, so the friction force between fabrics starts to reduce as long as some areas has started the movement. However, because some parts are still in static state, so the friction force decrease slowly. With the increase of relative movement, the asperities of the area where movement is difficult and late might be flattened as shown in Figure D. 4. Gradually, two fabrics in the contact area could move at a similar pace, which means the transition from static friction to dynamic friction is finished, and the friction between fabric and fabric is in a stable rate.

The comparison between fabric-paper and fabric-fabric friction could also explain the difference between ripstop fabric and plain woven fabric shown in Figure D. 2. Ripstop fabric has smoother surface than plain woven fabric. It suggests that, compared with plain fabric, the asperities of two contacted surfaces have smaller interaction in friction test. Therefore, the change of fabric surface of ripstop fabric produced by repeated shearing effect is not as serious as that of plain fabric, and the decrease of μ_d is not as obvious as that of plain woven fabric. In addition, because of the smaller friction coefficient of ripstop fabric, less force is needed to start the movement. Less extension is produced, and most of extension is elastic deformation. Because of the small friction, the elastic deformation could recover quickly and all fabrics in the contact area could start move within a short displacement.

D.2 Rectification of the residue linear decrease of the friction force

Because the frequency coefficient of LUFHES test might have a decreasing trend, the influence of this trend on FFT spectrum is studied at first. A normal sine curve and a modified decreasing sine curve are analysed by FFT. According to the frequency values obtained in FFT results, wavelengths are calculated. Two curves and their FFT spectrum are shown in Figure D. 5.

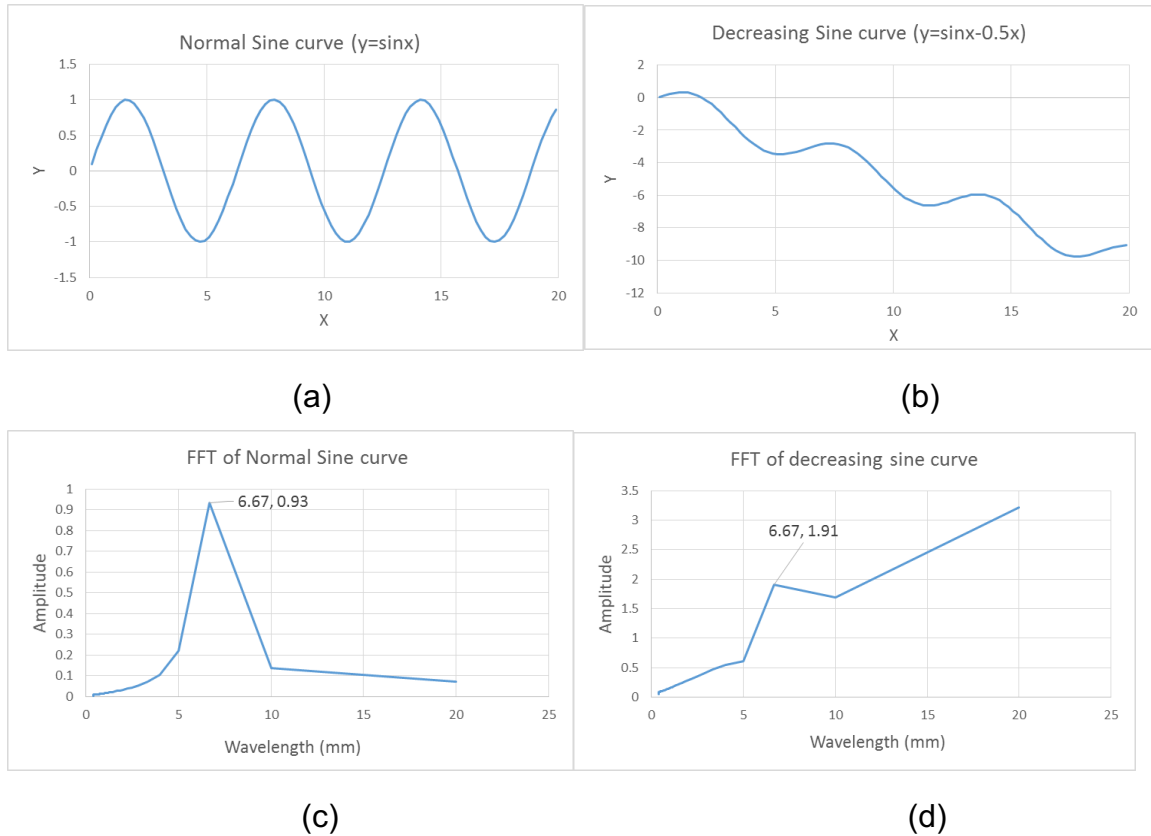
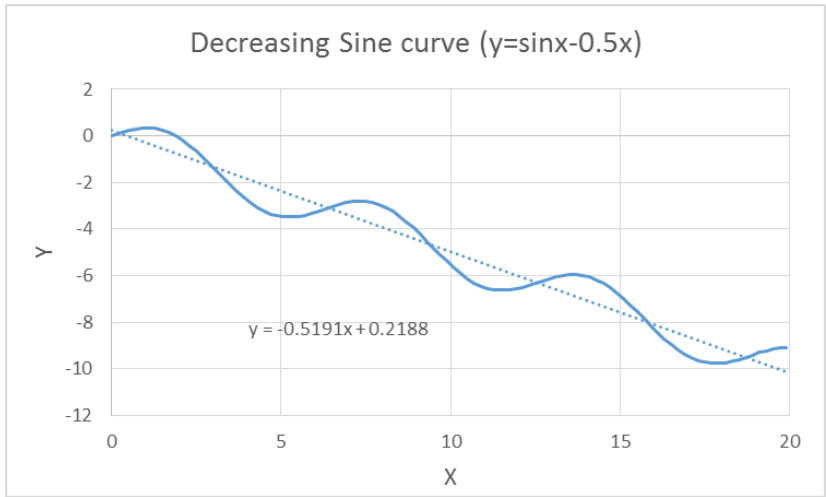


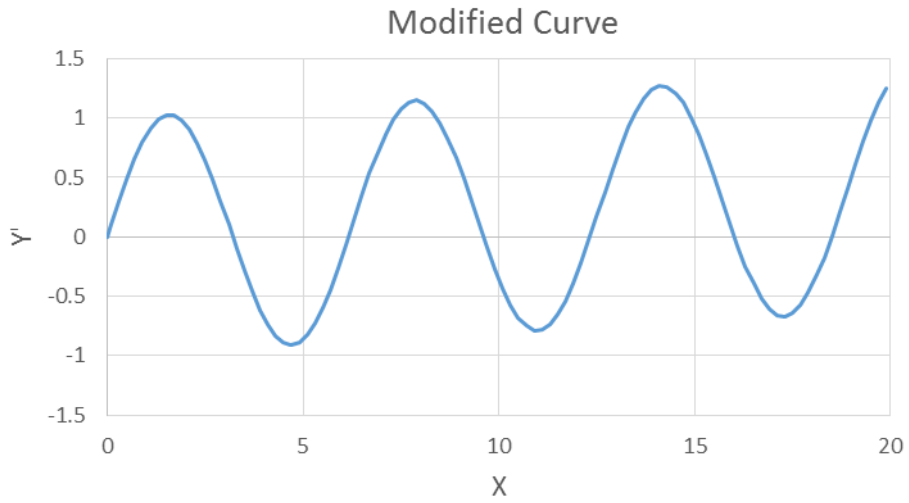
Figure D. 5 FFT study of flat sine curve and decreasing sine curve. (a) Flat sine curve. (b) Decreasing sine curve. (c) FFT results of flat sine curve. (d) FFT results of normal sine curve.

It is found that the decreasing trend could produce high amplitudes at long wavelengths. It is also noticed that FFT spectrum of two curves have peaks at the same wavelength, but their amplitudes have a significant difference. A possible reason is that the FFT transforms the straight line ($y = -0.5x$) into sine waves as well, and these sine waves of straight line significantly affect the final FFT spectrum. As analysed before, the decreasing trend might be because asperities on fabric surface structure have temporarily changed with the increase of relative movement, so the effect of the decreasing trend is unnecessary or can even produce errors in the analysis of fabric original structure. Therefore, it is better to eliminate the influence of the decreasing trend and, the decreasing curve is modified in following ways:

1. A trend line of the original decreasing curve is drawn, and the equation of the trend line is obtained as well: $Y = aX + b$ ($Y = -0.5191X + 0.2188$ of example).



2. The modified data is calculated by: $Y' = Y - aX$ ($Y' = Y + 0.5191X$)



The modified flat curve is not absolutely flat, but this error is ignored in the study.